

Targeting Neuroinflammation in mTORC1 Driven Brain Tumours



A thesis presented for the award of

Doctor of Philosophy

Darius McPhail

June 2023

Supervisors: Prof. Andrew Tee, Prof. Adrian Harwood, Dr Mark Davies

Acknowledgements

I would first like to thank my supervisors, Professor Andrew Tee, Professor Adrian Harwood, and Dr Mark Davies. I could not have asked for a more supportive team to guide me through this project. The guidance offered by Andy has been invaluable in helping me grow as a scientist. His patience, understanding, and expertise has made the past few years in his lab an excellent formative experience. Andy is truly an inspiring supervisor. My thanks also go to Mark Davies. I am consistently amazed by his incredible expertise, and the clinical and cellular perspectives offered by Mark have added invaluable to this project and my development as a scientist. Thank you to Adrian for the assistance in the daunting field of neuroscience, and his excellent input on the neurological side of this project. The research environment he has fostered in the Harwood group has made the difficult stem-cell side of this research project into a more enjoyable experience. Within the Harwood group, I would like to thank Laura Kleckner for the excellent training she provided, as well as the helpful discussions between our projects. I would also like to thank Karolina Dec, Gemma Wilkinson, and Shane Wainwright for their help in neural and iPSC culture. I would also like to thank Dr Jesse Champion. Discussions with Jesse on our projects have been an excellent source of inspiration for the directions in which to take my work. I would also like to thank Dr Brian Calver for his smooth running of the lab, assistance in experiments, and proof reading. My thanks go to Dr Sara Seifan and Dr Elaine Dunlop for their support and expertise throughout the years. My heartfelt thanks also go to Mr Mohammad Alzahrani for his kind and bright personality during stressful times, and his work alongside Dr Brian Calver in the generation of transcriptomic data. My gratitude also goes to Prof. Jeffrey Mackeigan for his generous donation of transcriptomic data which formed the backbone for this project. The continued support provided by Cancer Research Wales has been invaluable through the years, and I would like to sincerely thank them for the financial support they have provided during this project. I would especially like to thank Dr Lee Campbell and Dr Peter Henley. Incredibly important aspects of this project would not have been possible without their knowledge, input, and support.

Lastly, I would like to thank my family and friends for their support throughout the years. I have been incredibly lucky to have such a supportive group of people around me.

Abstract

Tuberous sclerosis complex (TSC) is a rare genetic disease that results in the system-wide growth of benign lesions. TSC patients often present with brain tumours and TSC-associated neuropsychiatric disorders (TANDs) including epilepsy and autism. Pharmaceutical intervention for TSC involves the use of mTORC1 inhibitors. Growing evidence suggests that chronic inflammation is a feature of TSC. Inflammatory processes arising in TSC-derived brain tumours are also implicated in the development of TANDs. There is limited research on inflammation in the context of TSC-derived brain tumours and TANDs, and models to explore this are limited. Furthermore, mTORC1 inhibitors are often unsuitable for total tumour clearance and reducing the severity of TANDs. Therefore, this project aims to investigate inflammation in TSC-derived brain tumours and identify new treatments to target this. Inflammatory signalling mechanisms were investigated within *in vitro* models of TSC and compared to TSC patient-derived brain tumour transcriptomic data. A *TSC2*-deficient iPSC model was developed, which was used to generate *TSC2*-deficient neural cells for inflammatory pathway analysis. Results showed that inflammatory pathways were dysregulated in *TSC2*-deficient cell models. NF- κ B was identified as an anti-inflammatory drug target in TSC. mTORC1 inhibition was found to be insufficient to target dysregulated NF- κ B signalling. The activation of TBK1 was also dysregulated, which may be a central mechanism that drives inflammation in TSC. *TSC2*-deficient neurons also showed dysregulated neurodevelopment, coinciding with dysregulated inflammatory activation of the NF- κ B and STAT3 pathways. Lastly, targeting of the IL-1 β pathway with a rheumatoid arthritis drug, diacerein, was shown to be efficacious at reducing inflammatory signals in TSC. Diacerein also reduced mTORC1 activation in *TSC2*-deficient neurons. Overall, this study showed that NF- κ B and other inflammatory pathways are hyperactive in TSC. These may contribute to the development of TANDs and TSC disease pathology and may be targeted with drugs that inhibit NF- κ B signalling.

Table of Contents

Chapter 1: Introduction.....	1
1.1 TSC and the mTOR complexes.....	1
1.1.1 Tuberous Sclerosis Complex.....	1
1.1.2 Additional TSC or mTORC1-regulated pathways	4
1.1.3 The mTOR complexes	8
1.1.3.1 mTORC1	8
1.1.3.2 mTORC2.....	10
1.1.4 Current drug treatments of TSC.....	12
1.1.4.1 Rapamycin (Sirolimus) and rapalogs.....	13
1.1.4.2 Vigabatrin.....	14
1.1.4.3 Surgery	15
1.1.4.4 Cannabidiol	15
1.1.4.5 Future Therapies	16
1.1.5 mTOR in Brain Tumours	16
1.1.5.1 Glioma and Glioblastoma Multiforme.....	17
1.1.5.2 Malignancy in TSC.....	20
1.2 Inflammation and the Immune System in Brain Tumours.....	20
1.2.1 Neuroinflammation and the immune system of the CNS	20
1.2.2 The NF- κ B and STAT3 signalling axes: disease and crosstalk.....	21
1.2.2.1 TNF α and NF- κ B	22
1.2.2.2 IL-1 β	23
1.2.2.3 cGAS/STING/TBK1	24
1.2.3 IL-6/STAT3 signalling	24
1.2.4 Crosstalk between the NF- κ B and STAT3 pathways	26
1.3 TSC-derived brain tumours.....	28
1.3.1 Normal neuronal development.....	28
1.3.2 SEN/SEGAs.....	31
1.3.3 Cortical tubers.....	32
1.3.4 TSC-associated neuropsychiatric disorders	34
1.3.5 Neuroinflammation in TSC.....	35
1.4 Aims and Objectives	38
Chapter 2 – Materials and Methods	40
2.1 Cell culture and maintenance.....	40
2.1.1 MEF, AML, and ELT3	40
2.1.2 iPS cell culture	41
2.1.3 iPSC single-cell cloning.....	42

2.2 Sodium Dodecyl Sulphate Polyacrylamide Gel Electrophoresis (SDS-PAGE) and western blotting	43
2.2.1 Protein lysate generation	43
2.2.2 SDS-PAGE	43
2.2.3 Electrophoretic Transfer and western blotting	43
2.3 Drug Treatments	44
2.4 Patient-Derived TSC Transcriptomic Analysis and Gene Ontology Analysis	45
2.5 RNA-Sequencing	45
2.6 Transcriptional Activation Enzyme Linked Immunosorbance Assays (ELISAs)	45
2.7 Cytokine/Chemokine Profiling	46
2.8 Viability Assays	46
2.9 DuoSet ELISAs	47
2.10 Anchorage-independent colony formation assays	47
2.11 Wound scratch cell migration assays	48
2.12 CyQUANT Cell Proliferation Assays	48
2.13 Reverse Transcriptase quantitative Polymerase Chain Reaction (RT-qPCR)	48
2.14 Neurodifferentiation	50
2.15 PGP1 <i>TSC2</i> -knockout validation	51
2.15.1 DNA extraction and qPCR	52
2.15.2 BigDye and Sanger sequencing	53
2.16 Statistical analysis	54
Chapter 3 - Exploring Inflammatory Pathways	55
3.1 Introduction	55
3.2 Results	56
3.2.1 The TNF α and STAT3 pathways are differentially regulated in <i>TSC2</i> -deficient MEFs and AMLs.	56
3.2.2 Inflammatory and immune pathways are upregulated in SEN/SEGA <i>in vivo</i>	62
3.2.3 STAT3 hyperactivation in <i>Tsc2</i> ^(-/-) MEFs can be diminished by NF- κ B inhibition.	67
3.2.4 NF- κ B activity controls dysregulated cytokine secretion in <i>TSC2</i> ⁽⁻⁾ AMLs	70
3.2.5 Cytokine and chemokine profiling	72
3.2.6 <i>TSC2</i> -deficiency confers sensitivity to NF- κ B inhibition	77
3.2.7 The NF- κ B pathway is differentially regulated in <i>Tsc2</i> ^(-/-) MEFs	80
3.2.8 Inflammatory signals within <i>TSC2</i> -deficient AMLs can be reduced by NF- κ B inhibition. ..	84
3.2.9 Hypoxia Response	91
3.3 Discussion	94
3.4 Conclusion	96
Chapter 4 – NF- κ B and Surrounding Pathways Within TSC	97
4.1 Introduction	97

4.2 Results.....	98
4.2.1 Inflammatory signalling in the growth of TSC-derived tumours.....	98
4.2.1.1 NF- κ B inhibition slows tumours growth	98
4.2.1.2 NF- κ B inhibition when combined with rapamycin reduces tumour growth after treatment discontinuation.....	100
4.2.1.3 NF- κ B reduces migration of <i>TSC2</i> -deficient cells	102
4.2.1.4 NF- κ B/mTORC1-dependent gene regulation	105
4.2.2 Alternative pathway targeting	111
4.2.2.1 Effects of pathway inhibitors in TSC-associated inflammatory pathways	113
4.2.2.2 IL-1 β and rheumatoid arthritis in TSC.....	117
4.3 Conclusion	132
Chapter 5: <i>TSC2</i> -deficient iPSC Model for Neuronal Model Generation	133
5.1 Introduction.....	133
5.2 Results.....	135
5.2.1 <i>TSC2</i> knockout verification and sequencing.....	135
5.2.2 Neurodifferentiation Optimisation for <i>TSC2</i> -KO PGP1	136
5.3 <i>TSC2</i> ⁽⁻⁾ iPSC model final usage	139
5.3.1 Neurodifferentiation of PGP1-A5 cells.....	139
5.3.2 Protein expression during neurodifferentiation of <i>TSC2</i> ⁽⁻⁾ PGP1-A5	146
5.3.3 Protein expression during neurodifferentiation of <i>TSC1</i> ⁽⁻⁾ iBJ4	155
5.3.4 Inflammatory pathways in mature <i>TSC2</i> ⁽⁻⁾ neurons.....	165
5.3.4 NF- κ B and mTORC1 inhibition in <i>TSC2</i> ⁽⁻⁾ neural cells.....	173
5.3.6 IL-1 β inhibition in <i>TSC2</i> ⁽⁻⁾ neural cells.....	176
5.4 Conclusion	178
Chapter 6 – Discussion	180
Bibliography	193

List of Figures

Figure/Table	Title	Page #
Figure 1.1	Diagram of mTORC1 and mTORC2 Signalling.	12
Figure 1.2	Positive feedback activity between NF- κ B and STAT3 pathways.	27
Figure 1.3	Neuroinflammation contributes to the development of TANDs.	37
Table 2.1	Drug supplier and stock concentrations.	44
Table 2.2	Primer pair sequences and optimization.	50
Table 2.3	N2B27 +/-RA Neurodifferentiation media composition.	50
Figure 2.1	Sequencing data of PGP1 <i>TSC2</i> -CRISPR-Cas9-transfected cell pool.	52
Figure 3.1	Inflammatory signalling in <i>TSC2</i> -deficient cells.	57
Table 3.1	Fold increases of STAT3 and RelA phosphorylation between <i>TSC2</i> - deficient and <i>TSC2</i> -restored MEF and AML cell lines.	59
Figure 3.2.1	Inflammatory and immune pathways are dysregulated in TSC patient-derived SEN/SEGAs.	63
Figure 3.2.2	Inflammatory and immune pathways are dysregulated in TSC patient-derived cortical tubers.	63
Figure 3.2.3	<i>TSC2</i> -deficient cells demonstrate dysregulated NF- κ B Signalling.	66
Figure 3.3.1	NF- κ B inhibition of STAT3 in <i>TSC2</i> -deficient cells.	67
Figure 3.3.2	STAT activity is regulated in a biphasic manner through NF- κ B inhibition.	68
Figure 3.4	Enhanced cytokine secretion can be regulated via NF- κ B.	71
Figure 3.5.1	Differential inflammatory activation between <i>Tsc2</i> ^(-/-) and <i>Tsc2</i> ^(+/+) MEFs, shown by cytokine profiling.	73
Figure 3.5.2	Cytokine profiling with intracellular transport inhibition.	76
Figure 3.6	NF- κ B inhibition causes selective cell death in <i>TSC2</i> -deficient cells.	78
Figure 3.7	NF- κ B, unlike C/EBP β is not regulated through mTORC1.	81
Figure 3.8.1	Dysregulated protein expression in <i>TSC2</i> ⁽⁻⁾ AMLs cannot be fully restored by mTORC1 inhibition.	85
Table 3.2	Fold changes in multiple gene expressions within TSC-patient derived SEN/SEGA.	86
Figure 3.8.2	mTORC1 inhibition is not suitable for restoring dysregulated NF- κ B signalling.	90

Figure 3.9	Hypoxia induces differential expression in NF- κ B target genes, and this can be affected by mTORC1.	92
Figure 4.1	NF- κ B inhibition reduces anchorage-independent colony formation <i>in vitro</i> .	99
Figure 4.2	combining inhibition of NF- κ B and mTORC1 has greater efficacy to reduce tumour growth.	101
Figure 4.3	NF- κ B inhibition reduces proliferation of TSC2-deficient cells <i>in vitro</i> .	102
Figure 4.4	NF- κ B inhibition reduces migration of <i>tsc2</i> -deficient AML cells.	104
Figure 4.5.1	Various inflammatory genes are upregulated within TSC2-deficient AML cells.	106
Figure 4.5.2	Combinatory NF- κ B and mTORC1 inhibition may be beneficial for reducing enhanced immune checkpoint expression.	107
Figure 4.5.3	Immune checkpoint regulators within TSC patient-derived SEN/SEGAs.	108
Figure 4.5.4	combinatorial NF- κ B and mTORC1 inhibition can be used to target cytokine gene expression.	109
Figure 4.5.5	NF- κ B inhibition may reduce migration via downregulation of <i>FNI</i> and <i>ICAM1</i> .	110
Figure 4.6.1	Exploratory experiments show potential for anti-inflammatory effects in TSC2 ⁽⁻⁾ AMLs in trialled drugs.	113
Figure 4.6.2	SAHA and R-7050 show efficacy in reducing STAT3 phosphorylation, but not RelA phosphorylation within TSC2-deficient AML cells.	115
Figure 4.6.3	SAHA reduces anchorage-independent colony growth in <i>Tsc2/TSC2</i> -deficient cells.	116
Figure 4.7.1	IL-1 β signalling is dysregulated in TSC.	118
Figure 4.7.2	Rheumatoid arthritis-associated genes were upregulated within TSC2-deficient cells.	120
Figure 4.8.1	Diacerein potentially reduced STAT3 tyrosine-phosphorylation in <i>TSC2/Tsc2</i> -deficient cells.	121
Figure 4.8.2	Diacerein potentially increases IL-6 secretion in <i>TSC2</i> -deficient AML cells.	123
Figure 4.9	Diacerein reduced colony growth in TSC2-deficient cells.	124
Figure 4.10	Diacerein has limited selective cytotoxicity on TSC-diseased cells.	126

Figure 4.11	Diacerein reduces migration of <i>TSC2</i> -deficient AML cells.	127
Figure 4.12	Diacerein was not effective at reducing cell proliferation in <i>TSC2/Tsc2</i> -deficient cells.	128
Figure 4.13.1	Diacerein was effective at reducing some immune checkpoint regulators.	129
Figure 4.13.2	Diacerein reduced inflammatory cytokine gene expression.	129
Figure 4.13.3	Diacerein may reduce migration via inhibition of <i>FNI</i> and <i>ICAM1</i> gene expression.	130
Figure 4.14	IL-6 secretion can be increased in <i>TSC2</i> -deficient neural cells by rapamycin, and reduced by DCN.	131
Figure 5.1	Steps of neurodifferentiation and markers of cell types.	134
Figure 5.2	Confirmation of purified <i>TSC2</i> -KO PGP1 iPSCs.	136
Figure 5.3.1	PGP1-A5 iPSCs demonstrate reduced viability in neurodifferentiation.	138
Figure 5.3.2	PGP1-A5 iPSCs do not express <i>TSC2</i> protein.	139
Figure 5.4.1	PGP1-A5 cells can progress with neurodifferentiation following passage to fibronectin if passaged at a higher ratio than iBJ4-WT.	141
Figure 5.4.2	Differentiation of PGP1-A5 cells and iBJ4 cells.	142
Figure 5.4.3	Maturation of iBJ4-WT and PGP1-A5 neurons.	143
Figure 5.4.4	Neuronal differentiation of <i>TSC2</i> ⁽⁻⁾ iPSCs results in mixed cell outcomes and differential macroscopic structures.	144
Figure 5.5.1	Differential protein expression in PGP1-A5 vs iBJ4-WT.	147
Figure 5.5.2	mTORC1, NF-κB, and STAT3 signalling is dysregulated through neurodifferentiation in PGP1-A5 iPSCs.	148
Figure 5.5.3	Neurodifferentiation markers are dysregulated in <i>TSC2</i> -deficient cells.	149
Figure 5.5.4	Later stage neural markers develop more slowly in <i>TSC2</i> ⁽⁻⁾ PGP1-A5 cells.	151
Figure 5.6	<i>TSC1</i> ⁽⁻⁾ cells develop more astrocytes than wild-type during differentiation.	153
Table 5.2	Transcriptomic neurodevelopmental markers in TSC patient-derived brain tumours.	154
Figure 5.7	Pre-neural cell types are upregulated in SEN/SEGA.	155
Figure 5.8.1	Differential protein expression in iBJ4- <i>TSC1</i> ⁽⁻⁾ vs iBJ4-WT during neurodifferentiation.	156
Figure 5.8.2	Early to intermediate neurodifferentiation markers are	

	dysregulated in <i>TSC1</i> -deficient cells.	157
Figure 5.8.3	Late neurodifferentiation markers are dysregulated in <i>TSC1</i> -deficient cells.	158
Figure 5.9.1	Neurodifferentiation of <i>TSC2</i> ⁽⁻⁾ cells produces neurons and GFAP positive cells.	166
Figure 5.9.2	Morphology and cell types vary within populations of <i>TSC2</i> -deficient neural cells.	167
Figure 5.9.3	<i>TSC1</i> -deficient neurons exhibit enhanced STAT3 signalling at day 60.	169
Figure 5.10	<i>TSC2</i> -deficient neurons exhibit enhanced NF- κ B signalling and decreased STAT3 activity.	170
Figure 5.11	NF- κ B or mTORC1 inhibition can reduce some inflammatory signalling in <i>TSC2</i> -deficient PGP1-A5 cells.	173
Figure 5.12	Diacerein is highly effective at inhibiting mTORC1 and STAT3 activity in <i>TSC2</i> -deficient cells.	176
Figure 6.1	Indirect inhibition of phospho-STAT3 activity by NF- κ B inhibition leads to an increase in available unphosphorylated STAT3.	188
Figure 6.2	Proposed mechanism of the development of inflammation in <i>TSC2</i> -deficient cells.	190

List of Abbreviations

4E-BP1	4E-Binding Protein 1
AML	Angiomyolipoma
ANOVA	Analysis of Variance
ANXA2	Annexin A2
BBB	Blood Brain Barrier
BDNF	Brain Derived Neurotrophic Factor
CBD	Cannabidiol
C/EBP	CCAAT enhancer binding protein
cGAMP	Cyclic GMP-AMP
cGAS	Cyclic GMP-AMP Synthase
CNS	Central Nervous System
CRISPR	Clustered Regularly Interspaced Short Palindromic Repeats
CSF	Cerebrospinal Fluid
DAMP	Damage Associated Molecular Pattern
DCN	Diacerein
DEG	Differentially Expressed Gene
DEPTOR	DEP-domain-containing mTOR Interacting Protein
DMSO	Dimethyl Sulfoxide
eIF4E	Eukaryotic translation Initiation Factor 4E
ELISA	Enzyme Linked Immunosorbent Assay
ELT3	Eker rat Leiomyoma Tumour
EMT	Epithelial to Mesenchymal Transition
EOMES	Eomesodermin
EphA	Erythropoietin-producing human hepatocellular-A
FKB	FKBP-Rapamycin Binding
FKBP12	FK506 Binding Protein 12
GABA	Gamma-Aminobutyric Acid
GAP	GTPase-Activating Protein
GBM	Glioblastoma Multiforme
GFAP	Glial Fibrillary Acidic Protein
GO	Gene Ontology
HvHKu	Hypoxia vs Hypoxia + Ku0063794

ICE	Interleukin-1 β Converting Enzyme
IKK	I κ B Kinase
IPC	Intermediate Progenitor Cell
iPSC	Induced Pluripotent Stem Cell
I κ B	Inhibitor of κ B
JAK2	Janus kinase 2
LAM	Lymphangioliomyomatosis
LARP1	La-Related Protein 1
LGALS3	Galectin-3
LITAF	Lipopolysaccharide Induced TNF Factor
MAP2	Microtubule-associated protein 2
MEF	Mouse Embryonic Fibroblast
MHC	Major Histocompatibility Complex
mLST8	Mammalian Lethal with SEC14 Protein 8
mSIN1	Mammalian Stress-activated protein kinase-Interacting protein 1
mTOR	Mammalian Target of Rapamycin
mTORC1	Mammalian Target of Rapamycin Complex 1
mTORC2	Mammalian Target of Rapamycin Complex 2
NEC	Neuroepithelial Cell
NF- κ B	Nuclear Factor Kappa-light-chain-enhanced of activated B cells
Ngn2	Neurogenin 2
NSC	Neural Stem Cell
NvH	Normoxia vs Hypoxia Dataset
OG	Oligodendroglioma
PAMP	Pathogen Associated Molecular Pattern
PBS	Phosphate Buffered Saline
PDL	Poly-D-Lysine
PI3K	Phosphoinositide 3-Kinase
Pol1	RNA-Polymerase I
Pol2	RNA-Polymerase II
Pol3	RNA-Polymerase III
PRAS40	Proline-Rich Akt substrate of 40 kDa
PTEN	Phosphatase and Tensin homolog
RA	Retinoic Acid

RAPTOR	Regulatory-Associated Protein of mTOR
RGC	Radial Glia Cell
RhA	Rheumatoid Arthritis
RHEB	Ras Homolog Enriched in Brain
RICTOR	Rapamycin Insensitive Companion of mTOR
RpS6	Ribosomal protein S6
RT-qPCR	Reverse Transcriptase-quantitative Polymerase Chain Reaction
S100B	S100 calcium-binding protein B
S6K1	Ribosomal Protein S6 Kinase beta-1
SAHA	Suberoyl Anilide Hydroxamic Acid
SDS-PAGE	Sodium Dodecyl Sulphate Polyacrylamide Gel Electrophoresis
SEGA	Subependymal Giant Cell Astrocytoma
SEN	Subependymal Nodule
SOCS3	Suppressor of Cytokine Signalling 3
SOX2	SRY-Box transcription factor 2
STAT3	Signal Transducer and Activator of Transcription 3
STING	Stimulator of Interferon Genes
SVZ	Subventricular Zone
TAE	Tris Acetic Acid EDTA buffer
TANDs	TSC-Associated Neuropsychiatric Disorders
TBK1	TANK Binding Kinase 1
TBR1	T-box brain protein 1
TLR	Toll-Like Receptor
TNF	Tumour Necrosis Factor
TSC	Tuberous Sclerosis Complex
VEGF	Vascular Endothelial Growth Factor

Chapter 1: Introduction

1.1 TSC and the mTOR complexes

1.1.1 Tuberous Sclerosis Complex

Tuberous sclerosis complex was first described in 1835 as a manifestation of facial angiofibromas. However, a description of the most prominent neurological manifestation (cortical tubers) coined the name “Tuberous Sclerosis”, which was made by Désiré-Magloire Bourneville in the 1880s (1). As such, the condition has sometimes been referred to as Bourneville’s disease. Research on the disease was slow to progress due to the rarity of TSC, which is now known to manifest at around 1 in 6,000 to 10,000 live births (2). TSC does not affect any particular race or sex at different frequencies (3,4). Alongside Bourneville, John James Pringle is also one of the earlier describers of the disease, drawing a correlation between several patients sharing similar traits in 1890, and (incorrectly) identifying the facial lesions as adenoma sebaceum (5). As such, by the early 1900s, correlations between the clinical manifestations of TSC were identified, meaning that TSC could now be diagnosed as a clinical triad of intellectual disability, epilepsy, and adenoma sebaceum (now known as angiofibromas) (6). The final name of “Tuberous Sclerosis Complex” was proposed by Sylvan E. Moolten in 1942, highlighting the multi-organ nature of the disease (7). Moolten also labelled the lesions as hamartomas (non-cancerous tumours).

In the late 20th century, the mutated proteins responsible for TSC were identified as hamartin and tuberin, encoded by the *TSC1* and *TSC2* genes, respectively (8,9). It was postulated that these proteins functioned as tumour suppressors. It is now known that hamartin and tuberin form a complex to function as a GTPase-activating protein (GAP). Here, hamartin stabilises tuberin, preventing degradation (10). In turn, the TSC1/TSC2 protein complex is then able to act as a GAP towards Ras homolog enriched in brain (RHEB), a small G-protein, thus inactivating it. Without the inhibitory activity of the TSC complex, RHEB functions as a positive regulator of mechanistic Target of Rapamycin Complex 1 (mTORC1) activation. Therefore, loss of either TSC proteins means that mTORC1 is hyperactive. RHEB is typically associated with the lysosome, where two molecules of RHEB interact with mTORC1, inducing a conformational change in mTOR, leading to mTORC1 activation (11). This leads to the excessive cell growth and subsequent formation of the hamartomas which are characteristic of TSC. TSC has been identified as an autosomal dominant negative disorder, wherein patients are heterozygous for either *TSC1* or *TSC2* since birth. The phenotypic

abnormality and tumour growth within TSC derives from a somatic second-hit mutation, as described in the Knudson's two-hit hypothesis (12). A germline mutation first occurs within either *TSC1* or *TSC2*, and tumour formation follows a somatic "second-hit" later in life. However, second-hit mutations to the *TSC1* or *TSC2* genes are not always required for tumour growth in TSC, as discussed in later sections.

An interesting characteristic of TSC is that it is both phenotypically and genetically heterogeneous. Mutations can occur within either the *TSC1* or *TSC2* genes, where *TSC2* mutations are more common and manifest more severely. Even within this subset of *TSC2*-deficient patients, there is heterogeneity, with varying severities of neurological and other symptoms (13,14). Of over 2000 known pathogenic variants within the *TSC1* and *TSC2* genes, 69-72% of these affect the *TSC2* gene versus 21-26% in *TSC1* (15), involving a range of mutation types on nearly all exons of the genes (16).

Tireless effort and research on TSC have now granted a more in-depth understanding of the genetic basis of the disease as well as elucidating effective treatments. A basic summary of the TSC disease and current treatments will now be described:

A loss of function mutation occurs *de novo* within either the *TSC1* or *TSC2* genes, or more rarely can be passed from the parent. This results in patients who are heterozygous for either *TSC1* or *TSC2*. During early development and subsequent life, somatic second-hit mutations occur on the remaining functional gene, conferring a loss of heterozygosity and thus resulting in *TSC1* or *TSC2* deficient cells. A loss of one protein effectively results in a loss of the other since each protein is required to stabilise the other within a TSC1/TSC2 complex, alongside a third protein known as TBC1D7 (17). Functionally, this heterotrimer complex serves to inhibit mTORC1 activity by reverting RHEB to an inactive GDP-bound form. Notably, the RHEB GAP domain of the TSC tumour suppressor complex is located on TSC2, while TSC1 typically functions to stabilise TSC2 (18). Under normal non-stimulated conditions, TSC1 and TSC2 form a complex to exert their inhibitory function. However, after growth factor stimulation through a receptor tyrosine kinase, or energy stimulation, or amino acid sensing, the TSC complex is inactivated. This occurs typically through either the AKT or Extracellular signal-Regulated Kinase (ERK) pathways, but also the Wnt and Tumour Necrosis Factor (TNF) pathway (19–21). For example, AKT can phosphorylate TSC2 on multiple residues, leading to sequestering of the protein away from RHEB and allowing subsequent mTORC1 activation (22,23).

This aberrant mTORC1 activity leads to systemic growth of hamartomas across every organ in the body, most notably the skin, central nervous system (CNS), heart lungs, eyes, and kidneys (24). As expected, these tumours cause complications within the resident organs, leading to complications such as renal disease, cardiac failure (although typically only in newborns), and disrupted lung function (particularly for predominantly female patients who also develop lymphangiomyomatosis (LAM)) (25). However, the leading cause of fatality within TSC, excluding LAM, is tumours of the CNS. These typically exist as three types: cortical tubers, subependymal nodules (SEN), and subependymal giant cell astrocytoma (SEGA). It is naturally assumed that the presence of these lesions is causative of the neurological symptoms of TSC, including autism, epilepsy, sleep disorders, and intellectual disability (26). TSC-related brain tumours arise early in development or shortly after birth, with infantile spasms arising at a mean age of 0.4 years, which will often progress to epilepsy at a rate of over 80% in TSC patients. Unfortunately, up to two-thirds of TSC patients present with refractory-epilepsy. A higher prevalence of seizures in TSC patients is often correlated with more severe TANDs (27).

LAM is a notable co-occurrent condition, presenting in between 29-49% of female patients, although it can also occur sporadically in a TSC-independent manner (28). The condition is characterised predominantly by the infiltration of smooth muscle-like cells to the lungs, leading to neoplastic growth and the destruction of lung tissue by newly formed cystic structures. As age increases, the occurrence of LAM in TSC patients also greatly increases by up to 81% (29). While the basic understanding of LAM has increased over the last few decades, the rate of mortality in TSC patients due to LAM is still significant (30). The origin of the tumour-forming LAM cells is still not understood, nor are the differences in prevalence between male and female patients. However, LAM cells express high levels of hormone (oestrogen and progesterone) receptors, hinting that female sex hormones play a significant role in the pathology of LAM (31,32). This is further supported by the fact that LAM symptoms increase during menopause, the menstrual cycle, pregnancy, or following the usage of the contraceptive pill (33).

The first line of treatment for TSC (and LAM) is rapamycin (Sirolimus) or Everolimus, which is prescribed upon diagnosis with either SEGAs, renal angiomyolipomas (AMLs), or epilepsy (34). Rapamycin is a naturally derived inhibitor of mTOR (35). As such, rapamycin specifically targets the dysregulated pathway within TSC and is effective in managing symptoms in the disease by shrinking tumours and reducing the prevalence of seizures

(although notably, seizures are not controlled in all cases of TSC treatment with rapamycin) (36,37). Furthermore, rapamycin tends to only shrink the tumours of TSC patients, not remove them completely (35). Due to the cytostatic nature of rapamycin on TSC cells, TSC-derived tumours will regrow upon discontinuation of the treatment. Further detail on the mTOR pathway as well as rapamycin and its analogues, commonly known as rapalogues (or rapalogs) will be described in later sections. Aside from rapamycin, other symptoms of TSC can be treated on a symptom-based basis. Vigabatrin, an anti-seizure medication, has proven to be effective in the treatment of seizures in TSC and is as such recommended as the primary means of seizure control for infantile spasms and epileptic seizures (38).

Seizures associated with TSC are just one of many neurological manifestations. TSC patients present with TANDs which include psychosocial, neuropsychological, intellectual, and behavioural manifestations (39,40). *TSC2* mutations result in worse neuropsychiatric manifestations than *TSC1* mutations (41). TANDs represent the greatest burden of disease in TSC patients, and while TANDs are experienced by over 90% of patients until recently, only 20% of patients received appropriate treatment. Accordingly, a TAND checklist was developed in 2015 that consolidates the different terms used to identify TANDs, while also providing a basis for tracking and evaluation of TANDs annually by professionals and caregivers (39).

While the discovery of the genetic basis of TSC has yielded significant progress in the treatment of the disease, predominantly with the identification of mTORC1 inhibitors as an effective treatment strategy, much is still unknown about the true pathology of TSC.

1.1.2 Additional TSC or mTORC1-regulated pathways

As discussed in the previous section, the pathology of TSC typically is ascribed to dysregulation of the mTORC1 pathway. *i.e.*, dysfunctional TSC1 or TSC2 leads to a lack of functional TSC complex, meaning that hyperactive mTORC1 subsequently drives cell growth and inhibits autophagy.

While mTORC1 is likely a key signalling pathway that drives TSC pathology, studies increasingly show that other signalling pathways may be involved. It is likely that TSC2/mTORC1 acts as a signalling nexus to various divergent cellular pathways that then contributes to the diverse patient phenotype exhibited in TSC. It is generally unclear how loss of *TSC1* or *TSC2* function may guide these phenotypes. We do not know if further pathway dysregulation is propagated through mTORC1 hyperactivity or rather non-characterised

functions of the TSC proteins. Furthermore, we do not know whether loss of heterozygosity is explicitly required for many of the symptoms experienced by TSC patients. Despite this lack of context, TSC research is continually identifying new potential therapeutic targets for the treatment of TSC. For example, a 2020 study identified that TSC-deficient neural cells exhibit a lower degree of ciliation which was mTORC1 inhibition insensitive. Inhibition of the heat shock pathway, specifically Hsp90, was able to restore cilia within these TSC-deficient cells, highlighting the heat-shock response as a druggable target in TSC (42).

Furthermore, TSC deficiency is known to influence inflammatory pathways. The Signal Transducer and Activator of Transcription (STAT) signalling pathways may be directly influenced by mTOR. Typically, the STAT pathways are activated in response to the detection of cytokines such as interleukins. As both the mTOR and STAT pathways are involved in immune responses and cellular growth/proliferation, it is unsurprising that the two pathways may exhibit signalling crosstalk. Specifically, a loss of either the TSC1 or TSC2 protein can lead to an increase in STAT3 phosphorylation (conferring activation), at both the tyrosine-705 and serine-727 phosphorylation sites (43,44). Furthermore, total STAT3 also appears to be upregulated by mTORC1 hyperactivity. While it is thought that the serine-727 site of STAT3 can be directly phosphorylated by mTORC1 (as a serine kinase), the mechanism behind the phosphorylation of STAT3 at tyrosine-705 by mTORC1 is not understood (45). Studies have shown that STAT3 and mTORC1 are intricately linked, however this linkage is cell-line dependent. In a rapamycin-sensitive bone cancer cell line, mTORC1 inhibition decreased Y705-STAT3 phosphorylation but not at serine-727. In a rapamycin insensitive cell line the opposite was true (46). Furthermore, the knockdown of STAT3 reversed the state of rapamycin insensitivity, suggesting that mTORC1 and STAT3 signalling crosstalk is relevant in maintaining cell viability. If this were applied to the context of TSC, we may postulate that the cytostatic nature of rapamycin may be derived from inflammatory pathway activation.

mTORC1 activity has also been shown to have links to the Nuclear Factor Kappa-light-chain-enhancer of activated B cells (NF- κ B) pathway, with rapamycin treatment inhibiting IKK activation in prostate cancer cells (47). Typically, NF- κ B activation in TSC is variable and poorly understood. One study found that siRNA targeting TSC2 led to an increase in NF- κ B activity (48), increasing the phosphorylation of I κ B Kinase (IKK) α/β and the NF- κ B subunit RelA. This increase in NF- κ B activity was likely propagated through mTORC1 hyperactivity. However, the study noted that the effect of TSC2 loss on NF- κ B activity was also likely dependent on the state of AKT activity, meaning that NF- κ B activation in TSC would likely

be variable across cell types. Most notably, Phosphatase and tensin homolog (PTEN) deficiency and subsequent AKT hyperactivation alongside TSC2 loss were required for an increase in NF- κ B activation. When PTEN was not lost in this model, TSC2 loss caused a reduction in NF- κ B activity instead. Another study also identified that increased NF- κ B activity was mediated by AKT hyperactivation by mTORC1 (47), with further research identifying an interesting link between mTORC1 inhibition and the impact on NF- κ B and STAT3 activation within *TSC2*-deficient immune cells (49). Notably, *TSC2* mutation resulted in a decrease of NF- κ B activity via mTORC1-dependent modulation of the transactivation domain in the NF- κ B subunit phospho-RelA. Inhibiting mTORC1 reversed this reduction in NF- κ B activity and caused subsequent NF- κ B hyperactivation. The ties to NF- κ B and TSC are further complicated by the identification that IKK β could phosphorylate TSC1, resulting in suppression of the TSC tumour suppressor complex and subsequent mTORC1 activation (21). Aside from these studies, research on direct links between NF- κ B and TSC is limited, and warrants further investigation.

Heterogeneity within the symptoms experienced by TSC patients may be explained through alternative or unknown functions of TSC protein. This could in part be evidenced by the vast difference in the severity of disease experienced by patients with mutations in *TSC1* compared to those with mutations in *TSC2*, wherein *TSC2* mutation is more common and typically presents with more severe symptoms (34). The classical explanation of TSC pathology may suggest that since *TSC1* expression is required primarily for the stability of TSC2 protein stability and activity, a loss of either gene would confer a highly similar phenotype, but this is not the case. The heterogeneity of TSC symptom expression will additionally be defined by which organs are affected, but also by the type of mutation. For example, while *TSC1* is typically inactivated through frame shift or nonsense mutations (and therefore the mutation generates a totally inactivated protein), *TSC2* mutations are typically frame-shift, missense, and splice-site mutations (50). It is currently unclear how these different mutations may confer the broad range of symptom severity experienced by TSC patients.

The role of loss of heterozygosity as a confounding factor in the disease phenotype may have been overstated. While the loss of heterozygosity is generally associated with the formation of the larger, more obvious lesions within TSC-derived brain tumours, *in vitro* studies have identified that mono-allelic mutations to *TSC1/TSC2* are also capable of inducing brain abnormalities.

A study by Martin *et al.* detailed how TSC-linked brain lesions tend to demonstrate a lesser degree of biallelic inactivation (when compared to the lesions within other organs) (51). Specifically, less than 35% of cortical tubers appear to possess a loss of heterozygosity. As the presence of brain lesions correlates with increased severity of TANDs, this information suggests that mono-allelic inactivation is sufficient for the development of the neurological manifestations of TSC (52). However, mouse studies suggest that neurological manifestations of TSC are not dependent on the presence of cortical tubers (53). Rather, TANDs may instead manifest from microstructural changes in the brain, such as decreased myelination complexity, or astrocytic changes (54).

Another study found that mono-allelic mutations to *TSC2* within a human induced pluripotent stem cell (iPSC) model were sufficient to promote dysregulation of a variety of pathways within Purkinje cells, including modification to differentiation status, activation of autophagy, oxidative stress, and cell death (55). Alongside this, mTORC1 activation was increased within *TSC2*^(+/-) neuronal cells, with mTORC1 inhibition seeming to partially reverse the dysregulated neuronal phenotype. Interestingly, differences in mTORC1 activation within *TSC2*^(+/-) cells and wild-type only seem to occur slightly later in neurodifferentiation, demonstrating the importance of the stage of neural development in TSC pathology. mTORC1 hyperactivation within *Tsc2*^(+/-) mice also demonstrated variations in brain regions, showing the importance of cell type in the neuropathology of TSC (54). It has been known since relatively early in TSC research that a loss of heterozygosity is not altogether necessary for tumour growth and brain abnormalities within TSC (56–58). While not explicitly highlighting a specific alternative pathway in which TSC1 or TSC2 proteins might play a role in, these studies do highlight that the neurological manifestations of TSC are not dependent entirely on loss of heterozygosity, with a study in 1996 suggesting that only 6% of TSC-derived brain tumours exhibited biallelic inactivation of TSC1 or TSC2 (59). A later, broader study identified that biallelic mutation was only present in roughly one-third of cortical tubers (51).

Another study identified that heterozygosity is capable of inducing the formation of abnormal retinogeniculate projections within *Tsc2*^(+/-) mice, likely caused by *TSC2*-linkage to the function of erythropoietin-producing human hepatocellular-A (EphA) receptors (60). This was further validated by *in vitro* data which demonstrated that *Tsc2*^(+/-) neuronal cells exhibited less sensitivity to EphA receptor signalling, thus desensitizing *Tsc2* haploinsufficient cells to EphA mediated cytoskeletal rearrangements, and therefore neuron axonal guidance.

Interestingly, *TSC2* may also regulate transcription directly, and has been shown to bind to the promoter of epiregulin (61). Therefore, loss of *TSC2* promotes heightened levels of epiregulin in TSC patients which promotes cell proliferation.

Overall, *TSC2* is involved in more pathways than the typically ascribed activation of mTORC1. The broad range of symptom severity that TSC patients experience may be indicative of this and could be dependent on the poorly understood role of monoallelic inactivation of *TSC2*.

1.1.3 The mTOR complexes

Both mTORC1 and mTORC2 possess the mTOR catalytic subunit; a serine/threonine kinase of the Phosphoinositide 3-Kinase (PI3K)-related kinase family. Despite this similarity, their activation and cell signalling outcomes are distinct. TSC research primarily focuses on mTORC1 signalling, and as such, it is far better understood. The reasoning for this is relatively clear; the TSC tumour suppressor complex (and the resultant downstream effects on RHEB) govern mTORC1, but not mTORC2 activity.

1.1.3.1 mTORC1

The outcomes of mTORC1 signalling have been briefly described in section 1.1.1, however, this was mainly described in the context of *TSC2* or *TSC1* loss. A more detailed summary of mTORC1 and mTORC1 signalling outcomes will be provided here.

mTORC1 and mTORC2 both possess mTOR, DEP domain containing mTOR interacting protein (DEPTOR) and mammalian Lethal with SEC13 protein 8 (mLST8). Aside from their cell signalling outcomes, mTORC1 and mTORC2 can be distinguished by their responsiveness to rapamycin; mTORC1 is rapamycin sensitive, whereas mTORC2 requires long-term rapamycin treatment to reduce activity (62).

mTORC1 is composed of mTOR, mLST8, DEPTOR, and Regulatory-Associated Protein of mTOR (RAPTOR). While mTOR is the catalytic core of the mTORC1 complex, additional components are necessary for proper kinase activity (63). mTORC1 substrates possess a TOR signalling motif that is recognised by RAPTOR and allows the association of the mTORC1 complex to promote kinase activity (64). mLST8 is believed to associate with the complex to stabilise the active substrate-binding domain of mTORC1 (65). Conversely, Proline-Rich Akt Substrate of 40 kDa (PRAS40) is believed to be an endogenous inhibitor of mTORC1 activity, and associates with mTORC1 via RAPTOR to inhibit substrate binding (66).

DEPTOR is also a negative regulator of mTORC1 (67). mTORC1 functions to integrate growth factors, amino acids, and energy levels into pro-growth signalling. The overall outcome of activation of the mTORC1 pathway is typically regarded as an increase in cellular metabolism, inhibition of autophagy, and an increase in cellular growth (68).

Since mTORC1 possesses serine/threonine kinase activity (69), mTORC1 activation results in the phosphorylation of various downstream regulators that ultimately result in the known effects of mTORC1 pathway activation. Two of the key targets of mTORC1 are Ribosomal Protein S6 Kinase beta-1 (S6K1) and 4E-Binding Protein 1 (4E-BP1). Protein synthesis is initiated by the phosphorylation of 4E-BP1 by mTORC1. 4E-BP1 suppresses mRNA translation by binding to eukaryotic Translation Initiation Factor 4E (eIF4E) at the 5'-ends of mRNA awaiting translation and possesses 7 phosphorylation sites in humans (70). Four of these are regarded as key for activity, with phosphorylation of Thr37/Thr46 priming the protein for further phosphorylation at Ser65/Thr70 (71). Phosphorylation of 4E-BP1 leads to the dissociation of 4E-BP1 from eIF4E, allowing the recruitment of eIF4G and the ribosomal 40s subunit to progress with protein translation (68). Another mTORC1 substrate is S6K1. S6K1 is a serine/threonine kinase, and upon activation by mTORC1 can phosphorylate a variety of translation-promoting proteins (72). This includes the ribosomal protein S6 (rpS6) on the Ser235/Ser236 sites. Phosphorylation of rpS6, while regarded as a key marker of mTORC1 activity, is relatively poorly understood. However, as a component of the 40s ribosomal subunit, rpS6 phosphorylation is believed to enhance the translation of proteins with AU-rich proximal untranslated region sequences, such as IL-8 and TNFAIP6 (73). S6K1 can also phosphorylate eIF4B to promote the helicase activity of eIF4A, allowing the translation of mRNA secondary structures that which would otherwise inhibit translation (74). To further enhance protein translation, mTORC1 and S6K1 can phosphorylate the recently discovered protein La-Related Protein 1 (LARP1), causing the dissociation of LARP1 from the translation initiation complex (75). Dissociation of LARP1 allows the recruitment of eIF4F, and this promotes the translation of mRNAs containing a 5'-terminal oligopyrimidine sequence (76). These sequences are typically associated with mRNAs encoding ribosomal proteins, meaning that LARP1 inhibition by mTORC1 promotes the generation of protein assembly cellular machinery.

mTORC1 also promotes nucleic acid synthesis via poorly understood positive regulation of RNA polymerases. It has been shown that mTORC1 can regulate RNA-polymerase-I, II, and III (Pol1, Pol2, and Pol3, respectively). mTORC1 can phosphorylate TIF1A, which is

responsible for the co-activation of Pol1 (77). This would promote Pol1-dependent production of rDNA, leading to ribosomal biogenesis. Strangely, while mTORC1 is characteristically believed to associate with the lysosome, mTORC1 may also be found within other sub-cellular compartments, including the nucleus (78). While all components of mTORC1 can be found within the nucleus, it is generally believed that they do not associate to form the full mTORC1 complex (79), and instead, nuclear mTOR may be responsible for much of the poorly characterised nuclear mTOR activity. It is believed that in this case, nuclear mTOR plays a role in transcriptional regulation via promoter binding (78). Nuclear mTOR may play a role in Pol2 activity in this way by enhancement of Pol2-regulated transcription (80). Within the nucleus, mTOR has also been shown to bind to the promoters of rDNA and tRNA genes in a rapamycin-sensitive manner, suggesting that mTOR may be able to promote RNA polymerase-I and RNA polymerase-III-mediated transcription by a poorly defined mechanism (81). This may occur by phosphorylating other recruited factors to the transcriptional machinery of the RNA polymerases. Altogether, mTORC1/mTOR-dependent upregulation RNA polymerase activity would assist in the generation of building blocks for cellular growth.

mTORC1 can also modulate the activity of various transcription factors. Most relevant to the following thesis is the phosphorylation of STAT3 on the S727 residue. mTORC1-dependent phosphorylation of S727-STAT3 likely contributes to the overall activity of STAT3, working in tandem with the inflammatory-associate Y705 phosphorylation site of STAT3 (82). The review by Giguère (2018) (83) effectively outlines a broad range of transcription factors that are regulated by mTORC1, including HIF1 α , NRF1, STAT3, and UBF. mTORC1-dependent regulation of these transcription factors directs a variety of cellular processes including angiogenesis, metabolism, and cell growth/proliferation. mTORC1 activity also can guide inflammatory processes. mTORC1 inhibition has been shown to dampen immune responses and reduce IL-8 and IL-1 β levels, highlighting the importance of this pathway in propagating inflammatory signalling (84). As such, rapamycin is a potent immune inhibitor, functioning to inhibit cytokine-stimulated differentiation and activation of various immune cells (85,86).

1.1.3.2 mTORC2

As previously described, mTORC2 shares the mTOR, DEPTOR and mLST8 subunits, but is functionally distinct from mTORC1. As in mTORC1, mLST8 is essential for proper mTORC2 function, mTOR is the central catalytic component (87), and DEPTOR functions as

an endogenous inhibitor (67). mTORC2 is also composed of Rapamycin Insensitive Companion of mTOR (RICTOR), mammalian stress-activated protein kinase-interacting protein 1 (mSIN1), and protein observed with RICTOR (Protor-1) (88). RICTOR functions as a scaffolding protein and promotes mTORC2 function, and is believed to be the reason for the insensitivity of mTORC2 to rapamycin; rapamycin binding is mediated through the interaction of RAPTOR to mTOR, preventing mTORC1-substrate binding (89). mSIN1 stabilises RICTOR, and together are essential for the kinase activity of mTORC2 on AKT (90,91). The function of Protor-1 is poorly understood and not believed to be essential for mTORC2 activity. However, it is believed to assist in the phosphorylation of SGK1 (92).

The functional role of mTORC2 is less well-characterised than that of mTORC1. mTORC2 is typically localised to the ribosome, and mTORC2 activity is stimulated through growth factors and is activated downstream of PI3K/AKT (93). One role that mTORC2 plays is within the AKT pathway, wherein mTORC2 can phosphorylate AKT (alongside PDK1) for the activation of AKT (94). mTORC2 can stabilise the structure and enhance the function of AKT by phosphorylating an additional distinct residue at synthesis of AKT (95). mTORC2 also phosphorylates SGK1 and PKC, with the ultimate cell signalling outcome conferring actin cytoskeletal reorganisation, cell migration, and an increase in protein synthesis and metabolism (96). As mTORC2 is capable of altering cell metabolism, mTORC2 dysregulation could be implicated in various cancers (97).

mTORC2 is typically regarded as rapamycin insensitive. The activity of mTORC2 is not directly regulated by rapamycin. However, prolonged rapamycin treatment can reduce mTORC2 activity. This process is not entirely understood, and not all mTORC2 hyperactive cells can be targeted with rapamycin (98). It is believed that rapamycin may interfere with mTORC2 complex assembly (62), but this is dependent on a high FK506 Binding Protein 12 (FKBP12) expression (98).

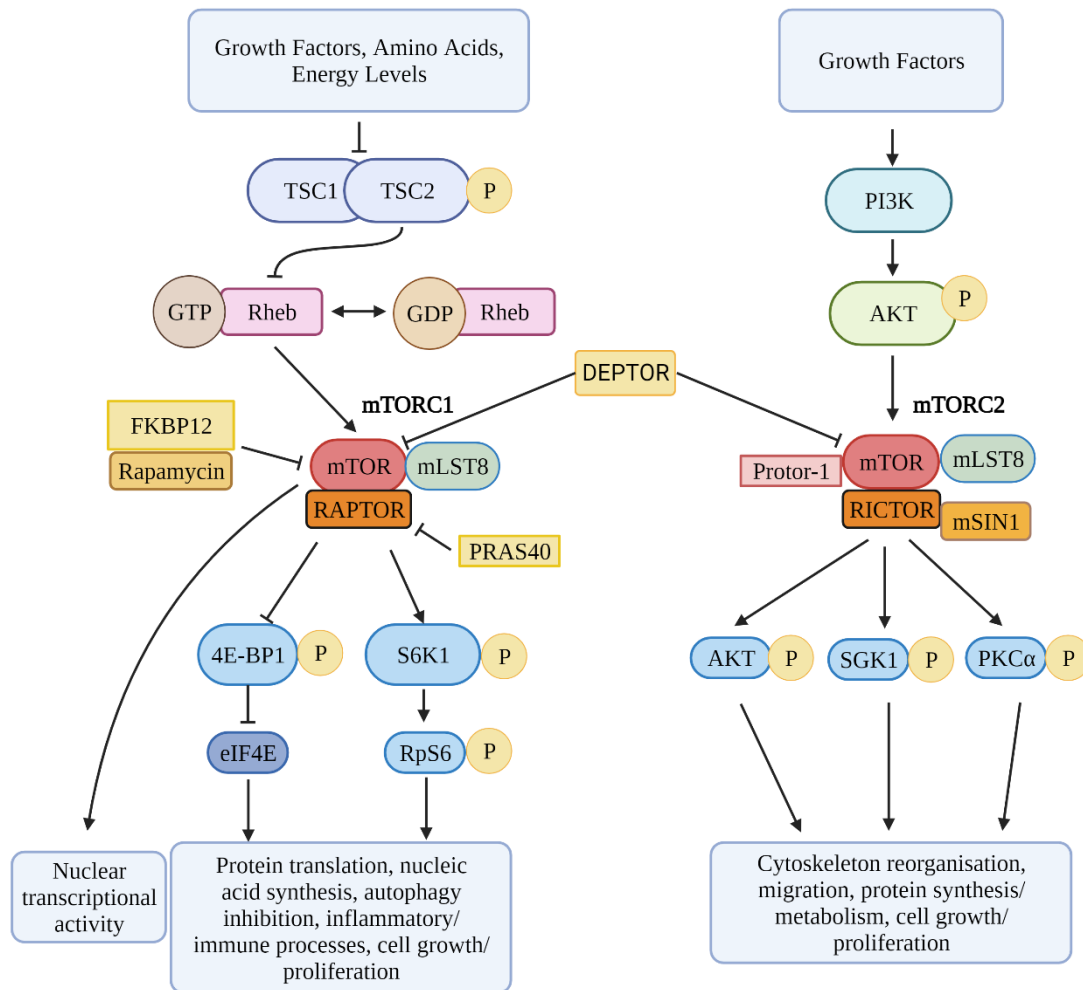


Figure 1.1. Diagram of mTORC1 and mTORC2 signalling. mTORC1 signalling (left) is activated by growth factors, amino acids, and energy levels. TSC1/TSC2 act as a tumour suppressor complex via the GTPase activating domain of TSC2. Pathway activation results in the phosphorylation and dissociation of TSC2. Growth factor stimulation also activates mTORC2 downstream of PI3K (right). The mTORC1 complex is composed of mTOR, mLST8, and RAPTOR. PRAS40 functions as an endogenous inhibitor of mTORC1. mTORC2 is composed of mTOR, RICTOR, mLST8, mSIN1, and Protor-1. Both mTORC1 and mTORC2 share DEPTOR as an endogenous inhibitor. Rapamycin inhibits mTORC1 via association with FKBP12. mTORC1 and mTORC2 activity result in distinct cell signalling outcomes. Illustration produced in BioRender.

1.1.4 Current drug treatments of TSC

While earlier treatments may be beneficial in reducing the severity of neurological manifestations (99), TSC is typically treated symptomatically. This is typically done with a range of licensed drugs or surgery. Non-pharmacological or non-surgical treatments can be taken too, including a ketogenic diet (which is believed to reduce seizures via a reduction in mTORC1 activity (100)) and vagus nerve stimulation (101).

1.1.4.1 Rapamycin (Sirolimus) and rapalogues

In 1964, in an attempt to identify new antimicrobial compounds, Georges Nogrady obtained soil samples from Rapa Nui, also known as Easter Island. *Streptomyces hydroscopicus* was discovered within this soil and found to be producing a molecule with antifungal properties. This macrolide molecule named after the island was called rapamycin (102). In 1999, rapamycin, renamed as Sirolimus, was approved for use as an immunosuppressant (FDA application 021083). Following the identification of the genetic pathology of TSC, Everolimus, a rapamycin analogue with an attached ethyl ester group, was approved for the treatment of TSC-associated SEGA in 2010 (103). Sirolimus and Everolimus have also been demonstrated to have limited applicability for the treatment of seizures in TSC (103,104). The benefit of rapamycin in LAM was also investigated and was shown to have potential benefit in the treatment of the TSC-associated disease (105). Following a clinical trial, rapamycin was also approved for the treatment of LAM in 2015 (NCT02432560). Rapamycin was also effective at reducing the size of TSC-derived kidney AMLs (106). Despite being one of the primary methods of treatment for TSC, Everolimus and Sirolimus are not without drawbacks. Rapamycin is relatively safe but known to present with mild side effects such as an increased likelihood of infection (107) due to immunosuppressive properties. Perhaps unsurprisingly, Everolimus has proved ineffective at improving neurocognitive function in children with TSC over 6 or 12 months (108,109). An ongoing study is attempting to assess the impact of Everolimus on neurocognitive function and autism (NCT01730209). Refractory epilepsy occurs in roughly 45% of TSC patients, and Everolimus is effective at reducing epilepsy in around half of these cases (110). Of course, Everolimus is highly beneficial in this regard but demonstrates that mTORC1 inhibition alone cannot effectively manage neuropsychiatric disorders in TSC. This is especially prudent when epilepsy is highlighted as such a high cause of mortality in TSC (111), whilst also being highly treatment-resistant (112). Additionally, despite the apparent benefits of rapamycin and Everolimus, tumour regrowth occurs after discontinuation of treatment, highlighting the cytostatic nature of these treatments (113). Further analogues of rapamycin, dubbed ‘rapalogues’, are in the process of investigation for clinical use in TSC and various cancers (114). However, Everolimus is the only approved drug for the management of SEGA and AML (115). Second-generation mTOR inhibitors, which bind directly to the mTOR catalytic site, are also in development (115). It could be argued that these may lack enhanced efficacy in TSC compared to conventional rapalogues, as mTORC2 activity may be downregulated in TSC (116). Recently, a topical gel of

Sirolimus demonstrated applicability for use on facial skin lesions in TSC (117) (NCT02635789).

In terms of biological activity, Everolimus is more effective than rapamycin but also more expensive (118). The difference in biological activity may be attributed to the greater efficacy in reducing mTORC2 signalling by Everolimus (119). However, some differences in biological activity may also be attributed to overall differences between the two compounds in bioavailability and pharmacokinetics (119). Rapamycin and Everolimus function by initially binding to FKBP12. FKBP12 then binds to mTOR by the FKBP-Rapamycin Binding (FKB) domain. Interaction of FKBP12-Rapamycin with the FKB domain results in the dissociation of RAPTOR, thus inhibiting mTORC1 activity (89).

1.1.4.2 Vigabatrin

Infantile spasms typically occur as a precursor to epilepsy in TSC, and Vigabatrin is currently recommended for the treatment of infantile spasms in TSC (13,38). Vigabatrin functions by mimicking the inhibitory neurotransmitter Gamma-Aminobutyric Acid (GABA). By doing this, Vigabatrin competes with the GABA breakdown enzyme, GABA transaminase, resulting in increased levels of GABA in the synaptic cleft (120). Vigabatrin is not able to reduce epilepsy in all TSC patients, with one study reporting a reduction in seizures with 13 patients, and a lack of efficacy leading to treatment discontinuation in 21 patients (121). Additionally, Vigabatrin demonstrates retinal toxicity, leading to a loss of peripheral visual field over prolonged treatment periods. This means that visual ability must be continuously assessed during treatment (122). Other side effects of Vigabatrin include memory loss, depression, drowsiness, confusion, and diarrhoea. Vigabatrin side effects are prevalent in up to 50% of adults, and 15-31% in infants/children (123). Therefore, while Vigabatrin shows excellent efficacy in the management of TSC-associated seizures, side effects of the drug must be considered. Patients will often discontinue Vigabatrin treatment, and this is believed to be due to the development of tolerance to Vigabatrin, reducing the efficacy of the drug (124). Similar to tumour regrowth after cessation of mTORC1 inhibitors, seizures will often reoccur after a discontinuation of Vigabatrin (125). Despite these setbacks, Vigabatrin is effective in reducing seizures in many cases, and as such, is the first-line treatment for TSC-associated infantile spasms. Data are mixed on the need to continue Vigabatrin treatment after seizure reduction. In some cases, Vigabatrin can be withdrawn after a seizure-free period of 6 months, while other data suggests that seizures can reoccur if treatment is rescinded (126).

1.1.4.3 Surgery

In the case of TSC-associated brain tumours, surgery can be employed as a treatment option. It is typically relatively effective in the reduction of seizures, providing that there is correct identification and resection of the epileptogenic region of the brain. One analysis reported seizure freedom in patients with refractory epilepsy between 48-57 % over a follow-up period (127), while another reported a reduction in 51 % of surgery-treated patients (128). While surgery can be highly effective in achieving seizure freedom in TSC patients, it is a highly invasive procedure, and it therefore could be argued that the roughly 51 % seizure freedom rate makes surgery a last-resort option in the treatment of epilepsy in TSC. Many patients are also unable to undergo surgery due to deeply residing epileptogenic regions in TSC patients. However, new surgery techniques such as MRI-guided laser therapy may offer highly effective means of therapy in the future (129,130).

1.1.4.4 Cannabidiol

The mechanism of cannabidiol (CBD) on seizure reduction and the anti-inflammatory properties of CBD are, in general, poorly understood. GPR55 is a cannabinoid-sensitive receptor which typically increases neurotransmitter and calcium release during neurotransmission (131). The broadest understanding of CBD action appears to be that CBD can reduce neuronal excitability by antagonizing GPR55 at excitatory synapses, as well as lowering calcium and adenosine uptake, thus reducing neurotransmission (132,133). CBD also has anti-inflammatory and anti-oxidative properties, able to reduce the production of TNF α and other cytokines (134). The anti-cancer effects of CBD have had an increase in research recently (135). CBD induces damaging oxidative stress in glioma cells but not healthy control cells (136). CBD increases oxidative stress in breast cancer and also inhibits mTORC1 signalling (137). CBD has shown benefits in the treatment of various cancers, including melanoma, glioblastoma, and breast, prostate, lung, and colon cancer (138,139).

When CBD is employed in combination with rapamycin or Everolimus, there appear to be drug interactions between the two in TSC, demonstrating that care needs to be taken when prescribing both medications for TSC patients. Specifically, CBD appeared to increase the overall concentration of Everolimus within the blood of one patient when both treatments were taken (140). This was demonstrated to be more significant when 25 patients were tested, wherein CBD increased the blood trough concentrations of either rapamycin or Everolimus to dangerous levels (141). Because of this, mTOR inhibitor therapies need to be adjusted

accordingly when taken in combination with CBD. CBD has also shown drug interactions with other medications in the treatment of seizures, including clobazam (an epilepsy drug), wherein clobazam was elevated in patients who were also taking CBD (142). Another study reported increases in serum levels of topiramate, rufinamide, and N-desmethyclobazam (all common antiepileptic drugs) when administered alongside CBD (143). It is possible that these interactions occur due to competition between CBD and other drugs for metabolism in the cytochrome P450 pathway. Overall, CBD has proven to be highly effective at reducing the prevalence of treatment-resistant seizures (144–146). Following a clinical trial by Jazz Pharmaceuticals (NCT02544763) wherein CBD was shown to be effective and well-tolerated, CBD has been approved for the treatment of seizures in TSC (147).

1.1.4.5 Future Therapies

As outlined in the review by Schubert-Bast and Strzelczyk (2021), a range of therapies are currently being explored for the treatment of epilepsy in TSC (148). A phase III trial recently concluded for Ganaxolone (NCT03572933), demonstrating applicability in refractory epilepsy in TSC. The 2021 review outlines multiple potential therapies which are being typically researched for usage in other seizure-causing conditions but suggests that many of these treatments could have impacts on TSC. These include the CH24H inhibitor, Soticlestat, and the serotonergic drug, Fenfluramine. A novel formulation of Sirolimus is also being investigated for the treatment of epilepsy in infants with TSC (NCT04595513).

1.1.5 mTOR in Brain Tumours

mTOR acts as the central catalytic component within two distinct protein complexes, mTORC1 and mTORC2, and possesses serine/threonine kinase activity (149,150). mTORC1 activity is induced by cellular energy, oxygen, nutrient levels, and growth factors, and transduces these signals into cellular growth and metabolism via increased ribosomal biogenesis, protein synthesis, and the inhibition of autophagy (151,152).

As such a central component of cellular growth, it is unsurprising that cancer will often hijack mTOR to guide its growth, with mutations in upstream signalling pathways often converging on mTORC1 to guide oncogenesis (153). As a disease, TSC demonstrates the profound impact of TSC1/TSC2 mutations on tumour formation, and therefore the key role that mTORC1 dysregulation may play in cancer progression.

Loss of *TSC2* is implicated in various brain tumours. One study reported that loss of heterozygosity of *TSC2* was found in 1/16 astrocytomas, 3/15 ependymomas, 5/16 gangliogliomas, 0/7 oligodendrogliomas (OG), and 2/14 glioblastoma multiforme (GBM) (154). While mTOR activity can drive the development and pathology of cancerous brain tumours, *TSC2* is rarely the causative mutation. Regardless, it can be beneficial to look at the role of mTORC1 activity within malignant brain tumours to hopefully identify parallels between cancer and TSC. Despite a clear profile of *TSC2* mutations in malignant brain tumours, *TSC2* mutations (or otherwise lowered expression of *TSC2*) has been observed in various other cancer types, including breast cancer, oral squamous cell carcinoma, and renal cell carcinoma (155,156). Cancer patients with mutations of *TSC1*, *TSC2*, or *MTOR* seem to show greater response rates to rapalogues (156).

1.1.5.1 Glioma and Glioblastoma Multiforme

While playing an important role in normal brain development and neurogenesis, aberrant mTORC1 activation has a correspondence with various brain tumours and is involved in multiple facets of cancer progression (157). Gliomas are brain tumours of the supportive glial cells that can progress to GBM which is among the deadliest types of cancer (158); the 5-year survival rate of GBM is below 5%. Furthermore, the survival of GBM has shown little increase over the past few decades of research (159). GBM usually arises from a primary glioma. It is generally believed that they are astrocytic in origin, but newer research points towards mutations in neural epithelial cells (NECs) and glial-committed precursor cells, which then become dysregulated astrocytes (160). GBM often have a high activation of mTORC1 (161), resulting in greater unc-51 like autophagy activating kinase 1 (ULK1) inhibition and protein translation via 4E-BP1 (162). Notably, inhibition of mTORC1 in this scenario does not always produce the desired therapeutic goal, as mTORC1 inhibition can lead to resistance to hypoxia-induced cell death (162,163). It is believed that this is due to the activation of autophagy which serves to protect the cells in nutrient and oxygen-starved conditions. High mTORC1/mTORC2 activity has also been observed in low-grade glioma, including pilocytic astrocytoma (164).

mTORC1 activity in GBM is often conferred through loss of PTEN, leading to increased AKT activity and consequently high mTORC1 activity (150). The levels of S6K1 and AKT phosphorylation are clinically correlated with radiation resistance in treatment (165). There is also a correlation between AKT, Nuclear Factor Kappa-light-chain-enhancer of activated B

cells (NF- κ B) activity, and tumour grade in GBM (166). Overall, high-grade gliomas tend to demonstrate higher AKT, mTOR, and S6K1 phosphorylation when compared to low-grade non-invasive gliomas, demonstrating the disease-progressing nature of mTORC1 signalling (167,168). mTORC1 can also be activated within tumour-associated microglia via secreted signals from glioblastoma; mTORC1 activity in microglia reduces T-cell infiltration and reduces reactivity, aiding in tumour immune evasion (169). Within this context, mTORC1 activity promotes STAT3-mediated secretion of anti-inflammatory factors also, limiting T-cell infiltration. mTORC1/mTORC2 activity is also shown to progress GBM by activating the Wnt pathway, leading to the promoted transcription of pro-invasive factors and guiding Epithelial to Mesenchymal Transition (EMT) (170).

Similarly, mTORC2 activity is upregulated within glioma (171). mTORC2 has been shown to play a role in glioma formation, where heightened protein and mRNA levels of the mTORC2 complex component, RICTOR, have been found. RICTOR overexpression leads to increased mTORC2 activity, and consequently higher AKT phosphorylation (171). mTORC2 guides GBM towards aerobic glycolysis by increasing the expression of glucose transporter 4, and activating hexokinase 2 and phosphofructokinase-1 (150), thus promoting a Warburg effect. mTORC2 activity also has implications with chemoresistance, and treatment with a mTOR inhibitor (called PP242) sensitized chemo-resistant GBM to cisplatin-induced cell death (172).

Overall, first-generation mTORC1 inhibitors were ineffectual in the treatment of GBM, largely due to limited pharmacodynamics and an inability to suitably target mTORC2 (150). Newer therapies with dual mTOR kinase inhibitory activity such as Ku-0063794 may prove more effective by more potently inhibiting AKT activity (173). The immunosuppressive properties of first-generation mTOR inhibitors are a concern in the treatment of GBM. However, newer dual kinase inhibitors such as PP242 appear more effective at suppressing mTOR activity with reduced inhibition on the immune system (174). These studies generally highlight the prevalent role of mTORC2 in GBM, as well as mTORC1. It is generally accepted that sirolimus (and other rapalogues such as everolimus and temsirolimus) can cross the blood brain barrier (BBB) (175,176). While first generation mTOR inhibitors showed limited penetration of the BBB, second generation mTOR inhibitors (such as Ku-0063794) appear to penetrate the brain more effectively (177).

OG are a type of glioma brain tumour which were initially believed to arise from mature oligodendrocytes; the myelin-producing supportive cells of the brain. However, recent research indicates that OGs are more likely to develop from glial precursors which then differentiate to oligodendrocyte-like cells with non-functional myelination capability (178,179). Compared to GBM, OGs are far less common, making up roughly 5% of CNS tumours (180). OGs are also far less deadly, with a 5-year survival rate of roughly 50.2% for high-grade OG (181). Research of mTOR signalling within OG is relatively low, likely due to the relative infrequency of the condition, and the comparatively favourable prognosis compared to other brain tumours. The role of mTOR signalling in OG was revealed by the finding that PI3K/AKT/mTOR activity was necessary for the successful engrafting of OG xenografts in mice (182). A lack of PI3K/AKT/mTOR activity prevented xenograft formation. Implanted xenografts were also sensitive to mTOR inhibition with Everolimus. Overall, this demonstrated that PI3K/AKT/mTOR was able to promote oncogenesis.

Ependymomas are a rare type of glioma which typically occurs in the ependymal lining of the ventricular system. Due to their often subependymal nature, ependymomas can obstruct the flow of cerebrospinal fluid (CSF), leading to hydrocephalus (183); a feature shared by TSC-derived SEGA, discussed later. While ependymomas affect children more frequently than adults, children aged 10 to 14 years have a 5-year survival rate of 81.4% (184,185). A study found that a patient with a childhood ependymoma demonstrated high activation of mTORC1 (186). In this study, the patient's tumour was highly susceptible to Sirolimus for 18 months. mTORC1 inhibition also suppressed ependymoma xenograft growth in mouse studies (187). mTORC1 inhibitors have been evaluated for the treatment of ependymomas. However, a recent clinical trial (NCT02155920) (188) showed that Everolimus for up to 2 years did not appear to be effective in treating recurrent or highly progressive subtypes of ependymoma in children. Notably, this study was carried out in the most aggressive and treatment-resistant subtype of ependymoma, meaning that mTORC1 inhibition may prove beneficial in other, less aggressive subtypes. It has also been suggested that ganglioglioma can gain enhanced growth from mTORC1 activation (189). Epilepsy is a common symptom of gangliogliomas (190), demonstrating parallels between this low-grade rare brain tumour and TSC. Generally, gangliogliomas do not usually possess mutations within components of the mTORC1 pathway. A sequencing experiment of 40 gangliogliomas revealed no mutations to *TSC1*, *TSC2*, *AKT3*, *MTOR*, *PI3KCA*, or *PTEN*, except for one *PTEN* mutation (190). mTORC1

activity is also present in neuroblastoma, with potential cytostatic and cytotoxic benefits shown via inhibition of the AKT/mTORC1 signalling nexus (191).

1.1.5.2 Malignancy in TSC

It might be expected that due to a large number of benign tumours in TSC patients, there would be an increased risk of the development of cancerous tumours. However, this does not appear to be the case. In terms of renal tumours, the lifetime risk of the development of malignant renal tumours is only around 2-3 % (192). This is not different from the risk of renal cancer in non-TSC patients, according to Cancer Research UK (193). Despite this, cases of malignancy in TSC have been observed. One example of this was the development of GBM in a 58-year-old male TSC patient. However, it should be noted that this tumour did not appear to arise from any previous TSC-derived tumours (194). The same case report by Azriel *et al.* (2019) details how malignant brain tumours in TSC have only been reported within six patients, none of which presented with a SEGA at the previous site of glioma/GBM development. TSC contrasts with cancerous tumour development in the sense that most malignant tumours are believed to initiate follow mutations to *TP53*

1.2 Inflammation and the Immune System in Brain Tumours

1.2.1 Neuroinflammation and the immune system of the CNS

The inflammatory response is an essential mechanism which is triggered by various stimuli, including infection, trauma, toxins, or cell damage/stress. An acute inflammatory response is necessary to reduce damage and begin healing and repair, and will self-regulate to switch itself off (195). However, loss of control over an acute inflammatory signal leads to chronic inflammation. Chronic inflammation is implicated in a wide array of diseases, including cancer (196). Inflammation involves the activation of signalling pathways which result in the recruitment and accumulation of immune cells, as well as increased blood flow to the affected area.

The CNS is an immune privileged site. Typically, cells of the immune system which are present within the rest of the body are not permitted within the CNS. As outlined in the review by Muldoon *et al.*, (2013) (197), the Blood Brain Barrier was identified following the observation that immune responses in the peripheral immune system were not apparent within the CNS. Overall, the blood brain barrier can be most broadly defined as a tight network of endothelial cells with tight junctions lining the capillaries, with a selection of

highly specific transport channels (198). The result is a protective layer which separates circulating blood from the highly regulated CSF to maintain homeostasis. Antibodies and circulating immune cells have limited penetration of the BBB (199).

Typically, leukocytes will not cross the BBB and instead will reside near the BBB to capture antigens. Certain inflammatory cytokines are known to cross the BBB, stimulating inflammation and immune responses within the CNS, such as IL-6 and TNF α . Cytokines can also damage the BBB, increasing their permeability to immune cells and other molecules (200). Therefore, under conditions of injury, infection, or otherwise inflammation, the BBB can be compromised to allow the influx of non-typically residing cells and molecules to the CNS.

Under normal conditions the microglia are the primary immune mediators of the CNS. Rather than just fighting infection and mediating inflammatory signals, microglia interact with neurons and other CNS-resident cells to regulate synaptic plasticity, synapse maturation, myelination, neuron survival, and differentiation of supporting cells (201). As outlined in the review by Li & Barres (2018) (202), microglia play a variety of roles during neurodevelopment, and also maintain homeostasis in later life. It is thought that microglia can attenuate the activity of highly-active neurons via contact (203).

Microglia go through a range of activation states. During normal, non-stimulated/non-inflammatory conditions they are involved in the maintenance of synapses and neurons through the secretion of factors such as Brain Derived Neurotrophic Factor (BDNF) (204,205). When stimulated by injury, inflammation, or infection, microglia are activated. This is mainly characterised by an increase in proliferation, a larger cell body, and the secretion of pro-inflammatory cytokines and chemokines (206,207). Neuroinflammation is often damaging to neural function, and is associated with neurodegenerative diseases such as Alzheimer's and Parkinson's disease (208). Neuroinflammation is also heavily associated with epilepsy (209–211). It is believed that microglia play significant roles in the propagation of these conditions, however microglia can also be anti-epileptic (211). Neuroinflammation and lesion-associated activated microglia are also believed to play a role in the development of epilepsy in TSC, and are also activated by epilepsy (212,213).

1.2.2 The NF- κ B and STAT3 signalling axes: disease and crosstalk

The NF- κ B and STAT3 signalling pathways are regarded as key drivers of epilepsy-linked neuroinflammation. Both pathways play a prominent role in the activity of microglia and

surrounding glial cells in the CNS (214,215). TNF α is a known mediator of epilepsy with both epilepsy promoting and epilepsy suppressing mechanisms (216). IL-1 β also plays significant roles in the development of epilepsy, and has been demonstrated to contribute to neural hyperexcitability states (217). IL-6 is also believed to contribute to neural hyperexcitability and enhance the production of glial cells (210). As discussed later, these pathways also demonstrate significant crosstalk with one another. As activators of NF- κ B, the inflammatory stimulating mechanisms of TNF α and IL-1 β will be summarised below. Similarly, STAT3 activation will be summarised in the context of IL-6.

1.2.2.1 TNF α and NF- κ B

As a key modulator of inflammation, TNF α plays a relevant role in cancers, infection, and various inflammatory diseases. TNF α is released from the cell membrane by proteases, followed by trimerization and subsequent binding to either TNFR1 or TNFR2 (218). TNF α is highly pleiotropic and thus is a key player in the regulation of many important processes including embryo development, defence from pathogens, wound repair, and fever. However, unregulated, or aberrant TNF α signalling can cause disease states, and is implicated in depression, cancer, and other inflammatory diseases. While it is possible for some tumours to be sensitive to TNF α stimulation, causing their death, others may be bolstered by it, by driving the inflammatory phenotype that can be associated with malignant processes. As such, there are various reviews on TNF α discussing its dual nature as both a pro- and anti-cancer cytokine (218). TNF α binding to its receptors can present with contrasting effects depending on the cellular context and relative abundance of complex assembly proteins. Formation of complex I is typically associated with inflammation and pro-survival via NF- κ B and Mitogen-Activated Protein Kinase (MAPK) activation, whereas complex II formation leads to apoptosis or necrosis (219). The pathway undergone after complex I formation depends on an intricate set of cellular conditions and is generally integrated into complex formation via ubiquitination of RIPK1. Activation of complex I is determined by recruitment of TRADD to the TNF receptor followed by precise ubiquitination of RIPK1 by cIAP1 and cIAP2. RIPK1 is recruited to NEMO, leading to recruitment and ubiquitination of the TAK1 complex (TAK1-TAB1-3) (219–221). This complex is capable of phosphorylating and triggering the MAPK pathway. This means that complex I formation and activation promotes survival through the MAPK pathway, mainly via activation of JNK, but also ERK

(219,222,223). The canonical NF- κ B pathway is also triggered by complex I. TNF-receptor associated factor (TRAF) adaptor proteins are responsible for the recruitment of the IKK complex, and IKK is phosphorylated by a variety of other recruited factors, notably RIPK1, TAK1, and MAP3K3 (224).

The canonical NF- κ B pathway is a cell signalling pathway which results in the transcription of pro-inflammatory genes, and the activation of NF- κ B is laid out in the review by Yu *et al.*, (2020) (225). The NF- κ B family contains five members which interact with each other through the REL homology domain. However, the most important of these in canonical signalling are regarded to be RelA and p50. Phosphorylation of the IKK complex is crucial for initiation of the canonical NF- κ B pathway, and is followed by IKK complex-mediated phosphorylation of the inhibitor of κ B (I κ B). This is followed by ubiquitin-mediated degradation of I κ B (225). I κ B α is the most well defined I κ B protein and typically associates with p50/RelA heterodimers. Rapid degradation of I κ B α via IKK-mediated phosphorylation is essential for the nuclear translocation and activity of p50/RelA (226). The IKK complex (composed of IKK α , IKK β , and NEMO) also phosphorylates S536 of RelA, which is the NF- κ B subunit with transcriptional activity. IKK also phosphorylates p105, leading to p105 cleavage to generate mature p50 (227). p50 is phosphorylated by PKA to allow DNA binding (228). Phospho-RelA and p50 form the most well characterised heterodimer with NF- κ B transcriptional activity, and DNA binding results in the transcription of genes corresponding to the immune response, cell growth, and survival (229,230). The less characterized RelA homodimer can also bind to DNA, and likely has differential transcriptional activity (231). Conversely, p50 homodimers are inhibitory as they compete for NF- κ B binding motifs with transcriptionally active NF- κ B dimers (228).

1.2.2.2 IL-1 β

NF- κ B is stimulated by a variety of cytokine and crosstalk between other signalling pathways. IL-1 β also stimulates NF- κ B (232,233). IL-1 β is processed by caspase-1 after inflammasome activation, and after secretion is able to bind to the IL-1R1/IL-1RAcP receptor complex. After receptor binding, MYD88 and IRAK4 are recruited, the latter of which autophosphorylates and phosphorylates IRAK1 and IRAK2. TRAF6 is then recruited. The IRAK1-IRAK2-TRAF6 complex then dissociates from the IL-1 β receptor complex and results in the recruitment and ubiquitination of TAK3. TAK3 activation and recruitment of TAB1, TAB2, and TAB3 leads to the phosphorylation of IKK and subsequent stimulation of

NF- κ B in a similar mechanism as described above. In this way, both TNF α and IL-1 β mediated activation of NF- κ B is propagated through the TAK3-TAB complex.

1.2.2.3 cGAS/STING/TBK1

The cyclic GMP-AMP synthase (cGAS)/Stimulator of Interferon Genes (STING) pathway functions to activate inflammatory mechanisms in response to cytosolic foreign DNA (234). As foreign cytosolic DNA is indicative of bacterial or viral infection, the predominant purpose of the cGAS/STING pathway is immunity, and helps to guide inflammation in order to neutralise invading pathogens (235). Cytosolic DNA can also be indicative of cellular stress, resulting from leakage of nuclear or mitochondrial DNA (236). As a strong stimulator of inflammation, it is unsurprising that in certain contexts the cGAS/STING pathway can be aberrantly activated, thus guiding oncogenic processes, as well as other immune-related disorders (237). cGAS exists within the cytosol and serves as a DNA sensing molecule. The surface of cGAS is positively charged, and it possesses a zinc thumb binding site which allows it to interface with the sugar-phosphate backbone of DNA (238). This allows binding to dsDNA which induces a conformational change to activate the nucleotidyl transferase catalytic core of cGAS (239). This is followed by binding of GTP and ATP, resulting in the formation of the secondary messenger, cyclic GMP-AMP (cGAMP). cGAMP then binds to STING which is located on the endoplasmic reticulum, activating STING and inducing oligomerization and translocation to the golgi (234,240). At the golgi, STING recruits various kinases. This includes Tank-Binding Kinase 1 (TBK1), which phosphorylates interferon regulatory factor 3 (IRF3) and in turn stimulates the expression of genes that are dependent on type I interferon signalling (241). STING recruits and activates the IKK complex (242). TBK1 can also phosphorylate IKK, leading to NF- κ B activity (243).

1.2.3 IL-6/STAT3 signalling

IL-6, like TNF α , is a key pleiotropic cytokine that plays significant roles in the immune response. Initially IL-6 was identified under various pathways and circumstances, and thus garnered a selection of names such as B-cell stimulatory factor 2, or hepatocyte-stimulatory factor. However, eventually it was realised that these functions were all incurred by a singular molecule, now known as IL-6 (244). IL-6 is involved in the mediation of multiple immune responses to both endogenous and exogenous stimuli and may be regarded as one of the strongest cytokines in inducing large pro-inflammatory processes. Under normal conditions, IL-6 would be produced transiently in response to injury or infection. As such a powerful key

regulator of inflammation, IL-6 is also implicated in many inflammatory diseases including cancer (245). IL-6 is a member of the IL-6 family of cytokines, which includes 9 other cytokines. This family of cytokines all require the ubiquitously expressed cell-surface gp130 anchor as a co-receptor in order to transduce their inflammatory signal (246).

In the initial stages of infection or tissue damage, IL-6 is rapidly and transiently produced to send out a warning message to the entire body. For example, upregulation of IL-6 can be induced via pathogen associated molecular patterns (PAMPs), toll-like receptors (TLRs), or damage associated molecular patterns (DAMPs) (244,247). The IL-6 receptor, IL6R is expressed on monocytes, hepatocytes, B-cells, and neutrophils, but this does not mean that IL-6 signalling effects are restricted to these cell types. This is because IL-6 signalling can occur through the trans pathway, wherein IL-6 receptors can be secreted by neutrophils or cleaved from their surfaces, following neutrophil attraction by a chemoattractant like IL-8 (248). This allows soluble receptor binding, followed by binding to the membrane-bound gp130 receptor in order to facilitate the signal (249). Perhaps counterintuitively, binding of IL-6 to a membrane bound IL-6R is associated with an anti-inflammatory signal, whereas soluble IL-6 interactions instead mediate a pro-inflammatory signal (250). The capability of IL-6 for trans signalling is not a shared property among IL-6 family members, and this may be why IL-6 signalling is so dominant (251). While expression of soluble IL-6 or soluble IL-6R promotes the trans pathway, soluble gp130 inhibits trans-signalling and can be used as a treatment for inflammatory diseases (252).

Upon IL-6R binding through either the cis or trans pathway, gp130 receptor dimerisation occurs. The major pathways activated by IL-6 signalling are the STAT3 pathway, the MEK/ERK pathway, and the PI3K/AKT pathway (246,250,253). The STAT3 pathway is better understood and occurs by recruitment and phosphorylation of JAK to the active dimerized gp130, leading to subsequent recruitment of the SH2-domain containing STAT3. STAT3 is then phosphorylated at tyrosine 705, leading to p-STAT3 dimerisation and p-STAT3 dimer translocation to the nucleus where it can act as a transcription factor. As a transcription factor, Y705 p-STAT3 is heavily implicated in governing a wide array of tumorigenic processes, including invasion/metastasis, transformation, proliferation, survival, migration, and angiogenesis (254). Furthermore, p-STAT3 activity can upregulate unphosphorylated STAT3, enhancing available STAT3 levels for phosphorylation or the non-transcription factor functions of STAT3 (255). STAT3 phosphorylation occurs in a biphasic pattern during constant IL-6 stimulation, likely due to the repetitive action of the STAT3 induced suppressor

of cytokine signalling 3 (SOCS3) (256). One cytokine which may be upregulated by STAT3 nuclear activity is IL-1 β (257), which could then stimulate NF- κ B activity.

1.2.4 Crosstalk between the NF- κ B and STAT3 pathways

As two of the most important and pleiotropic cytokines, TNF α and IL-6 will often be implicated in similar pathways, and therefore may exhibit crosstalk and regulatory functions upon each other. For example, 55% of the genes that are upregulated greater than 2-fold by trans IL-6 signalling are also upregulated by TNF α signalling in fibroblast-like synoviocytes (258).

It is thought that TNF α may be able to induce IL-6 mRNA levels and protein secretion (259). TNF α -dependent IL-6 expression may be due in part to the fact that the *IL6* promoter possesses binding sites for NF- κ B (260). Thus, if TNF α upregulates NF- κ B, then IL-6 transcription may be enhanced. This has been confirmed as far back as 1990, wherein the promoter binding site for NF- κ B on the *IL6* gene was shown as essential for TNF α -induced IL-6 expression (261). This carries on to disease contexts, where head and neck squamous cell carcinoma displays increased IL-6 activity, which is dependent on an intact NF- κ B promoter site (262). As TNF α can induce NF- κ B, and IL-6 can induce STAT3 phosphorylation, crosstalk between TNF α and IL-6 could be also thought of as like crosstalk between NF- κ B and STAT3. This is further supported by the fact that a blockade at NF- κ B activity leads to significantly lowered STAT3 phosphorylation in both head and neck squamous cell carcinoma cells, and associated healthy epithelial cells (262). TNF α induced MAPK or AKT pathways may also upregulate other key transcription factors that induce IL-6 signalling (263). For instance, MAPK inhibition causes a decrease in IL-6 protein and mRNA levels (264). Curiously, inhibition of PPAR γ is also capable of inhibiting TNF α -induced IL-6 activity (265).

TNF α induced IL-6 signalling may be dependent on cell type, as human embryonic kidney cells did not demonstrate heightened IL-6 secretion following TNF α stimulation.

Alternatively, TNF α might aid in sensitising a cell to IL-6 activity (266). This idea is supported by a study which demonstrated that IL-6 was able to stimulate skeletal myoblast proliferation, when pre-treated with TNF α for 24 h (267). This led to enhanced cell growth through the ERK/MAPK and insulin-like growth factor signalling pathways. Interestingly, as well as increased mRNA of growth factors, gp130 levels were also increased 3.5-fold, but only after combined TNF α and IL-6 treatment.

NF- κ B activation and the MAPK pathway appear to enhance microRNA-365 (among other microRNAs), which lowers IL-6 mRNA stability (268). As detailed prior, these the NF- κ B pathway is activated by TNF α , suggesting signalling interplay between TNF α expression and IL-6 regulation at a post transcriptional level. Additionally, another study demonstrated that TNF α stimulation exerted negative regulation on IL-6 levels in macrophages (269). This mechanism requires suppressor of cytokine signalling 3 (SOCS3) and SHP2, likely because both SOCS3 and SHP2 can be recruited to the Y757-phosphorylated gp130. SOCS3 is known to inhibit gp130 activity (270). As TNF α can upregulate SOCS3 and recruitment of SHP2 protein, this provides a clear rationale for how TNF α may negatively regulate IL-6 signalling (270,271). Another component of this regulatory system functions by a reduction in the levels of gp130 following NF- κ B signalling, thus also inhibiting IL-6 signalling (269).

Overall, signalling crosstalk between the IL-6 and TNF α pathways is complex and varied. This complexity is likely due to differential activity and expression of the various receptors, meaning that some cell types will exhibit negative feedback regulation upon the expression of one pathway, while other cells will demonstrate positive feedback. A potential mechanism for a positive inflammatory feedback mechanism between NF- κ B and STAT3 is shown here (Figure 1.2).

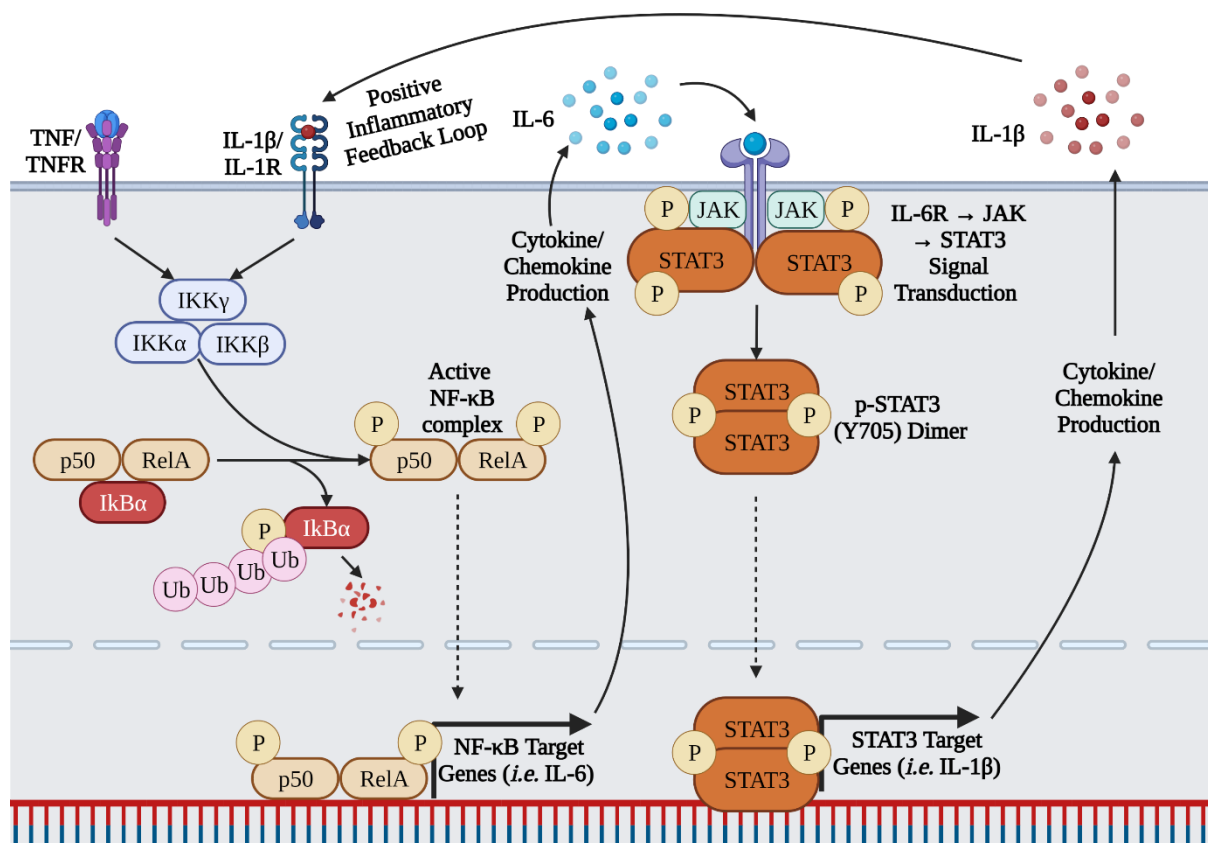


Figure 1.2. Positive feedback activity between NF- κ B and STAT3 pathways. NF- κ B stimulation initially occurs through TNF α or IL-1 β -receptor binding, leading to downstream activation of RelA/p50 heterodimers. This results in the upregulation of NF- κ B target genes, including cytokines such as IL-6. IL-6 production and secretion leads to autocrine stimulation of the STAT3 pathway, resulting in STAT3-target gene transcription. This can include cytokines such as IL-1 β , which then feed back into a positive inflammatory loop. Illustration produced in BioRender.

1.3 TSC-derived brain tumours

As detailed prior, brain tumours and their associated neuropsychiatric conditions are among the lead causes of mortality in TSC patients. Brain tumours are also the leading cause of cancer-related death in people under the age of 40 (272). TSC-derived brain tumours include SENs, SEGAs, and cortical/subcortical tubers.

1.3.1 Normal neuronal development

To understand the abnormal neuronal development of TSC-associated brain tumours, it is necessary to understand normal neuronal development. Neurogenesis is the process by which neurons are formed. This process relies on complex and precise signal interplay in order to direct progenitor cells to terminal differentiation states in the correct locations. Accordingly, gliogenesis is the development of the glial (non-neuronal, supporting) cells of the CNS.

Neurulation is a process of neural development that begins prenatally and results in formation of the neural tube after four distinct steps: formation of the neural plate, neural plate shaping, neural plate bending, and finally closure of the neural plate to generate the neural tube.

Neurulation initiates with a rapid proliferation event within the ectoderm to develop a high number of NECs, resulting in a structure known as the neural plate. High rates of cell division force this plate to bend inwards, known as the neural groove, before pinching into the neural tube: a folded structure of NECs which appears after around 4 weeks of prenatal development (273). The neural tube will go on to form the brain, spinal cord, meninges, and bones.

Incidentally, 2-dimensional neural cultures (described in Chapter 5) attempt to mimic the neural tube via the development of neural rosettes, which serve as an *in vitro* cross-section of the neural tube (274). The neural tube is accompanied by neural crest stem cells, which migrate and differentiate to become a variety of cell types including peripheral neuron types, glia, melanocytes, and skeletal/connective cells (275). The fluid filled lumen of the neural tube will become the cerebral ventricles of the brain. The neural tube may be regarded as the

key neurogenerative structure of the cortex. From around the 40th day of gestation, the process of neuronal development from the neural tube begins (276). This process moves outwards from the lumen (ventricle) to the outer (pial) regions. Layers of cells are formed from the ventricular zone, and sequentially through the subventricular zone (SVZ), the intermediate zone, the cortical plate, and finally the marginal zone which is lined with laminin. A description of these processes is summarised in the article by Bystron *et al.* (2008) (277). Within the subventricular zone, NECs form radial glia cells (RGCs). The apical side of RGCs contact the luminal side of the neural tube. RGCs extend and divide, reaching long processes up to form the edge of the marginal zone. The intermediate zone coalesces in the middle and is generally composed of the long processes of radial glia. Symmetrical cell division dominates the earlier stages of neurogenesis, increasing the levels of RGCs. Conversely, from around week 7 of development, asymmetrical division of RGCs occurs, leading to the generation of early neuroblasts. These migrate to the marginal zone to become the very first immature neurons. Following from this, asymmetrical division of RGCs produces TBR2-expressing intermediate progenitor cells (IPCs) (278). The SVZ is typically populated by IPCs which divide and migrate up the processes of RGCs to the marginal zone before differentiating into neurons. Each subsequent progeny of IPCs must migrate past the original layering of neurons, constructing the brain outwards in a layered fashion. An exception of this is the first population of migrating neurons that remain in the marginal zone and secrete reelin to guide the migration of IPCs, and generally assist with guiding the structural development of the cortex (279). Later in development, a new subset of RGCs arise. The apical side of these RGCs resides in the SVZ, and these continue to provide IPCs which migrate and develop into neurons. Sub-ventricular RGCs can also differentiate to generate glia such as astrocytes and oligodendrocytes, whereas RGCs can become the ependymal cells that line the BBB. Overall, the above described process is responsible for the generation of excitatory glutamatergic neurons of the cerebral cortex (280), whereas inhibitory neurons (GABAergic) are produced in the ganglionic eminences and migrate into the cortex (281).

Following corticogenesis, the relative regions within the cortex become demarcated as layers: layer 1 corresponds to the marginal zone, and layer 2 houses the last born neurons, with the earliest neurons forming layer 6 in what was once the ventricular zone (277). These layers contain varying mixes of neuronal cell types as well as glia. Postnatally, RGC retract their processes from the pia, and proliferation slows (282). Accordingly, the rate of neurogenesis slows.

Microglia are not explicitly developed within the brain. The most commonly accepted theory of microglial derivation is that microglia originate early in development, in the yolk sac, then migrate to the developing brain prior to the closure of the BBB. Here, microglia proliferate and maintain their own population (283). Microglial proliferation can be induced by injury or cytokines such as IL-1 β , and high proliferation of microglia are associated with neuroinflammatory neurodegenerative diseases (284,285).

As described by Tee *et al.* (2016) (286), mTOR signalling is a crucial aspect of neurogenesis and helps to direct progenitor migration as well as influences progression through differentiation states. Specifically, mTORC1 signalling guides the generation of RGCs from NECs as well as NEC proliferation. mTORC1 also influences the migration and proliferation of IPCs.

The review by Zimmer *et al.* (2020) (287) provides an excellent view of the mechanisms by which mTOR hyperactivation impacts the various glial cell types in the TSC brain. In summary, astrocytes in the TSC brain can be a mixed population of poorly differentiated mTORC1 hyperactive astrocytes, and reactive (pro-inflammatory) astrocytes. Giant cells are formed also as poorly differentiated intermediate cell types with a mix of glial and neuronal markers, and these are believed to arise from mTORC1 hyperactive RGCs. mTORC1 also guides oligodendrocyte maturation, cytoskeletal remodeling, oligodendroglial branching, and myelination. Dysregulation of mTORC1 in TSC leads to hypomyelination in and around cortical tubers. Defective myelination may contribute to epilepsy and TANDs in TSC (288). Microglia are also heavily impacted by mTORC1 hyperactivation. Microglia localise to mTORC1 hyperactive neurons and are typically upregulated in TSC-derived brain lesions. Microglia in TSC are generally shown to be more active, and mTORC1 activity in microglia also promotes the production of pro-inflammatory cytokines. Microglia can be activated through heightened neural activity such as epilepsy (289). Pro-inflammatory cytokines released from microglia like IL-1 β can promote neuron hyperexcitability, leading to epilepsy (290).

A study by Wildonger *et al.* (2008) (291) provided an interesting perspective on the role of mTORC1 in regulating neural polarity. Normally in the developing cortex, dendrites extend from neurons in an mTORC1-regulated process, and the longest of these (which trails behind during migration) will become the axon. Hyperactive mTORC1 may lead to a loss of

neuronal polarity and lead to the presence of multiple axons. The presence of multiple axons in non-polarised neurons may lead to dysregulated signalling in the TSC brain.

Overall, the current literature suggests that mTORC1 hyperactivity likely leads to the dysregulated neural phenotype in TSC in two primary ways. Migration of neural precursors is disrupted by mTORC1 hyperactivity. Also, mTORC1 hyperactivity causes neuroinflammation, and this results in enhanced recruitment and activation of immune cells and glial cells.

1.3.2 SEN/SEGAs

SENs are small, non-cancerous growths that normally arise near the foramen of Monro at the caudothalamic groove (292). They are typically highly calcified, making them easy to identify in brain imaging (293). SENs are believed to occur in between 70-84% of TSC patients (294), although one study identified SENs in up to 95 % of TSC patients (295). They are mostly composed of abnormally formed, enlarged glial cells. Histologically, SENs and SEGAs are believed to be mostly identical, but are differentiated based on their size and growth rate. Generally, the differentiation between SENs and SEGAs occurs when nodules have exceeded 1 cm in size, at which point they are regarded as SEGAs (296). Usually patients have more than one SEN (297).

SEGAs occur in roughly 20 % of TSC patients, are symptomatic in roughly 42% of these patients, and typically develop at a young age (298). SEGA can also rarely occur in non-TSC patients (299). SEGAs typically demonstrate a loss of heterozygosity of *TSC2*, or less commonly, *TSC1* (56,300). While SEGAs are often non-symptomatic, their proximity to the lateral and third ventricles means that they can obstruct CSF flow and cause obstructive hydrocephalus, coinciding with a substantial increase in neuropsychiatric symptoms and mortality (301). Symptoms associated with this are an increase in intracranial pressure, headaches, diplopia, photophobia, and ataxia. Seizures typically worsen with increased SEGA size and obstructed CSF flow, as well as an increased severity in cognitive deficits (302). SEGA are usually non-invasive, and unlike malignant GBM, have well contained borders (303). It is hypothesised that SEGAs (and by extension, SENs) develop from progenitor cell types in the early development of the brain, wherein mTORC1 hyperactivation confers altered differentiation states. While the histological cell basis is not fully known, three separate cell types are believed to composite the main mass of SEN/SEGAs. These are spindle cells (likely glial), enlarged (gemistocytic) astrocytes, and enlarged pyramidal

neuron-like cells (304). However, astrocytes are believed to be the main component of this based on glial fibrillary acidic protein (GFAP) and S100b expression (299). Studies attempting to investigate models of SEGAs have previously employed mTORC1 hyperactive astrocyte cultures (305). However, this scenario may not fully mimic the situation of TSC-derived SEGA, since a *Tsc1* mutation was used (rather than the more pathogenic *Tsc2* mutation). Additionally, murine astrocytes were employed rather than human astrocytes, which differ notably in complexity. Interestingly, however, the astrocytes employed in this study seemed to partially revert to earlier differentiation states, with a decrease in GFAP expression and an increase in SRY-box transcription factor 2 (SOX2) expression.

TSC patients are routinely screened with computed tomography (CT) or magnetic resonance imaging (MRI) to detect the presence of growing SEGAs (306). Following detection, the primary treatment for SEGA is surgical resection, although if SEGAs are underneath a certain size and do not appear to be actively growing, surgery may be delayed (307,308). Conversely, rapid worsening of symptoms ascribed to hydrocephalus/intracranial pressure warrants emergency surgery. CSF shunts can also be applied before or after surgery to help CSF flow, although shunts are typically avoided due to the risk of infection and need for revisions. Surgery can be highly effective at removal of SEGAs and can also help alleviate epilepsy in some cases. However, surgical mortality can also occur, with one literature review citing the SEGA surgery mortality rate to be 4.9 % (307). Surgery can also result in memory problems, infections, and hemiparesis, among other postoperative adverse events. Regardless, surgery results in complete removal of the SEGA in approximately 80 % of cases. While severe SEGAs that results in obstructive hydrocephalus are normally treated with surgery, a study demonstrated that Everolimus or Sirolimus were capable of reducing hydrocephalus by shrinkage of the SEGA (309). Furthermore, clinical trials have demonstrated the efficacy of mTORC1 inhibitors to shrink SEGAs, with long-term usage (>5 years) proving to be safe and effective (NCT00411619 (310), NCT00789828 (311)) with between 50-60% of patients experiencing shrinkage of SEGAs.

1.3.3 Cortical tubers

Cortical tubers develop in the cortex, arise early in development, and are apparent in approximately 90% of TSC patients (312). They are believed to be non-functioning since tubers can be resected with little apparent induction of mental deficiency (313). Like SEN/SEGAs, cortical tubers are generally composed of a mix of malformed neurons and glial

cells, demonstrating an upregulation in the number of astrocytes (2,314). They can also demonstrate calcification, but this is less common than in SEN/SEGAs (315). Over time, cortical tubers can develop into cyst-like structures, and these are correlated with worse epilepsy (316). Tubers can be separated into three subtypes, based on their relative levels of calcification and the prevalence of giant cells, and dysmorphic neurons (317). Martin *et al.* (2017) (51) highlighted some key differences between the SEN/SEGAs and cortical tubers. Unlike SEN/SEGAs, the majority of cortical tubers do not demonstrate loss of heterozygosity of *TSC2* (or *TSC1*). Another key difference between cortical tubers and SEN/SEGAs is that the latter tends to display more angiogenesis. Tubers also do not typically grow over time, and instead form prenatally and then persist through development. However, larger tubers can exist and are typically correlated with more severe TANDs (318). Cortical tubers as well as the perilesional cortex display enhanced mTORC1 activity, and lower mTORC2 activity (319). The same study showed that neurons in these areas are hyperconnective, hyperexcitable, and hypomyelinated.

A study by Mühlebner *et al.* (2016) (320) provides an interesting look at the presence of cortical layer markers within cortical tubers. The neurons in cortical tubers are dysmorphic and demonstrate dysregulated migration; TBR1-expressing neurons are increased throughout the white matter and upper cortical layers, and this dysregulated structuring may contribute to epileptogenic signalling. Overall, the precisely ordered cortical layers required for normal neural development appear highly dysregulated within cortical tubers. Consequently, this leads to an abundance of dysmorphic and incorrectly spaced neurons. A high number of TBR1-expressing neurons are also present within the perilesional cortex, which likely also promotes epilepsy. *CUX2* expression was also dysregulated. While *CUX2* expression should normally be confined to neurons in L2-3, *CUX2*-expressing cells were found in deeper layers in cortical tubers. *SATB2* is also typically found in L2, 3, and 5, however cortical tubers demonstrate a reduction in *SATB2*-expressing cells within layer 5, suggesting that earlier developmental cues are being lost. Further research has shown that abnormal neurons within cortical tubers have higher levels of excitatory neurotransmitter receptors, demonstrating a mechanism of their epileptic origin (321). These neurons also possess reduced GABA receptors which could confer heightened excitability (322).

Cortical tubers are highly associated with epilepsy. In the case where cortical tubers are known to be the epileptogenic focus, they are referred to as “hot tubers” (323). If epilepsy proves pharmacologically resistant, these tubers must be resected via surgery (324). Surgery

must also target the perituberal area, as it has been demonstrated that this tissue is also epileptogenic (319). A difficulty in targeting tubers with surgery for the relief of epilepsy is that TSC patients often present with multiple tubers. This means that correct identification of the epileptic focal point must be determined for effective surgical targeting. Singular tubers can be often identified as focal points of epilepsy (41). According to meta-analysis, surgical excision of epileptogenic tubers results in seizure freedom in 59 % of TSC patients (325). Cortical tubers are primarily targeted through surgery as a means of alleviating epilepsy. However, mTORC1 inhibition with Everolimus may prove especially useful if used at the appropriate time, as reduction in hyperactive mTORC1 activity may help to relieve the aberrant neuronal development and maturation that is observed within these lesions (322).

As an aside, white matter abnormalities are typically also present in the brains of around 80% of TSC patients (314). TSC patients normally possess heterotopia. Similar to cortical tubers, heterotopia is associated with treatment-resistant epilepsy (315). Heterotopia is believed to arise from a failure of neuronal migration from the subependymal area to the cortex, leading to abnormal organisation of neurons (326). General white matter abnormalities with no apparent well defined lesion may be a significant cause of epilepsy and TANDs in the TSC brain (319).

1.3.4 TSC-associated neuropsychiatric disorders

As previously described, TSC patients typically present with various neuropsychiatric disorders known as TANDs. Around 90% of TSC patients will present with these conditions throughout their lives (39). Healthcare professionals use the TAND checklist to identify TANDs and assess the need for further treatment and management in TSC patients. As outlined in the paper by de Vries *et al.*, (2014) (39) the TAND checklist was delineated. TANDs can be broadly described in five separate categories. Behavioral elements refer to the typically caregiver-reported trends such as anxiety, issues in temper control, eating and sleep difficulties, and general social issues. Psychiatric disorders refer more closely to patterned behavioral observations which can be grouped into broader conditions, including autism spectrum disorder, attention deficit hyperactivity disorder, and depressive and anxiety disorders. The intellectual aspects of the checklist focus on intellectual disabilities or an overall lowering in cognitive ability. The academic level of the checklist is distinct from the intellectual level; some children with TSC have apparently normal intellectual capability, but still perform worse in an academic setting. Neuropsychological aspects of the checklist

observe neuropsychological deficits in executive, attention, language, memory, and visuospatial skills. Notably, TSC patients may exhibit very specific deficiencies in some of these abilities. For example, one patient may present with normal language and visuospatial skills, but struggle with memory and attention. The psychosocial area of the checklist focuses on the quality of life and relationship aspects. Overall, the TAND checklist aims to facilitate conversation between healthcare professionals and caregivers in order to more effectively identify causes for concern in TSC patients.

While epilepsy is not directly assessed through the checklist, epilepsy is another key TAND. Epilepsy occurs in over 80% of TSC patients (27), and is refractory in 62.5% of these cases (327). Generally, seizures present in infants with TSC in the form of infantile spasms. Infantile spasms occur within the first year of life, and TSC patients account for 10-20% of infantile spasm cases (328). Higher severity and earlier occurrence of infantile spasms correlates with more severe epilepsy in later life, and more severe cognitive impairment. While it has been shown that the overall tuber load (the proportion of brain occupied by tuber) has a stronger correlation to the severity of epilepsy and cognitive dysfunction than the number of tubers, the key determining factor in worsened TANDs is the age of seizure onset (329). It is likely that the best control measure in TSC to target TANDs would be to control seizures (27). TSC may exhibit some differences in the pathogenicity of epilepsy when compared to other epileptic disorders. Most cases of non-TSC-linked epilepsy originate in the temporal lobes (330). Conversely, cortical tubers are regarded as the epileptogenic foci in TSC, and are more often located in the frontal and parietal lobes, with one study reporting only 8% of tubers being found in the temporal lobes (331).

1.3.5 Neuroinflammation in TSC

While both cortical tubers and SEN/SEGA seem to present inflammatory signalling and immune recruitment, inflammatory signalling appears to be more abundant in SEN/SEGAs (51). Martin *et al* (2017) postulated that 20% of the mRNA within SEN/SEGAs corresponded to leukocytes. It is believed that mTORC1 activation and inflammation can develop prenatally, and this may contribute to the development of brain lesions and TANDs (332). A mouse model demonstrated that IL-1 β and CXCL10 in particular were enhanced in the brains of *Tsc1*-deficient mice, and this likely contributes to epilepsy (333). These cytokines were shown to be downstream of mTORC1, as observed by their sensitivity to mTORC1 inhibitors. Mouse models also revealed that pro-inflammatory signalling appeared to develop

prior to epilepsy onset (333). Another study reported high levels of IL-1 β and IL-1RI within cortical tubers and SEN/SEGAs of the TSC brain. This was particularly within giant cells, activated microglia, and reactive astrocytes (290). IL-1 β activity likely contributes to neural hyperexcitability and seizures (334). TSC-derived brain tumours also exhibit a high degree of immune invasion, as observed by the heightened expression of major histocompatibility complex (MHC) class II-antigen positive immune cells around mTORC1-hyperactive brain cells (290,335). It is likely that seizures trigger the activation of invading immune cells that then engage in further pro-inflammatory signals, leading to more seizures. This may provide the rationale for why early presentation of infantile spasms correlates with worsened TANDs in later life. The complement cascade is also highly active in TSC-derived brain tumours (336), providing further evidence for immune infiltration and inflammatory activation in TSC brain lesions. The complement system is also likely implicated in epilepsy (337). Anti-inflammatory treatments in other seizure disorders seem to have efficacy. For example, inhibition of IL-1 β production (via inhibition of Interleukin-1 β converting enzyme (ICE)) has shown to reduce chronic epileptic activity in a mouse model (338).

Neuroinflammation is also believed to contribute to permeability of the BBB, although research on this in the context of TSC is relatively limited. A study has implicated BBB leakage in TSC via enhanced uptake of serum albumin by astrocytes, and this is known to impact neural hyperexcitability (290). Another study found enhanced blood vessel length and branching in cortical samples of TSC patients, suggesting disruption of the BBB in TSC (339). Pro-inflammatory cytokines result in migration of leukocytes across the BBB (340), and these would likely upregulate inflammatory processes in TSC-derived brain lesions. Vascular endothelial growth factor (VEGF) production also likely disrupts the carefully organized vasculature of the BBB, further driving this process (341). Disruption of the BBB is associated with epilepsy, wherein it is believed that BBB permeability can be influenced by seizures (342), but may also contribute to the development of seizures (343). Through the above-described research, epileptic seizures seem to follow a mechanism of positive feedback; inflammatory mechanisms can trigger epilepsy, leading to the generation of further inflammatory and immune signals. This process is mediated by cytokine/chemokine production, immune cell invasion/activation, activated/dysregulated glial cells, and disruption to the BBB. While there is limited research on the actual state of the BBB in TSC, the available knowledge on inflammation in TSC and the effect of inflammation on the BBB makes it highly likely that the BBB is compromised in TSC. mTORC1 activity is also known

to influence vasculature formation in neurodegenerative diseases (344), lending further credibility to this hypothesis.

Various other neuropsychiatric conditions can be associated with neuroinflammation. Autism spectrum disorder has been characterized as a neuroinflammatory condition, as well as Alzheimer's disease, Multiple Sclerosis, narcolepsy, and Parkinson's disease (345). Dysfunctional microglia can often play a role in autism, wherein the synaptic regulatory effects of dysregulated microglia after inflammatory stimulation results in altered synaptic function (346). In general, neuroinflammation leads to overactive microglia and astrocytes, leading to altered synaptic connections and neural function (347). NF- κ B signalling in microglia may also be present in autism spectrum disorder (348), however this notion was contested in other studies (349). NF- κ B in epilepsy is similar, in that NF- κ B is thought to have both neuroprotective effects during seizures, but heightened NF- κ B in immune cells is also undoubtedly detrimental to the CNS (214). Overall, it is believed that neuroinflammation alongside mTORC1 hyperactivity likely contributes to the pathology of epilepsy and other TANDs in TSC (Figure 1.3).

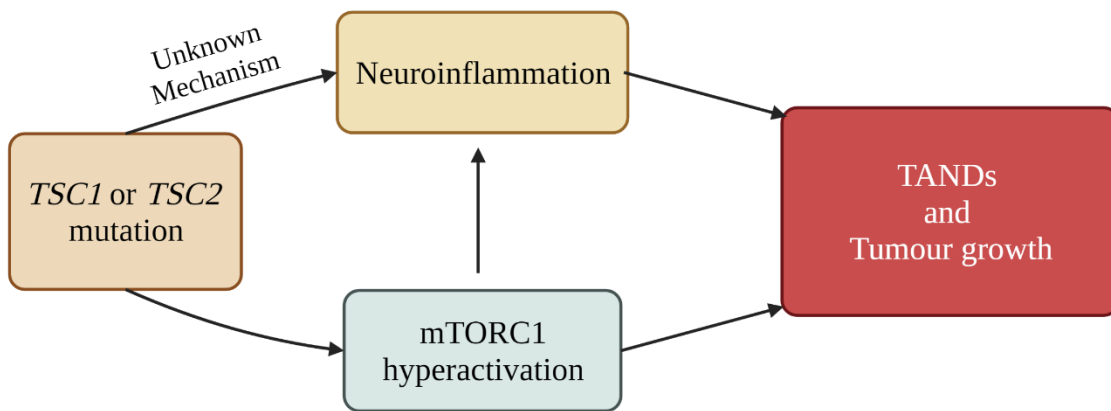


Figure 1.3. Neuroinflammation contributes to the development of TANDs. Mutation to either *TSC1* or *TSC2* results in mTORC1 hyperactivation. mTORC1 hyperactivation contributes to the development of neuroinflammation. *TSC1/TSC2* loss may also confer neuroinflammation through unknown mTORC1-independent mechanisms. Both neuroinflammation and mTORC1 contribute to abnormal neurodevelopment, leading to the development of TANDs and brain tumour growth. Illustration produced in BioRender.

1.4 Aims and Objectives

In this project, it is hypothesised that inflammatory signalling is dysregulated within TSC patients, and that this inflammatory signalling is linked to the development of TANDs in TSC patients, and inflammatory signalling may guide dysregulated neurodevelopment.

Furthermore, it is suggested that NF- κ B, which is poorly researched in TSC, may play an important role in the development of neuroinflammation in TSC, and targeting of NF- κ B may prove effective in the management of TSC symptoms. Lastly, it is hypothesised that the current standard models of TSC (specifically MEF, AML, and ELT3 cells) do not accurately reflect neuroinflammation in TSC, and therefore neural models may be required to further the understanding of TAND development.

There are three broad aims of this project.

Aim 1: Currently, the origination of inflammatory signalling in *TSC2*-deficient cells is unclear. The project aims to characterize the inflammatory processes in *TSC2*-deficient cells with a focus on the NF- κ B and STAT3 pathways, while observing the crosstalk between these two inflammatory pathways. The project also seeks to determine a potential cause for inflammatory mechanisms in TSC by exploring activation of TBK1. To do this, the project will explore the effects of inflammatory stimuli on *TSC2*-deficient cells and explore cytokine activity in these cells. Since TSC-associated epilepsy is treatment refractory and often not modulated by mTORC1 inhibitors such as Sirolimus or Everolimus, the project also aims to assess the effects of mTORC1 inhibition on inflammatory pathways in TSC.

Aim 2: Models exploring neuroinflammation in TSC are currently limited, and research on the state of NF- κ B in TSC-derived brain tumours is also limited. Furthermore, it is generally unclear how dysregulated inflammatory processes may influence the development of TANDs in TSC. For this reason, the project aims to develop a *TSC2*-deficient iPSC model using CRISPR-Cas9 technology. This iPSC model will be used in neurodifferentiation experiments alongside a wild-type control to analyse the differences in neural development. Throughout the differentiation process, neurodifferentiation biomarkers will be analysed as well as inflammatory activation biomarkers (STAT3 and NF- κ B). Data will be compared between this *in vitro* neural model and existing *TSC2*-deficient *in vitro* models to observe how inflammatory processes are maintained throughout the disease state of TSC. Data will also be compared to *in vivo* transcriptomic analyses of TSC patient-derived brain tumours to determine how inflammatory processes in the models compare to *in vivo* brain tumours.

Aim 3: Aside from a recent approval for the use of CBD, the exploration of anti-inflammatory treatments is limited in TSC. This is especially relevant if we consider that many TANDs such as epilepsy may be inflammatory in origin. Therefore, the project aims to identify currently available drugs which may a) reduce inflammation in *TSC2*-deficient cells, b) exert anti-proliferative, anti-tumour formation, and other phenotypic effects in *TSC2*-deficient cells, and c) be useful in conjunction with traditional mTORC1 inhibitors to reduce mTORC1 hyperactivity, or otherwise reduce mTORC1 hyperactivity in mono-treatment.

Chapter 2 – Materials and Methods

2.1 Cell culture and maintenance

Mycoplasma-free frozen cell stocks were used for this study, all cells were routinely checked with Venor GeM Advance Mycoplasma Detection Kit (Minerva Biolabs, 11-7024) as per manufacturers guidelines and were negative to the presence of contaminating Mycoplasma spp.

2.1.1 MEF, AML, and ELT3

621-101 TSC2-deficient ($TSC2^{(-)}$) and 621-103 TSC2-addback ($TSC2^{(+)}$) AML cells were used as a human *in vitro* model of TSC and were gifted by Prof. Elizabeth Henske. $Tsc2^{(-/-)}$ mouse embryonic fibroblast (MEF), and $Tsc2^{(+/+)}$ MEF cells (both $Tp53^{(-/-)}$) were used as an additional *in vitro* cell line model of TSC. 621-101 AMLs are an angiomyolipoma cell line lacking functional TSC2, which are derived from a LAM patient and reported to be homozygous for a missense mutation in TSC2 (G1832A), resulting in TSC2 with an amino acid substitution (R611Q) (350). The mutation is frequently found in TSC patients (351) and results in TSC2 being unable to interact normally with other proteins. Wild-type human TSC2 was added back to the 621-101 AML cells to generate 621-103 AML cells, a rescue cell line with functional TSC2 (352). The study by Yu *et al.* describes the process of establishing this culture, wherein freshly extracted AML tissue was minced and plated, prior to DNA sequencing. The MEF cell line was a generous gift from Prof. D. Kwiatkowski. $Tsc2^{(-/-)}$ MEFs are an immortalised, $Tsc2$ null, MEF cell line derived from early-stage embryos produced by interbreeding studies (353). Development of this cell line required $TP53^{-}$ mice. Day 10-12.5 embryos were collected as described in (353), prior to trituration and plating. Eker rat leiomyoma-tumour-derived $Tsc2$ -deficient cells (ELT3-V3) and matched controls re-expressing $Tsc2$ (ELT3-T3) were generated by Astrinidis *et al.* (354) and were gifted in 2006 by Prof. C. Walker (M.D. Anderson Cancer Center, Houston, USA). The development of these cell lines are described in (354), wherein ELT3 cells were transfected with retrovirus containing either full-length human $TSC2$ or an empty vector, resulting in establishment of ETLT-T3 or ELT3-V3 cell lines, respectively. MEF, AML, and ELT3 cells are heterogeneous populations.

Cells were maintained at 37 °C, 5% CO₂ in a humidified incubator using Gibco™ TC reagents (Thermo Fisher) and TPP™ coated TC plasticware (Helena Biosciences Europe)

throughout. When indicated cells were incubated under hypoxic conditions of 1% O₂ achieved with N₂ displacement. Cells were cultured in TC media consisting of DMEM (Merck, D6429) supplemented with FBS (Merck, F7424) at either 10% (v/v) or 15% (v/v) for MEF or AML cell lines, respectively, with 50 IU/mL penicillin and streptomycin (Merck, P0781).

Cells were passaged via washing three times in trypsin-EDTA (Thermo Fisher, 25200-056) prior to incubation at 37°C for 5 min. Cells were then resuspended in DMEM, and the appropriate volume of media was removed to generate the correct passaging dilution. *Tsc2*^(+/+) and *Tsc2*^(-/-) MEF cells were typically passaged at ratios of 1:10 and 1:20, respectively. *TSC2*⁽⁺⁾ and *TSC2*⁽⁻⁾ AML cells were typically passaged at a ratio of 1:6. ELT3-T3 and ELT3-V3 cells were typically passaged at a ratio of 1:10. MEF, AML, and ELT3 cells were used below passage numbers of 45, 25, and 45, respectively.

To freeze cells for long-term storage, cells were detached via trypsinisation. Cells were then centrifuged at 200 × g for 5 min. Cells were then resuspended in Recovery™ cell culture freezing medium (Thermo Fisher, 12648010) at a density of 500,000 cells/mL. Cells were then cooled at a rate of -1 °C/min to -80 °C. Cells were then stored in liquid N₂. To thaw cells, vials were rapidly thawed in a 37 °C water bath and added directly to cell culture medium. Media was changed the following day.

2.1.2 iPS cell culture

iBJ4 wild-type (iBJ4-WT) cells were gifted by the Harwood lab of the NMHRI, Cardiff. *TSCI*-deficient iBJ4 cells were generated and kindly gifted by Dr Laura Kleckner. iBJ4 cells are an induced human pluripotent cell line derived from male fibroblasts (355). A mixed pool of *TSC2*-deficient PGP1 iPS cells were purchased from Synthego prior to subcloning and sequencing (section 2.1.3 and section 2.15, respectively). PGP1 cells are an induced human pluripotent cell line derived from male fibroblasts (356). *TSC2* knockout by CRISPR-Cas9 was performed by Synthego. Subcloning, Sanger sequencing, and downstream characterisation was performed post-acquisition.

iPSCs were cultured in a feeder free system using Gibco Essential 8 Medium (E8) (Thermo Fisher, A1517001) on a basement membrane of Cultrex (R&D Systems, 3434-005) diluted in DMEM-F12 at a 1:100 dilution. Cells were maintained in a humidified incubator at 37 °C with 5% CO₂. Medium was replaced every 24 h. Cell confluency was monitored, and cells were passaged at 80% confluency. Prior to passaging, cells were treated with 10 μM Y27632-

dichloride (Tocris, 1254) for at least 1 h to prevent detachment-induced cell death. iPSCs were then washed once with D-PBS (Thermo Fisher, D8537) before being incubated for 3 min at 37 °C with gentle cell dissociation reagent (GCDR) (Stemcell Technologies, 100-0485). Following incubation, GCDR was aspirated and replaced with E8 containing 10 µM Y27632. Cells were scratched and/or gently resuspended via pipetting before transferring to new Cultrex pre-coated plates containing E8 with Y27632. After 24 h, media was replaced with fresh E8 without Y27632. If spontaneous differentiation appeared to be occurring, cells were passaged in ReLeSR™ passaging reagent (Stemcell Technologies, 05872) to maintain pure iPSC cultures.

Prior to freezing, cells were treated for at least 1 h with Y27632 before detachment with GCDR. Cells were then resuspended in E8 with 10% (v/v) Dimethyl Sulfoxide (DMSO) containing Y27632 and brought to -80 °C at a cooling rate of -1 °C per min. For long-term storage, cells were stored in liquid N₂.

Cells were thawed with E8 + ReviADAM171I™ supplement (Gibco, A2644501) and allowed to attach to Cultrex-coated plates. Media was replaced after 24 h. Cells were maintained for at least 2 passages prior to usage in experiments.

2.1.3 iPSC single-cell cloning

To generate solutions of singular cells, iPSCs were incubated with Y-27632 for at least 1 h. Cells were then washed and incubated in accutase cell detachment reagent (Stemcell Technologies, 07920) for 10 min at 37 °C. Cells were collected in accutase and diluted within E8 before centrifugation at 200 × g for 5 min. Excess media was aspirated, and the resulting pellet was resuspended in 1 mL E8 + Y27632. 10 µL of this cell solution was added to a Cultrex pre-coated 100 mm dish in E8 with Y27632. The dish was gently rocked from side to side to ensure an even distribution of cells. Cells were checked under a microscope to ensure a lack of clumping before incubation overnight. Media was then replaced with fresh E8, and cells were maintained until sizeable (but not touching) colonies were formed.

When colonies were of a sufficient size, cells would be treated with Y27632 for 1 h. Colonies would then be selected under a microscope via pipetting and transferred to a pre-coated 48-well plate and cultured as described above. These cells were then allowed to grow before splitting to larger plates for subsequent sample generation and assays.

2.2 Sodium Dodecyl Sulphate Polyacrylamide Gel Electrophoresis (SDS-PAGE) and western blotting

2.2.1 Protein lysate generation

Tsc2^(-/-) and wild-type MEFs were seeded within 6 cm plates at a seeding density of 3×10^5 and 9×10^5 cells/mL, respectively. *TSC2*-deficient and *TSC2*-rescued AMLs were seeded at a density of 8×10^5 and 1.2×10^6 , respectively. ELT3-T3 and ELT3-V3 cells were seeded at a density of 6×10^5 . Cells were grown until 80-90% confluency. Various treatments were then administered as specified in relevant sections before cells were washed with ice-cold PBS and lysed directly in sample buffer 62.5 mM Tris-HCl (pH 7.6), 10% (v/v) glycerol, 2% (w/v) SDS, 50 mM fresh dithiothreitol (DTT). Samples were then sonicated using a Diagenode Bioruptor and boiled at 95 °C for 10 min, and finally centrifuged at $17,000 \times g$ for 10 min. Total protein was quantified at OD₆₆₀ using Pierce™ 660 nm reagent plus ionic detergent compatibility reagent (ThermoFisher, 22663), before normalisation of each sample to the lowest sample protein concentration per sample set, using sample buffer containing bromophenol blue. Samples were then stored at -20 °C until needed.

2.2.2 SDS-PAGE

SDS-PAGE was performed using NuPAGE™ Bis-Tris 4-12% (Thermo Fisher, NP0326BOX) and NuPAGE™ Tris-acetate 3-8% (Thermo Fisher, EA0375BOX) gels, using NuPAGE™ MES SDS running buffer (Thermo Fisher, NP0002) and NuPAGE™ Tris-acetate SDS running buffer (Thermo Fisher, LA0041), respectively. Gels were run in XCell SureLock Mini-cell electrophoresis chambers (Thermo Fisher, EI0001) with BLUeye pre-stained protein ladder (10-240 kDa) (Geneflow, S6-0024). 5-10 µg of total protein were loaded per well. Gels were run at 180 V for 5 min, followed by 150 V for 55 min.

2.2.3 Electrophoretic Transfer and western blotting

Resolved proteins were transferred to Immobilon®-P polyvinylidene difluoride membranes (Merck Life Science, IPVH00010) using wet transfer. Membranes were then blocked in 5% (w/v) dry powder milk in Tris-buffered saline (50 mM Tris-Cl pH 7.5, 150 mM NaCl) with 0.1% Tween 20 (TBS-T). Membranes were then probed with primary antibodies overnight at 4 °C on an orbital shaker. Primary antibodies were diluted in TBS-T with 2% (w/v) bovine serum albumin (BSA) (Merck, A7908). All antibodies were purchased from Cell Signalling Technology except mTOR antibody. The mTOR antibody was custom generated in sheep and

gifted from the MRC Protein Phosphorylation Unit (Dundee University, epitope: LGTGPAATAATTSSNVS). Most antibodies were used at a dilution of 1:1000 except for β -actin (1:30,000), Annexin A2 (ANXA2) (1:10,000), Galectin-3 (LGALS3) (1:10,000), phospho-rpS6 (S235/236) (1:4000), and STAT3 (1:4000). Membranes were washed in TBS-T prior to secondary staining with either anti-rabbit, anti-mouse, or anti-sheep HRP-conjugated secondary antibodies (1:10,000) (Merck) in TBS-T with 2% (w/v) dry powder milk. Membranes were incubated for 1 h at room temperature on an orbital shaker. Membranes were then washed in TBS-T prior to addition of enhanced chemiluminescence (ECL) reagent. Membranes were incubated for 1 min and then detected using Cytiva Amersham™ ECL Select™ western blotting detection reagent (Cytiva, RPN2235). Pixel densitometry was performed in ImageJ. (version 1.52i). Densitometry values were normalised to β -actin band intensity, and relative intensities were used to calculate relative protein abundance and fold changes.

2.3 Drug Treatments

Drug	Supplier	Stock concentration dissolved in DMSO
Rapamycin	(Merck, 553210)	100 μ M
BMS345541	(Selleckchem, S8044)	20 mM
Diacerein	(Selleckchem, S4267)	50 mM
SAHA	(Selleckchem, S1047)	10 mM
R-7050	(Selleckchem, S6643)	10 mM
Resatorvid	(Selleckchem, S7455)	10 mM
IMD0354	(Selleckchem, S2864)	10 mM
C188-9	(Selleckchem, S8605)	20 mM

Table 2.1 Drug supplier and stock concentrations.

Recombinant human TNF α and recombinant IL-6 (Abcam, 259410 and 198571, respectively) were reconstituted in sterile ddH₂O with 0.2% (w/v) BSA to 50 μ g/mL and 100 μ g/mL, respectively.

The stock drug solutions were added to culture media to reach the required concentration without exceeding 0.5% (v/v) DMSO. The total DMSO concentration was adjusted within experiments to maintain a consistent % (v/v) of DMSO per condition.

2.4 Patient-Derived TSC Transcriptomic Analysis and Gene Ontology Analysis

Samples of TSC patient-derived SEN/SEGAs ($n = 15$) were collected by Prof. J. MacKeigan (Center for Cancer and Cell Biology in Grand Rapids, MI, USA). Differentially expressed gene (DEG) analysis was performed as described by the lab of Prof. J. MacKeigan (51). A list of genes, fold changes, and adjusted p-values was provided by Prof. J. MacKeigan, and subsequent analysis was performed for this study. Gene ontology (GO) analysis was performed with GeneAnalytics (LifeMap Sciences Inc., Covina, CA, USA). A similar analysis was performed with TSC patient-derived cortical tubers ($n = 15$). GO analysis was used to identify dysregulated inflammatory and immune system processes in TSC patient-derived tumours. Volcano plots were generated in R Studio version 1.3.959.

2.5 RNA-Sequencing

Samples for RNA-sequencing were generated by Mr Mohammad Alzahrani and Dr Brian Calver (Cardiff University). Cells were washed in PBS and lysed in RNAprotect® Cell Reagent (Qiagen, 76104). RNA was extracted from six biological repeats using QIAshredder® (Qiagen, 79654) and RNeasy® Mini kits (Qiagen, 74104) and then stored at -80°C . RNA library preparation and sequencing were performed through a commercial service/collaboration with Wales Gene Park (Cardiff University, UK), as described previously (357), except the Illumina® TruSeq® RNA sample preparation v2 kit (Illumina, RS-122,2001) was used for library preparation, according to the manufacturer's instructions. Following validation, the libraries were normalised to 8 nM and the pool was sequenced on the MiSeq with a 150 cycle, version 3, cartridge (both Illumina Inc) according to the manufacturer's instructions. Differentially expressed transcripts were identified using the DeSeq2 package in R (358). Analysis was carried out on all pairwise comparisons in the dataset. P-values were corrected for multiple testing using the Benjamini-Hochberg false discovery rate (FDR) method. The initial bioinformatic work was carried out by Wales Gene Park.

2.6 Transcriptional Activation Enzyme Linked Immunosorbent Assays (ELISAs)

Transcriptional activation ELISAs for STAT3, p50, p65, and CCAAT enhancer binding protein β (C/EBP β) were purchased from ActiveMotif. *Tsc2*^(-/-) and wild-type MEFs were grown over a two-day period until 80-90 % confluent. Full-serum media was then replaced with serum-depleted media, including pathway inhibitors or DMSO where applicable for a

duration of 24 h. When assaying TNF α responsiveness, TNF α was supplemented for the final 2 h to match the end point of this timepoint. Alternatively, IL-6 was supplemented at 1 h prior to the end of the treatment period. Cells were then washed in ice-cold PBS containing phosphatase inhibitors (supplied in kit), and lysis/nuclear sample preparation was then performed as directed by the kit manufacturer. When assaying the effect of *TSC2*-deficient cell-conditioned media on *TSC2*-expressing cells, *TSC2*-deficient MEFs or AMLs were grown until 80% confluency before media was replaced with serum depleted media. Cells remained under starved conditions for 24 h before the media was collected, briefly centrifuged, and added to *TSC2*-expressing cells. Control points were performed using media taken from *TSC2*-expressing cells. Total protein of each sample was quantified by Bradford assay before samples were stored at -80°C . ELISAs were carried out as directed by the kit manufacturer's instructions.

2.7 Cytokine/Chemokine Profiling

A mouse cytokine array kit was purchased from Biotechne (Biotechne, ARY006). MEFs were grown over a 24 h period until 80-90% confluent before media was replaced with serum-free media. After an 24 h starvation period, cells were then treated with 30 ng/ml TNF α for 2 h before lysis was performed according to the kit manufacturer's instructions in NonIdet P40 substitute (Merck, 11755699001) supplemented with PhosSTOP (Merck, 4906845001) and cComplete Mini Protease Inhibitor Cocktail Tablets (Merck, 04693124001). Total protein concentration was quantified, and 200 μg was used for each sample on each profiler membrane. Membranes were imaged on photosensitive film using ECL SelectTM western blotting detection reagent, with 15 s used as the optimum exposure time.

2.8 Viability Assays

MEF cells were grown over a two-day period until 80-90% confluent before media was replaced with serum starved media containing the inhibitor/protein to be assayed. Cells were then left for a further 24 h before media was collected. Cells were then washed three times with trypsin/EDTA with each wash also collected alongside the media. Cells were then trypsinised, collected, and pelleted alongside the collected media and trypsin washes. Cells were resuspended in a lower volume to generate a high cell-density, before 18 μL of each suspension was added to 2 μL of propidium iodide/acridine orange solution (Logos Biosystems, F23003) and incubated for 5 min. Viability counts were then performed on a Luna cell counter (Logos Biosystems).

2.9 Duoset ELISAs

IL-6 and VEGFA ELISA duoset kits (R&D, #DY206, #DY293B) were purchased from R&D Systems alongside an ancillary reagent kit (R&D, #DY008B). ELISAs were performed according to the manufacturer's instructions. *TSC2*⁽⁺⁾ or *TSC2*⁽⁻⁾ AMLs were grown in 12-well plates to 70-80% confluency before media was replaced with drugged media (where applicable). Cells were kept under full serum conditions in these assays. Neural samples were used at day 70 of neurodifferentiation with or without 48 h treatments. Media was collected and diluted at a ratio of 1:10 within reagent diluent and kept on ice prior to use.

Lysates or media preparations were then loaded onto ELISA plates which had been pre-coated with the appropriate capture antibody and blocked. Sample incubation was performed overnight at 4 °C.

Readings were later quantified by either total protein concentrations in Pierce™ 660 nm reagent of cell lysates or by cell count.

2.10 Anchorage-independent colony formation assays

Noble agar (Difco, 214230) was dissolved via boiling in 1X PBS to 1. % (w/v). This was maintained at 50 °C when not in use. 1. % (w/v) agar was mixed 1:1 with warmed DMEM (refer to 2.2 for media composition) to give 0.6% (w/v) agar. 2 mL of 0.6% (w/v) agar was quickly added to the bottom of 6 well plates and allowed to cool to form a solid layer for 15 min. The cells to be used in the tumour formation assay were then passaged and counted, with special attention made to ensure a single-cell solution. 1.2% (w/v) agar was then mixed with warmed DMEM at a ratio of 1:3 to give a 0.3% (w/v) agar solution. After cooling to a suitable temperature, cell solution was added to give a final concentration of 20,000 cells (for AML cells) or 10,000 cells (for MEFs) per well. After gentle mixing, 3 mL of 0.3% (w/v) agar cell suspension was added on top of the existing 0.6% (w/v) agar plug. The agar was allowed to cool for 1 h to allow the agar to solidify, before overnight incubation at 37 °C. The following day, 3 mL of media (containing drug if applicable) was added carefully on top of the solidified agar layers. Media was changed twice per week and colonies were allowed to grow to a suitable size (typically 2 weeks for the MEF cells, 3-4 weeks for AML cells). Conditions were run in triplicate (3 wells per condition) with multiple images taken per well. Every colony per image was counted. Colony diameter was measured in ImageJ in pixels and

converted by a scaling factor of 2.15 to calculate the diameter in μm . In regrowth assays, media was replaced with fresh media in the absence of drug treatments (twice weekly) and colony growth was assessed 2-4 weeks later.

2.11 Wound scratch cell migration assays

Cells were seeded at a high confluency in 12-well plates (350,000 cells/well) and grown to full confluency overnight. Next, cells were scratched in a straight vertical line using a 200 μL pipette tip to form a wound within the confluent cell layer. Media was next aspirated before being replaced with serum starved media (2% (v/v) FBS) including the drug to be assayed or vehicle (DMSO). “Wounds” were immediately imaged via stereomicroscopy at 4x, and a pen marking was made for later reference of the area to be observed. At set time points (typically 24 h and 48 h), wounds were imaged again to visualise closure of the wound over time. When wound closure was complete (or after 72 h had elapsed) the assay was stopped. The area of wound scratches was calculated in ImageJ and closure was recorded as a percentage.

2.12 CyQUANT Cell Proliferation Assays

CyQUANT cell proliferation assays were purchased from ThermoFisher (C7026). 1000 cells were seeded per well. After a 4 h attachment period, cells were washed and media was replaced with drugged full-serum media and cells were allowed to proliferate for 24 h. After 24 h, media was removed completely, and plates were frozen briefly at -80°C prior to lysis in 200 μL of the provided cell lysis buffer supplemented with CyQUANT GR dye. Samples were incubated for 4 min in the dark prior to fluorescent measurement with 480 nm excitation and 520 nm emission.

A standard curve was also produced. 0, 500, 1000, 1500, 2000, 4000, 8000, and 12,000 cells were seeded per well in triplicate. After a 4 h attachment period, media was removed, and plates were frozen and then quantified as described above. The curve was used to quantify the cell counts in treated samples after the 24 h proliferation period. Results are reported as a fold change from 1000 seeded cells. Separate standard curves were produced for each cell line used.

2.13 Reverse Transcriptase quantitative Polymerase Chain Reaction (RT-qPCR)

TSC2⁽⁺⁾ or *TSC2*⁽⁻⁾ AML Cells were grown in 6-well plates until 70-80% confluency. Cells were washed and media was replaced with drugged (where applicable) serum reduced (2% (v/v) FBS) media. Cells were treated for 24 h prior to washing in PBS and collection in

RNAprotect reagent (Qiagen, 76106). Samples were frozen at -80°C . RNA was extracted from samples using Qiagen's RNeasy mini kit (Qiagen, 74014) with QIAshredder spin columns (Qiagen, 79656). RNA was stored at -80°C . RNA was quantified using QubitTM broad range RNA assay (ThermoFisher, Q10210). cDNA was generated from extracted RNA using Reverse Transcriptase Core Kit (Eurogentec, RT-RTCK-03). cDNA samples were then quantified using QubitTM dsDNA broad range assay (ThermoFisher, Q32850) and normalised to $5\ \mu\text{g}/\text{mL}$. RT-qPCR was performed using TakyonTM ROX Sybr mastermix dTTP blue (Eurogentec, Belgium). Fold changes were calculated with the $\Delta\Delta\text{Ct}$ method. When comparing between *TSC2*-deficient or expressing AML cells, Ct values were normalised to *HMBS*. Initially *TUBA1A* and *IPO8* were used to normalise drugged *TSC2*-deficient cell experiments, however RNA sequencing data showed that *TUBA1A* may be influenced through mTORC1 inhibition, so *IPO8* was used as the sole housekeeping gene. Primers were designed on Primer-BLAST and were purchased from Integrated DNA Technologies. Primers were optimised for annealing temperature and efficiency prior to use. Primer pairs for *IL6*, *HMBS*, *IPO8*, *TNFRSF1A*, and *TNFRSF1B* were optimised and provided by Mr Jesse Champion. Dissociation curves were run to validate primer specificity.

Primers:

Gene	Forward Primer (5' – 3')	Reverse Primer (5' – 3')	Annealing Temperature (°C)	CPE	Amplicon Length (bp)
<i>ICAM1</i>	CCCTGATGG GCAGTCAAC AG	GGCAGCGTA GGGTAAGGT TC	58.4	1.9799	119
<i>FN1</i>	ACAACACCG AGGTGACTG AGAC	GGACACAAC GATGCTTCCT GAG	60	1.9656	143
<i>IL6</i>	CAGCCACTC ACCTCTTCAG A	GCCTCTTTGC TGCTTTCACA	56.4	2	119
<i>CCL2</i>	AGAATCACC AGCAGCAAG TGTCC	TCCTGAACCC ACTTCTGCTT GG	60.5	2.3868	98
<i>IL1B</i>	CCACAGACC TTCCAGGAG AATG	GTGCAGTTC AGTGATCGT ACAGG	60	2.0448	131
<i>IL15</i>	AACAGAAGC CAACTGGGT GAATG	CTCCAAGAG AAAGCACTT CATTGC	61.6	2.0783	148
<i>LAG3</i>	GCAGTGTAC TTCACAGAG CTGTC	AAGCCAAAG GCTCCAGTC ACCA	62	2.0514	143

<i>IPO8</i>	ACTGTTGCAC ATTGTTAGA G	ACTTTGCCAA ATATCTCAGC	51.7	1.85	138
<i>HMBS</i>	ATGGGCAAC TGTACCTGAC T	TCCTCAGGG CCATCTTCAT G	58.2	1.97	115
<i>VSIR</i>	CAGAAGTTC CTCTGCGCGT C	ACATACAGG GAATACGGC GTG	63	1.9263	158
<i>PDCD1LG2</i>	GAACCCAGG ACCCATCCA AC	TTCAGATAG CACTGTTTAC TTCCC	59	2.0765	184
<i>TNFRSF1A</i>	AGGAAATGG GTCAGGTGG AG	GGTGTCTGT TTCTCCTGGC	56.4	1.83	173
<i>TNFRSF1B</i>	GGGCCAACA TGCAAAAGT CT	CCACCTGGTC AGAGCTACA G	56.4	2.01	140

Table 2.2 Primer pair sequences and optimisation.

2.14 Neurodifferentiation

N2B27 Media Composition	Volume for 150 mL Media
DMEM/F12 1:1 (Thermo Fisher, 12634-010)	100 mL
Neurobasal (Thermo Fisher, 21103049)	50 mL
B27 supplement $-/+$ retinoic acid (Thermo Fisher, 12587010, 17504001)	1 mL
N2 supplement (Thermo Fisher, 17502001)	1 mL
Penicillin streptomycin glutamine (Thermo Fisher, 10378016)	1.5 mL
β -mercaptoethanol (Sigma Aldrich, M3148)	150 μ L

Table 2.3 N2B27 $+/-$ RA Neurodifferentiation media composition.

The following protocol is the standard protocol used by the Harwood lab group for the generation of glutamatergic forebrain neurons from iPSCs. Prior to the start of neurodifferentiation (day -2) confluent well of iPSCs were passaged with GCDR as described previously and plated onto cultrex-coated 12-well plates. Cells were typically passaged at a ratio of 1:5-1:6. iPSCs were maintained in E8 until they were 70-80% confluent. After which, cells were washed with D-PBS before media was swapped to N2B27 $-$ RA (day 0) (see Table 2.3). Cells were maintained in 1.5 mL N2B27 $-$ RA with 100 nM LDN193189 (Tocris, 6053) and 10 μ M SB431542 (Tocris, 1614), with half medium changes

every 1-2 days. Cells were maintained for 8-12 days until multi-layered colonies of cells were apparent. From day 10 onwards, N2B27 –RA without LDN193189/SB431542 was used.

Once multi-layered colonies were apparent, cells were pre-treated for 2 h with 10 μ M Y27632. Following this, cells were washed with D-PBS prior to incubation in 500 μ L 0.05 mM versene (Thermo Fisher, 15040066) at 37 °C for 3 min. Versene was then aspirated and 500 μ L fresh N2B27 –RA with 10 μ M Y27632 was added to each well. Cells were detached from the plate by gently scratching with a 1000 μ L pipette tip. Cells were collected and split at a ratio of 1:1.5 onto fibronectin- (Millipore, FC010) coated plates with 1.5 mL fresh N2B27 –RA + 10 μ M Y27632. In the case of PGP1-*TSC2*^(-/-) cells, a splitting ratio of 1:1 was used instead. Cells were maintained for around 9-10 days, at which point multilayer colonies of neural rosettes could be seen (day 18-22).

When neural rosettes were present (day 18-20), cells were pre-treated with Y27632 prior to passaging with versene as described before (1-2 min 37 °C) onto Poly-D-Lysine (PDL)-laminin coated plates. Plates were prepared by incubation with 0.5 mL/well 0.001% (w/v) PDL in sterile ddH₂O (Sigma Aldrich, P6407-5MG) before washing with D-PBS. Plates were then incubated overnight with laminin 15 μ g/mL (Sigma Aldrich, L2020, 1MG) in sterile ddH₂O at 37 °C. Cells were passaged at a ratio of 1:3, or 1:2 for *TSC2*^(-/-) cells.

From day 26 onwards, N2B27 –RA was replaced with N2B27 +RA media. From day 25 onwards neurites were visible. The early neuronal stage occurred at roughly day 30, with mature neurons typically forming around day 50.

Cells were passaged again at day 30 at a ratio of 1:3 (or 1:4 for *TSC2*^(-/-) cells) as described before, onto PDL-laminin coated plates to account for proliferation of remaining NPCs.

2.15 PGP1 *TSC2*-knockout validation

Initially, work was carried out to develop a clustered regularly interspaced short palindromic repeat (CRISPR)-Cas9 induced knockout of *TSC2* within iPSCs. This process was unsuccessful. Following this, a mixed pool of CRISPR-Cas9-induced *TSC2*-knockout PGP1 iPSC cells were purchased from Synthego (Redwood City, California). Sequencing revealed a 55% knockout score within the mixed pool (Figure 2.1)

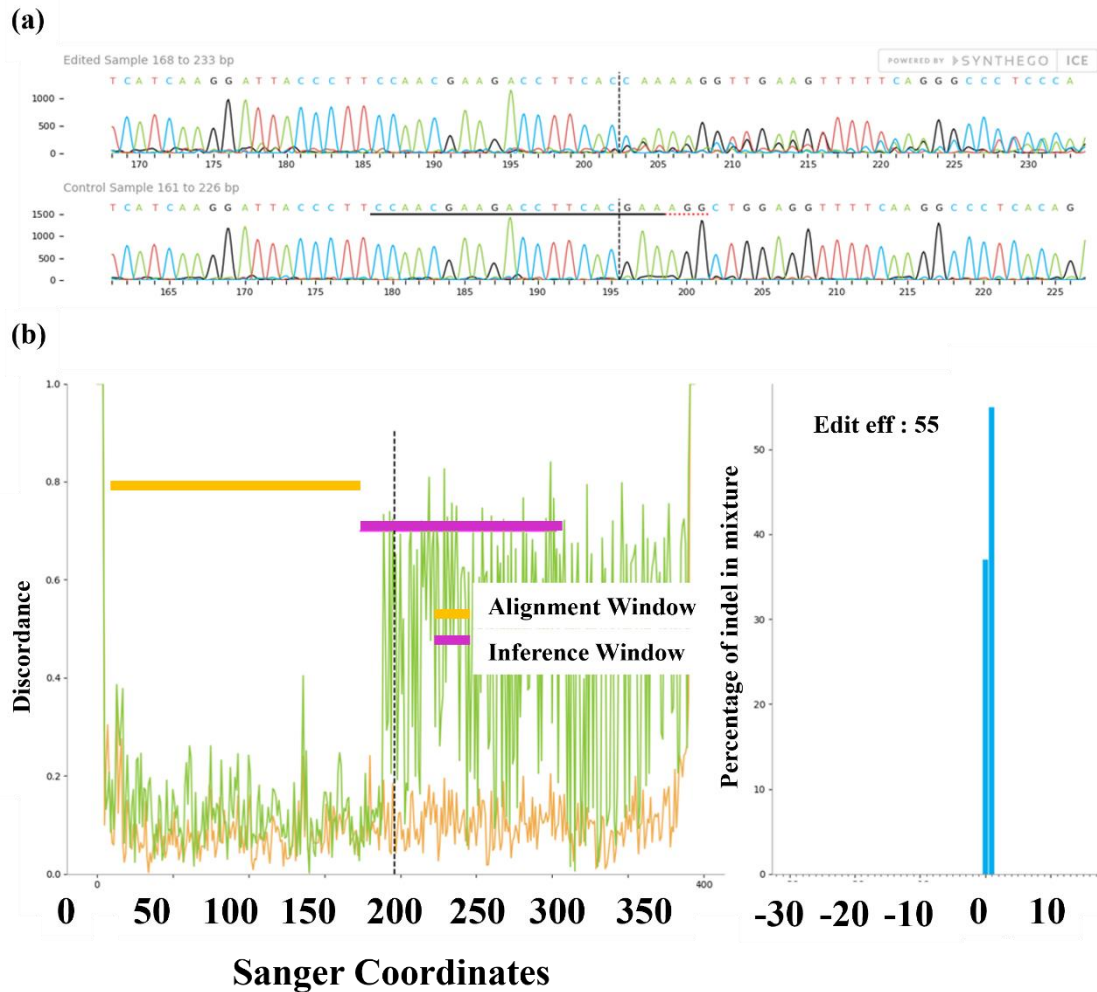


Figure 2.1. Sequencing data of PGP1 *TSC2*-CRISPR-Cas9 transfected cell pool. (a) Sanger sequence read showing the edited region (top) of DNA around the selected guide sequence following CRISPR-Cas9 transfection. The horizontal black line represents the guide sequence. The black dotted line shows the cut site, with error prone repair causing a mixed insertion of base sequences that follows the cut site. (b) The discordance and indel plot show a change in overall alignment between bases of the wild-type control and the edited sample around the interference window. The indel plot demonstrates a 55% presence of 1-base insertions within the sample population.

PGP1 iPSCs were single cell cloned and sequenced to generate pure *TSC2*-knockout clones.

2.15.1 DNA extraction and qPCR

iPSCs were cultured prior to dissociation with GCDR. Cells were collected, pelleted, and then frozen at $-20\text{ }^{\circ}\text{C}$. DNA was extracted using an AllPrep DNA/RNA/Protein kit (Qiagen, 80004) following the manufacturer's instructions. To confirm successful DNA extraction, samples were run on a 1.0% (w/v) agarose Tris acetic acid EDTA (TAE) gel with GelRed

nucleic acid gel stain (Biotium, 41003) (100 V, 30 min) and samples visualised under UV. Primers targeting the sequence site were purchased from Integrated DNA Technologies (Forward 5'-3': AATGCTGATGCTGCAGACCT; Rev 5'-3': ATGAAGCAGGGTGGGCATAC). An optimal annealing temperature of 65.4 °C was used. PCR was carried out using megamix gold (Microzone, 2MMG) with 12.5 µL megamix, 50 pM (each primer final concentration), 5 ng/µL DNA, made to 25 µL in PCR-grade water. The following cycle conditions were used.

<u>Cycle Condition</u>	<u>Time</u>
Initial denaturation: 95 °C	5 min
<u>Cycle begin: 35x</u>	-
Denaturation: 95 °C	1 min
Annealing: 65.4 °C	1 min
Extension: 72 °C	1 min
<u>Cycle end</u>	-
Final extension: 72 °C	5 min
Store: 4 °C	∞

To confirm product amplification, samples were run on a 1.5% (w/v) agarose gel (100 V, 30 min) and visualised under UV. Excess nucleotides were removed using a mixture of shrimp alkaline phosphatase (Thermofisher, 783901000UN) and Exonuclease 1 (*ExoI*) (Thermofisher, EN0581) with a ratio of 2:1, with 1 µL of ExoSAP mixture added to 20 µL of PCR product. Samples were then processed with the following conditions.

<u>Cycle Condition</u>	<u>Time</u>
Activate: <i>ExoI</i> 37 °C	1 h
Deactivate: <i>ExoI</i> 95 °C	15 min
Store: 4 °C	∞

2.15.2 BigDye and Sanger sequencing

In preparation for Sanger sequencing, BigDye terminator (Thermofisher, 4337449) was used to generate variable fluorescently-capped transcripts of the PCR transcripts. Reactions include 2 µL 5x sequencing buffer, 0.75 µL BigDye terminator mix v1.1, 1 µL template, and

1 μL of either the forward or reverse primer. Samples were then processed with the following conditions.

<u>Cycle Condition</u>	<u>Time</u>
Initial denaturation: 96 °C	5 min
<u>Cycle begin: 30x</u>	-
Denaturation: 96 °C	30 s
Annealing: 50 °C	15 s
Extension: 60 °C	4 min
<u>Cycle end</u>	-
Store: 4 °C	∞

Following BigDye, samples were purified with isopropanol. 40 μL of 75% (v/v) isopropanol was added to each 10 μL reaction volume and allowed to incubate at room temperature for 30 min. Samples were then centrifuged at 4000 rpm at 4 °C for 45 min. Isopropanol was blotted off, prior to spinning plates inverted over a paper towel at 500 rpm for 30 s. Plates were allowed to dry at room temperature for 10 min in the dark. 10 μL of HiDi formamide (Thermofisher, 4311320) was added to resuspend DNA. Sequences were analysed on an ABI 3730 analyser (Applied Biosystems) and read using the online inference of CRISPR edits tool provided by Synthego.

2.16 Statistical analysis

Normality testing in Prism9 was carried out with a D'agostino & Pearson and Shapiro-Wilk test. Normally (Gaussian) distributed data was then analysed by an ordinary one-way analysis of variance (ANOVA) with Tukey's multiple comparisons or two-way ANOVA with Šídák's multiple comparisons tests. If comparing treated samples to only a DMSO control, data was analysed by one-way ANOVA with Dunnett's multiple comparisons. When analysing 2 groups only, a parametric unpaired t-test was carried out. Data are presented as mean \pm SEM. Non-normally distributed data were assessed by the Kruskal-Wallis test, with Dunn's multiple comparisons tests. If the comparison was between only two groups, nonparametric Wilcoxon t-tests were instead carried out. p-values: * < 0.05, ** < 0.01, *** < 0.001, **** < 0.0001, and not significant (ns). Repeats for *in vitro* experiments were performed (unless specified) by simultaneous culture of separate cell-culture flasks, prior to passage of these into individual wells to generate multiple samples. One repeat represents sample collected from one well. In this sense, "*n* = 3" refers to three biological replicates.

Chapter 3 - Exploring Inflammatory Pathways

3.1 Introduction

As discussed within Chapter 1, the most well-characterised phenotype of TSC is hyperactive mTOR resulting in aberrant cell growth and the system-wide formation of tumours. However, inflammatory signatures have also been identified in TSC and are suspected to be related to many of the neurological manifestations of the disease (333). Inflammation plays significant roles in a variety of cancers, as well as various neurological and neuropsychiatric diseases, marking inflammatory processes as being fundamental in our understanding of effective treatment for such conditions. Little research so far has addressed these inflammatory pathways in TSC, and less so specifically in TSC-derived brain tumours. This is potentially a serious oversight, given that conditions such as epilepsy and autism have links to neuroinflammation (210,359) and are prevalent in TSC.

Neuroinflammation has been identified in the brains of TSC patients, as well as within *in vitro* studies (290,333,360,361). It should be noted that many current studies either focus on *in vivo* heterogeneous cell populations or instances of *TSC1* deficiency, rather than *TSC2*. This may be detrimental in the analysis of TSC-linked neuroinflammation as the pro-inflammatory transcription factor, Y705-pSTAT3, appears enhanced more so in *TSC2* null cortical spheroids than *TSC1* and wild-type (362). Few studies have investigated *TSC2*-deficiency in a pure *TSC2*-null *in vitro* model of brain tumours, meaning that we lack information on the true disease-causing cell of TSC-derived brain tumours. Also, the true pathophysiological role that inflammatory pathways play in TANDs are not currently well understood. It is also not clearly known how TSC results in the activation of inflammatory pathways. Complex signal interplays have been hinted at in some studies, wherein rapamycin treatment causes enhanced NF- κ B activation, but diminished pSTAT3 (49). Interestingly, this pattern is reversed upon loss of *TSC2*.

It is suggested that mTORC1 inhibition by rapamycin has some effect on reducing the inflammatory phenotype, proving efficacy in reducing STAT3 activation in *TSC1* or *TSC2* null brain cells *in vitro* (362). However, the efficacy of rapamycin in the treatment of neurological symptoms is not always effective, with occurrences of treatment resistant epilepsy reported as two thirds in the sufferers of TSC-linked epilepsy (36,363). In addition, mTOR inhibition often presents side effects, notably immunosuppression and in serious cases, can lead to infection (364). Treatment with mTORC1 inhibitors must also be continual

as they are cytostatic rather than cytotoxic, meaning that tumours regrow upon discontinuation of treatment. Additionally, *in vitro* models suggest that rapamycin treatment must fall within a certain time window during neurodevelopment, as treatment left too late cannot reverse the (highly glial) phenotype in *TSC2* deficiency (362).

Data on the use of anti-inflammatories in TSC is limited. While reduction in inflammatory pathway activation (such as STAT3) has been noted, these are normally identified as a response to mTORC1 inhibition, rather than direct inhibition of offending pathways (49,365,366). Interestingly, treatment with cannabidiol (a well-tolerated anti-inflammatory (367)) has offered a remarkable reduction in the prevalence of epilepsy that are refractory to standard anti-epileptic drugs (368). This offers a tantalising insight into the potential of anti-inflammatory medications for the treatment of TANDs.

The aim of this chapter was to confirm whether inflammatory pathways were upregulated within TSC, both *in vitro* and *in vivo*. This would provide an initial basis with which to continue further research on inflammatory pathways and subsequent consequences in TANDs and neural development in TSC. For this, it was hypothesised that cells harbouring defective *TSC2* would exhibit heightened inflammatory pathways and demonstrate a differential response to inflammatory stimuli than wild-type counterparts. Another aim was to identify whether this enhanced inflammatory response was dependent on mTORC1 hyperactivity and was carried out with an array of pathway inhibitors.

3.2 Results

3.2.1 The TNF α and STAT3 pathways are differentially regulated in *TSC2*-deficient MEFs and AMLs.

The first aim of the study was to identify a dysregulated inflammatory response in *TSC2*-deficient cells. To identify this, *Tsc2*-deficient MEFs alongside their wild-type counterparts (as described in section 2.1.1) were assayed for inflammatory markers. The key markers which were analysed were S536 pRelA, and Y705 pSTAT3. The former is a marker of NF- κ B activation, and the latter is typically phosphorylated in to the active form through IL-6 signalling, and is implicated as a key inflammatory proponent in a variety of neurological conditions as well as glioblastoma (369–371).

Tsc2/TSC2-deficient or control MEFs or AMLs were treated with TNF α or IL-6 to determine differential responses to cytokine stimulation. Additionally, control cell lines were treated with media conditioned by their *TSC2*-deficient counterparts to determine if secreted factors contributed to the inflammatory condition (Figure 3.1).

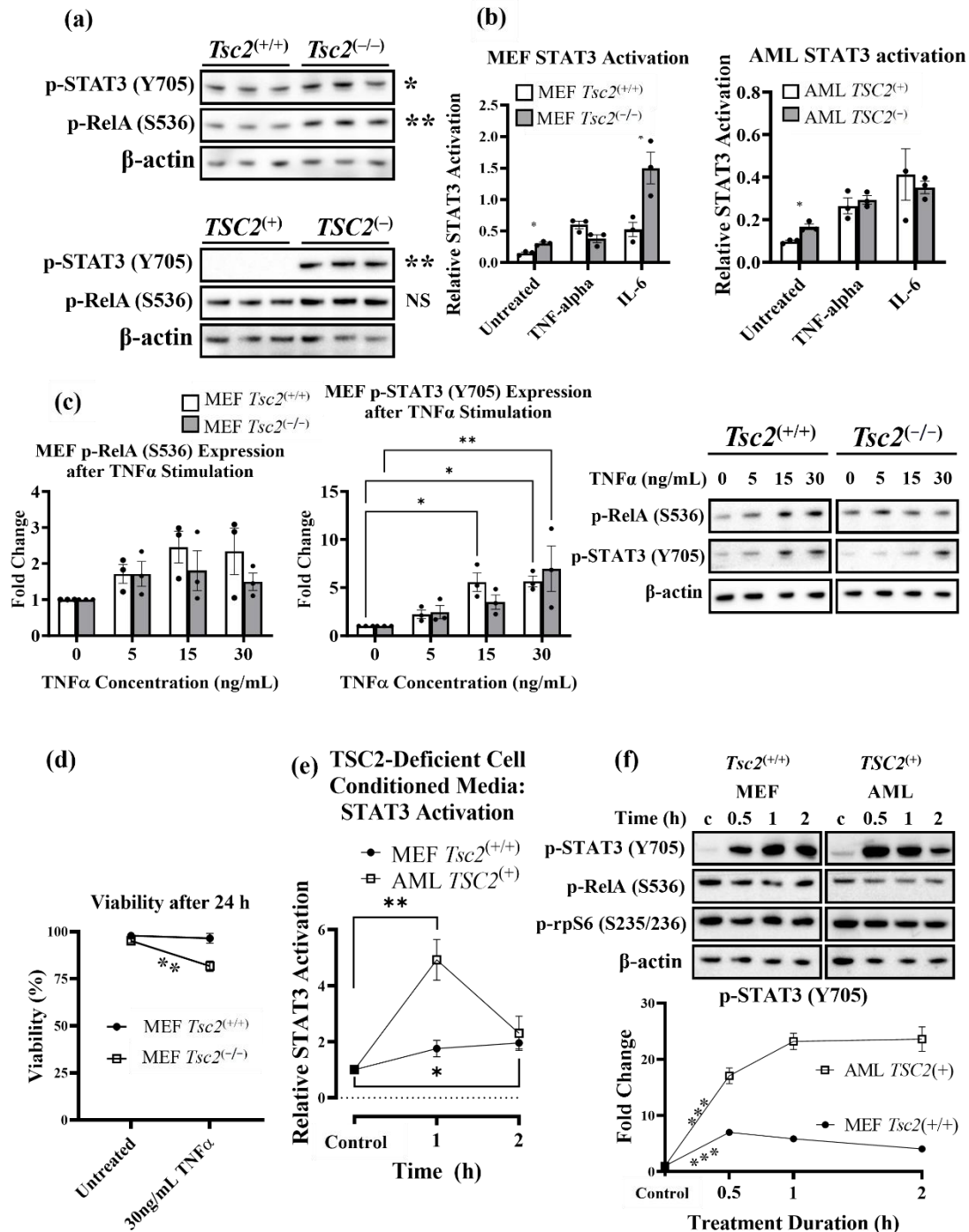


Figure 3.1. Inflammatory signalling in TSC2-deficient cells. (a) Confluent cells were serum-starved for 24 h and lysed. Western blot analysis of S536-phospho RelA and Y705-phospho STAT3 was carried out in *Tsc2*^(-/-) MEFs (top panel) and 621-101 AMLs (bottom panel), respectively. β -actin was used as a loading control, $n = 3$, unpaired t test. No signal was detected in *TSC2*⁽⁺⁾ AMLs, and a value

of zero was used for statistical analysis. The three wells for each cell type correspond to three separate replicates, as described in section 2.16. **(b)** Serum-starved *Tsc2*^(-/-) and *Tsc2*^(+/+) MEFs, and 621-101 and *TSC2*-rescued AML cells were stimulated with either 30 ng/mL TNF α for 2 h or 50 ng/mL IL-6 for 1 h, as indicated. STAT3 activity assays were carried out. $n = 3$, unpaired t-tests. **(c)** Serum-starved *Tsc2*^(+/+) and *Tsc2*^(-/-) MEFs were stimulated with TNF α (0, 5, 15, or 30 ng/mL for 2 h). S536-phospho-RelA and Y705 phospho-STAT3 were assessed by western blot analysis. Fold changes from untreated samples for each respective cell line are shown. β -actin levels were analysed as a loading control and used to normalise densitometry analysis ($n = 3$). **(d)** Viability assays were carried out on *Tsc2*^(+/+) and *Tsc2*^(-/-) MEFs treated with either DMSO or 30 ng/mL TNF α for 24 h. $n = 3$, unpaired t-test. **(e)** Serum-starved *Tsc2*^(+/+) MEFs or *TSC2*⁽⁺⁾ AMLs were stimulated with conditioned media from serum-starved *Tsc2*^(-/-) MEFs or *TSC2*⁽⁻⁾ AMLs, respectively, and STAT3 transcription assays were carried out after 1 and 2 h of stimulation. *Tsc2*^(+/+) MEFs or *TSC2*⁽⁺⁾ AMLs were treated for 2 h with media conditioned by *Tsc2*^(+/+) MEFs or *TSC2*⁽⁺⁾ AMLs, respectively, to act as controls (“Control”). $n = 3$, one-way ANOVA with Tukey’s multiple comparisons. **(f)** Serum-starved *Tsc2*^(+/+) MEFs or *TSC2*⁽⁺⁾ AMLs were stimulated with conditioned media from serum-starved *Tsc2*^(-/-) MEFs or *TSC2*⁽⁻⁾ AMLs, respectively, and western blot analysis of S536-phospho RelA, Y705-phospho STAT3, and S235/235-phospho RPS6 was assayed at 0.5, 1, and 2 h of treatment duration. *Tsc2*^(+/+) MEFs or *TSC2*⁽⁺⁾ AMLs were treated for 2 h with media conditioned by *Tsc2*^(+/+) MEFs or *TSC2*⁽⁺⁾ AMLs, respectively, to act as controls (“c”). Y705-phospho STAT3 is also shown graphically via densitometry analysis. figures e-f were analysed with two-way ANOVA with Tukey’s multiple comparisons. Western blot densitometry was normalised to β -actin.

While varied in direction, this data clearly shows dysregulation within inflammatory pathways in *TSC2*-deficient cells. Two main inflammatory markers have been picked out for these analyses. These were S536-pRelA and Y705-pSTAT3 to signify NF- κ B and JAK/STAT3 pathway activation, respectively. Notably, these pathways were enhanced within both *Tsc2*^(-/-) MEFs and *TSC2*⁽⁻⁾ AMLs when compared to their respective *TSC2*-expressing cells (Figure 3.1a, densitometry results shown in Table 3.1). Not shown in this analysis was a third cell model. These were ELT3 cells, derived from rat kidney tumours with non-functional *Tsc2*. In this cell model, STAT3 and RelA phosphorylation on the Y705 and S536 residues was also significantly upregulated within *Tsc2*-deficient cells, compared to their *Tsc2*-re-expressing counterpart.

	Pixel density average fold increase in $Tsc2^{(-/-)}$ MEFs	MEF p-value	Pixel density average fold increase in $TSC2^{(-)}$ AMLs	AML p-value
Y705-pSTAT3	1.438	0.0141	(No signal detected in $TSC2^{(+)}$ cells)	<0.00001
S536-pRelA	1.828	0.0116	1.810	0.2792

Table 3.1. Fold increases of STAT3 and RelA phosphorylation between *TSC2*-deficient and *TSC2*-restored MEF and AML cell lines, determined by western blot pixel densitometry. Average pixel densitometries: (**p-RelA (S536)**): *Tsc2*^(-/-) MEFs: 4067; *Tsc2*^(+/+) MEFs: 2225; *TSC2*⁽⁺⁾ AMLs: 5640; *TSC2*⁽⁻⁾ AMLs: 10207. (**p-STAT3 (Y705)**): *Tsc2*^(-/-) MEFs: 4877; *Tsc2*^(+/+) MEFs: 3667; *TSC2*⁽⁺⁾ AMLs: 0; *TSC2*⁽⁻⁾ AMLs: 6707.)

The study next aimed to investigate whether STAT3 and NF- κ B pathway activation could be attributed to a greater sensitivity of *TSC2*-deficient cells to cytokine activity, with the rationale that this could account for the increased inflammatory activity. To do this, STAT3 activity was assayed via transcriptional activation ELISA in *Tsc2*^(-/-) and wild-type MEFs, as well as *TSC2* and *TSC2*-restored AMLs after treatment with either TNF α or IL-6 (Figure 3.1b). While this experiment confirmed that STAT3 was more active within *TSC2*-deficient cells (MEF $n = 4$ ($p = 0.0041$), AML $n = 4$ ($p = 0.0089$)), we generally saw no significant difference in STAT3 activation from cytokine stimulation between *TSC2*-deficient and *TSC2*-expressing cells. This was with one exception, where the *Tsc2*^(-/-) MEFs showed a greater degree of STAT3 nuclear activation after stimulation with IL-6 ($n = 4$, $p = 0.0041$) than the *TSC2*-expressing counterpart. Predominantly, this data demonstrates that the NF- κ B pathway (as activated by TNF α) and STAT3 pathway are linked, since TNF α stimulation causes STAT3 activation in all cell types. The data also hints towards at least some degree of enhanced sensitivity to cytokine stimulation within *TSC2*-deficient cells.

To further investigate the crosstalk between TNF α -induced NF- κ B and Y705 STAT3 activation, MEF cells were stimulated with a dose range of TNF α cytokine. In initial experiments that were underpowered, a higher sensitivity to TNF α stimulation was observed within *Tsc2*^(-/-) MEFs, when compared to wild type. However, this finding was not evident with related TNF α stimulation experiments. For instance, with further experiments it appears that *Tsc2*^(+/+) MEFs exhibited a greater phosphorylation of STAT3 on Y705 than *Tsc2*^(-/-) MEFs (Figure 3.1c). In this set of experiments, it should be noted that untreated samples of each respective cell line were used as their own control, *i.e.*, *Tsc2*^(+/+) MEFs

treated with TNF α are reported as fold changes from untreated *Tsc2*^(+/+) MEFs, and not compared directly to *Tsc2*^(-/-) MEFs. Comparisons between untreated cells show an average fold change between *Tsc2*^(-/-) and *Tsc2*^(+/+) MEFs in RelA and STAT3 phosphorylation by 1.8-fold and 1.0-fold respectively (not shown).

Differences observed with inflammatory pathway activation could be linked to secreted inflammatory cytokines. To look at whether secreted cytokines could be involved, media was taken from *TSC2/Tsc2*-deficient AML/MEF cells. This conditioned media was then supplemented to their corresponding wild type MEF and AML cells for 1 and 2 h, before these wild-type cells were harvested and processed for STAT3 transcriptional activity assays (Figure 3.1e). As a control, media was taken from *TSC2/Tsc2* expressing AML/MEF cells and used to treat *TSC2/Tsc2*-deficient AML/MEF cells, respectively, to negate any effects caused by the act of media changes. Interestingly, a large spike in STAT3 activity was observed after 1 h of treatment within *TSC2*-restored AML cells ($n = 4$, $p < 0.0001$), followed by a decrease in STAT3 activity between the 1 h and 2 h time point ($p < 0.0001$). *Tsc2*^(+/+) MEFs also showed a significant enhancement after 2 h of treatment ($p = 0.0239$), although not to the same degree as observed in AML cells. This data provides a very clear picture that secreted factors may play a key role within the inflammatory state of *TSC2*-deficient cells.

Interestingly, the peak in STAT3 activation for AML cells occurred at the 1 h time point and then appeared to diminish at longer time points. In the earlier optimisation data (not shown), we found that IL-6 appeared to peak (in terms of Y705 STAT3 phosphorylation) around the 45-60 min time points before decreasing at longer times. Additionally, transcriptomic data of AML cells (discussed later) shows an 8.5-fold increase in IL6 mRNA levels ($n = 6$, $p < 0.00001$). Furthermore, *TSC2*-deficient AML cells showed a 9.5-fold increase in mRNA levels of the cysteine protease, *CTSS* ($p < 0.00001$), which has been shown to cleave IL-6R to promote trans-signalling as well as being secreted from the cell itself (372). Therefore, it may be hypothesised that the enhanced activation of STAT3 in *TSC2*-deficient cells may be attributed in part to an increased production of inflammatory cytokines such as IL-6 that then act in an autocrine or paracrine manner. *In vivo*, it may be possible to also find increased levels of sIL-6R generated from neighbouring cells in TSC-derived patient tumours, and this prediction is supported by increased levels of Cathepsin S (15.7-fold) within SEN/SEGAs, as ascertained from Jeffrey Mackeigan's transcriptomic dataset. Additionally, while TNF α production does not appear to occur in AML cells, *TSC2*-deficient AML cells have enhanced expression of lipopolysaccharide induced TNF factor (*LITAF*) mRNA (2.38-fold, $p <$

0.00001, when compared to wild type). LITAF is a secreted factor that functions to enhance the production of TNF α from neighbouring immune cells.

With the indication that cytokine signalling is enhanced within TSC patient-derived tumours and TSC cell models, the study attempted to determine whether TNF α signalling may exhibit a differential effect on cell viability within *TSC2*-deficient cells (Figure 3.1f). We found that 24 h of TNF α at 30 ng/mL was able to induce a significant reduction in cell viability (2-way ANOVA, $p = 0.0028$) within *Tsc2*^(-/-) MEFs, but not *Tsc2*^(+/+) MEFs. *TSC2*⁽⁻⁾ and *TSC2*⁽⁺⁾ AMLs both demonstrated a small, but not significantly different, reduction in cell viability. As discussed in Chapter 1, the cell fate undergone after TNF α signalling is complex and not fully understood, with inflammation, survival, and cell growth being possible outcomes, alongside apoptosis and necrosis. A key determinant in pathway propagation appears to be RIPK1 ubiquitylation, wherein high RIPK1 ubiquitylation drives NF- κ B activation and inflammation, whereas a lack of ubiquitylation instead activates the TRADD-linked apoptosis pathway. This pathway could be the reason why apoptosis was apparent in *Tsc2*^(-/-) MEFs after treatment with TNF α , although this cannot be confirmed from this experimentation. Of note, while the data did not reach significance, both western blots and STAT3 transcriptional activation ELISAs seem to suggest that wild-type MEFs exhibit a higher level of STAT3 activation after TNF α stimulation than their *Tsc2*-deficient counterparts. Overall, this may suggest that cells which are more susceptible to TNF α -induced cell death are less sensitive to TNF α induced inflammation.

While not conclusive, the data gathered here may suggest that some *TSC2*-deficient cells may exhibit a greater sensitivity to TNF family receptor-induced cell death. Transcriptomic data support this also, with the FAS death receptor demonstrating a 1.5-fold upregulation in *TSC2*-deficient AML cells, and a 5.66-fold upregulation within SEN/SEGAs. Lastly, the adaptor protein which links death-receptors to the caspase cascade, FADD, is also upregulated by 1.42-fold within AMLs ($p = 0.00005$). Thus, therapies that make use of a potential sensitivity to programmed death pathways within *TSC2*-derived tumours may prove as an effective means of chemotherapy for TSC patients for example TNF α isolated limb perfusion, which has shown efficacy in the treatment of certain tumours (373). However, the data presented in the current study is not sufficient to state whether this would be an effective treatment option for TSC patients.

Altogether, these results clearly demonstrate an enhancement of select inflammatory pathway, notably the NF- κ B and STAT3 pathways. The results show that there is unlikely to be a specific enhancement of inflammatory sensitivity to inflammatory stimuli in *TSC2*-deficient cells, however it is likely that *TSC2*-deficient cells are producing and secreting more cytokines such as IL-6, thus generating a self-propagating immune-reactive, inflammatory environment.

3.2.2 Inflammatory and immune pathways are upregulated in SEN/SEGA *in vivo*.

With a currently basic confirmation that NF- κ B/STAT3 activation appears higher in *TSC2*-deficient cells *in vitro*, the study now sought to confirm that these findings could be represented *in vivo*. To do this, a transcriptome was kindly donated by the lab of Jeffrey MacKeigan in Michigan State University, detailing transcriptional differences between SEN/SEGAs within TSC brain tumours to patient matched healthy brain tissue. Notably, this patient matched healthy brain tissue would still be heterozygous for *TSC2*. 15 SEN/SEGA were compared to patient matched healthy tissue for this analysis. The top 300 upregulated genes were analysed using the online GeneAnalytics software to enrich for pathways and processes that were upregulated in SEN/SEGA. Data analysis was refined to select for upregulated genes that were specifically and directly linked to the immune and inflammatory processes (Figure 3.2.1). DEGs were annotated within volcano plots to demonstrate the high prevalence of inflammatory pathways within *in vivo* TSC patient-derived tumours. GO analysis did not reveal an inflammatory signature within downregulated DEGs. A similar Bioinformatic analysis was also performed on 15 cortical tubers from the same dataset (Figure 3.2.2).

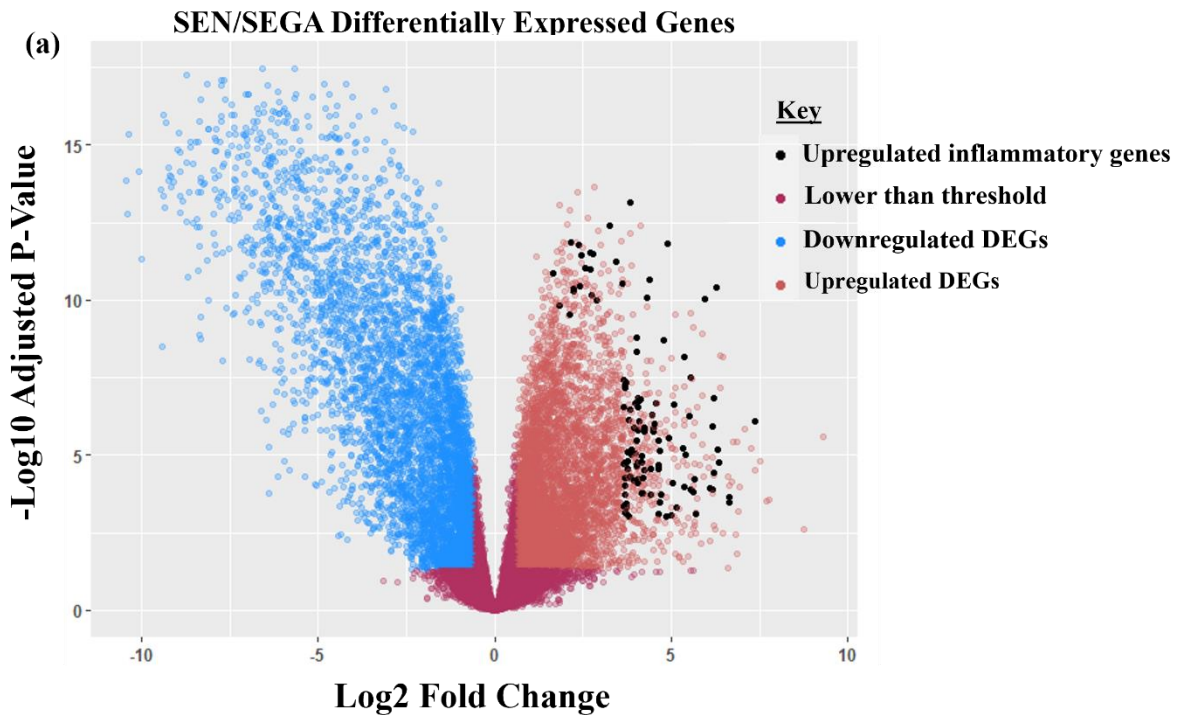


Figure 3.2.1. Inflammatory and immune pathways are dysregulated in TSC patient-derived SEN/SEGAs. (a) SEN/SEGA patient samples were collected and processed as described in (51). This dataset was used to generate a volcano plot. GO analysis was performed on the top 300 upregulated DEGs, and all inflammatory/immune response genes were emphasised on the plot to demonstrate the dysregulated inflammatory nature in these tumours.

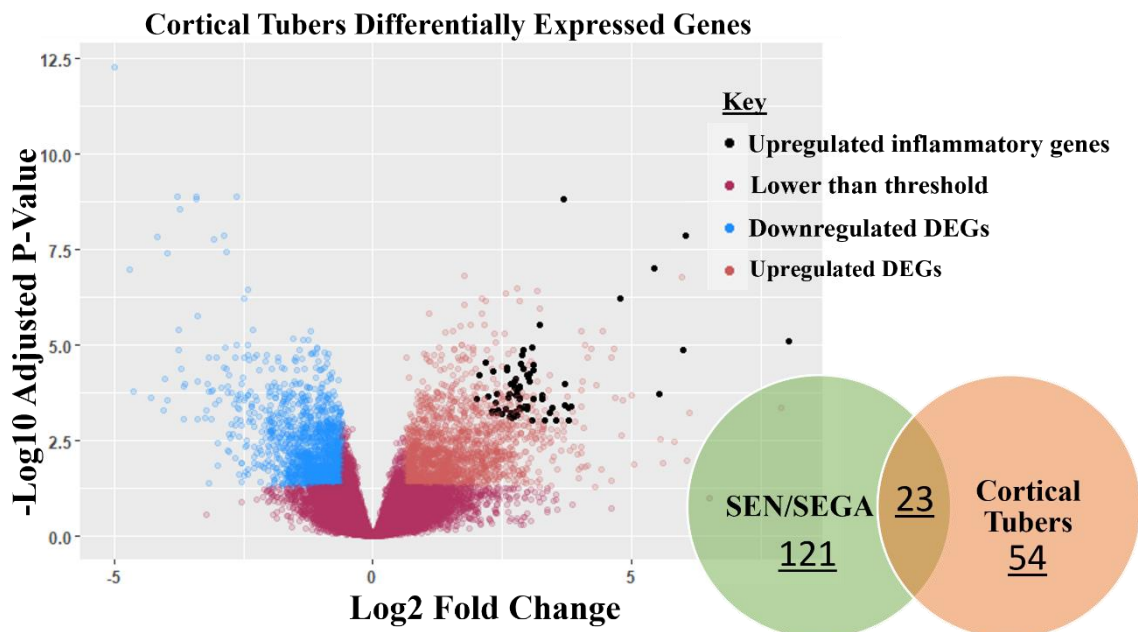


Figure 3.2.2. Inflammatory and immune pathways are dysregulated in TSC-patient derived cortical tubers. This figure is similar to Figure 3.2.1, except the cortical tuber dataset was used with the top 150 upregulated DEGs. A comparison between upregulated inflammatory DEGs between

SEN/SEGAs and cortical tubers is shown, demonstrating a relatively low overlap of dysregulated inflammatory genes in this GO analysis (23 shared DEGs). However, it should be noted that a lower number of DEGs was used in the cortical tuber analysis due to a lower number of overall DEGs in the dataset.

Data collected from the SEN/SEGA transcriptome offered an insight into some of the most differentially upregulated pathways within SEN/SEGAs. GO analysis of the top 300 upregulated DEGs in SEN/SEGA presented 64 high match GO terms. Out of these 64 terms, 20 terms were directly related to immune and inflammatory responses. Of note, the 15 highest scoring terms included 13 terms which were directly related to immune/inflammatory responses. These were: Immune response, antigen processing and presentation, immune system process, antigen processing and presentation of peptide or polysaccharide antigen via MHC class II, interferon-gamma-mediated signalling pathway, regulation of complement activation, antigen processing and presentation of exogenous peptide antigen via MHC class II, neutrophil degranulation, inflammatory response, cytokine-mediated signalling pathway, innate immune response, complement activation, and adaptive immune response.

Interestingly, many of the genes which were upregulated within this transcriptome bore similarities to highly invasive glioblastoma subtypes (374,375). Another study highlights 20 of the most significantly upregulated and downregulated genes within glioblastoma, of which 14 were identified as directionally matching in upregulation or downregulation within SEN/SEGAs (376). Similarly, ontology data demonstrated multiple high-match pathways which were upregulated in the top 300 upregulated genes within SEN/SEGA, including the NF- κ B pathway. This demonstrates potential similarities between TSC patient-derived brain tumours and cancerous brain tumours. Similar ontological analysis of the most downregulated genes in SEN/SEGA did not return any inflammatory or immune-related pathways/GO terms.

The same transcriptomic analysis also included data from 15 cortical tubers compared to patient matched healthy tissue. An analysis of the top 150 upregulated DEGs demonstrated a similar pattern to that in the SEN/SEGAs, with 19 out of 38 GO terms corresponding directly to inflammatory or immune response. Of note, these included “Positive Regulation of Tumour Necrosis Factor Production” and “Positive Regulation of Chemokine Secretion”, thus providing further support for the hypothesis posed in Figure 3.1 of cytokines guiding the inflammatory state in TSC. The 16 highest scoring GO terms were associated with

inflammatory/immune processes, and NF- κ B was once again one of many highly matched inflammatory pathways in tubers.

DEGs from SEN/SEGAs were plotted on a volcano plot in RStudio. A threshold of $p > 0.05$ and a \log_2 fold change of < 0.5 fold / > -0.5 fold was used to signify genes that were not significantly upregulated or downregulated. All genes which appeared in the highly scoring section of immune/inflammatory pathways were then superimposed on this plot to highlight the highly inflammatory nature of SEN/SEGAs (Figure 3.2.1). An additional plot was generated with cortical tubers which demonstrated the same trends (Figure 3.2.2).

Since differential RelA phosphorylation was observed in both the AML and MEF cell models (Figure 3.1), a general snapshot of NF- κ B activity in TSC-derived tumours was also generated. Here, a large collection of NF- κ B regulator and target genes were used from a list developed by the Gilmore lab at Boston University (<https://www.bu.edu/nf-kb/gene-resources/target-genes/> (accessed November 22nd, 2022)), and this dataset was used to generate volcano plots of NF- κ B-related genes within TSC-patient tumours (Figure 3.2.3a) and *in vitro* 621-101 AMLs (Figure 3.2.3b). A similar plot was also generated for patient-derived cortical tubers (data not shown), which showed similar trends.

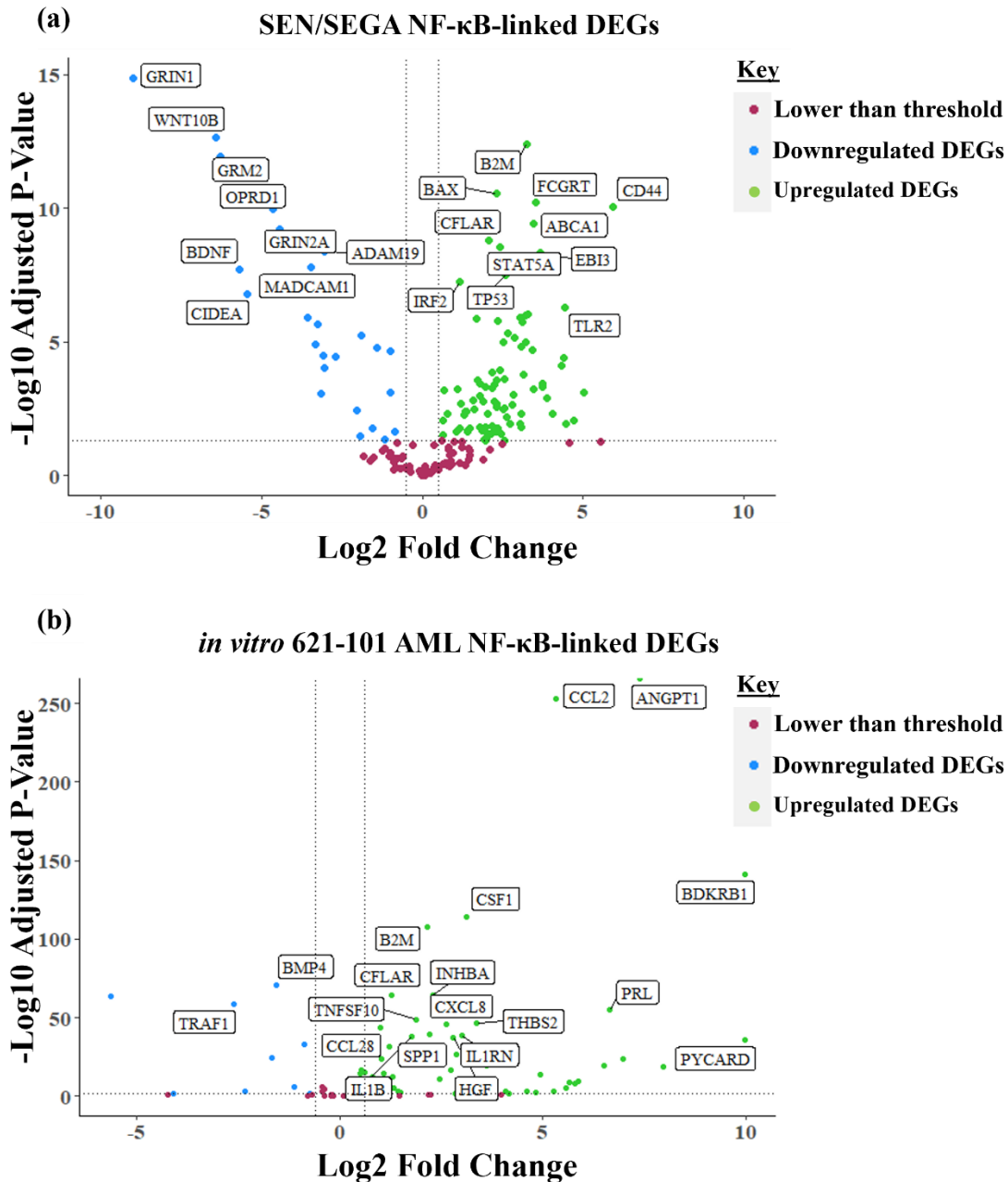


Figure 3.2.3. *TSC2*-deficient cells demonstrate dysregulated NF- κ B signalling. **(a)** NF- κ B regulator and target genes were plotted from the patient-derived SEN/SEGA dataset, the acquisition of which was described in Figure 3.1. **(b)** A similar analysis was performed in data generated from *in vitro* 621-101 *TSC2*⁽⁻⁾ AMLs. Both datasets show significantly dysregulated NF- κ B signalling.

This data highlights that NF- κ B signalling becomes dysregulated in TSC. While NF- κ B linked genes are both upregulated and dysregulated when compared to normal matched brain tissue in SEN/SEGAs, or 621-103 *TSC2* re-expressed AML cells, a general trend can clearly be seen within upregulation of the inflammatory pathway. Overall, this transcriptomic data confirms a highly inflammatory environment within TSC patient-derived brain tumours *in*

in vivo, and further suggests that *TSC2*-deficient cells propagate this environment by means of enhanced cytokine secretion, enhancing cytokine secretion in neighbouring cells, and attracting immune infiltrates.

3.2.3 STAT3 hyperactivation in *Tsc2*^(-/-) MEFs can be diminished by NF-κB inhibition.

With confirmation that the NF-κB and other inflammatory pathways are enhanced within TSC patient-derived tumours, the study next sought to identify signalling crosstalk between the NF-κB and STAT3 pathways. To do this, *Tsc2*^(-/-) and *Tsc2*^(+/+) MEFs were treated with BMS345541 or C188-9, inhibitors of IKKα/β or STAT3, respectively (Figure 3.3.1).

BMS345541 is a highly selective inhibitor of the IKK complex, with preferential inhibition of IKKβ to IKKα (377). C188-9 binds specifically with the Src homology 2 (SH2) domain of STAT3 (378)

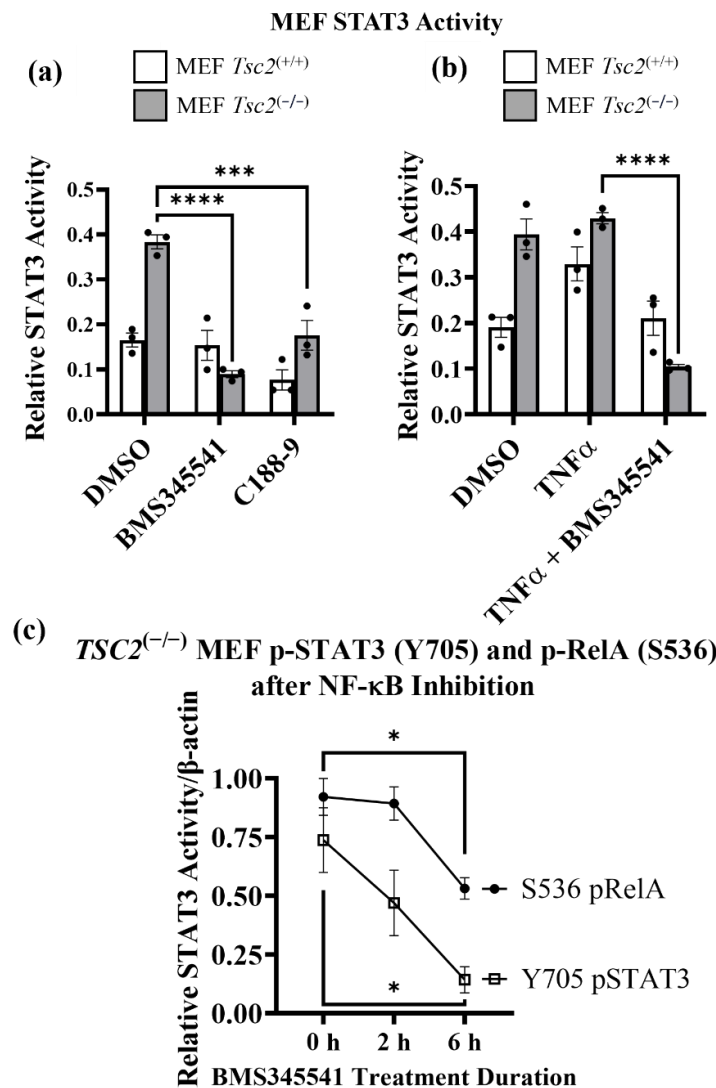


Figure 3.3.1 IKK inhibition results in STAT3 inhibition in *TSC2*-deficient cells. STAT3 activity ELISAs were carried out from nuclear lysates prepared from *Tsc2*^(-/-) and *Tsc2*^(+/+) MEFs treated with

either (a) DMSO, BMS345541 5 μ M or C188-9 15 μ M for 24 h or (b) TNF α (30 ng/mL 2 h treatment) after pre-treatment with BMS345541 5 μ M for 24 h, as indicated. $n = 3$, two-way ANOVA with Tukey's multiple comparisons. (c) Western blot analysis of p-RelA (S536) and p-STAT3 (Y705) was performed on *Tsc2*^(-/-) MEFs after treatment with BMS345541 5 μ M for either 0 h, 2 h, or 6 h. Over this time course, BMS345541 diminished both RelA and STAT3 phosphorylation. $n = 3$, one-way ANOVA with Tukey's multiple comparison. Western blot densitometry was normalised to β -actin, and relative intensity is normalised to the highest recorded signal intensity.

The impact of long-term treatment on RelA and STAT3 phosphorylation states of BMS345541 and/or rapamycin was also investigated in AMLs (Figure 3.3.2).

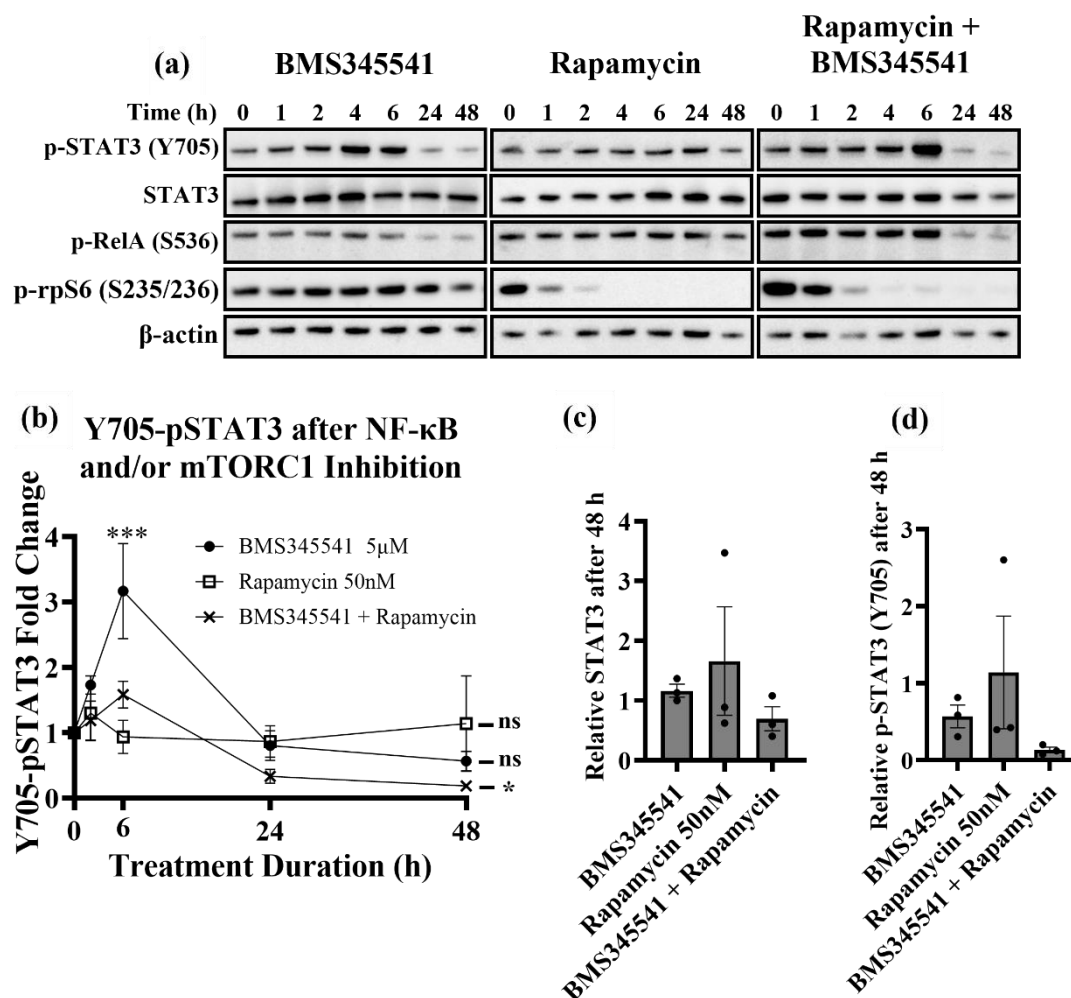


Figure 3.3.2. STAT3 activity is regulated in a biphasic manner through IKK inhibition. (a) Phosphorylation states of RelA, STAT3, and RPS6 were investigated following a time-course treatment with either 5 μ M BMS345541, 50 nM rapamycin, or a combination of the two in 621-101 AMLs ($n = 3$). (b) Subsequent densitometry analysis for p-STAT3 of Figure 3.3d. one-way ANOVA with Dunnett's multiple comparisons tests, comparing each data point to the 0 h treatment time point. (c) Analysis of the fold change after 48 h for total STAT3 protein, or (d) p-STAT3 (Y705), for Figure

3.3.2a. Western blot densitometry was normalised to β -actin. Fold changes are recorded from 0 h samples of each respective treatment condition.

Crosstalk between the NF- κ B and STAT3 pathways is a previously identified feature that is prominent in a range of cancers, including glioma (379,380). In these circumstances, factors upregulated through NF- κ B such as IL-6 would drive STAT3 activation (381). Therefore, *Tsc2*^(-/-) and wild-type MEFs were treated with 7.5 μ M BMS345541 for 24 h (Figure 3.3.1a), an inhibitor of IKK within the NF- κ B pathway, as well as 5 μ M C188-9 (a STAT3 inhibitor), and relative levels of STAT3 activation were assayed under serum-starvation. As previously observed, STAT3 activation is higher within *TSC2*-deficient cells. 24 h treatment with BMS345541 decreased STAT3 activation significantly within *TSC2*-deficient cells, but not the wild-type counterpart. As expected, C188-9 reduced STAT3 activation in both cell types. The apparent selective inhibition of STAT3 within *TSC2*-deficient cells by IKK inhibition seems to suggest that STAT3 activation within *TSC2*-deficient cells is propagated through the NF- κ B pathway. This data hints at potential beneficial uses of anti-inflammatory drugs for the treatment of TSC.

To further confirm the influence of NF- κ B inhibition within *Tsc2*^(-/-) MEFs, cells were also treated with 30 ng/mL TNF α for 2 h (Figure 3.3.1b) following a 24 h treatment with BMS345541. As before, an increase in STAT3 activation is seen after TNF α stimulation (particularly in *Tsc2*^(+/+) MEFs). As expected, this increase of STAT3 activity is negated by IKK inhibition, demonstrating that TNF α was activating STAT3 through the NF- κ B pathway.

To investigate this signalling crosstalk further, *Tsc2*^(-/-) MEFs were treated with 7.5 μ M BMS345541 for shorter durations and Y705 STAT3 phosphorylation was assayed (Figure 3.3.1c). IKK inhibition could reduce Y705 STAT3 phosphorylation significantly at these time points. Building on this data, 621-101 *TSC2*⁽⁻⁾ AML cells were treated with either 5 μ M BMS345541, 50 nM rapamycin, or a combination of the two over a time course of 0, 1, 2, 4, 6, 24, and 48 h. Relative levels of STAT3, RelA, and rpS6 phosphorylation on Tyr705, Ser536, Ser235/236, respectively, was analysed by western blot (Figure 3.3.2a). While IKK inhibition ultimately leads to a reduction in STAT3 phosphorylation at 24 and 48 h, the treatment first induced a transient spike in STAT3 phosphorylation up to the 6 h timepoint. This is notably different to the pattern observed within *Tsc2*^(-/-) MEFs and reflects different compensatory mechanisms and pathway cross talk between the two models. As expected, rapamycin treatment quickly reduced rpS6 phosphorylation, showing a reduction in mTORC1 activity, but was generally ineffective at reducing RelA or STAT3 phosphorylation.

The slight delay in reduction of rpS6 phosphorylation by rapamycin treatment may be because rpS6 is not directly phosphorylated by mTORC1 and is instead phosphorylated downstream of mTORC1 by S6K1. A combination of the two treatments reduced mTORC1 activity as well as reducing RelA and STAT3 phosphorylation, while somewhat mitigating the transient spike in phosphorylation of STAT3. Densitometry analysis is also shown (Figure 3.3.2b), highlighting these differences. The overall fold changes at 48 h of treatment from the 0 h time point are shown for total STAT3 (Figure 3.3.2c) and p-STAT3 (Y705) (Figure 3.3.2d), further demonstrating the benefit in anti-inflammatory activity within a combinatory treatment of the two inhibitors. It was previously identified that unphosphorylated STAT3 can activate NF- κ B (382), which may explain the delayed reduction in RelA phosphorylation observed in *TSC2*-deficient AMLs upon BMS345541 treatment. Furthermore, the high levels of cytokines such as IL-6 that *TSC2*-deficient AMLs are subjected to may bolster this biphasic response through transcription targets of unphosphorylated STAT3 (383).

3.2.4 NF- κ B activity controls dysregulated cytokine secretion in *TSC2*⁽⁻⁾ AMLs

Our previous data showed interesting trends in the dysregulation of NF- κ B and STAT3 signalling in *TSC2*-deficient cells. Notably, hyperactive STAT3 activity could be diminished via inhibition of IKK, and this appears to reduce levels of total and Y705-phosphorylated STAT3. Meanwhile, rapamycin proved generally ineffective at reducing this dysregulated inflammatory phenotype, while a combination of the two inhibitors appeared to demonstrate enhanced reduction in inflammatory signalling. We previously demonstrated that secreted factors were likely playing a large role in the propagation of these inflammatory signals (Figure 3.1). Therefore, we aimed to identify this dysregulation in a more targeted *in vitro* model. To accomplish this, the concentration of IL-6 and VEGFA was assayed by ELISA in media that had been conditioned by 621-101 *TSC2*⁽⁻⁾ and 621-103 *TSC2*⁽⁺⁾ AML cells (Figure 3.4a). 621-101 AML cells were also stimulated with TNF α and/or rapamycin to demonstrate crosslinks between NF- κ B, mTORC1, and STAT3 signalling (Figure 3.4b), and additionally, the impact of IKK versus mTORC1 inhibition was assayed on IL-6 levels (Figure 3.4c). Lastly, the impact of IKK or mTORC1 inhibition was assayed on VEGFA secretion (Figure 3.4d). The effect of rapamycin on IL-6 secretion in *TSC2*⁽⁺⁾ AMLs was also assayed, wherein rapamycin increased IL-6 by a small amount (data not shown).

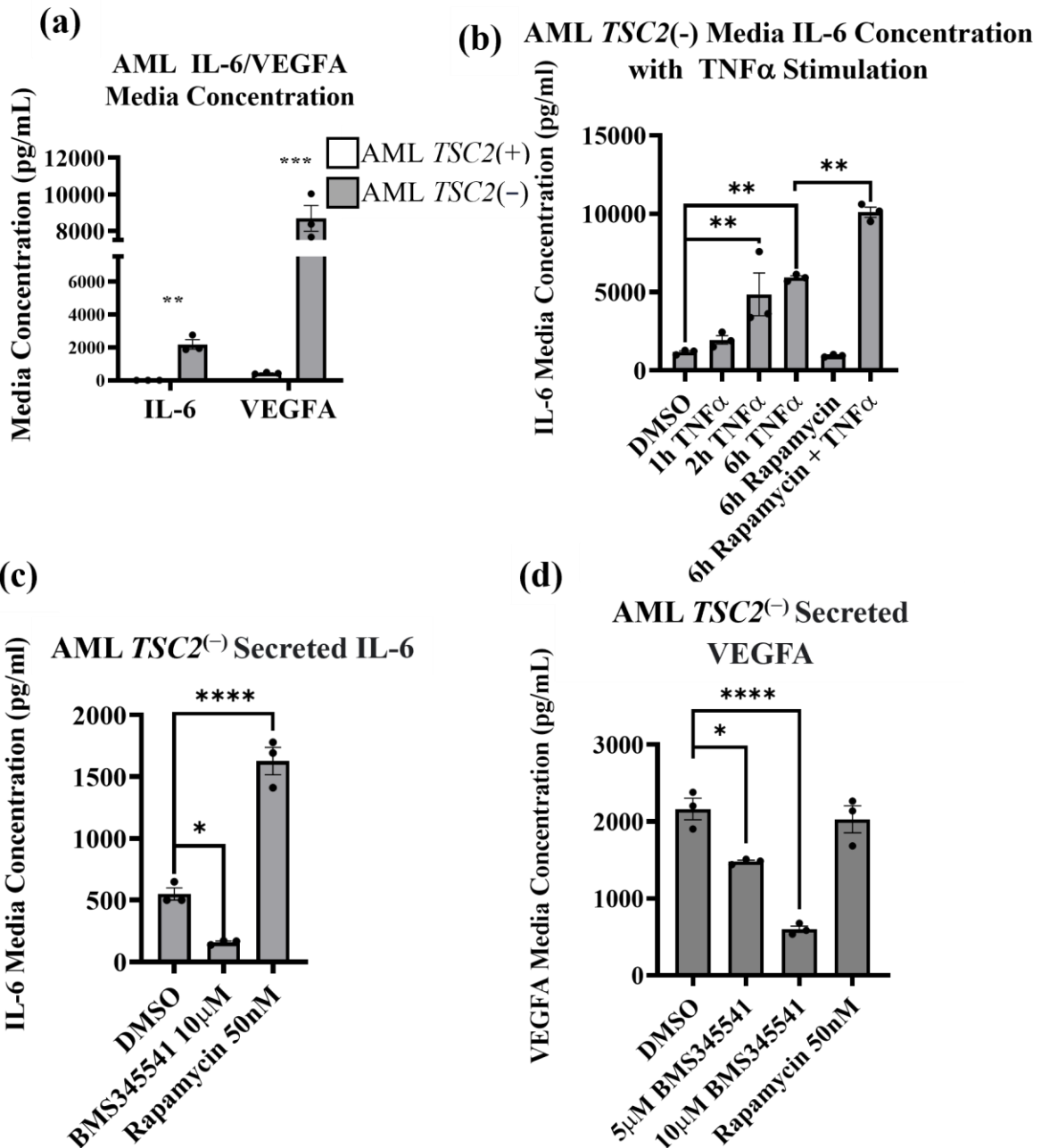


Figure 3.4. Enhanced cytokine secretion can be regulated via NF- κ B. Cytokine media concentration was assayed by ELISA. (a) Media was conditioned by 621-101 *TSC2*(⁺) or 621-103 *TSC2*(⁻) AMLs prior to collection and analysis via ELISA. *TSC2*-deficient AMLs secreted far more IL-6 and VEGFA than their *TSC2*-expressing counterparts. $n = 3$, unpaired t-test. (b) *TSC2*(⁻) AMLs were treated with various durations of TNF α , or 6 h rapamycin with or without 6h TNF α , and IL-6 media concentration was determined via ELISA. NF- κ B pathway stimulation via TNF α increased IL-6 media concentration, whereas rapamycin produced no effect. In combination with TNF α , rapamycin further enhanced IL-6 media concentration. $n = 3$, one-way ANOVA with Tukey's multiple comparisons. (c) IL-6 media concentration was determined in 621-101 AMLs after treatment with 24 h DMSO,

BMS345541 10 μ M, or rapamycin 50 nM. IKK inhibition with BMS345541 was able to reduce IL-6 secretion, whereas rapamycin raised IL-6 secretion by approximately 3-fold. $n = 3$, one-way ANOVA with Tukey's multiple comparisons. (d) *TSC2*^(-/-) AMLs were treated with BMS345541 or rapamycin, and secreted VEGFA was analysed by ELISA as described prior. IKK inhibition with BMS345541 reduced VEGFA secretion, whereas rapamycin was ineffective. $n = 3$, one-way ANOVA with Tukey's multiple comparisons.

3.2.5 Cytokine and chemokine profiling

To assay a range of cytokine and chemokine levels in parallel, a proteome profiler was used on lysates from wild-type and *Tsc2*^(-/-) MEFs before and after TNF α treatment (Figure 3.5.1). The rationale behind this experiment was to explore what cytokines/chemokines were enhanced or lowered between the two cell types as well as their difference in response to an inflammatory stimulus, since cytokines and chemokines are often enhanced within and related to inflammation within brain tumours (384). Samples were lysed as according to the kit manufacturer's instructions and protein concentration calculated using Pierce 660 nm reagent. 200 μ g/mL of each sample was added to profiler membranes and processed as according to the kit manufacturer's instructions, with a final exposure time of 15 s on X-ray film used for analysis. Films were then scanned and analysed using protein densitometry to determine relative protein amounts within lysed cells. As exploratory work, this was performed as $n = 1$.

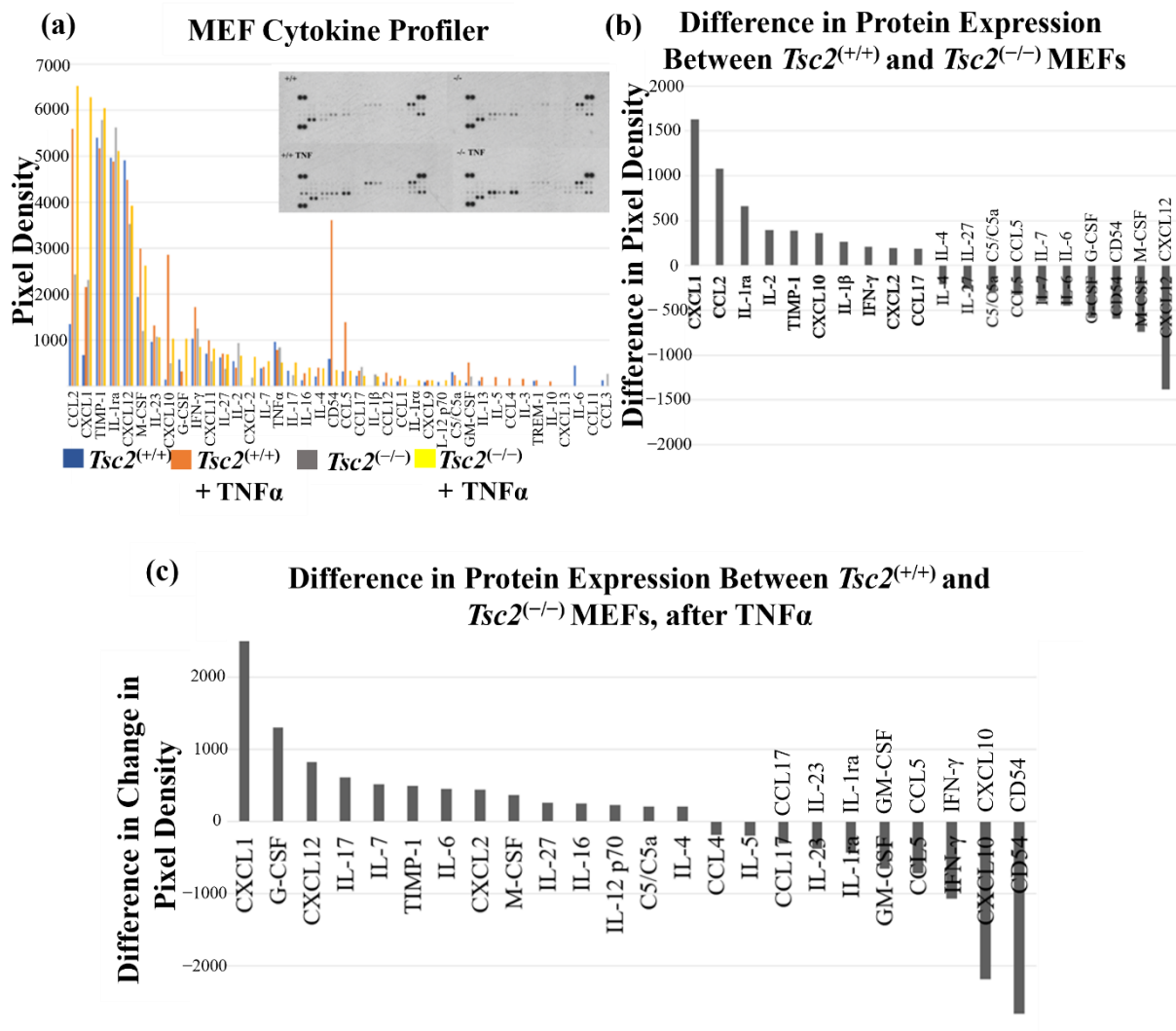


Figure 3.5.1. Differential inflammatory activation between $Tsc2^{-/-}$ and $Tsc2^{+/+}$ MEFs, shown by cytokine profiling. **(a)** Relative protein expression levels within $Tsc2^{-/-}$ and $Tsc2^{+/+}$ MEFs, both including or without treatment with 30 ng/mL $TNF\alpha$ for 2 h. Shown are the four proteome profile membranes used (top right), and the pixel densitometry analysis acquired from the membranes. Pixel density refers to the value obtained by image analysis in ImageJ, and represents relative protein abundance per sample **(b)** The levels of protein expression in wild-type MEFs were subtracted from their expressions in $Tsc2^{-/-}$ MEFs, showing the differential expression without extra NF- κ B pathway stimulation. Positive values denote higher expression in TSC2-deficient cells. **(c)** MEFs were stimulated with $TNF\alpha$ 30 ng/mL for 2 h prior to lysis. The difference in the change in protein expression was plotted, showing differential reactivity of $Tsc2^{-/-}$ to $TNF\alpha$ stimulation when compared to wild-type MEFs. Positive values therefore denote a greater sensitivity to $TNF\alpha$ stimulation, whereas negative values show a lessened sensitivity of $Tsc2^{-/-}$ MEFs. as CD54. $n = 1$, exploratory experiments.

By examining the expression levels of a broad range of cytokines, we may get a greater understanding of which inflammatory/immune pathways may become dysregulated within

TSC diseased cells. The graphs within Figure 3.5.1 shows differential changes in expression between the two cell types. Perhaps rather strikingly, we see a rather exaggerated activation of CD54: a pro-inflammatory receptor (also known as ICAM-1) (385) within wild-type MEFs after TNF α stimulation, but not in the *Tsc2*^(-/-) MEFs. This is interesting, since both *Tsc2*^(-/-) MEFs and wild-type MEFs seem to respond to TNF α with increased RelA and STAT3 phosphorylation. While this highlights a differential response to an inflammatory stimulus, it is important to also consider that the MEFs, as a murine cell model of TSC, may not truly reflect the microenvironment and pathway alterations that might occur within brain tumours of TSC patients. To demonstrate differences between model systems, RNA-sequencing data shows an upregulation of *ICAMI* of 3.5-fold in *TSC2*⁽⁻⁾ AMLs when compared to *TSC2*⁽⁺⁾ AMLs ($p < 0.0005$). In another example, another study showed that *ICAMI* is upregulated within the cortical tubers of *Tsc1* inactivated mice (335). However, it is important to note that this study focused on *Tsc1*, rather than *Tsc2*. The SEN/SEGA transcriptome data also shows significant upregulation of *ICAMI*, which is good evidence that ICAM-1 expression is increased in patient tumours. Altogether, these discrepancies in the expression of inflammatory markers such as ICAM-1 demonstrate that there is still a large gap in the knowledge of inflammation and neuroinflammation within TSC. Furthermore, this knowledge gap may not be reasonably filled in by utilising the commonly available models, demonstrating why novel models, such as the iPSC neural model proposed within this study, are needed.

On the flipside, we see a striking upregulation of CXCL1 within *Tsc2*^(-/-) MEFs both in unstimulated conditions (Figure 3.5.1b) and stimulated conditions (Figure 3.5.1c). CXCL1 is expressed at a higher basal level, and expression increased more in *Tsc2*^(-/-) cells after stimulation. Figure 3.5a also shows that CXCL1 expression in unstimulated *Tsc2*^(-/-) cells was higher than unstimulated or TNF α stimulated wild-type MEFs. CXCL1 is an inflammatory protein that belongs to the GRO superfamily. CXCL1 is activated through NF- κ B promoter binding, and is thus induced by TNF α or IL-1 stimulation (386,387). Within the brain, CXCL1 binds to its receptor, CXCR2, which is present on microglia, mature myelinating oligodendrocytes, and oligodendrocyte precursor cells (388). CXCR2 stimulation can lead to the recruitment of neutrophils to sites of injury, and thus regulates an inflammatory response element. Seizure onset can result in enhanced levels of CXCL1, originating in neurons and endothelial cells. This damage response appears to then recruit neutrophils, which may result in increased inflammation (389). Enhanced levels of CXCL1 as well as CCL2 (also shown to

be upregulated within the profiler) have also been linked in LAM cells of TSC patients (390). It might be possible that NF- κ B-induced expression of CXCL1 may be linked to epilepsy in TSC.

The next protein which is shown to be upregulated within *Tsc2*^(-/-) MEFs is CCL2. Notably, the basal level of CCL2 expression when not stimulated by TNF α is higher in the *Tsc2*^(-/-) MEFs when compared to the wild-type cells. The fold increase in CCL2 expression after stimulation with TNF α is similar between both cell types, showing that both cells are equivalently responsiveness to cytokine stimulating. Two other differentially increased immune regulatory proteins in *Tsc2*^(-/-) MEFs are G-CSF and CXCL12. It should be noted that the protein expression of G-CSF and CXCL12 decreases slightly after TNF α stimulation in wild-type MEFs, while increasing slightly in *Tsc2*^(-/-) MEFs. Additional repeats of this experiment would be required to determine if these results are significant or not.

While this data is underpowered, it still offers some insights into inflammatory proteins linked to TSC. The data may suggest that some inflammatory pathways are upregulated, or more sensitive to inflammatory stimulation than others. This is also shown in the AML RNA-sequencing data of NF- κ B linked genes (Figure 3.2.2b), wherein some NF- κ B linked genes are upregulated while others are downregulated in *TSC2*-deficient AMLs.

A second set of proteomic profilers were performed (Figure 3.5.2). Within this the conditions used were identical to as in Figure 3.5.1, except GolgiPlug and GolgiStop (BD Biosciences) were added alongside TNF α . These molecules serve to inhibit intracellular transport, thus preventing cytokine secretion. This was performed to enrich cytokine/chemokine levels within cell lysates, as it is possible that many cytokines/chemokines may be poorly shown in cell lysates due to secretion. In this scenario, data appeared significantly reduced (fewer different cytokines were detected, and at apparently lower levels).

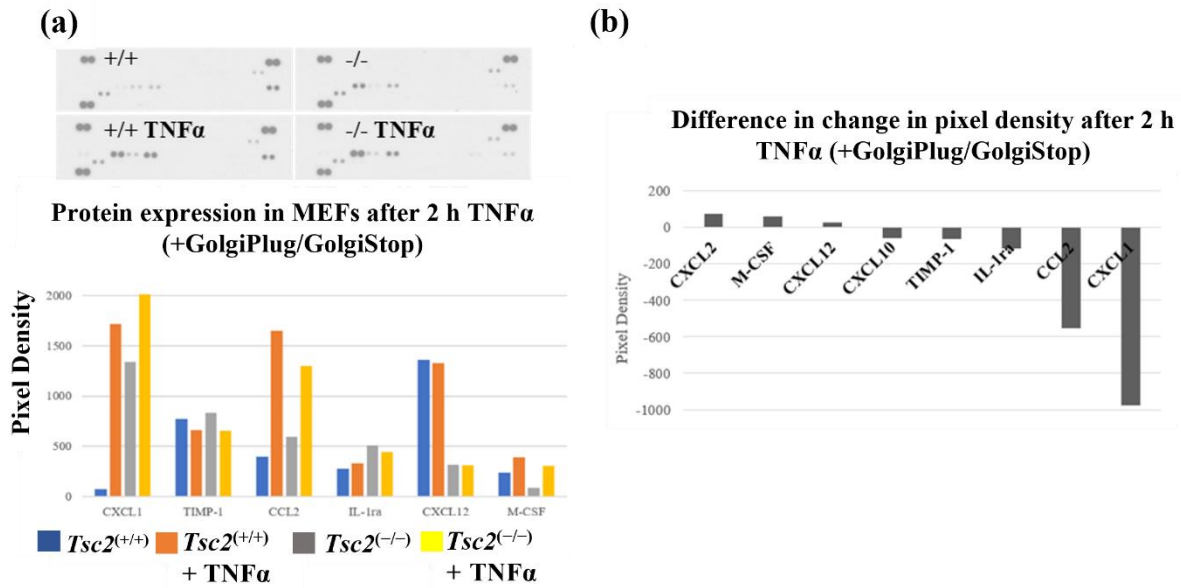


Figure 3.5.2. Cytokine profiling with intracellular transport inhibition. **(a)** Relative protein expression levels within *Tsc2*^(-/-) and wild-type MEFs, both before and after treatment with 2 h TNF α 30 ng/mL, with the addition of GolgiPlug and GolgiStop. **(b)** The difference in change in protein expression after TNF α stimulation, between *Tsc2*^(-/-) MEFs and wild-type MEFs. *n* = 1, exploratory experiments.

Notably, with the addition of intracellular trafficking inhibitors, while CXCL1 was once again at a slightly higher level at basal expression in *Tsc2*^(-/-) MEFs (Figure 3.5.2a), TNF α stimulation caused CXCL1 (and CCL2) expression to increase more so within wild-type MEFs rather than their TSC2 deficient counterparts (Figure 3.5.2b). This may suggest that by preventing cells from being able to secrete cytokines in response to TNF α , further stimulatory pathways are also inhibited, meaning that overall cytokine and chemokine protein expressions are reduced. Once again, this data is limited by a lack of repeats. However, the impression given is that TSC (and normal) chemokine/cytokine production is likely dependent on an autocrine signalling mechanism.

3.2.6 TSC2-deficiency confers sensitivity to NF- κ B inhibition

As previous results showed a sensitivity of *TSC2*-deficient cells to BMS345541, as well as differential responses to activation of the NF- κ B pathway via TNF α , it was hypothesised that NF- κ B inhibition may have a selective cytotoxic effect on *TSC2*-deficient cells. To test this, *TSC2*-deficient and control cells were treated with increasing concentrations of BMS345541 under serum starvation, and a live/dead cell count was obtained using acridine orange and propidium iodide. To confirm caspase-dependent apoptosis, lysates generated from *TSC2*⁽⁻⁾ AML cells were also probed for PARP cleavage and caspase 3 cleavage after treatment with BMS345541. Levels of the anti-apoptotic factor BCL-2 were compared between wild-type and *Tsc2*^(-/-) MEFs, and after BMS345541 treatment.

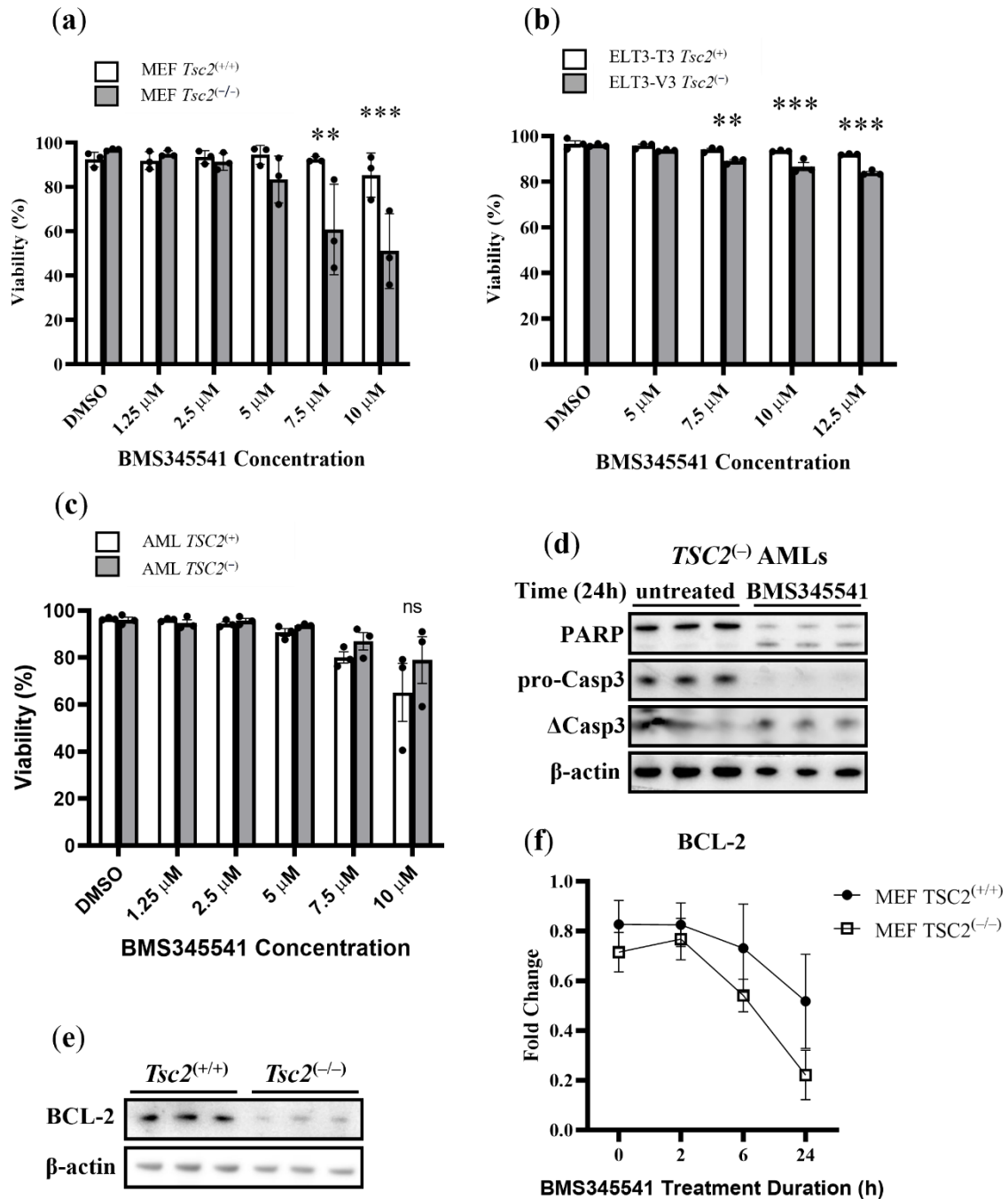


Figure 3.6. IKK inhibition causes selective cell death in *TSC2*-deficient cells. Viability assays were performed over a range of concentrations of BMS345541 in *TSC2*-deficient or *TSC2*-expressing (a) MEF, (b) ELT3, and (c) AML cells. $n = 3$, two-way ANOVA with Tukey's multiple comparison test. (d) *TSC2*⁽⁻⁾ AMLs were treated with 15 μ M BMS345541 for 24 h and assayed for apoptotic markers by western blot (PARP and Caspase 3). (e) Relative levels of the anti-apoptotic protein BCL-2 were compared within wild-type and *Tsc2*^(-/-) MEFs. (f) BCL-2 levels in MEFs after treatment with BMS345541 10 μ M, determined by western blot. Western blot densitometry was normalised to β -actin.

Interestingly, *Tsc2*^(-/-) MEFs displayed a significantly greater sensitivity to BMS345541-induced cell death than wild-type (Figure 3.6a). This was particularly apparent after 7.5 μ M BMS345541 ($p = 0.0016$), and 10 μ M ($p = 0.0006$). However, it should be noted that differences in viability can be seen at earlier lower concentrations of BMS345541, but without reaching significance. *Tsc2*-deficient ELT3-V3 cells did exhibit a greater sensitivity to BMS345541-induced cell death than *Tsc2*-reexpressing ELT3-T3 cells, although generally seemed to be less sensitive than MEFs (Figure 3.6b). ELT3-V3 cells had a significant difference in viability compared to ELT3-T3 cells at 7.5 μ M, 10 μ M, and 12.5 μ M. It is unlikely that induction of cell death is due to off target effects manifesting at higher concentrations, since BMS345541 has shown to be selectively inhibitory to IKK at concentrations up to 100 μ M (391).

Conversely, *TSC2*-deficient AMLs appeared to demonstrate the opposite trend, with *TSC2*-expressing AMLs exhibiting a greater sensitivity to BMS345541-induced cell death (Figure 3.6c). However, these trends did not reach significance.

To further confirm BMS345541-induced cell death within *TSC2*-deficient cells, *TSC2*^(-/-) AMLs were treated with 15 μ M BMS and probed for apoptotic markers after 24 h (Figure 3.6d). Caspase-3 cleavage was clearly detected at the 24 h time point. PARP cleavage was also shown. Bcl-2, an NF- κ B induced anti-apoptotic marker, was detected at lower levels in *Tsc2*^(-/-) MEFs than *Tsc2*^(+/+) MEFs ($p = 0.0481$, unpaired t-test). Conversely, BIM, a pro-apoptotic regulator, was expressed at much higher levels in *Tsc2*^(-/-) MEFs ($n = 3$, unpaired t-test, $p = 0.0009$, data not shown). The anti-apoptotic protein Bcl-xL was also tested, but no significance difference was detected. Bcl-2 appears to be depleted within *Tsc2*^(-/-) MEFs after treatment with BMS345541 and also decreases in *Tsc2*^(+/+) MEFs (Figure 3.6f).

Interestingly, AML RNA-sequencing data shows that *BCL2* is expressed at a 1.6-fold increase within *TSC2*⁽⁺⁾ AMLs when compared to *TSC2*⁽⁻⁾ AMLs ($p = 0.02025$). Meanwhile, *BCL2L1* (Bcl-xL) is expressed at a slight increase of 1.1-fold in *TSC2*⁽⁻⁾ AMLs ($p = 0.01393$).

However, perhaps most striking is expression of the NF- κ B-induced anti-apoptotic regulator *CFLAR*, with a 2.4-fold increase in *TSC2*⁽⁻⁾ AML RNA sequencing data and a 4-fold increase in SEN/SEGAs (both $p < 0.00001$). These apoptotic regulators are often controlled through NF- κ B activity, meaning that we could suggest that heightened NF- κ B is partially responsible for the non-cytotoxic nature of rapamycin treatment in *TSC2*-deficient cells. Indeed, later discussed data seems to show that rapamycin enhances relative Bcl-2 levels in MEFs.

Conversely, while the pro-apoptotic gene *HRK* is expressed 7-fold lower in SEN/SEGAs to matched healthy tissue, it is expressed highly in the transcripts of *TSC2*⁽⁻⁾ AMLs, but not *TSC2*⁽⁺⁾ AMLs. One study demonstrated that tumour cells which expressed high levels of Hrk were particularly sensitive to TNF α -related apoptosis inducing ligand (TRAIL) (392). For this reason, we might have expected to see a markedly increased level of cell death in prior experiments with TNF α treatments, although rationale for this has already been posed in 3.3.1.

It was previously identified that aberrant mTORC1 signalling could also activate NF- κ B, resulting in an increase in the transcription of NF- κ B regulated genes such as *BCL2L1* and *BCL2* (393). As anti-apoptotic proteins, Bcl-2 and Bcl-xL upregulation is often seen in cancer (394). Selective cell death may occur within *TSC2*-deficient cells after IKK inhibition due to a reduction in anti-apoptotic proteins such as Bcl-xL and Bcl-2. Interestingly, the *TSC2* protein has been shown to also negatively regulate Bcl-2, meaning that *TSC2* loss would incur an increase in the anti-apoptotic activity (395).

Previously, it was shown that cells that express high levels of RelA activity are more sensitive to BMS345541-induced apoptosis, and furthermore RelA inhibition causes a downregulation of anti-apoptotic genes, including Bcl-2 (396). Overall, this selective induction of cell death with BMS345541 treatment demonstrates a strong reliance upon inflammatory pathways by *TSC2*-deficient cells for survival, and possibly demonstrates upregulation of anti-apoptotic NF- κ B target genes that could be exploited in TSC as therapy.

3.2.7 The NF- κ B pathway is differentially regulated in *Tsc2*^(-/-) MEFs.

Since cells with inactive *TSC2* appear to be sensitive to IKK inhibition (both in terms of STAT3 activation and cell survival), it stands to reason that NF- κ B is likely dysregulated in these cells. For example, NF- κ B activity may be propagating pro-survival signals at an elevated level within *TSC2*-deficient cells. Upon inhibition of NF- κ B signalling, *TSC2*-deficient cells undergo cell death due to a shift in pro- versus anti-apoptosis protein expression.

Therefore, using transcriptional activation ELISAs on nuclear fractions, *Tsc2*^(-/-) and wild type MEFs were assayed for activation of the NF- κ B subunit RelA, as well as cEBP β after treatment with either 10 μ M BMS345541 or 50 nM rapamycin. The effects of NF- κ B

inhibition on TNF α responsiveness were also assayed by treating cells with 30 ng/mL TNF α for 1 h after 7.5 μ M BMS345541 treatment for 24 h. We also examined the effect of rapamycin on STAT3 activity in MEFs.

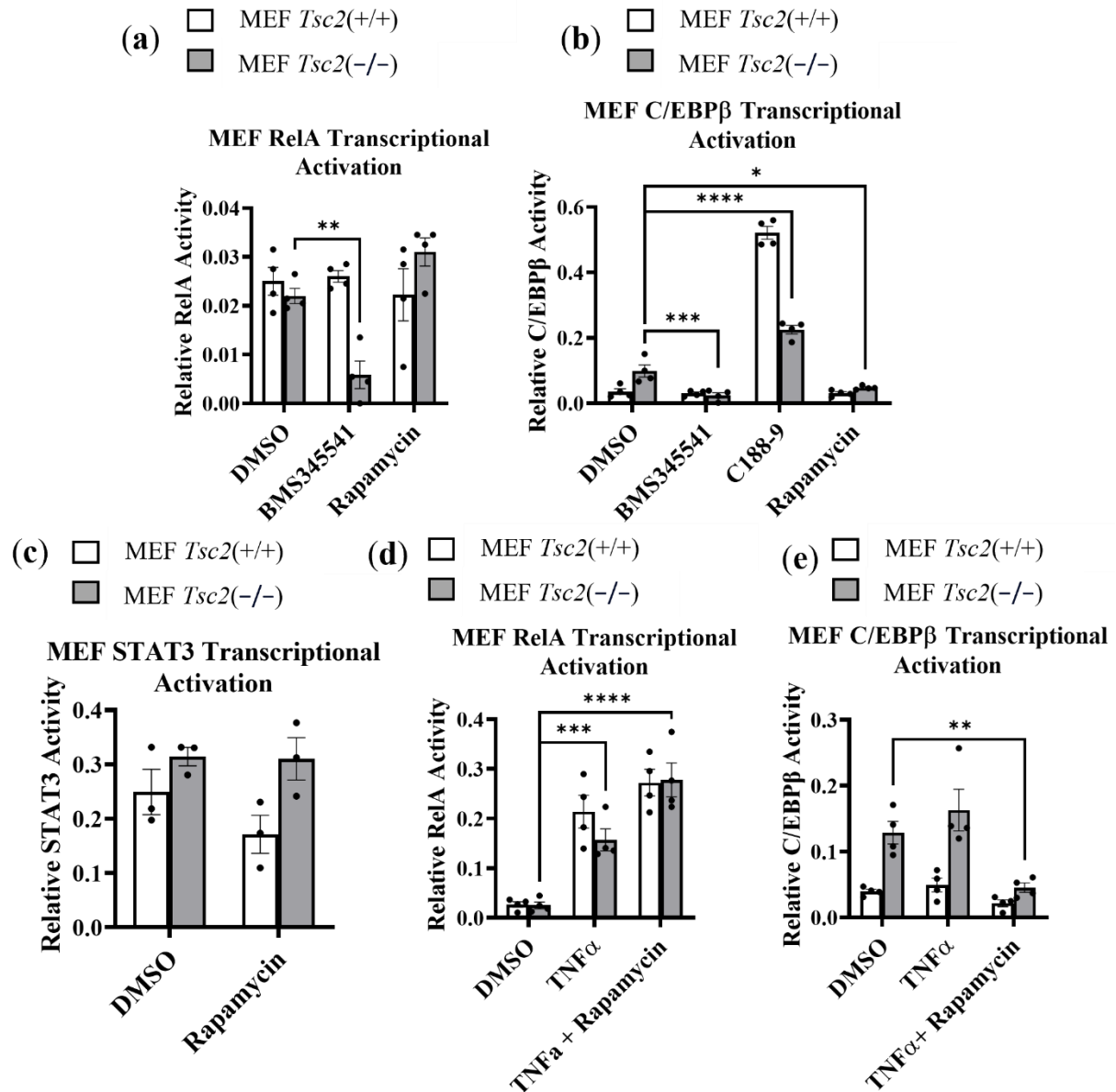


Figure 3.7. NF- κ B, unlike C/EBP β is not regulated through mTORC1. (a) RelA transcriptional activation ELISA performed on *Tsc2*^(-/-) or *Tsc2*^(+/+) MEFs after IKK, STAT3, or mTORC1 inhibition. (b) C/EBP β transcriptional activity within *Tsc2*^(-/-) or *Tsc2*^(+/+) MEFs after inhibition of IKK, STAT3, or mTORC1. (c) *Tsc2*^(-/-) or *Tsc2*^(+/+) MEFs were treated with either DMSO or rapamycin and STAT3 transcriptional activity was assayed. $n = 3$, two-way ANOVA with Tukey's multiple comparison test. (d) RelA transcriptional activity in *Tsc2*^(-/-) or *Tsc2*^(+/+) MEFs after treatment with TNF α or TNF α + rapamycin. (e) C/EBP β transcriptional activity in *Tsc2*^(-/-) or *Tsc2*^(+/+) MEFs after treatment with TNF α

or TNF α + rapamycin. **a, b, d, e:** $n = 4$, compared by two-way ANOVA with Tukey's multiple comparison test.

If the assumption is made that the STAT3 pathway is indeed hyperactive in *TSC2*-deficient cells, it may be reasonable to state that as a cause and/or consequence of this, the NF- κ B pathway is also hyperactive since there are interlinkages between these two pathways. This is to say that the NF- κ B pathway can activate the STAT3 pathway through NF- κ B-induced factors such as IL-6, and in turn STAT3 activation can promote the production of factors which then in turn stimulate both STAT3 and NF- κ B (380). Furthermore, it has been shown that NF- κ B subunits and STAT3 can interact with one another both in the cytoplasm and nucleus, granting either pro- or anti-transcriptional effects (397–399).

However, previous research has demonstrated that NF- κ B activation in TSC is variable, and that a loss of *TSC2* function can either activate or repress NF- κ B based on the genetic context (48). For this reason, it was interesting to see that a difference in RelA activation in unstimulated conditions was not significant between *Tsc2*^(-/-) and wild type MEFs, especially since prior blots (Figure 3.1) seemed to show enhanced RelA phosphorylation. Higher RelA nuclear activity has been shown in similar studies between *Tsc2*-deficient and expressing MEFs, however this was under hypoxia (400). IKK inhibition by BMS345541 selectively diminished RelA nuclear activity (Figure 3.7a). This is unexpected, as we would expect BMS345541 to diminish RelA activation in both cell lines, since it works simply by allosterically inhibiting IKK (396). Conversely, STAT3 inhibition with C188-9 increased RelA phosphorylation in *Tsc2*^(+/+) MEFs, but not *Tsc2*^(-/-) MEFs, demonstrating differential inflammatory pathway regulation and compensatory mechanisms between the two cell types. BMS345541 also significantly diminished C/EBP β activity in *Tsc2*^(-/-) MEFs ($p = 0.0008$), but not wildtype MEFs (Figure 3.6b). Since increased levels of S536 phospho-RelA were observed in prior experiments, but nuclear-located DNA-binding RelA was relatively unchanged, this may suggest that *TSC2*-deficient cells have a greater pool of RelA in reserve that can shuttle into the nucleus. RelA may also interact with other transcription factors such as STAT3 for alternative inflammatory signalling. While not reaching significance, mTORC1 inhibition with rapamycin appeared to slightly increase RelA activity.

C/EBP β levels were greatly elevated in *Tsc2*^(-/-) MEFs when compared to wild type ($p = 0.0034$) (Figure 3.7b). This is expected, as C/EBP β is an inflammatory transcription factor that is upregulated by, and in turn further stimulates STAT3 activation via IL-6 (401,402). For this reason, it is possible that C/EBP β activation is functioning as a surrogate marker

downstream of STAT3. As expected, C/EBP β levels closely mirror the patterns seen with STAT3: an increased basal activation, a large reduction in activation upon BMS345541 treatment, and a smaller reduction in activation by rapamycin (Figure 3.7b). Interestingly, in contrast to the previously seen STAT3 results, C/EBP β responsiveness to rapamycin seems to be greater than the responsiveness to BMS345541 after TNF α stimulation. The lack of effectiveness of rapamycin in reducing STAT3 activity was also shown via a transcriptional activation ELISA (Figure 3.7c). This may suggest that alternative pathways are targeting C/EBP β activation which are more mTORC1-dependent. For example, STAT3 can be directly activated by mTORC1 via phosphorylation on Ser727, rather than the mTORC1-independent pathway involving IL-6, which induces Y705-STAT3 phosphorylation via Janus Kinase 2 (JAK2). However, the link between C/EBP β to STAT3 activity is likely more complex. STAT3 inhibition with C188-9 caused a dramatic increase in C/EBP β activation for both *Tsc2*^(-/-) MEFs and wildtype ($p < 0.0001$). This may suggest a compensatory activation of C/EBP β after inhibition of STAT3, although this does not seem to be suggested elsewhere in literature.

The effects of TNF α on transcription factor activation levels was also observed. As expected, TNF α causes a significant increase in RelA activation for both cell lines. Notable is the fact that treatment with rapamycin appears to sensitise *Tsc2*^(-/-) MEFs to TNF α , bolstering RelA activation, or otherwise caused NF- κ B activation through alternative means (Figure 3.7d).

Conversely, TNF α did not appear to enhance C/EBP β activation significantly (Figure 3.7e). This is unexpected, since we would expect that if TNF α was able to activate NF- κ B and consequently activate STAT3, we would also expect to see an increase in C/EBP β nuclear activity. It is possible that the duration of TNF α stimulation was not sufficient to induce C/EBP β activity through these two separate pathways. However, rapamycin caused a decrease in C/EBP β activity in *Tsc2*^(-/-) MEFs ($p = 0.0044$), even with exogenous NF- κ B activation with TNF α . Overall, this suggests that C/EBP β activity within *Tsc2*^(-/-) MEFs is linked more closely to mTORC1 hyperactivation, unlike STAT3 and NF- κ B activity. Indeed, this has been identified previously, wherein mTORC1 inhibition with rapamycin also causes a decrease in C/EBP α and C/EBP β levels (403). However, this decrease was specifically for the shorter, truncated isoforms which act as repressors of gene activation (404). Conversely, a more recent study identified that *TSC1*-deficient macrophages expressed lower levels of C/EBP β that could be restored by rapamycin (405), although this study did not directly examine nuclear-localised active C/EBP β . Overall, it seems that mTORC1 activity plays a

significant role in the modulation of C/EBP β activity, particularly in terms of the expression of C/EBP β isoforms via control of translation (404). This contrasts with NF- κ B and STAT3 activation, where the inhibition of mTORC1 does not appear to decrease the inflammatory phenotype. C/EBP β is known to exhibit crosstalk with the NF- κ B pathway. Specifically, C/EBP β can promote NF- κ B signalling by negative regulation of I κ B α (406).

An ELISA for active nuclear p50 was also performed alongside the ELISAs for RelA and C/EBP β . Despite similar patterns emerging between p50 and RelA levels, the data lacked significance and demonstrated particularly low absorbance values, so this data has not been shown. It should also be noted that the data used in the RelA transcriptional activation ELISA (Figure 3.7a) also demonstrated very low absorbance values, however the data did show statistical significance upon analysis.

Ultimately, this data collectively suggests a complex set of interactions and signalling interplay that occurs between the NF- κ B, STAT3, and other inflammatory pathways in the TSC diseased setting. Still, we may postulate on reasons for clinically observed trends that are linked to the pathology of TSC and current treatments with mTOR inhibitors. For example, it is known that rapamycin and associated rapalogues are cytostatic to tumour growth in TSC patients rather than being selectively cytotoxic (35). For this reason, upon discontinuation of the treatment, shrunken tumours grow back. It may be possible that rapamycin fails to fully terminate TSC tumours due to the prolonged and persistent activation of pro-survival signals from inflammatory pathways such as NF- κ B or STAT3. These observations suggest that rapamycin treatment alone is not sufficient to block inflammation within this TSC disease model. It further supports the rationale that rapamycin treatment in combination with anti-inflammatories as an adjunct therapy may offer a greater clinical efficacy to restore the disease state.

3.2.8 Inflammatory signals within *TSC2*-deficient AMLs can be reduced by IKK inhibition

Work presented above indicates that *TSC2*-deficient cells exhibit a multitude of differential inflammatory phenotypes when compared to wild-type cells. Inflammatory pathways are also upregulated *in vivo* within the SEN/SEGAs and cortical tubers of TSC patients. A key target of TSC-related inflammation appears to be the NF- κ B pathway, with notably differential responses between *Tsc2*^(-/-) and wild-type MEFs upon its inhibition. The study now aimed to consolidate *in vivo* data with *in vitro* data by comparing biomarkers which were significantly

dysregulated within SEN/SEGAs and those which were dysregulated within *in vitro* cell line models of TSC. With such close signalling crosstalk between the inflammatory pathways in TSC, the next step was to identify whether IKK inhibition could influence other dysregulated inflammatory effectors in TSC.

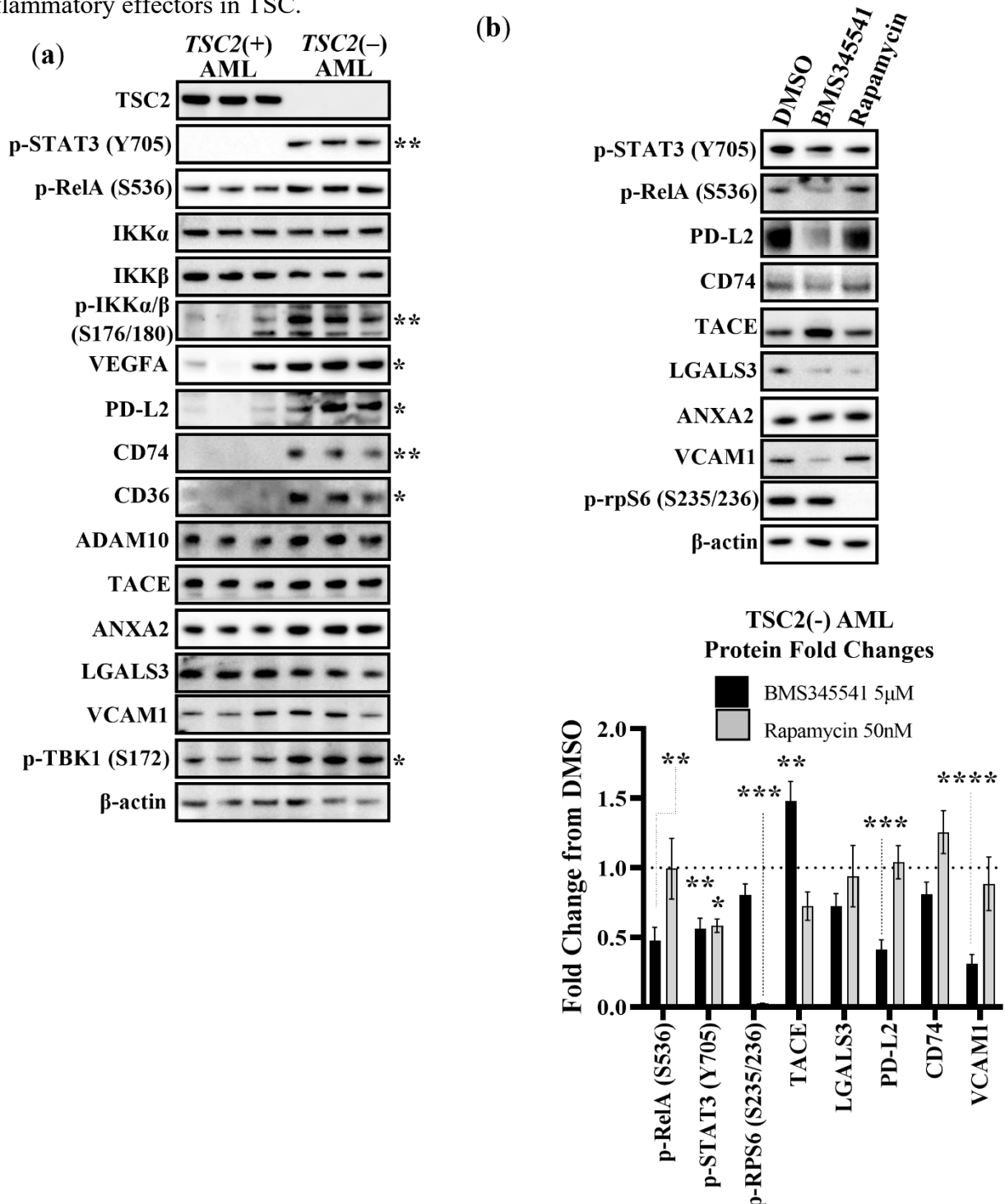


Figure 3.8.1. Dysregulated protein expression in $TSC2^{-}$ AMLs cannot be fully restored by mTORC1 inhibition. (a) Western blot panel demonstrating dysregulated inflammatory protein expression in $TSC2^{-}$ AMLs. Cells were serum starved for 24 h prior to lysis. $n = 3$, unpaired t-tests. Note: this western blot panel is derived from the same set of experiments as the AML western blot panel in

figure 3.1a. Pixel densitometry analysis was used to determine relative protein abundance, and statistical significance was determined by multiple t-tests (b) Western blot and corresponding pixel densitometry analysis showing that 24 h BMS345541 5 μ M is able to reduce expression of some proteins, whereas rapamycin was less effective. $n = 3$, two-way ANOVA with Tukey's multiple comparisons test. Western blot densitometry was normalised to β -actin.

A range of inflammatory proteins were compared between *TSC2*⁽⁻⁾ and *TSC2*-restored AMLs by western blot (Figure 3.8.1a). The majority of these were selected as they were transcriptomically upregulated within *TSC2*⁽⁻⁾ AMLs, as identified by RNA-sequencing data (as mentioned in 3.2.4.) The fold changes here can also be compared with that of the SEN/SEGA transcriptome (table 2).

Gene	Fold Change (SEN/SEGA)	Fold Change (Cortical Tuber)	Fold Change (AML)	Significant? (SEN/SEGA; Cortical Tuber; AML)
<i>STAT3</i>	3.0	1.8	1.5	(Y; Y; Y)
<i>RELA</i>	2.8	1.9	1.0	(Y; Y; N)
<i>IKK1</i>	1.4	1.1	1.2	(Y; N; Y)
<i>IKK2</i>	3.2	1.9	0.8	(Y; Y; Y)
<i>VEGFA</i>	1.6	0.8	8.3	(N; N; Y)
<i>PDCD1LG2</i>	15.3	5.2	6.5	(Y; Y; Y)
<i>CD74</i>	20.7	7.5	142.0	(Y; Y; Y)
<i>CD36</i>	68.6	1.7	5.0	(Y; N; Y)
<i>ADAM10</i>	0.9	0.8	1.8	(N; N; Y)
<i>ADAM17</i>	2.8	1.2	0.78	(Y; N; Y)
<i>ANXA2</i>	41.1	11.1	1.4	(Y; Y; Y)
<i>VCAM1</i>	13.4	7.7	N/A	(Y; Y; N)
<i>LGALS3</i>	13.0	3.8	1.7	(Y; Y; Y)
<i>TBK1</i>	0.8	0.8	0.8	(Y; Y; Y)

Table 3.2. Fold changes in multiple gene expressions within TSC-patient derived SEN/SEGA, Cortical Tubers, or *in vitro* AMLs.

Given this data, the AML proteome and transcriptome may be regarded as at least somewhat similar to the SEN/SEGA transcriptome in terms of select inflammatory protein expressions. These trends were similar in the cortical tuber transcriptome. This will grant further insight to the inflammatory pathology of TSC.

Heightened expression of multiple inflammatory and immune markers (*VEGFA*, *PD-L2*, *CD74*, *CD36*, *ADAM17*, *ADAM10*, *ANXA2*, and phosphorylation of *Y705-STAT3* and *S536-RelA*) were observed in *TSC2*⁽⁻⁾ AMLs when compared to control (Figure 3.8.1a). Total

levels of IKK α and IKK β were not different between the two cell types, but phospho-IKK α/β (S176/180) phosphorylation was markedly upregulated in the *TSC2*⁽⁻⁾ AMLs. Dysregulation of many of these targets was also noted in transcriptomic data of SEN/SEGAs, cortical tubers, and *in vitro* AMLs (Table 3.2).

We sought to identify if these NF- κ B-linked genes could be modulated with inhibitors of the NF- κ B pathway or mTORC1 (Figure 3.8.1b). *TSC2*⁽⁻⁾ AML cells were treated with 5 μ M BMS345541 or 50 nM rapamycin for 24 h and probed via western blot. Many targets remained unchanged by both treatments, such as ANXA2, CD74, and CD36. However, one target of note was PD-L2. PD-L2 shows high levels of protein expression in *TSC2*⁽⁻⁾ AMLs (Figure 3.8.1a) and was transcriptionally upregulated in patient tumours (Table 2). Notably, rapamycin treatment was not able to reduce expression of PD-L2, whereas IKK inhibition was able to significantly reduce PD-L2 levels (Figure 3.8.1b).

PD-L2 is an immune checkpoint regulator, and is closely associated with immune invasion within various cancers (407). It is unclear why the immune system is unable to clear TSC-derived tumours, however expression of proteins such as PD-L2 may partially explain this. Therefore, reducing PD-L2 (and other immune checkpoint co-inhibitors) could be a viable strategy to allowing the immune system to detect and to clear TSC-derived tumours.

Strangely, LGALS3 protein levels do not appear to be upregulated within *TSC2*-deficient AMLs (Figure 3.8.1a), which does not fit accordingly with the transcriptomic data of TSC-derived brain tumours, where *LGALS3* transcripts are enhanced by 13-fold within SEN/SEGAs and 3.8-fold within cortical tubers. *LGALS3* does appear slightly upregulated in *TSC2*-deficient AMLs in RNA-sequencing, but this was not significant. LGALS3 could be reduced by both IKK and mTORC1 inhibition (Figure 3.8.1b), demonstrating anti-inflammatory properties of both treatments.

Protein expression of VCAM1 is slightly upregulated in *TSC2*⁽⁻⁾ AMLs by 1.3-fold (not statistically significant) and can be seen as significantly enhanced within SEN/SEGA and cortical tubers. IKK inhibition was able to reduce VCAM1 expression, whereas rapamycin was ineffective. This is somewhat expected, since VCAM1 has previously reported to be regulated by NF- κ B (408). Seizures can enhance VCAM1 expression (409), which could explain the difference in upregulation between SEN/SEGAs, cortical tubers, while differences in expression of VCAM1 is less apparent in *TSC2*⁽⁻⁾ AMLs. It is worth noting that RNA-sequencing of AMLs showed close to zero VCAM1 mRNA expression, suggesting that

VCAM1 protein must be stabilised in these cells. Consequently, the ability of the NF- κ B inhibitor to reduce VCAM1 protein is unlikely through mRNA expression, but rather via reduced protein stability of VCAM1. The mechanism to how this might occur is unknown.

CD74 and CD36 are also significantly dysregulated in this data. However, their expression could not be significantly altered with either IKK or mTORC1 inhibition. CD36 functions as a receptor for a broad range of ligands, typically responsible for recognising molecules on pathogens or pathogen-infected cells. Furthermore, dysregulated CD36 typically promotes inflammation, including NF- κ B activation upon complexing with TLRs (410,411). TLR2 and TLR6 (and most other TLRs) are upregulated by 21.6 and 8.6-fold, respectively, in the SEN/SEGA transcriptome. Our data showed that IKK inhibition was unable to reduce CD36 levels, suggesting that CD36 expression may be causative, and not resultant of NF- κ B activity. Various other transcription factors contribute to CD36 upregulation, including STAT3 (412). CD74 is a cell surface receptor for macrophage migration inhibitory factor (MIF), the binding of which causes CD74 intracellular release and downstream effects conferring survival and NF- κ B activation (413,414). Interestingly, MIF transcripts are upregulated within AMLs by 1.7-fold ($p < 0.00005$). Furthermore, midkine, a downstream target cytokine of CD74 activation is upregulated in both AMLs and SEN/SEGAs ($p < 0.00005$). It is possible that the pro-survival pathways undergone by CD74 activation may contribute to the cyostatic nature of TSC-derived tumours during rapamycin treatment. Taken together, this may present CD74 as an attractive target for TSC treatment. CD74 has already been identified as a potential target in some cancers, with antibody therapy targeted to CD74 by Milatuzumab presenting as a potentially effective treatment (415). CD74 stimulation of NF- κ B and ERK1 would stimulate pro-survival and inflammatory pathways, and CD74 is also highly expressed in inflammatory disorders and cancer (416). TNFSF12 is upregulated within the *in vitro* TSC2⁽⁻⁾ AML RNA-sequencing data by 1.7 fold and could potentially stimulate production of CD74 (417). However, significant dysregulation of TNFSF12 is not seen in the SEN/SEGA or cortical tuber data. The intracellular domain of CD74 interacts with NF- κ B and thus stimulates NF- κ B activity (413), so in this scenario, NF- κ B activity could be both causative and resultant of CD74 upregulation. However, this is not observed in our treatments, wherein CD74 appeared marginally, but not significantly reduced by IKK inhibition (Figure 3.8.1b). Conversely, mTORC1 inhibition had a similarly marginal increase in CD74 expression, but again this was not significant.

Of particular interest, serine 172 phosphorylation on TBK1 is upregulated in *TSC2*⁽⁻⁾ AMLs, despite slight (but statistically significant) downregulation of *TBK1* in all tested mRNA datasets. Phosphorylation of TBK1 demonstrates the recruitment of TBK1 via the cGAS/STING pathway, which is activated through viral infection or cellular stress (234,239). The cGAS/STING pathways can also be activated by cytosolic mitochondrial DNA (418). Following TBK1 phosphorylation, TBK1 can exert serine/threonine kinase activity on IRF3 or IκBα, leading to NF-κB pathway stimulation (419). Clearly, this may be highly significant in terms of hyperactive NF-κB signalling in *TSC2*⁽⁻⁾ cells. Unsurprisingly, activation of the cGAS/STING/p-TBK1 pathway is often implicated in cancers and immunological disorders (237). TBK1 activity will be explored further in later chapters.

ANXA2 is also upregulated in all datasets, although less-so within *in vitro TSC2*⁽⁻⁾ AMLs than the TSC-patient derived brain tumours. As a promoter of angiogenesis and proliferation, it correlates strongly with poor prognostic metastatic and mesenchymal phenotypes of glioma (420,421). It is also known to modulate NF-κB signalling, although this is through non canonical NF-κB signalling leading to p50 nuclear localisation (422), whereas the focus on NF-κB signalling in this chapter has been on p65 (RelA). Importantly, mTORC1 signalling is known to be important in ANXA2 upregulation, however ANXA2 was not reduced in our experiments by mTORC1 inhibition. Similar, IKK inhibition was unable to reduce ANXA2 levels. If chronic mTORC1 activity could increase ANXA2 levels, this may lead to enhanced non-canonical NF-κB signalling which is not possible to reverse with short-term rapamycin treatment. Further experimentation would be required to observe non-canonical NF-κB signalling. ANXA2 dysregulation is significantly more upregulated within TSC-patient brain tumours than the *in vitro* AML model (41.1-fold vs 1.4-fold) so it is possible that inhibition in neuronal models would provide different results.

Lastly, two metalloproteinases, ADAM10 and ADAM17 demonstrate heightened levels within *TSC2*⁽⁻⁾ AMLs, when compared to *TSC2*-restored AMLs. The difference in protein expression did not reach significance but appeared visually apparent. ADAM10 demonstrated transcriptomic down-regulation within TSC-patient derived brain tumours, whereas ADAM17 showed upregulation. Conversely, ADAM17 expression appeared to be downregulated within the transcriptome of *in vitro TSC2*⁽⁻⁾ AMLs. ADAM17 is responsible for the cleavage and release of mature TNFα (and various other membrane-bound cytokines and receptors (423)) from the cell-membrane, leading to downstream signalling via soluble-

TNF α binding on neighbouring cells. Higher TNF α levels from ADAM17 expression may be implicated in the seizures and other neuropsychiatric symptoms of TSC (216).

Altogether, this data reveals a heightened inflammatory response in *TSC2*-deficient cells and highlights NF- κ B and STAT3 as potential pathways responsible for this phenotype. Although similar in some regards, such as general directional trends in gene dysregulation, the data also demonstrates some differences between the *in vitro* AML model used and the inflammatory gene transcriptional signature found in brain tumours of TSC patients. An example of this is the expression of *ANXA2*, wherein TSC patient-derived brain tumours exhibit hugely upregulated mRNA of this gene, which is not matched to the same extent within *in vitro* AMLs. As the AML cells were derived from the kidney, it is unlikely that AML cells would accurately mirror brain tumours. Clearly, better models of TSC brain tumours are required. Later experimentation will highlight inflammatory dysregulation within *in vitro* neural models of TSC in an attempt to consolidate this data.

RNA-sequencing was also used to analyse the effect of mTOR inhibition with Ku-0063794 on dysregulated NF- κ B-related genes in *TSC2*-deficient AMLs under hypoxia. Ku-0063794 inhibits both mTORC1 and mTORC2 activity by inhibition of mTOR. Notably, mTOR inhibition appears generally insufficient for reducing dysregulated NF- κ B signalling at the transcriptomic level (figure 3.8.2).

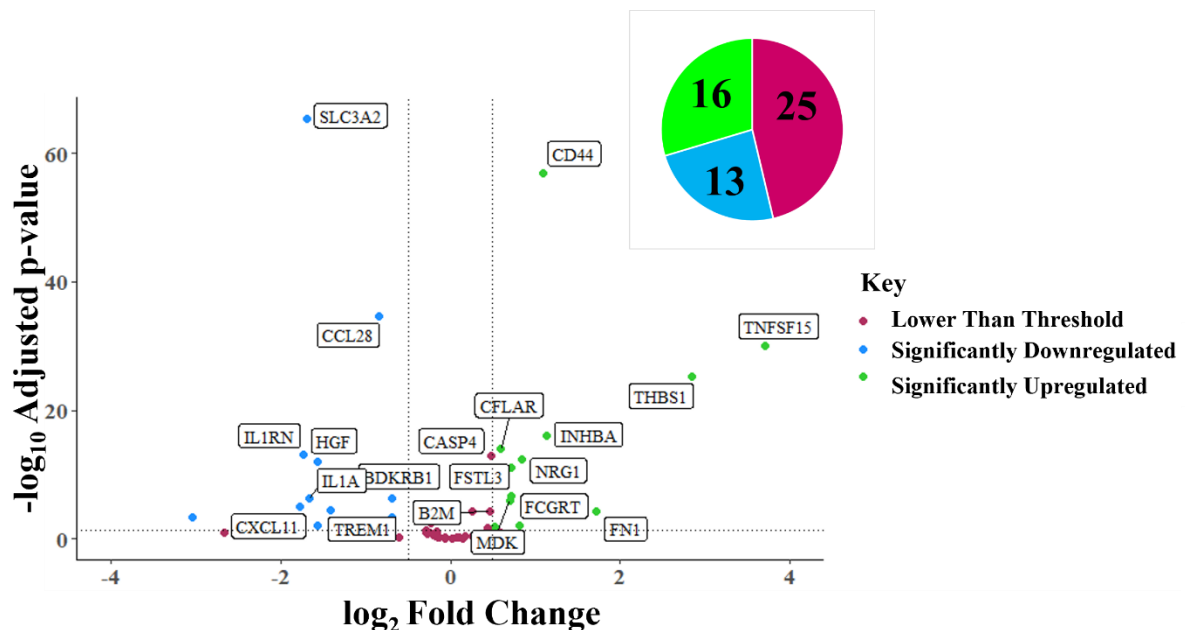


Figure 3.8.2. mTOR inhibition is not suitable for restoring dysregulated NF- κ B signalling.

Upregulated NF- κ B-linked genes in *TSC2*⁽⁻⁾ AMLs (as detailed in 3.3.2) were selected. This gene list was then plotted using RNA-sequencing data for *TSC2*⁽⁻⁾ AMLs under hypoxia versus *TSC2*⁽⁻⁾ AMLs under hypoxia which had been treated with an mTORC1 inhibitor, Ku-0063794 1 μ M.

Overall, mTOR inhibition was unable to restore the inflammatory state effectively. 25 of the genes tested were not significantly upregulated or downregulated with mTOR inhibition, while 16 NF- κ B-linked genes were upregulated even further. 13 out of the 54 genes tested were downregulated by mTOR inhibition.

3.2.9 Hypoxia Response

Hypoxia is the state where cells are deprived of an adequate oxygen supply, resulting in the activation of the hypoxic response pathways. While necessary for normal cellular function, hypoxia has links to various neurological diseases due to neuronal damage stemming from oxygen deficiency, as well as altered vascular formations resulting in defective blood flow and nutrient delivery (424–426). Furthermore, hypoxia has ties to cancer due to faulty vasculature in tumours, often leading to a hypoxic core (427). In GBM, this results in more invasive tumours into the surrounding healthy brain tissue, severely impacting the efficacy of treatment and raising patient morbidity (428). Hypoxia also has links to inflammation, wherein the hypoxia inducible factor system can trigger inflammatory pathways including NF- κ B and STAT3 (429,430).

Therefore, activation of these inflammatory pathways under hypoxia may be key in understanding the pathology of TSC. For this purpose, the general status of the NF- κ B pathway within *TSC2*⁽⁻⁾ AMLs under normoxia and hypoxia was investigated (Figure 3.9a). Similarly, the effect of Ku-0063794 was investigated in these conditions. The overall impact of hypoxia and mTOR inhibition was compared within a table (Figure 3.9b). An analysis of the impact of mTOR inhibition on DEGs which were dysregulated under hypoxia was also performed (Figure 3.9c).

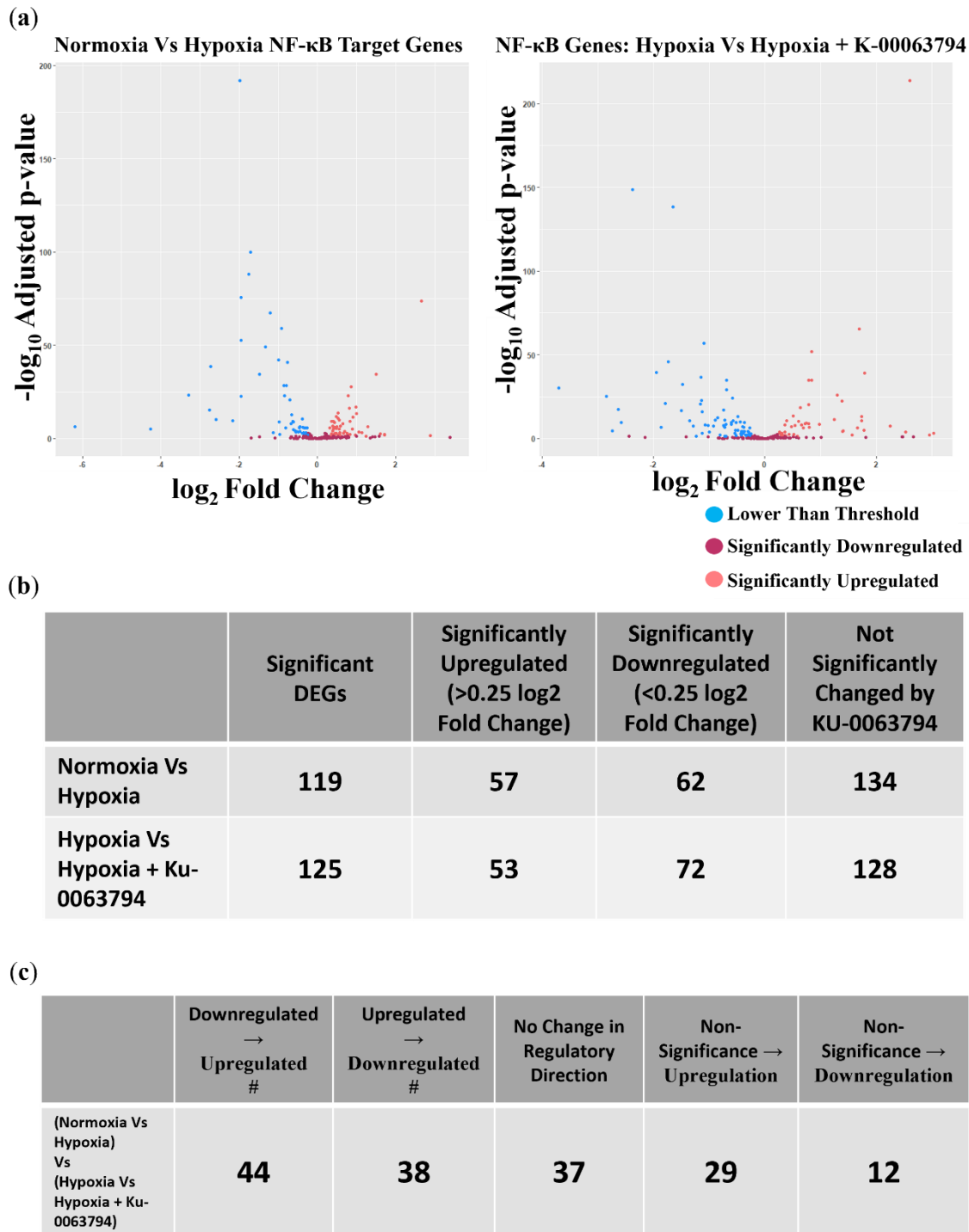


Figure 3.9. Hypoxia induces differential expression in NF-κB target genes, and this can be affected by mTOR inhibition. (a) Volcano plots of NF-κB target DEGs within *TSC2*⁽⁻⁾ AMLs comparing normoxia and hypoxic conditions (left), and NF-κB target DEGs within AMLs between hypoxic and hypoxic conditions with mTOR inhibition by Ku-0063794 (right). (b) Table demonstrating the numbers of significantly upregulated or downregulated genes within 3.9a. Significantly upregulated and significantly downregulated were defined as a greater-than 0.25 log₂ fold change, or less-than -0.25 log₂ fold change, respectively, with an adjusted p-value below 0.05. *n* = 6. (c) Comparison

between two DEG datasets: Normoxia vs Hypoxia, and Hypoxia vs Hypoxia + Ku-0063794. Here, the directional change in gene dysregulation (*i.e.* upregulated, downregulated, or no change) was noted between the datasets with the aim of determining how mTOR inhibition may influence hypoxia-dependent inflammation through NF- κ B. Directional change was categorised as either a shift from upregulated to downregulated, downregulated to upregulated, or a change between non-significance to either upregulation or downregulation (# = “or non-significance”).

Prior data (not shown) reveals that STAT3 activation is highly dysregulated within *TSC2*-deficient cells under hypoxia. Thus, the study aimed to investigate whether *TSC2*-deficiency may also modulate the NF- κ B pathway under similar circumstances. Prior studies have already identified that NF- κ B can be activated by hypoxia, and of particular interest, hypoxia induced NF- κ B activation may be reduced via inhibition of IKK (431).

Here, we see that hypoxia indeed appears to regulate NF- κ B within *TSC2*-deficient AMLs (Figure 3.9a). Notably, some pathways appear downregulated whereas others appear upregulated, although these will not all be modulated predominantly via NF- κ B. After inhibition of mTOR with Ku-0063794 under hypoxia we can see that the dysregulated NF- κ B phenotype is not restored, showing that inhibition of mTORC1/mTORC2 hyperactivity does not restore the disease state of NF- κ B activation under hypoxia. These results are consolidated within the table of Figure 3.9b, wherein the balance of upregulated to downregulated genes is not shifted by any large degree.

To try and identify how mTOR inhibition would affect these pathways, two datasets were compared: Normoxia vs Hypoxia (NvH) (as in Figure 3.9a, left), and Hypoxia vs Hypoxia + Ku-0063794 (HvHKu) (as in Figure 3.9a, right). The rationale for this analysis was to see if mTOR inhibition could alter, or otherwise reduce a pro-inflammatory NF- κ B activated phenotype. DEGs were counted based on their directional change in regulation and notated within the table (Figure 3.9.c). *i.e.*, if a gene which is upregulated in the NvH dataset changes to downregulated, or changes to a statistically equal expression between conditions within the HvHKu dataset, it would be counted as “Upregulated \rightarrow Downregulated or non-Significance”.

Here, we see that 44 genes which were previously upregulated within the NvH dataset were either downregulated or equally expressed within the HvHKu dataset. Conversely, 38 genes which were downregulated within the NvH dataset shifted in the opposite direction within the HvHKu dataset. 37 genes exhibited no directional change between the datasets. 29 genes changed from no significant difference in expression within the NvH dataset to a significant

upregulation within the HvHKu dataset, whereas 12 changed from non-significance to a significant downregulation. This may be taken further to suggest that a total of 73 NF- κ B-target genes increase in expression following mTOR inhibition under hypoxia, with a total of 50 NF- κ B-target genes decreasing in expression.

Ultimately, this data suggests that NF- κ B is dysregulated under hypoxia in *TSC2*-deficient AMLs. Furthermore, mTOR inhibition is not sufficient to revert inflammation under hypoxia, and in some cases, may appear to even exacerbate the inflammatory condition.

3.3 Discussion

This chapter investigated the heightened inflammatory responses within *TSC2*-deficient cells. Data indicates that this heightened state of inflammation was not as a direct consequence of mTORC1 signalling, which become aberrantly active when *TSC2* is lost. Therefore, this heightened inflammation upon loss of *TSC2* appears to be mTORC1-independent. Furthermore, this chapter illustrates that the inflammation observed in *TSC2*-deficient cell models was likely dependent on NF- κ B and STAT3.

It was found that NF- κ B and STAT3 activation (and other inflammatory biomarkers) were significantly expressed to higher levels within *TSC2*-deficient cells, and upon treatment with rapamycin, this inflammatory signal was not reduced to a basal level. Of interest, IKK inhibition by BMS345541 was found to diminish this heightened level of STAT3 activity. This suggests that STAT3 activation in TSC is dependent on the NF- κ B pathway. IKK inhibition could also selectively induce apoptosis in *Tsc2*-deficient cells, but not when using the AML cell lines. Direct communication with the Tee lab and unpublished data have repeatedly shown that *TSC2*-restored AMLs tend to be highly sensitive to drug treatments, in terms of viability. This is likely because *TSC2*-restored AMLs are untransformed; they have regained their tumour suppressor function, thus losing the ability to transform. *TSC2*-restored AMLs are also unable to form colonies or tumours within soft agar, demonstrating that they have lost growth capability without cell-cell adhesion. It is likely that this is not seen in MEFs because both *Tsc2*^(-/-) and 'wild-type' MEFs are lacking TP53. During the generation of *Tsc2*^(-/-) MEFs, Prof. David Kwiatkowski identified that a knockout of TP53 was required to establish this cell line effectively (353), likely since TP53 mutation serves as an immortalizing component (432). Therefore, the transformed, TP53-deficient nature of wild-type MEFs may be serving to remove the same heightened sensitivity that we see within *TSC2*-deficient AML cells.

Excessive STAT3 activation is a phenomenon that has been observed previously within TSC in *Tsc2*-deficient MEFs [13], dissociated LAM cells [87] and in brain-tumours of TSC patients (56,365,433). Higher levels of soluble IL-6R have also been observed within the cortical lesions of TSC patients (434). The STAT3 pathway can become hyperactivated via IL-6 trans signalling. Comparatively, STAT3 hyperactivation is also observed within cancerous brain tumours, contributing significantly to their pathogenicity via enhanced angiogenesis, migration, immunity, treatment resistance, and stemness, whilst also impacting the differentiation state of neural stem cells (371,435,436). Like STAT3, excessive activation of NF- κ B is frequently observed within cancerous brain tumours, promoting invasion/metastasis, resistance to therapy, survival, and further propagating an inflammatory signal (379,437,438). This may suggest parallels in neuroinflammation for the research and treatment of TSC-derived brain tumours and cancerous brain tumours such as glioma, glioblastoma, and astrocytoma.

The data presented here also demonstrates some similarities to *in vivo* TSC-patient derived brain tumours. SEN/SEGAs and cortical tubers demonstrate inflammatory transcriptomic signatures and suggest a high degree of immune invasion. Specifically, NF- κ B signalling also appears to be upregulated in these brain tumours. It is possible that high cytokine and chemokine production in *TSC2*-deficient cells is recruiting and activating immune cells.

Interestingly, we can also match several of these upregulated and downregulated genes to those which are upregulated within glioblastoma. Specifically, one transcriptomic study identified 40 genes whose upregulation was correlated with poor-prognosis highly invasive glioblastoma (374). Out of these 40, 21 were also upregulated within SEN/SEGAs, with three (LGALS3, LITAF, ANXA1) playing direct roles in inflammatory processes. Another study identified several other genes which were prognostically poor within glioblastoma of the mesenchymal phenotype, notably including complement factors which are also upregulated within SEN/SEGAs (375). One final study noted 20 of the most significantly differentially expressed genes in glioblastoma, of which 14 were correspondent to genes in SEN/SEGAs (439). Taken together, these results may suggest a phenotypic similarity between SEN/SEGAs and glioblastoma, most notably those of the mesenchymal subtype which represent a similarly heightened inflammatory response (440).

3.4 Conclusion

In conclusion, the data in this chapter has demonstrated a heightened inflammatory response in TSC, which is present in both the currently available *in vitro* models (AML, MEF, and ELT3 cells), as well as transcriptomic studies of *in vivo* patient-derived brain tumours. NF- κ B likely plays an important role in the function of a positive inflammatory feedback loop which ultimately generates cytokines and chemokines for the recruitment of immune cells, as well as exacerbating the neurological conditions in TSC such as epilepsy. A link between heightened NF- κ B activity and STAT3 activity in TSC has also been identified, suggesting that dysregulated inflammatory pathways in TSC can be targeted via NF- κ B.

Chapter 4 – NF- κ B and Surrounding Pathways Within TSC

4.1 Introduction

The previous chapter characterised a hyperactive NF- κ B signalling nexus in TSC diseased cells. It is possible that restoring NF- κ B in TSC could be a potential therapy that warrants further investigation. Some related studies have been carried out. Bortezomib, a proteasome inhibitor, was initially developed for NF- κ B inhibition by inhibiting the degradation of the inhibitor I κ B α . However, studies showed mixed results on the regulation of NF- κ B activity after Bortezomib treatments (441,442). Bortezomib has been used in several studies in TSC. It was shown that Bortezomib when combined with nelfinavir, another ER-stress-inducing drug, enhances endoplasmic reticulum stress in TSC-deficient cells, subjecting them to ER-stress induced death (443). As a single drug treatment, Bortezomib had limited effect in pre-clinical models of TSC (444). Aside from these studies, research into potential therapeutics that may target NF- κ B in TSC is currently lacking. There are likely two key reasons for this. Firstly, the understanding of NF- κ B signalling in TSC is poorly understood and inconclusive. Secondly, the application of NF- κ B targeting therapeutics may also impact a range of other pathways that could cause off-target effects (225). It should also be noted that long-term treatments with anti-inflammatory drugs could result in serious side effects such as renal failure, heart issues, stroke, and gastrointestinal issues (445).

Despite this, further research into the dysregulation of NF- κ B in TSC is likely to be beneficial to better understand this complex disease. By understanding the pathways that are promoted by (or promoting) NF- κ B activation in the disease state, we may unlock new treatments for the various neurological symptoms that are presented within TSC. Inflammation is a hallmark of cancer progression, where inflammation can promote tumour formation via the promotion of proliferative pathways. Furthermore, inflammation can enhance metastasis and cell migration, and this is a highly relevant feature in the TSC-associated disease, LAM. NF- κ B also plays a key role in immune signals, likely involved in the recruitment of immune cells to tumours found in TSC patients.

This chapter seeks to identify how we may disrupt some phenotypic elements which correspond to the tumours which present themselves in TSC patients via inhibition of NF- κ B and related inflammatory pathways. To do this, assays will be employed to examine *in vitro* cancer-related features of TSC model cell lines, which includes *in vitro* colony formation and

cell migration assays. This chapter also aims to identify potential drug targets to accomplish anti-inflammatory action in TSC.

4.2 Results

4.2.1 Inflammatory signalling in the growth of TSC-derived tumours

4.2.1.1 NF- κ B inhibition slows tumours growth

Perhaps the most iconic aspect of TSC is the system-wide presentation of tumours. Specifically, renal angiomyolipomas are thought to be one of the main causes of death in TSC patients, with rapamycin treatment proving insufficient for the absolute removal of tumours (113); tumours shrink during rapamycin treatment and regrow upon discontinuation of treatment.

The generation of 3-dimensional tumours (or organoids) is being more commonly researched in the field of cancer research to better understand tumour microenvironments and the complex interplay between cell types (446). However, most models for 3D culture are either costly, expensive, or time consuming. Soft agar tumour growth assays offer a simple means of assaying the effects of drug treatment on the development of colonies *in vitro*. From this, we can extrapolate the effects of drug treatments on how tumours may grow within TSC patients. For this reason, colony formation assays were used to determine the potency of IKK inhibition on TSC tumour growth. To do this, colonies were grown over the course of 2-4 weeks in the presence of varying concentrations of BMS345541.

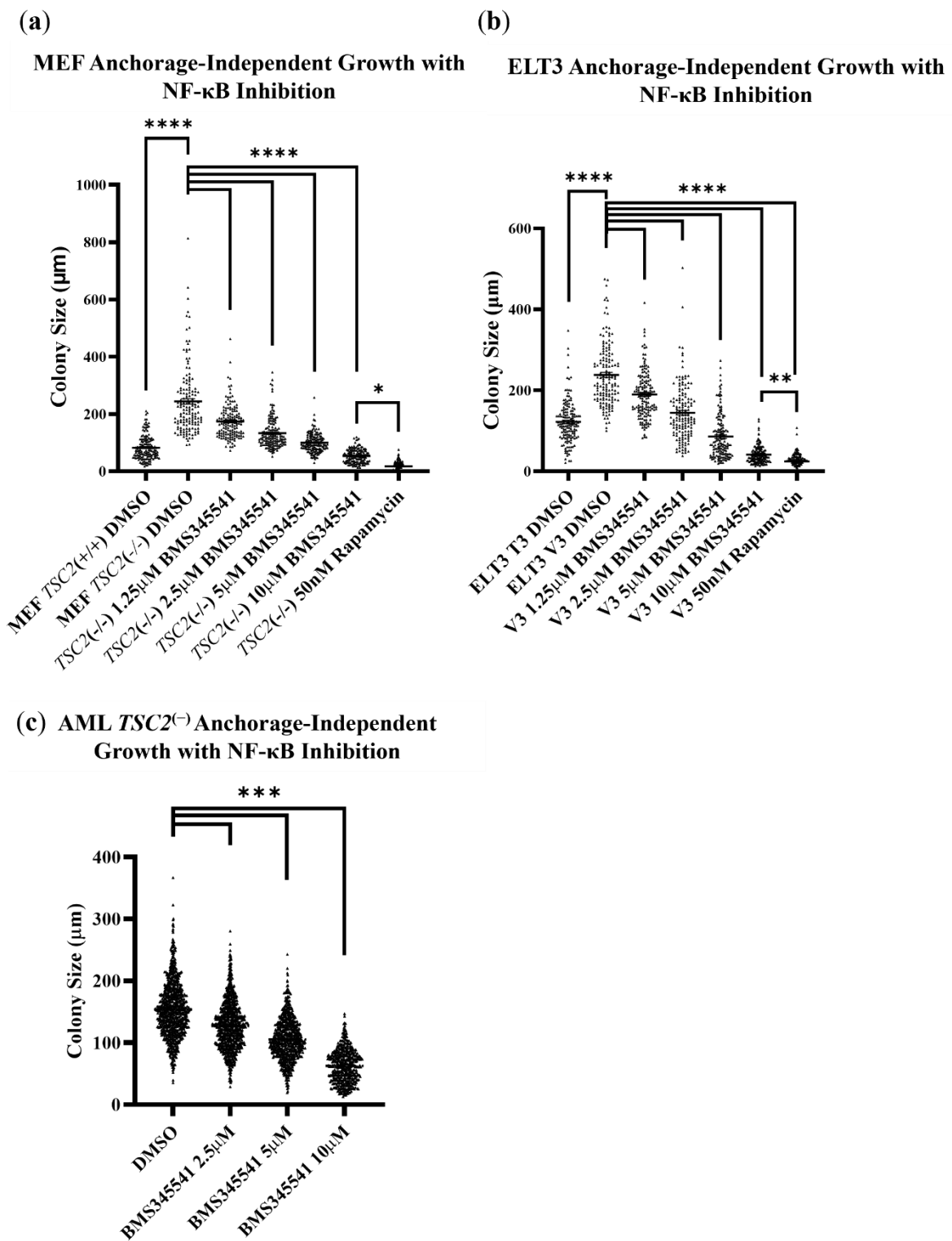


Figure 4.1. IKK inhibition reduces anchorage-independent colony formation *in vitro*. *TSC2*-deficient and their respective wild-type control cells were grown in soft agar assays for 2-4 weeks depending on cell line. (a) MEF, (b), ELT3, (c) and AML cells were grown in the presence of increasing drug concentrations of BMS345541, as indicated, prior to images of colony growth being taken.

Measurements of colony diameters was carried out in Image J. Three wells were counted per condition, all colonies per image were measured. Results were analysed by one-way ANOVA with Tukey's Multiple Comparisons. **(d)** Representative images are shown of colony size reduction after treatment with BMS345541 in *TSC2*-deficient MEF and AML cells. Note: *TSC2* re-expressing AMLs were not used due to an inability to form anchorage-independent colonies.

4.2.1.2 IKK inhibition when combined with rapamycin reduces tumour growth after treatment discontinuation

An issue with current mTORC1 inhibitor treatments for TSC is that tumours do not completely regress. Combinatorial treatments are commonly employed in cancer therapy to improve therapeutic outcomes. This often results in the need for lower total dosages of chemotherapeutics as well as a greater efficacy in reducing tumour burden (447).

Furthermore, since combinatorial treatments often use drugs which are already FDA-approved, the cost of development is significantly lower than the development of a novel drug. Combinatorial treatments can act synergistically or additively to reduce chemoresistance, as well as to induce apoptosis in otherwise hard to treat cancer cell populations.

This study previously demonstrated that combinatorial treatment of BMS345541 and rapamycin had greater efficacy to reduce STAT3 activation. Therefore, combinatorial approaches may be beneficial when treating TSC patient-derived tumours (Figure 4.2). To test this, *TSC2*-deficient AML cells were grown in soft agar as previously described in the presence of either rapamycin, BMS345541, or a combination of the two drugs. After untreated control tumours reached a suitable size, treatment was discontinued, and growth was resumed in drug-free conditions. This experiment would determine whether combinatory inhibition of both IKK and mTORC1 would have a more lasting benefit to prevent tumour growth, even after the discontinuation of treatment.

**Anchorage Independent Growth Assay:
Colony Regrowth After Treatment Discontinuation**

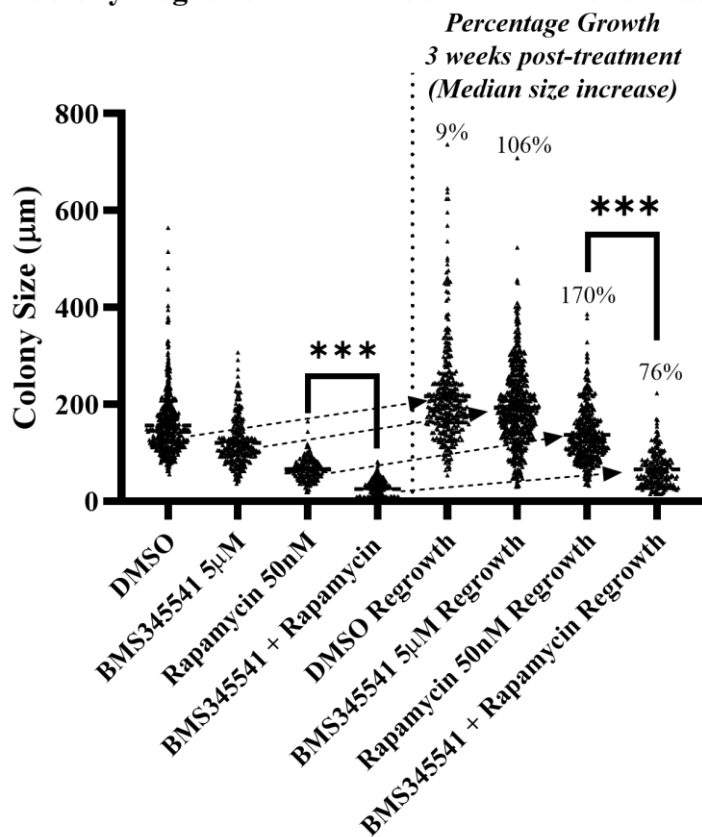


Figure 4.2. Combining inhibition of IKK and mTORC1 has greater efficacy to reduce tumour growth. *TSC2*-deficient AML cells were grown in soft agar over four weeks with either DMSO, BMS345541, rapamycin, or a combination of the two treatments. Colony formation was then measured, and colonies were grown for a further three weeks in the absence of inhibitors prior to re-measurement of tumour diameter. Median size increase is noted between the two timepoints. Three wells were counted per-condition, all colonies per image were measured. Results were analysed by Kruskal-Wallis test with Dunn's multiple comparisons.

Importantly, the data shown here demonstrates clearly that combinatorial treatment with mTORC1 and IKK inhibition is beneficial with regards to a reduction in colony diameter. Importantly, IKK inhibition in combination with rapamycin lead to a stark reduction in the regrowth of colonies, suggesting enhanced cytotoxicity with this drug combination. It is not possible to determine whether this effect was additive or synergistic, as the experiment was not structured in such a way to determine this.

Reducing the growth of colonies in this setting suggests that NF- κ B is having an anti-proliferative effect. To investigate the effects of IKK inhibition on cell proliferation,

Tsc2/TSC2-deficient MEF/AML cells were subject to CyQuant proliferation assays in the presence or absence of either BMS345541 or rapamycin (Figure 4.3). A second inhibitor of the NF- κ B pathway was also used (IMD0354), which functions via inhibition of IKK β .

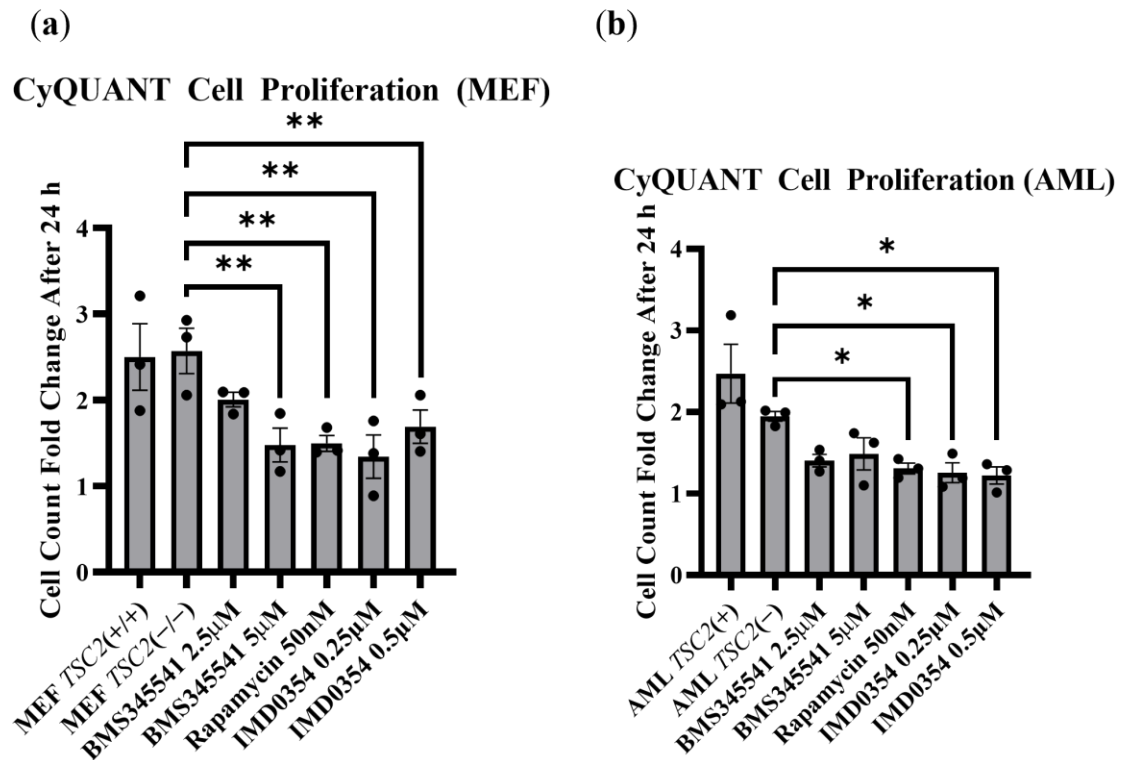


Figure 4.3. IKK inhibition reduces proliferation of *TSC2*-deficient cells *in vitro*. CyQuant assay was used to determine the effects of IKK or mTORC1 inhibition in (a) *Tsc2*-deficient MEF or (b) *TSC2*-deficient AML cells. IKK inhibition reduced proliferation after 24 h, to a level that was comparable with that of rapamycin in both cell lines. $n = 3$, one-way ANOVA with Dunnett's multiple comparisons. Statistics were performed on cell count values. Fold changes are shown.

IKK inhibition reduced cell proliferation significantly in both cell lines, demonstrating a reliance on inflammatory signalling for proliferation. With this data alongside the anchorage-independent growth assays previously described, we clearly show that NF- κ B signalling may play a key role in the growth of TSC-derived tumours.

4.2.1.3 IKK inhibition reduces migration of *TSC2*-deficient cells

A key characteristic of LAM is the propensity of TSC-derived tumour cells to migrate to the lungs in an oestrogen-dependent manner, leading to the growth of smooth muscle-like

tumours and leading to the subsequent loss of lung function (448). Epithelial to mesenchymal transition (EMT) and metastasis are key features of cancers with poor prognosis (449), and these processes rely on the migratory potential of cells. NF- κ B is well known within the context of EMT and migration (450,451), thus it is relevant to explore how NF- κ B signalling may impact migration of *TSC2*-deficient cells. This study aimed to determine whether IKK inhibition was effective at reducing cell migration. To accomplish this, wound scratch migration assays were performed on *TSC2*-deficient AML cells (Figure 4.4).

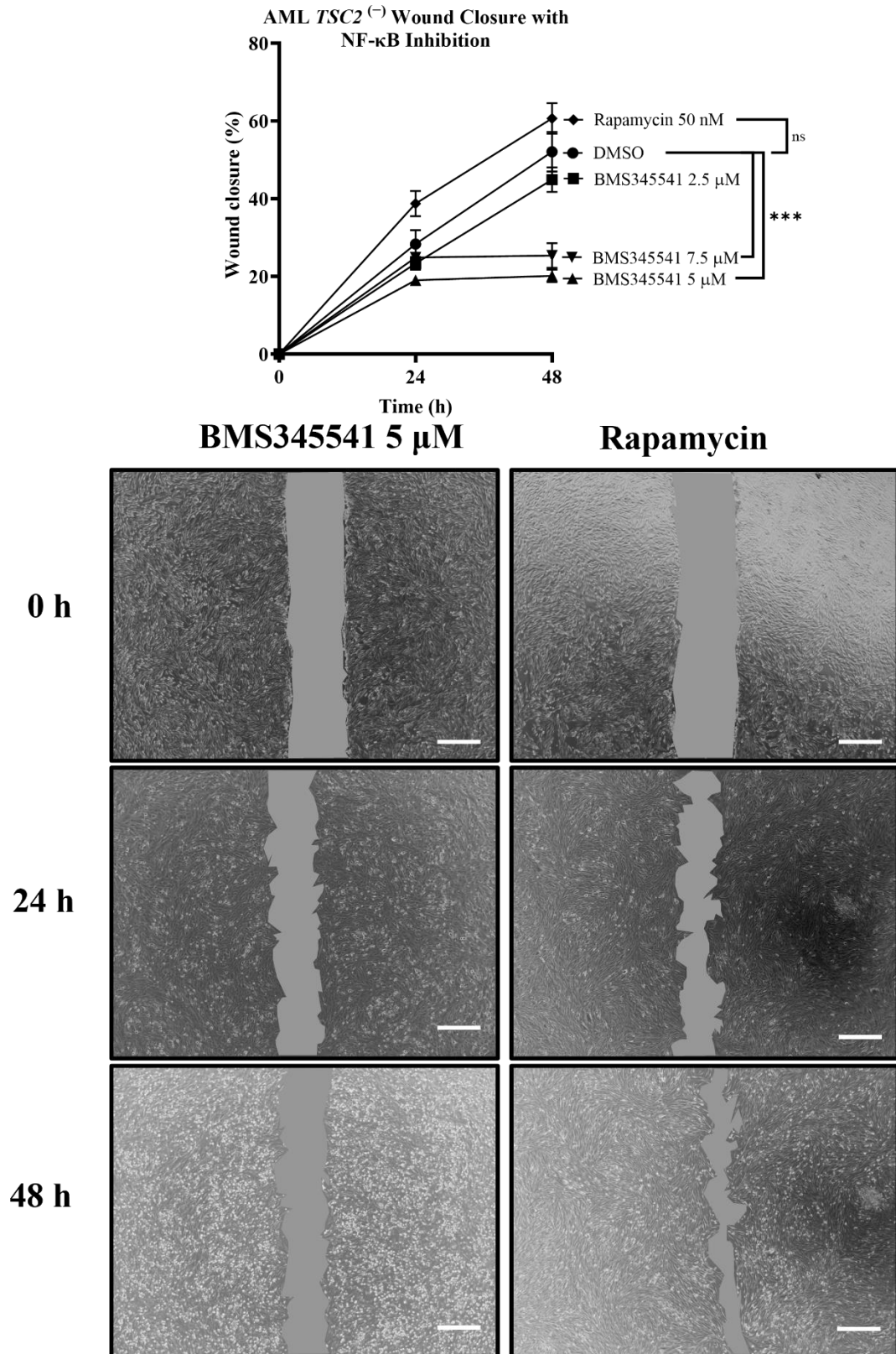


Figure 4.4. IKK inhibition reduces migration of *TSC2*-deficient AML cells. *TSC2*-deficient AMLs were grown to a confluent monolayer prior to treatment with either BMS345541 or rapamycin. A wound scratch in the monolayer was introduced, and cells were imaged at 24 h and 48 h to visualise

wound closure. IKK inhibition slowed wound closure, whereas mTORC1 inhibition was ineffective. Representative images of wounds are shown, with white scale bars at 500 μm . $n = 3$, two-way ANOVA with Tukey's multiple comparisons. Similar results were obtained in *Tsc2*^(-/-) MEFs (data not shown).

Wound scratch assays provide a relatively basic means to investigate cell migration. These assays were performed under conditions of serum depletion to reduce the rates of cell proliferation that occurs during the wound healing response. It was found that IKK inhibition markedly reduced wound closure of *TSC2*-deficient cells, indicating that cell migration was likely being impaired. This may be through regulation of a variety of migration/EMT-involved proteins. Indeed, transcriptomic data of *TSC2*-deficient AML cells demonstrates an upregulation in SNAIL, SLUG, and SIP1, which are considered as NF- κ B regulated EMT-promoting genes (452). mTORC1 inhibition with rapamycin had no effect to block wound closure, suggesting that cell migration of these *TSC2*-deficient cells are unlikely dependent on mTORC1.

4.2.1.4 NF- κ B/mTORC1-dependent gene regulation

The transcriptomic data presented suggests that expression of inflammatory gene targets may be driven through NF- κ B rather than mTORC1. The study aimed to examine a range of inflammatory gene targets in the AML cell line by qPCR (Figure 4.5). Genes were selected based on those that were found to be upregulated in both the AML cells (by RNA-sequencing) and the TSC patient-derived SEN/SEGAs transcriptomic dataset.

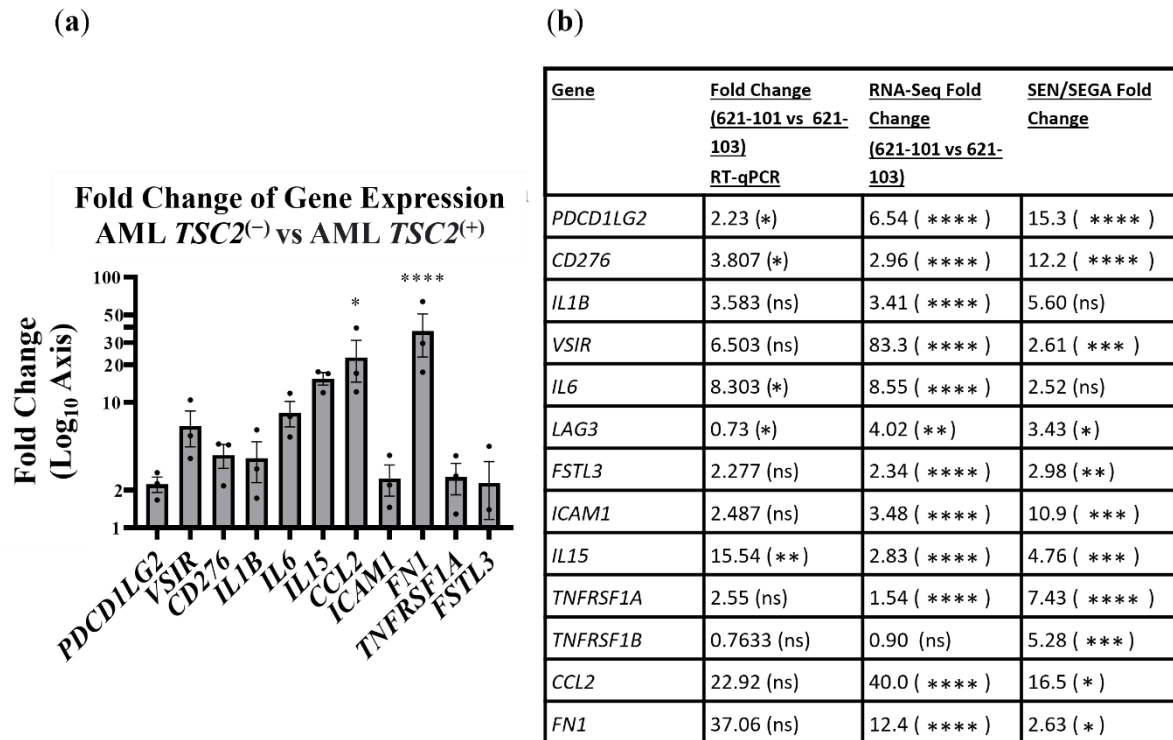


Figure 4.5.1. Various inflammatory genes are upregulated within *TSC2*-deficient AML cells. (a) Inflammatory gene mRNA expression was determined via qPCR, comparing *TSC2*-deficient to *TSC2*⁽⁺⁾ AML cells. Most genes appeared upregulated within the *TSC2*⁽⁻⁾ AML cells. $n = 3$, one-way ANOVA with Dunnett's multiple comparisons. Data was normalised to *HBMS* as the reference gene. (b) Comparison of gene expression between patient-derived SEN/SEGA, AML RNA-sequencing, and AML RT-qPCR. Most genes showed similar directional dysregulation between the datasets.

Figure 4.5.1 shows that the expression of various inflammatory genes were upregulated in *TSC2*-deficient AML cells. While significance was not found, there was a general trend for enhanced expression of genes, which was also found in the AML RNA sequencing data and patient-derived SEN/SEGA (described in Chapter 3). Not shown on the graph are *LAG3* and *TNFRSF1B*, both of which showed minor downregulation. Downregulation of *TNFRSF1B* was expected, as this is mirrored in the AML RNAseq data.

The next aim was to investigate how the expression of these dysregulated genes could be influenced with either IKK or mTORC1 inhibition. To test this, *TSC2*⁽⁻⁾ AMLs were treated for 24 h with either DMSO, 5 μ M BMS345541, 50 nM rapamycin, or a combination of the two inhibitors. RT-qPCR was used to analyse gene expression of various markers (Figure 4.5.2-4.5.5).

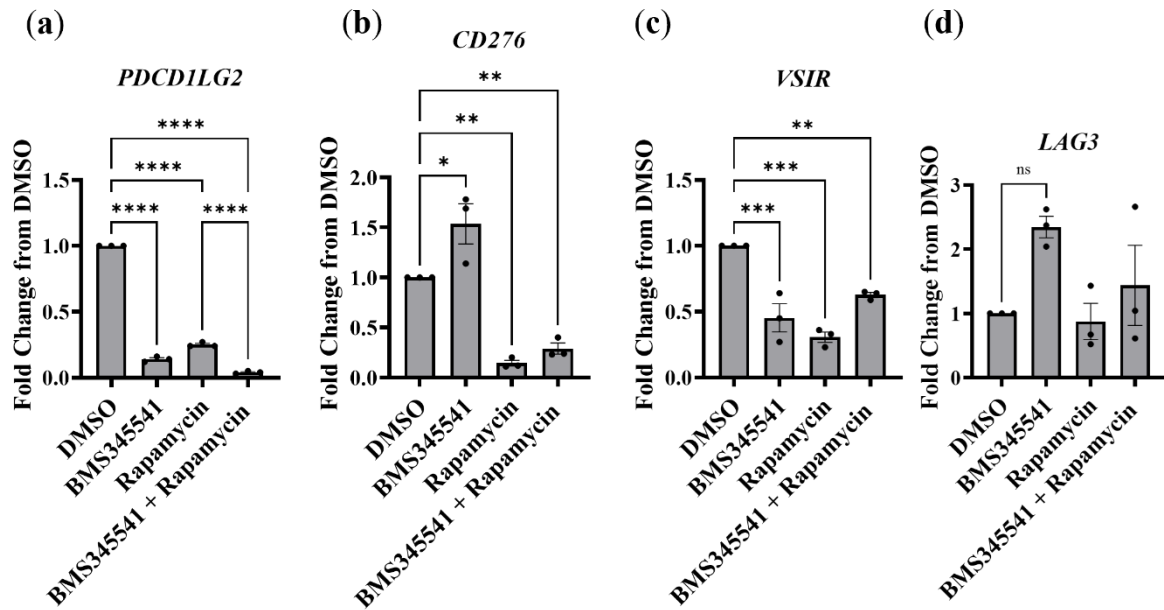


Figure 4.5.2. Combinatory IKK and mTORC1 inhibition may be beneficial for reducing enhanced immune checkpoint expression. RT-qPCR was used to analyse expression of (a) *PDCD1LG2*, (b) *CD276*, (c) *VSIR*, and (d) *LAG3* after singular or dual inhibition of IKK or mTORC1.. $n = 3$, one-way ANOVA with Tukey's multiple comparisons. Data normalised to *IPO8*.

The above genes represent immune checkpoint genes that typically function to suppress the immune system. Many cancers take advantage of immune checkpoints, utilising their upregulation to avoid detection by the immune system. As such, coinhibitory checkpoint regulators are being investigated in cancer therapies (453,454). Interestingly, this appears to also be a feature within TSC, shown by significant upregulation by various immune checkpoint coinhibitors in TSC patient-derived tumours (Figure 4.5.3).

SEN/SEGA: Immune Checkpoint Regulators

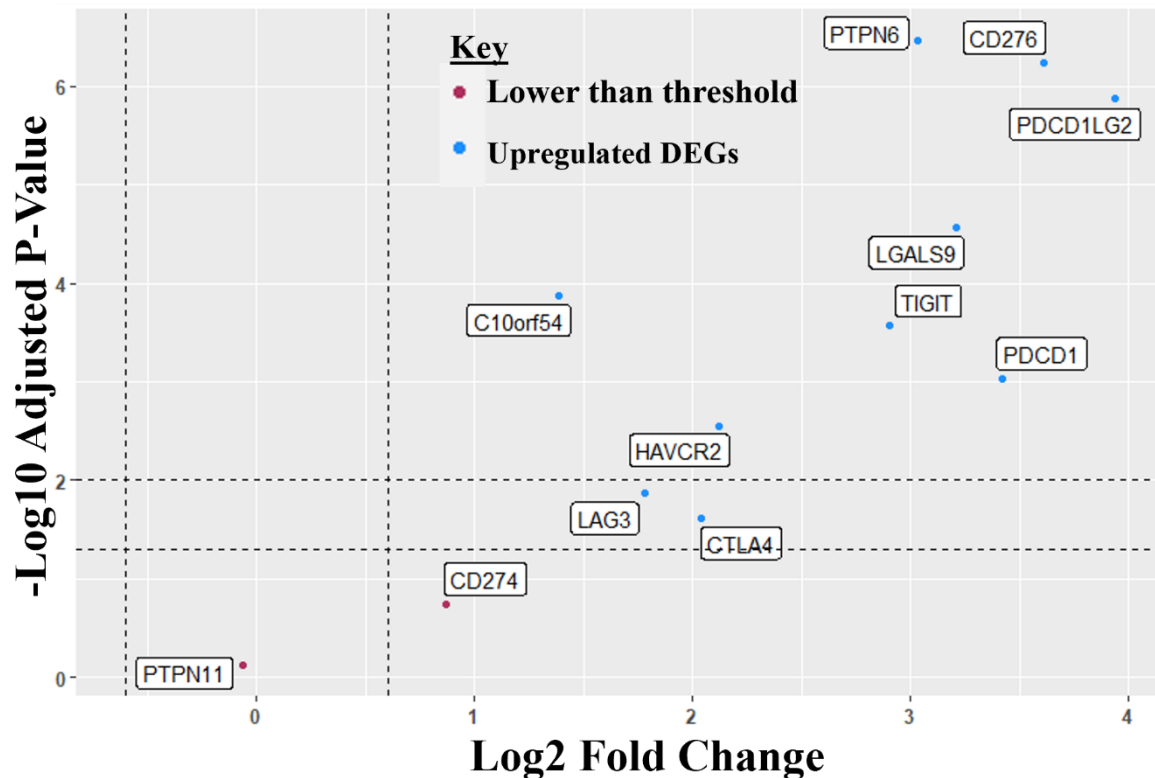


Figure 4.5.3. Immune checkpoint regulators within TSC patient-derived SEN/SEGAs. TSC patient-derived SEN/SEGAs exhibit highly upregulated expression of immune checkpoint regulators. Fold change of gene was from SEN/SEGA tumours versus matched unaffected tissue from TSC patients.

Notably, combinatorial inhibition appeared most effective at reducing *PDCD1LG2* expression (Figure 4.5.2a). This represents the possible importance of immune checkpoint regulators within TSC. However, while IKK and mTORC1 inhibition was beneficial to reduce *PDCD1LG2* and *VSIR* (Figure 4.5.2c), *LAG3* was upregulated by BMS345541 treatment (Figure 4.5.2d). *CD276* was also increased by BMS345541, but could be reduced by rapamycin or a combination of rapamycin and BMS345541 (Figure 4.5.2b). This suggests that single drug inhibition to target either IKK or mTORC1 is not sufficient to restore gene expression of multiple immune checkpoint regulators. Combined treatment was more effective. Current research on immune evasion within TSC is fairly limited, however two recent studies have highlighted potential applicability for immunotherapy in TSC. Firstly, it is known that mTORC1 upregulation can drive *CD276* expression, which agrees with our data (455). Secondly, and perhaps more interestingly, PD-L1 or CTLA4 blockade was highly effective at clearing tumours within *Tsc2*-deficient mice (456). Overall, since we can not

reliably inhibit the expression of immune checkpoint regulators with either mTORC1 or NF- κ B inhibition, further investigation into blockade of this class of molecules may prove beneficial for the treatment of TSC. However, it does appear that at least some of these genes may be upregulated through inflammatory signalling. In Chapter 3, we identified that BMS345541 treatment was highly effective at suppressing PD-L2 expression. BMS345541 also reduced expression of *PDCD1LG2* (the gene of PD-L2). Notably, the combinatorial approach with both mTORC1 and IKK inhibition appears more effective for suppressing PD-L2 gene expression.

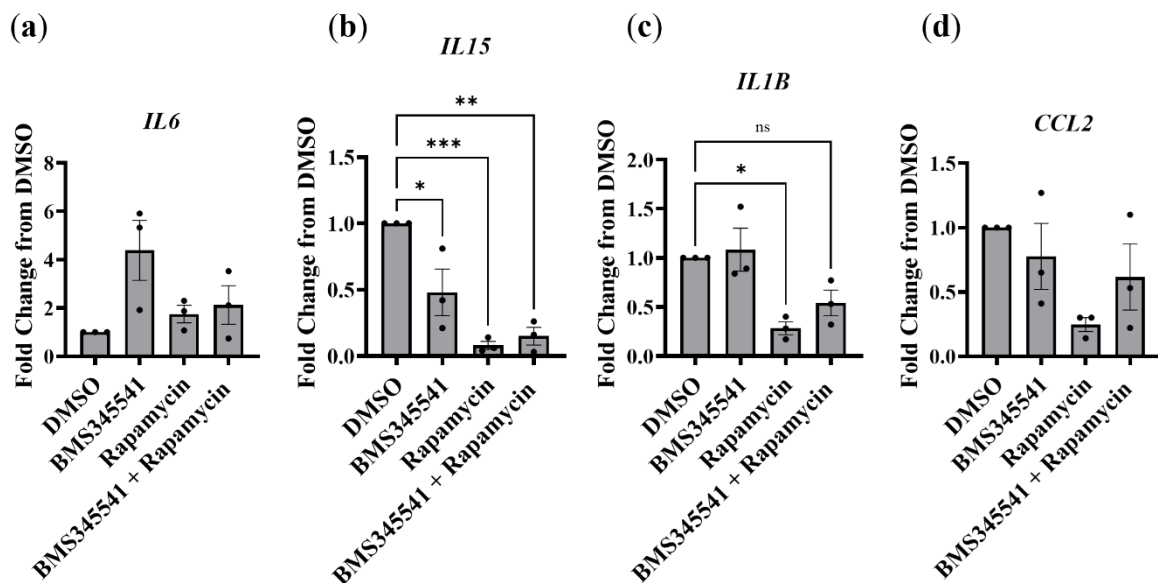


Figure 4.5.4. Combinatorial IKK and mTOR inhibition can be used to target cytokine gene expression. RT-qPCR data was generated as in Figure 4.5.2. The expression of (a) *IL6*, (b) *IL15*, (c) *IL1B*, and (d) *CCL2* was analysed after IKK and/or mTORC1 inhibition. Notably, neither treatment was consistently effective at reducing cytokine gene expression. $n = 3$, one-way ANOVA with Dunnett's multiple comparisons.

IL15 was drastically reduced by both IKK and mTORC1 inhibition (Figure 4.5.4b). Expression of both *IL1B* and *CCL2* was relatively unchanged by BMS345541 treatment, however this was sensitive to rapamycin (Figure 4.5.4 c-d). Some findings from this experiment might appear contradictory to previous results. Specifically, since we see a significant reduction in IL-6 secretion after IKK inhibition (Chapter 3). Given this previous finding, it might be expected that *IL6* mRNA expression would also be lower after IKK inhibition. However, this does not appear to be the case. Instead, *IL6* mRNA expression was highly upregulated after IKK inhibition (Figure 4.5.4a).

Several studies may help explain some of these findings (382,383). It was demonstrated that unphosphorylated STAT3 can drive the expression of a wide range of inflammatory genes, including *IL6*. Through this, STAT3 can engage in a self-propagating cycle. Previously, we identified that IKK inhibition stimulated an initial spike in phosphorylated STAT3 prior, followed by a decrease in both phosphorylated and unphosphorylated STAT3 over a longer period of time. It is important to note that high levels of mRNA gene expression does not necessarily conform to an equivariant high level of protein expression. For instance, high mRNA levels of *IL6* may not translate immediately to high protein levels of IL-6. This may be especially the case when we consider that rapamycin would likely slow down protein translation of gene transcripts, *i.e.*, since mTORC1 drives translation initiation via S6K1 and 4E-BP1 (457).

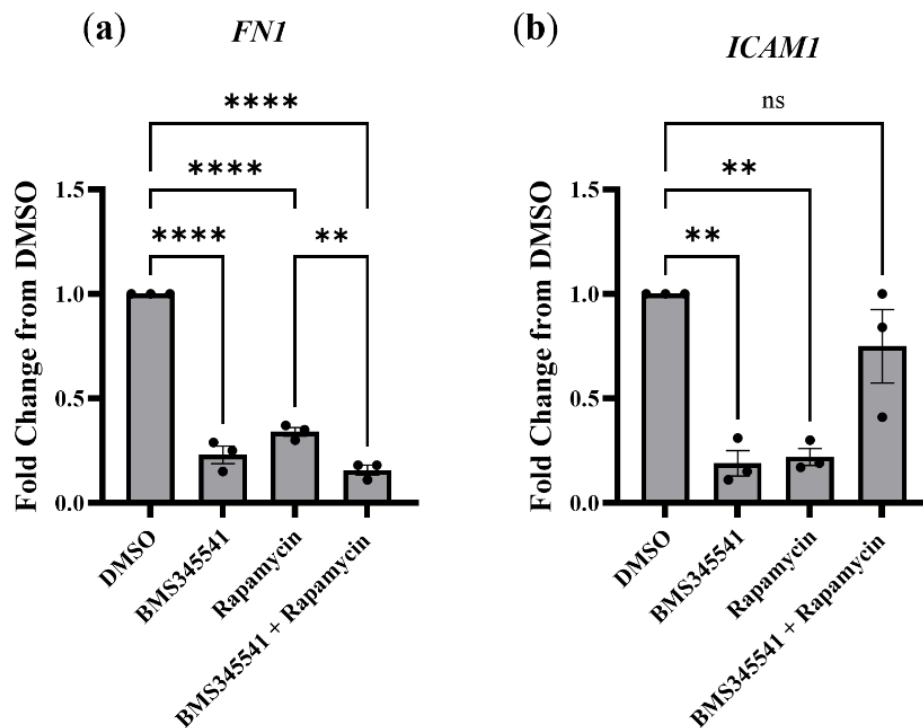


Figure 4.5.5. IKK inhibition may reduce migration via downregulation of *FNI* and *ICAMI*. RT-qPCR data was generated as in Figure 4.5.2. The expression of (a) *FNI*, and (b) *ICAMI* was analysed after IKK and/or mTORC1 inhibition. IKK inhibition proved effective at reducing the expression of both genes. $n = 3$, one-way ANOVA with Tukey's multiple comparisons.

Both *FNI* and *ICAMI* are very highly upregulated within *TSC2*-deficient AMLs by 12.3- and 3.5-fold, respectively. It is possible that this upregulation of fibronectin may even be

observed while handling the cells during tissue culture; *TSC2*-deficient AMLs have a tendency to slough off a thick unidentified substance during trypsinisation. This may be due to a heavy buildup of extracellular matrix components such as fibronectin. Tumour cells within a microenvironment of high fibronectin typically have higher migration, and cancer patients with high fibronectin expression also have a higher proportion of metastasis (458). ICAM1 is a cell surface glycoprotein that mediates intercellular adhesion. ICAM1 can be induced by NF- κ B stimulation (408). While ICAM1 is typically associated with the migration of leukocytes, ICAM1 has also been shown to mediate the migration of cancer cells (459). ICAM1 also plays a role in pro-inflammatory signal transduction, wherein ICAM ligation upregulates CCL5 (460) (which is notably also upregulated within AML cells and TSC patient-derived SEN/SEGA). Crucially, IKK inhibition was highly effective at reducing *FNI* expression, as was rapamycin to a lesser degree (Figure 4.5.5a). Both treatments were able to reduce *ICAMI* mRNA expression (Figure 4.5.5b). It is known in general that NF- κ B influences migration (as mentioned in section 4.3.1.3), and IKK inhibition reduced the migration of *TSC2*-deficient AMLs. It is likely that NF- κ B drives cell migration through pro-migratory factors, such as ICAM1 and FN1. It is unclear why combinatorial treatment reduced the inhibitory effect on *ICAMI*, although this may hint at crosstalk between mTORC1 and NF- κ B signalling.

The RT-qPCR data shown here provides insights into the mechanism behind how inhibition of the NF- κ B pathway may reduce an inflammatory state. Importantly, compensatory pathways appear to become activated upon inhibition of IKK, possibly mediated through the poorly understood mechanism of unphosphorylated STAT3 target activation (such as *IL6*). These feedback signalling mechanisms may not persist for longer durations of pathway inhibition, since in Chapter 3 it was shown that the biphasic response of IKK inhibition is reduced after 24 h. Therefore, it would be beneficial to explore the long-term effects of IKK inhibition on inflammatory pathways in the future.

4.2.2 Alternative pathway targeting

A key drawback of the study so far is a lack of clinical applicability. The IKK inhibitor used so far, BMS345541, is not a clinically approved drug. Rather, it has served as a means to investigating the role of NF- κ B in TSC *in vitro*. To progress this study, drugs that are clinically approved (or in the process of clinical approval) which target NF- κ B were required.

NF- κ B pathway inhibitors generally function through indirect mechanisms, rather than through the direct inhibition of NF- κ B pathway components. Several drugs were selected for this purpose:

Suberoyl anilide hydroxamic acid (SAHA), or Vorinostat, is a histone deacetylase inhibitor that is currently under development for a range of cancer types by Merck (461). SAHA has been shown to inhibit NF- κ B via enhanced degradation of the NF- κ B component IRAK1, leading to a reduction in TLR4 signalling (462). SAHA treatment has also been shown to increase NF- κ B hyperactivity and lead to lethal reactive oxygen species (ROS) production in cancer cells (463). This may not be beneficial in the context of TSC, since we see an upregulation in anti-oxidant genes such as GSS and GPX, which may counteract any ROS-induced lethality of such a treatment.

Lenalidomide is an approved treatment for multiple myeloma, which has immunomodulatory activity (464). The mechanisms of lenalidomide are diverse but a key feature is the ability to promote the proliferation and activity of immune cells. In this sense, *in vitro* applications for our purposes are limited, however lenalidomide has a more direct mechanism of action in cancer cells (465). Specifically, lenalidomide is able to reduce cytokine secretion (including IL-6, IL-1 β and TNF α) as well as exert anti-migratory and anti-angiogenic effects.

Lenalidomide has also been shown to downregulate NF- κ B (466).

Aspirin is known to inhibit NF- κ B (467) and STAT3 (468) activity, the latter of which is via blockade of IL-6. Of interest, a clinical trial (NCT03356769) of 98 participants with TSC also noted that aspirin showed efficacy in reducing refractive seizures, demonstrating potential applicability in the treatment of TANDs. This study attempted to look at the effect of aspirin on STAT3 and RelA phosphorylation, but no noticeable changes were observed (data not shown).

Resatorvid, like SAHA, is capable of reducing Toll-like receptor (TLR)4 signalling via direct binding and inhibition of TLR4 (469). Through this, Resatorvid would indirectly reduce NF- κ B and interferon signalling. Resatorvid has also shown to restore neuroinflammation via inhibition of IL-1 β , NF- κ B, and TNF α (470). Studies have also shown potential applicability for Resatorvid as an add-on therapy to treat cancer (471,472).

R-7050 is an antagonist for TNFR1 and has potential neuroprotective effects (473). As TNF α signalling appears to be dysregulated within TSC patient-derived brain tumours, it was considered that TNFR1 inhibition would help alleviate epileptic activity (474). Indeed, it was

shown that R-7050 reduced hyperexcitability in neural cells, thus reducing the severity of epilepsy (475). However, the role of TNF α in epilepsy is somewhat controversial (216).

Diacerein (DCN) will be discussed in greater depth later in this chapter. DCN is an approved treatment for rheumatoid arthritis (RhA) (476). In general, DCN is metabolised to rhein (cassic acid), a naturally occurring anthraquinone in rhubarb, and both DCN and rhein function to inhibit IL-1 β activity (477).

Of note, many of these pathway inhibitors were selected prior to the acquisition of the transcriptomic data from the *TSC2*-deficient AML cells. Thus, this selection of drugs was based on the inflammatory gene expression signatures of SEN/SEGAs and cortical tubers. This may partially explain the lack of efficacy in inhibiting NF- κ B signalling within the AML cell line. For example, SAHA functions to inhibit NF- κ B via inhibiting TLR4 signalling. While *TLR4* gene expression was significantly upregulated in SEN/SEGAs, *TLR4* expression was not affected in the AML cells. Therefore, these drugs might have had better capacity to block inflammatory signals in neural TSC cell line models, rather than the AML cells.

4.2.2.1 Effects of pathway inhibitors in TSC-associated inflammatory pathways

To begin to probe the efficacy of alternative inflammatory pathway inhibitors, initial drug dose experiments were carried out to identify appropriate concentration ranges of the drugs. These were trialed on *TSC2*⁽⁻⁾ AML cells for a 24 h treatment duration under serum starvation (Figure 4.6.1). Notably, the concentrations of all the drugs used did not appear to exert cytotoxicity after 24 h.

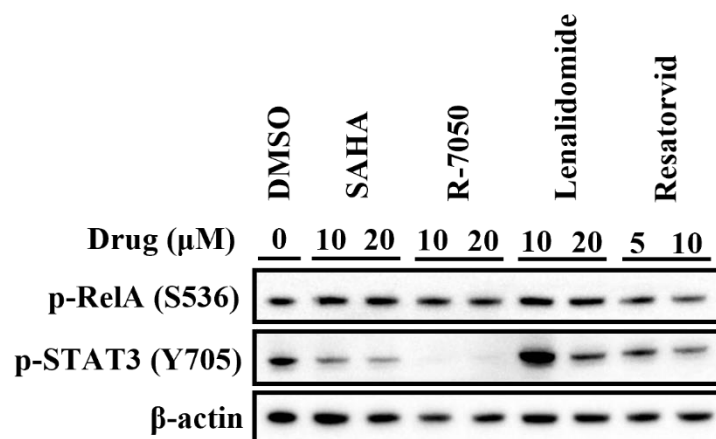


Figure 4.6.1. Exploratory experiments ($n = 1$) show potential for anti-inflammatory effects in *TSC2*⁽⁻⁾ AMLs in trialed drugs. *TSC2*⁽⁻⁾ AMLs were treated with SAHA, R-7050, Lenalidomide, Resatorvid, or DMSO for 24 h prior to lysis. RelA and STAT3 phosphorylation were then assayed by western blot. Results demonstrate potential anti-inflammatory activity, particularly within SAHA and R-7050-

treated samples. Resatorvid also appeared to reduce p-STAT3 phosphorylation, and also RelA phosphorylation.

As SAHA and R-7050 appeared to have the clearest effects on STAT3 activation, they were assayed further (Figure 4.6.2). *TSC2*-deficient AMLs were treated with varying drug doses for 24 h under serum starvation. Cells were lysed and RelA and STAT3 phosphorylation was determined by western blot (Figure 6.2a).

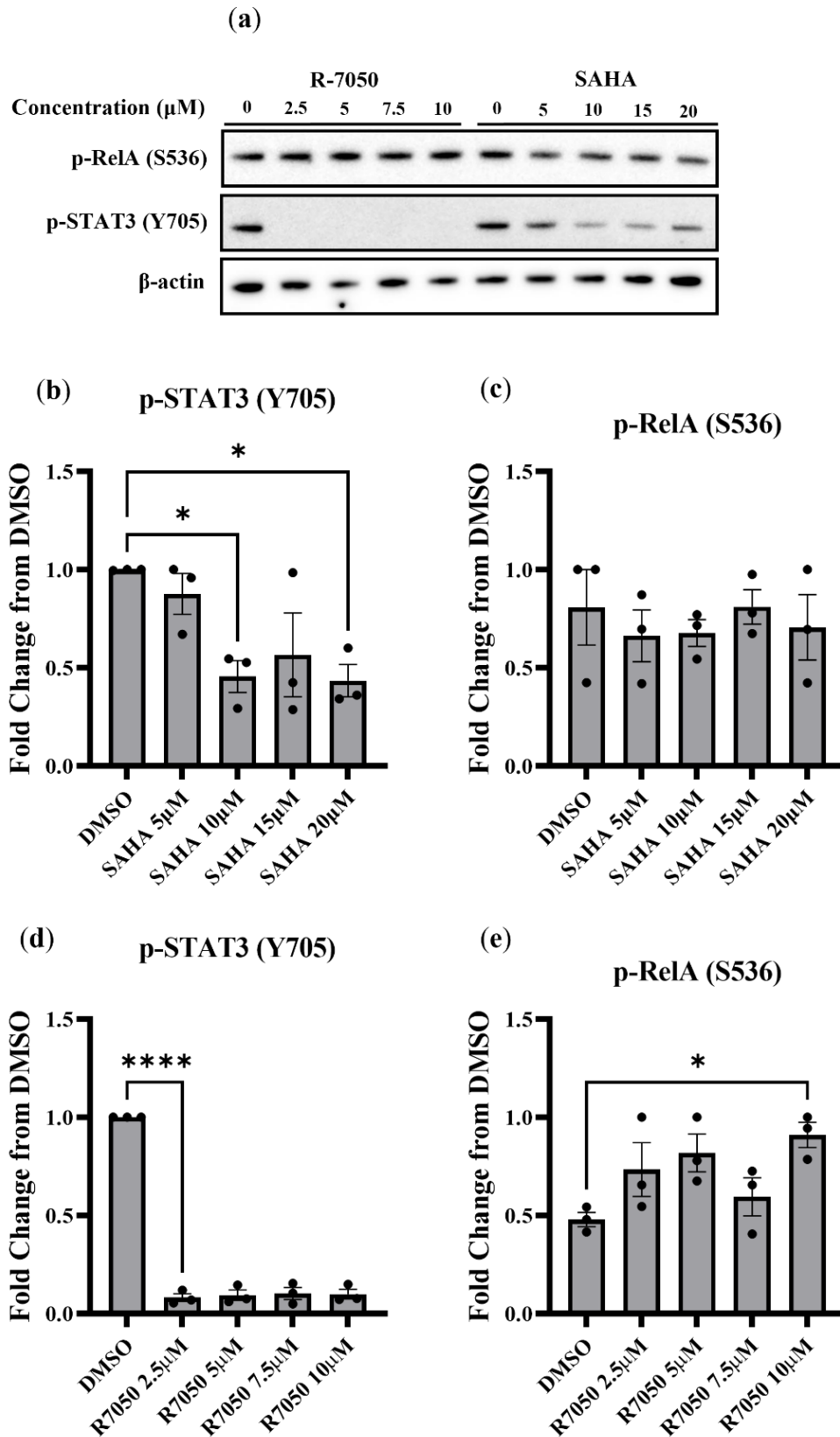


Figure 4.6.2. SAHA and R-7050 show efficacy in reducing STAT3 phosphorylation, but not RelA phosphorylation within *TSC2*-deficient AML cells. (a) Western blot was performed on samples of *TSC2*-deficient AML cells treated with increasing concentrations of R7050 or SAHA. Densitometry

analysis was performed, and the fold change in expression of (b) p-STAT3 (Y705), (c) p-RelA (S536) after treatment with SAHA was plotted. (d-e) A similar analysis was performed after treatment of cells with R-7050. $n = 3$, one-way ANOVA with Dunnett's multiple comparisons. Data normalised to β -actin.

SAHA was also able to reduce tumour growth in MEF and AML cells lacking TSC2 (Figure 4.6.3).

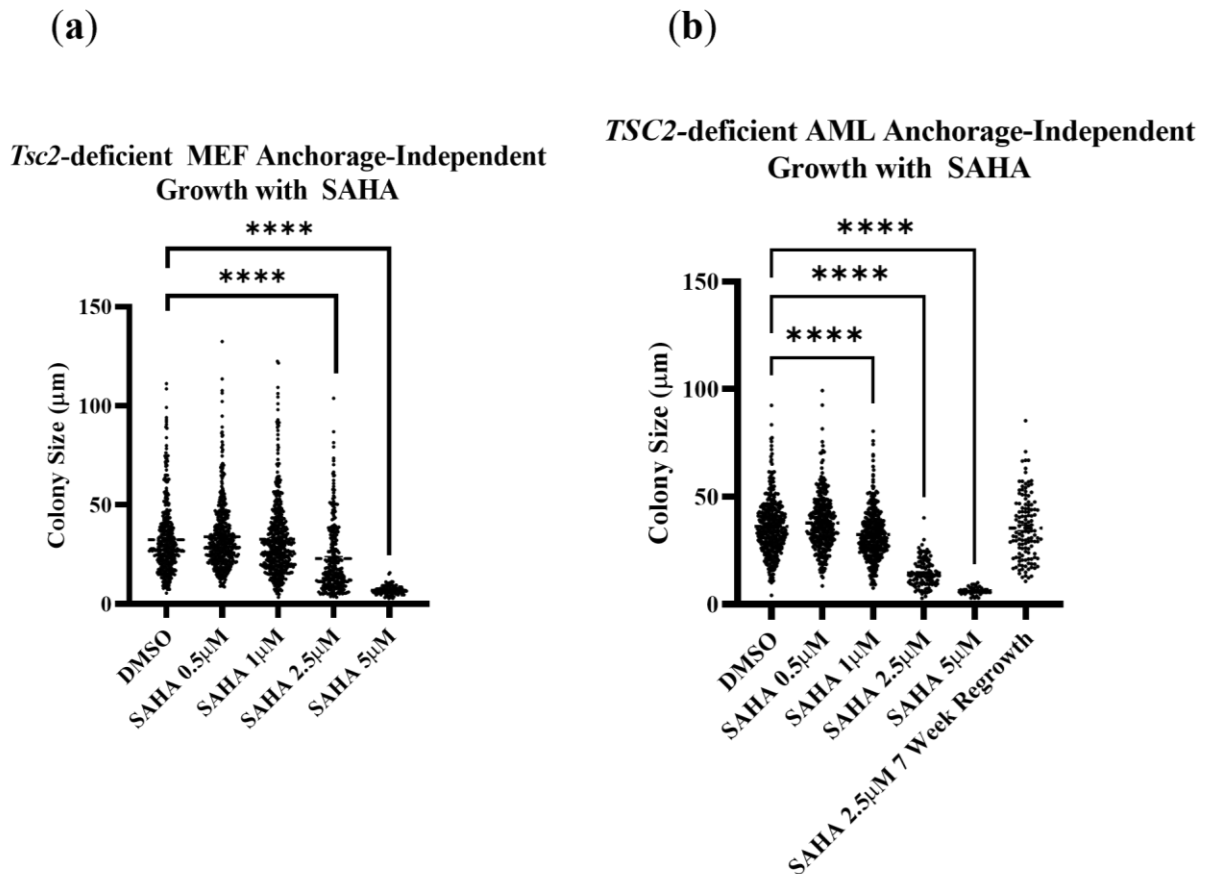


Figure 4.6.3. SAHA reduces anchorage-independent colony growth in *Tsc2/TSC2*-deficient cells. (a) *Tsc2*-deficient MEF cells were grown over 2 weeks with SAHA supplemented. SAHA significantly reduced the growth of *Tsc2*-deficient colonies. (b) Similarly, SAHA reduced growth of *TSC2*-deficient AML colonies over 4 weeks. Upon treatment discontinuation, colonies that were treated with 2.5 µM SAHA were able to regrow over 3 weeks, however with significantly fewer colonies present. Statistics performed as in Figure 4.2.

At the concentrations used, both R-7050 and SAHA appeared effective at reducing STAT3 activity (reduced Y705 phosphorylation of STAT3) but were not effective at reducing RelA phosphorylation. Similarly, SAHA reduced anchorage-independent colony formation. R-7050 proved too cytotoxic to cells over extended treatment durations, so soft-agar assays in R-7050 are not shown. Due to the epigenetic modality of SAHA, it will be difficult to ascertain how

SAHA exerts its anti-inflammatory effects. Methods such as ChIP-Seq may be beneficial in this regard. *HDAC1* and *HDAC3* (the proteins of which SAHA preferentially inhibits) are both slightly downregulated in *TSC2*-deficient AML cells. SAHA also had no effect on RelA phosphorylation. A brief experiment was also carried out wherein it was demonstrated that SAHA at 20 μ M also significantly enhanced TNF α -mediated apoptosis (data not shown). Altogether, this highlights a potential benefit of epigenetic therapies in TSC, however this was not further analysed within this study.

Conversely, R-7050 appeared to slightly increase RelA phosphorylation. This seems contradictory to the proposed mechanism of R-7050, assuming that it should block TNF α -related NF- κ B signalling. However, with transcriptomic data of *TSC2*-deficient AMLs, we can see that transcripts of *TNF* do not appear to be present within the cell line. Similarly, other known TNFR1 ligands such as RANK and CD40 do not appear to be highly expressed. This ultimately suggests that TNF α -related signalling is not driving NF- κ B activation within the *TSC2*-deficient AML cells, and that the effect of R-7050 on STAT3 inhibition is via a different mechanism from TNF α /TNFR1.

Given this information, it was curious that R-7050 had such a strong impact on STAT3 activity. This prompted further investigation into the mechanisms of R-7050. While it is known to block TNFR1, R-7050 also has effects on IL-1 β activity. This suggested that IL-1 β was a valid drug target in the context of TSC. This notion was explored further in the next set of experiments.

4.2.2.2 IL-1 β and rheumatoid arthritis in TSC

A hypothesis was made that IL-1 β signalling might be a key driver of NF- κ B and STAT3 signalling. Genes related to IL-1 β signalling were plotted from the RNAseq data sets from SEN/SEGAs and the AML cells (Figure 4.7). The gene list was compiled from an RNA-Seq analysis and cDNA microarray of IL-1 β responsive genes (478,479). A similar plot for cortical tubers was also made, showing similar trends but with lower significance (not shown).

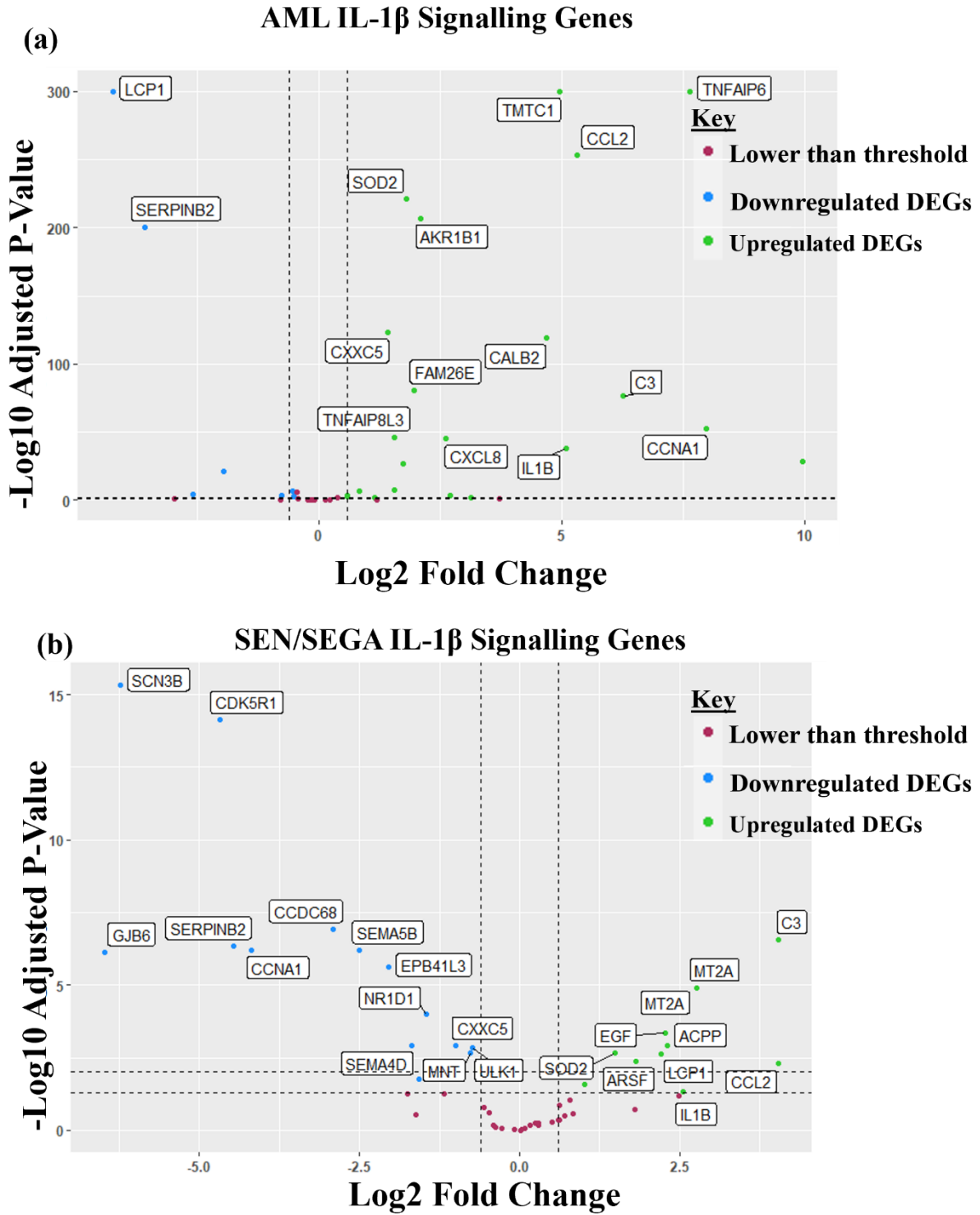


Figure 4.7.1 IL-1 β signalling is dysregulated in TSC. Volcano plots showing a set of IL-1 β related genes in **(a)** *in vitro* AML cells and **(b)** patient derived SEN/SEGAs. Notably, IL-1 β signalling appears far more upregulated within the AML dataset than SEN/SEGAs, although there was still a significant upregulation of *IL1B* in SEN/SEGAs.

GO analysis of SEN/SEGAs and cortical tubers highlighted that the most upregulated genes within these datasets shared a similar profile to RhA. To validate this, the top 50 associated

genes with RhA (obtained from Malacards.org (480)) were plotted from the SEN/SEGA and *in vitro* AML RNA-Seq dataset (Figure 4.7.2). A plot for cortical tubers was also generated and showed similar trends (not shown).

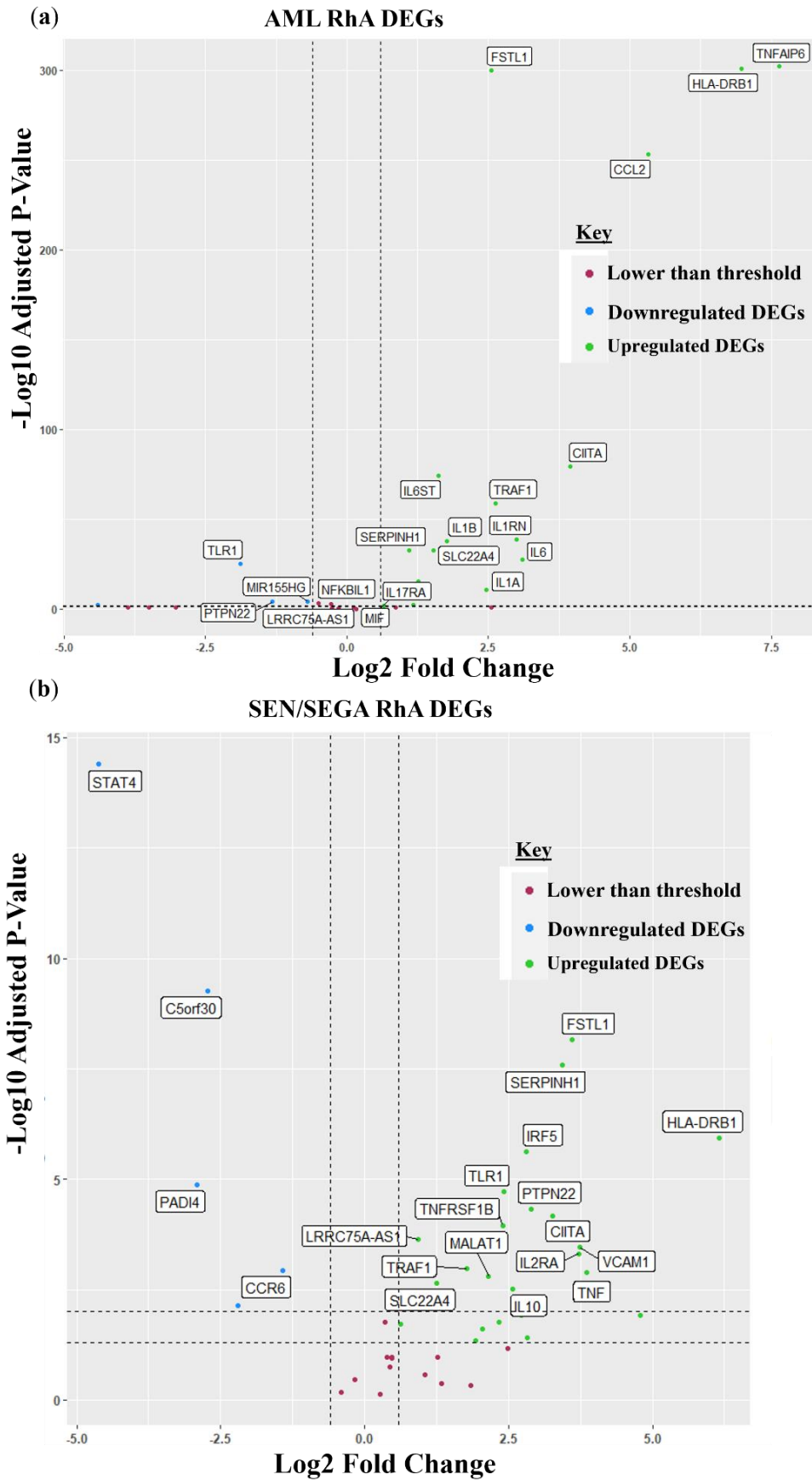


Figure 4.7.2. Rheumatoid Arthritis-associated genes were upregulated within *TSC2*-deficient cells. Volcano plots showing a set of RhA-associated genes within (a) *in vitro* AML cells and (b) TSC

patient derived SEN/SEGAs. Both the *in vitro* and *in vivo* datasets demonstrate upregulation of genes that are associated with RhA. The top 20 most significant genes are labelled.

To build from this, an IL-1 β inhibitor was purchased. As mentioned prior, DCN is a treatment for RhA, and works through inhibition of IL-1 β receptors and IL-1 β production within cells, wherein the latter function comes from the metabolite, rhein. Interestingly, while we see that IL-1 β signalling appears dysregulated in TSC (with IL-1 β scoring a 3.4-fold change), GO data also highlighted a disease similarity of TSC to RhA. RhA scored as the third highest disease match (preceded by TSC and lupus erythematosus) in the top 300 upregulated genes in SEN/SEGAs, and the eighth highest within cortical tubers. To begin this investigation, *TSC2*-deficient AML and *Tsc2*-deficient MEF cell lines were treated with DCN, and the effect on STAT3/NF- κ B activity was determined (Figure 4.8.1). DCN 25 μ M is within clinical relevance with respect to known systemic circulation (481). Due to metabolism of DCN to rhein, 50 μ M is also close to clinical relevance.

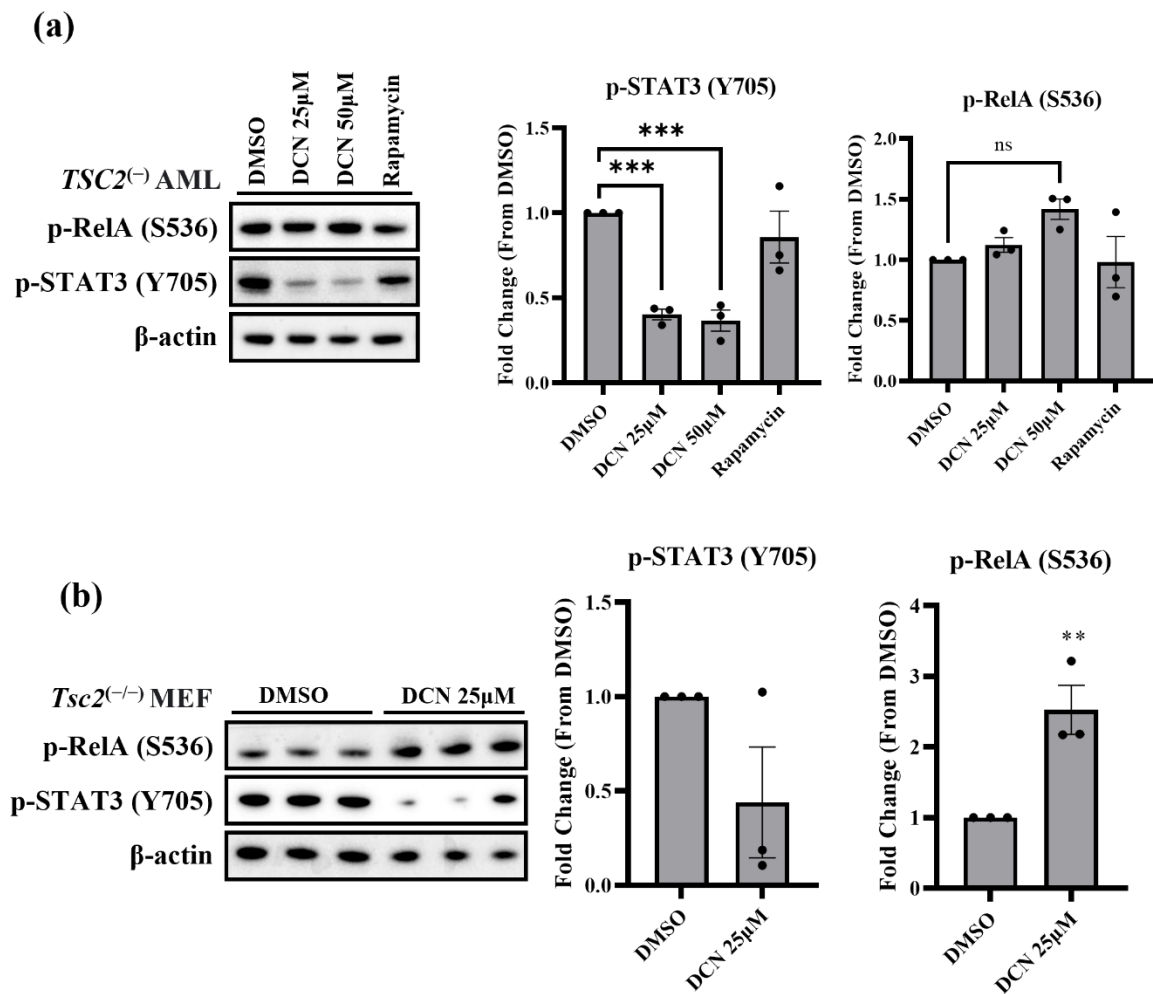


Figure 4.8.1 Diacerein potently reduced STAT3 tyrosine-phosphorylation in *TSC2/Tsc2*-deficient cells. (a) *TSC2*-deficient AMLs were treated with DCN (25 or 50 μ M), or rapamycin (50 nM) for 24 h

prior to lysis and analysis by western blot. $n = 3$, one-way ANOVA with Dunnett's multiple comparisons. Data normalised to β -actin. **(b)** *Tsc2*-deficient MEFs were treated with 25 μ M DCN for 24 h and analysed by western blot. $n = 3$, unpaired t-test. Data normalised to β -actin.

STAT3 phosphorylation in *TSC2*-deficient cells appears to be partially dictated by IL-1 β signalling. This is shown clearly by the inhibition of STAT3 phosphorylation by DCN in both cell lines. However, the apparent upregulation of RelA phosphorylation is contradictory, if we assume that RelA phosphorylation is a key marker of NF- κ B activity. This is unexpected when we consider the supposed mechanism of IL-1 β signalling. Typically, IL-1 β functions via binding to the dimerised IL1R1/IL1RAP receptor, leading to the phosphorylation and degradation of I κ B, leading to NF- κ B activation (482). This signalling mechanism can become a self-sustaining cycle, via NF- κ B-dependent stimulation of the NLRP3 inflammasome, which in turn upregulates caspase-1 to cleave IL-1 β to the active form (483). NF- κ B activity can also stimulate the production of IL-1 β directly (484). However, it would appear that this increase in NF- κ B activity via RelA phosphorylation (while lower in *TSC2*-deficient AMLs), is not sufficient to return the high level of Y705-phospho-STAT3. It is reasonable to point out a limitation in the work so far with regards to identifying NF- κ B activity: the phosphorylation of RelA on the serine site is not the only indicator on the current state of NF- κ B signalling. The state of NF- κ B could be further investigated in future experimentation by transcriptional activation ELISAs (as in Chapter 3). Furthermore, while RelA phosphorylation on S536 is typically considered as being the standard post-translational modification of RelA for pro-transcriptional activity, a recent study suggests that it may have inhibitory activity of NF- κ B signalling (485).

To expand on this, the effect of DCN on IL-6 secretion in *TSC2*-deficient AML cells was also assayed. Conditioned media was collected after 24 h treatment with DCN and assayed for IL-6 via ELISA as described in the previous chapter (Figure 4.8.2). ELISAs were performed as described in Chapter 3.

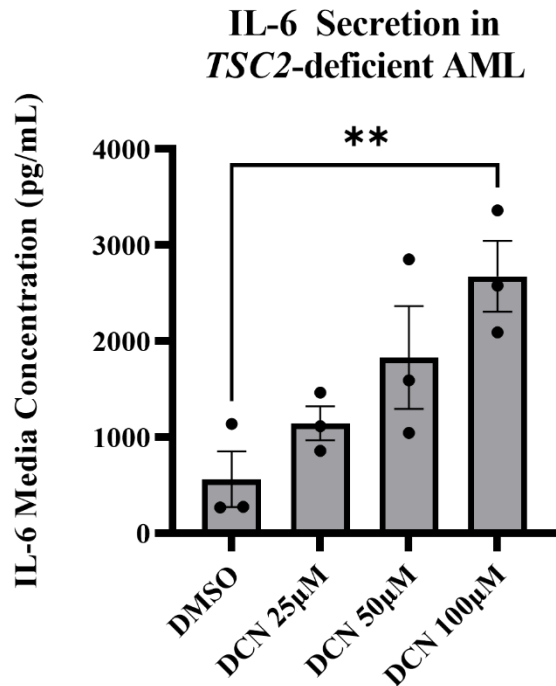


Figure 4.8.2. Diacerein potently increases IL-6 secretion in *TSC2*-deficient AML cells. *TSC2*-deficient AML cells were treated with DCN for 24 h and IL-6 media concentration was assayed by ELISA. $n = 3$, one-way ANOVA with Dunnett's multiple comparisons. Data normalised to total protein quantification.

Surprisingly, DCN significantly increased IL-6 secretion in the *TSC2*-deficient AML cells by around 5-fold (at 100 μ M DCN). This was unexpected, given that DCN could also greatly reduce Y705 STAT3 phosphorylation. These findings are in contrast with other studies. One study found that DCN reduced IL-6 concentration and Y705 p-STAT3 in the colon of rats after induced colorectal cancer (486). It could be expected that high IL-6 production would boost STAT3 phosphorylation after DCN treatment. This may not occur because DCN may be able to inhibit IL-6 binding to IL-6R (487). This strongly demonstrates the overall applicability of DCN in treating TSC; DCN may suppress dysregulated IL-1 β and IL-6 signalling. To further investigate the role of IL-1 β signalling in TSC, a specific IL-1 β inhibitor would need to be investigated in similar assays.

Currently, we see that despite an induction of IL-6 secretion, DCN can reduce phosphorylation of Y705 in STAT3, indicating a strong potential for combatting TSC-mediated inflammation. To further investigate this, anchorage-independent colony formation assays were used in *TSC2*-deficient AMLs and *Tsc2*-deficient MEFs (Figure 4.9).

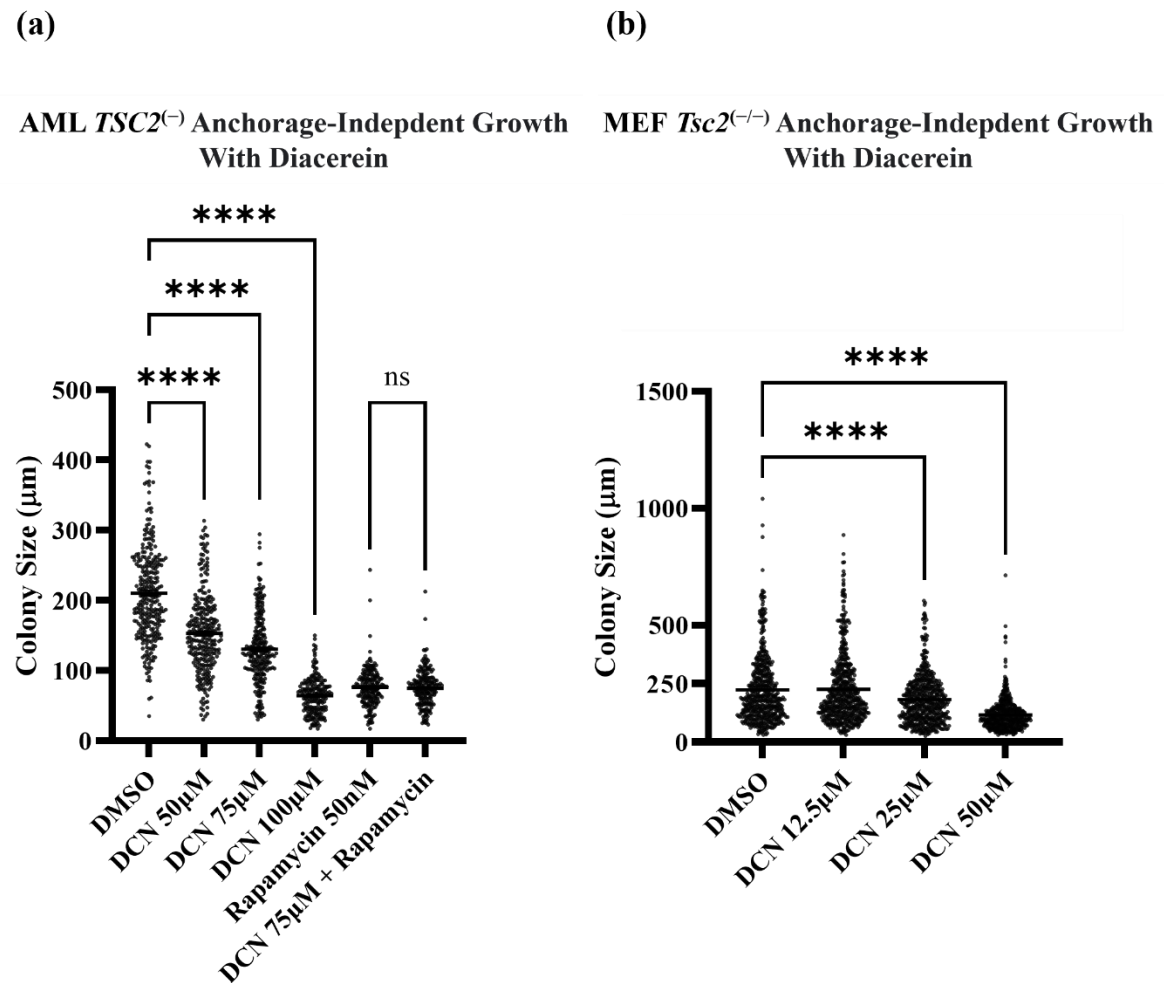


Figure 4.9. Diacerein reduced colony growth in *TSC2*-deficient cells. **(a)** *TSC2*-deficient AML cells were grown over a period of 4 weeks in soft agar. Cells were treated with increasing concentrations of DCN, rapamycin, or a combination of DCN (at 75 µM) and rapamycin. **(b)** *Tsc2*-deficient MEFs were grown over a period of 3 weeks in soft agar. Cells were treated with increasing concentrations of DCN. One-way ANOVA with Tukey's multiple comparisons.

Like the previously assayed inhibitors that reduced STAT3 phosphorylation, DCN was also able to reduce the formation of colonies, hinting at a potential anti-tumour activity when targeting IL-1 β . IL-1 β is upregulated in many cancers. Since IL-1 β stimulates NF- κ B activity, IL-1 β signalling promotes proliferation, angiogenesis, and migration through inflammatory pathway activation (488). Interestingly, while IL-1 β is acknowledged as having a pro-tumorigenic effect in some regards, the presence of IL-1 β in tumours is thought to have positive effects too. Specifically, IL-1 β recruits neutrophils which can combat tumour growth (489). Transcriptomic data suggests a high degree of immune invasion within TSC-derived tumours (which may be in part due to IL-1 β release), however it appears that TSC-derived

tumours are immune-evasive. This may be in part due to the high abundance of immune inhibitory regulators as mentioned in Figure 4.5.3. It is perhaps more likely that enhanced IL-1 β signalling contributes to a positive NF- κ B feedback loop in TSC-derived tumours. This has been observed within cancer cells with high RelA and IL-1 β , and typically confers chemoresistance (488).

Next, the study investigated whether diacerein had enhanced effects on cell viability within *TSC2*-deficient AML or *Tsc2*-deficient MEF cells, compared to wild type. To do this, *TSC2*⁽⁺⁾ and *TSC2*⁽⁻⁾ AMLs, or *Tsc2*^(+/+) and *Tsc2*^(-/-) MEFs were treated with DCN for 24 h, and cell viability was assessed (Figure 4.10).

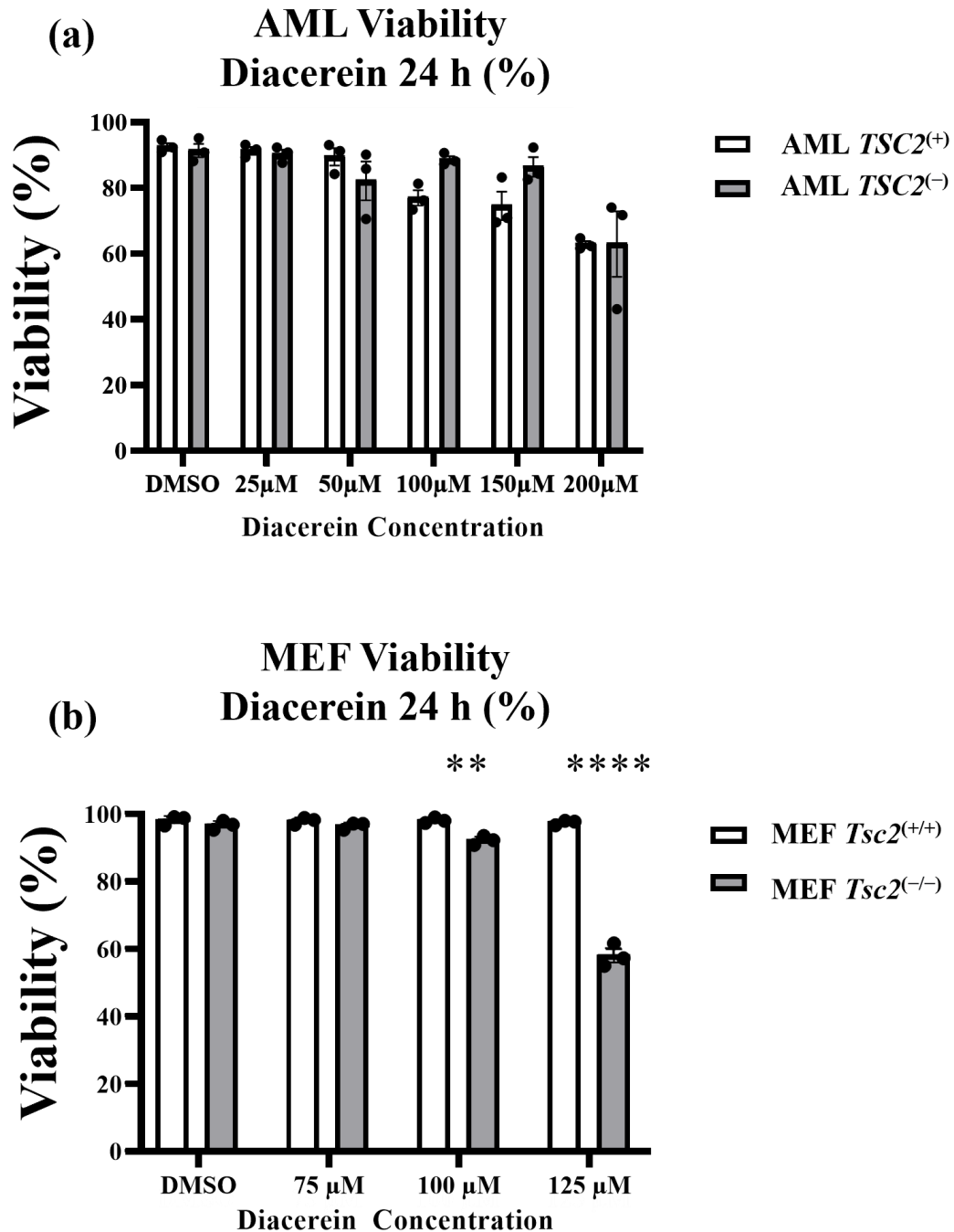


Figure 4.10. Diacerein has limited selective cytotoxicity on TSC-diseased cells. **(a)** AML cells and **(b)** MEF cells were treated with increasing concentrations of DCN for 24 h under serum starvation and viability was assayed. **(b)** MEFs were treated with increasing concentrations of DCN for 24 h and viability was assayed. $n = 3$, two-way ANOVA with Šidák's multiple comparisons.

DCN did not induce significantly different levels of cell death in either cell line, although *TSC2*⁽⁺⁾ AMLs did appear to lose viability at lower concentrations than *TSC2*⁽⁻⁾ AMLs (not significant) (Figure 4.10a). DCN induced selective cell death in *Tsc2*^(-/-) MEFs at a high drug

concentration of DCN (Figure 4.10b). As mentioned in Chapter 1, using $TSC2^{(+)}$ AMLs in viability assays could be problematic. As such, these results are relatively unclear, but could hint towards a level of cytotoxicity with DCN treatment in TSC-derived tumours.

The effects of DCN on cell migration was tested next via wound scratch assay (Figure 4.11).

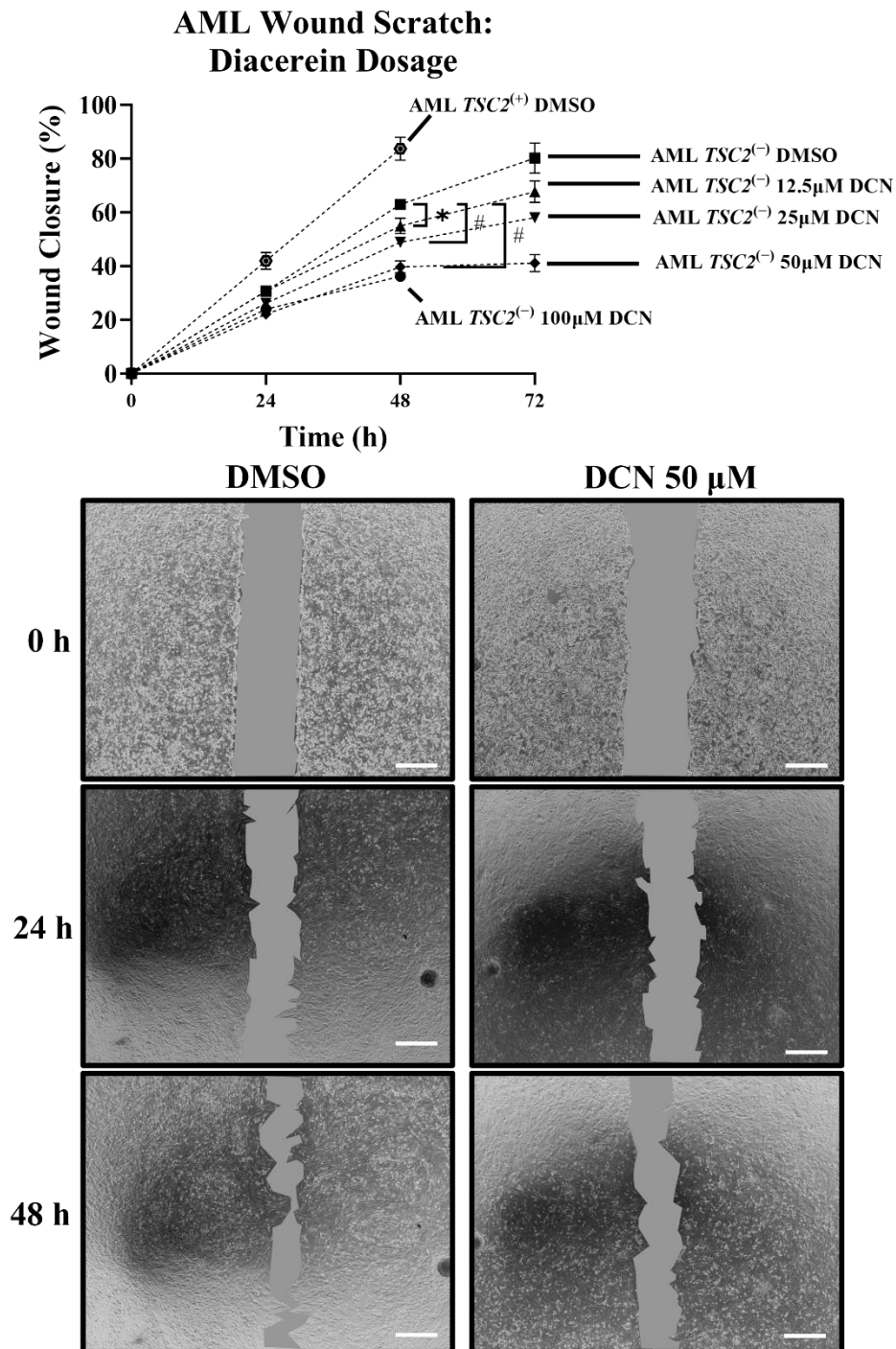


Figure 4.11. Diacerein reduces migration of $TSC2$ -deficient AML cells. Wound scratch assays were performed as before, with measurements taken at 0, 24, 48, and 72 h. 500 µm scale bars shown. $n = 3$, two-way ANOVA with Šidák's multiple comparisons. Data for 72 h timepoints was not used in

statistics due to heightened cell death at this time point. Comparisons were performed at the 48 h timepoints. #: $p < 0.0001$.

DCN significantly reduced wound closure compared to control (Figure 4.11). The effect of DCN on cell proliferation was also tested in *TSC2*-deficient AML and *Tsc2*-deficient MEF cells (Figure 4.12).

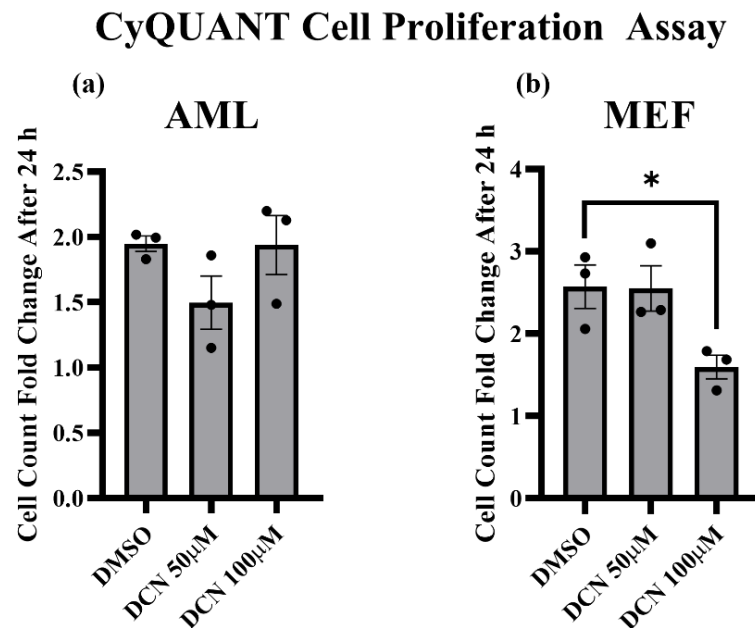


Figure 4.12. Diacerein was not effective at reducing cell proliferation in *TSC2/Tsc2*-deficient cells. CyQUANT cell proliferation assays were carried out on (a) *TSC2*-deficient AMLs and (b) *Tsc2*-deficient MEFs during treatment with DCN. $n = 3$, one-way ANOVA with Dunnet's multiple comparisons.

DCN appeared ineffective at reducing proliferation in *TSC2*-deficient AMLs but did slow proliferation in *Tsc2*-deficient MEFs at the higher concentration (Figure 4.12).

The previous set of experiments highlighted potential benefit to IL-1 β inhibition in TSC with the RhA drug, DCN. Specifically, DCN reduced anchorage-independent growth in *TSC2*-deficient cells while also slowing migration. Similarly, DCN reduced migration of *TSC2*-deficient cells. As described in section 4.3.1.3, this could be beneficial in the treatment of LAM which is characterised by tumour cell migration.

To further identify the role that IL-1 β could be playing on inflammatory processes in TSC, RT-qPCR was used to analyse gene expression of various markers, as before. *TSC2*-deficient AML cells were treated with either DMSO, 50 μ M DCN, 50 nM rapamycin, or a combination

of DCN and rapamycin for 24 h. RT-qPCR was then run on generated cDNA for these treated samples (Figure 4.13.1-13.3).

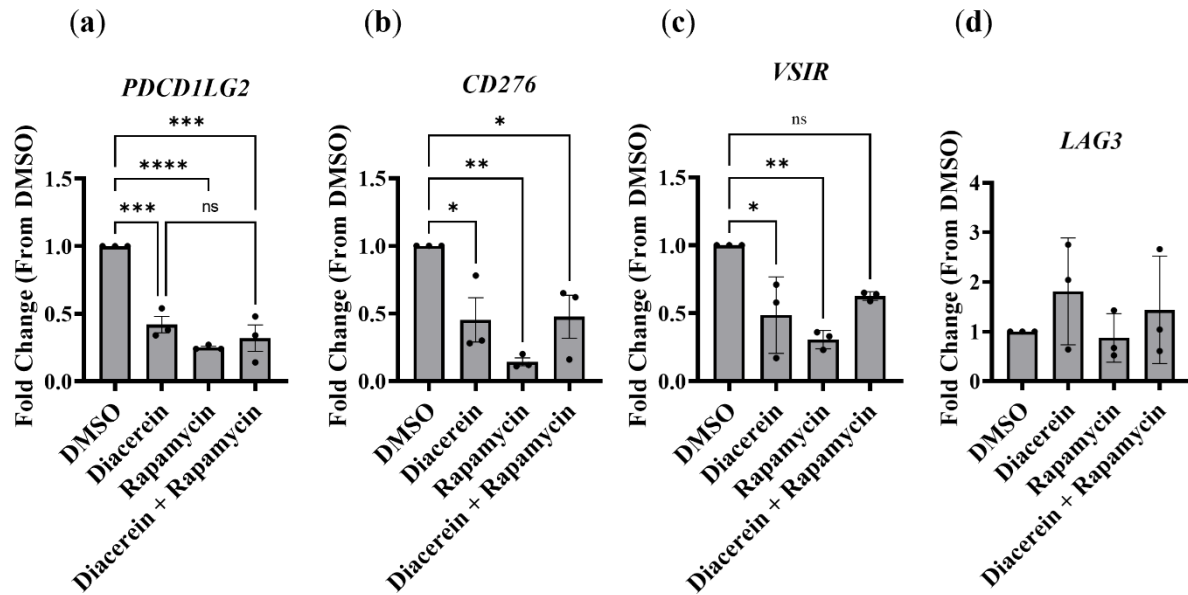


Figure 4.13.1. Diacerein was effective at reducing some immune checkpoint regulators. RT-qPCR was performed on *TSC2*-deficient AML cells. Gene expression of (a) *PDCD1LG2*, (b) *CD276*, (c) *VSIR*, and (d) *LAG3*. $n = 3$, one-way ANOVA with Tukey's multiple comparisons. Data normalised to *IPO8*.

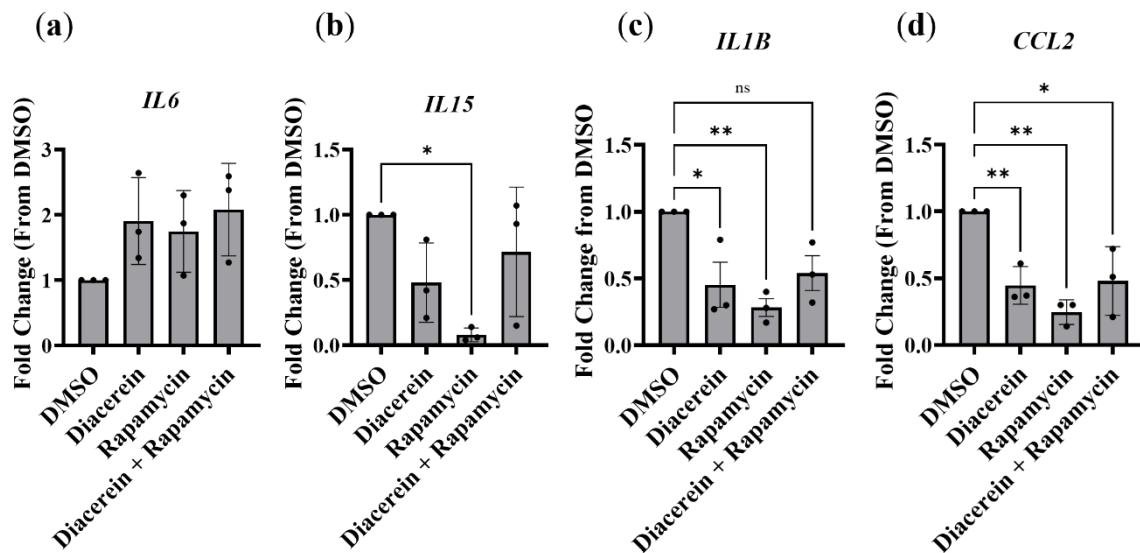


Figure 4.13.2. Diacerein reduced inflammatory cytokine gene expression. RT-qPCR was performed on *TSC2*-deficient AML cells. Gene expression of (a) *IL6*, (b) *IL15*, (c) *IL1B*, and (d) *CCL2*. $n = 3$, one-way ANOVA with Tukey's multiple comparisons. Data normalised to *IPO8*.

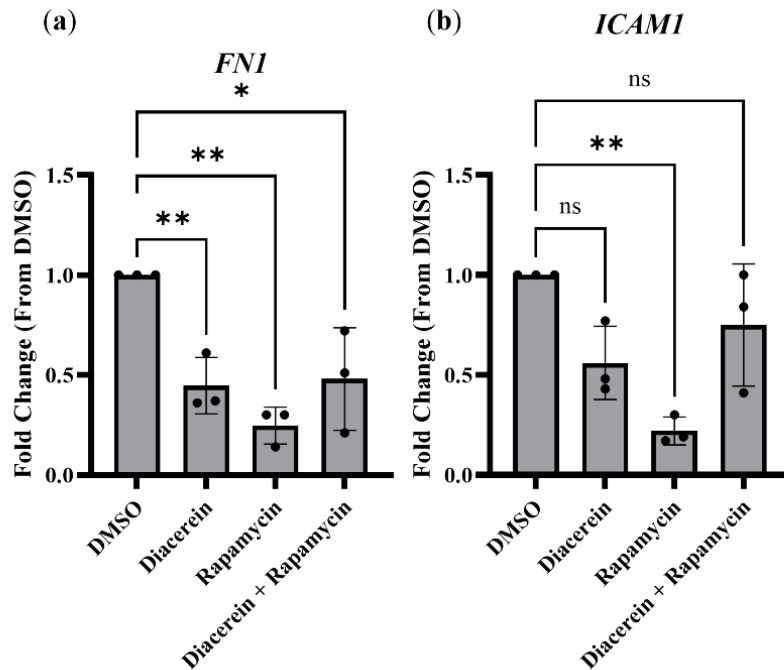


Figure 4.13.3. Diacerein may reduce migration via inhibition of *FNI* and *ICAMI* gene expression. RT-qPCR was performed on samples of *TSC2*-deficient AML cells. Expression of (a) *FNI*, and (b) *ICAMI* was analysed. $n = 3$, one-way ANOVA with Tukey's multiple comparisons. Samples normalised to *IPO8*.

Like BMS345541, DCN was able to reduce the gene expression of many inflammatory genes. Specifically, DCN was very effective at reducing expression of immune checkpoint regulators, cytokines, and pro-migratory genes. Samples for these experiments were generated simultaneously with those in figures 4.5.1-2, and 4.5.4-5. As such, the data for DMSO and rapamycin are the same. It is interesting to observe that no treatment used in these experiments could reduce *IL6* gene expression, and instead would increase *IL6* expression. As described earlier, this may be due to the duration of the treatments used. However, this data also suggests compensatory mechanisms that arise in the inflammatory state of TSC during pathway inhibition that may contribute to disease pathology. This may be apparent in the treatment of TSC patients with rapamycin. While rapamycin appears to be able to reduce some inflammatory signals within the data so far, the increase of other signals (such as IL-6) may contribute to the development of treatment resistant epilepsy. In the context of DCN treatment, the (low-significance) increase in *IL6* expression likely correlates with the strong increase in IL-6 secretion that was shown previously. However, this effect may be nullified if DCN suppresses IL-6 signalling via competitive binding of IL-6R.

Further work on the development and usage of an *in vitro* *TSC2*-deficient neuronal model will be shown in the following chapter. However, here it can briefly be shown that DCN was effective at reducing IL-6 secretion within *TSC2*-deficient neurons (Figure 4.14).

IL-6 Secretion in *TSC2*-Deficient Neurons

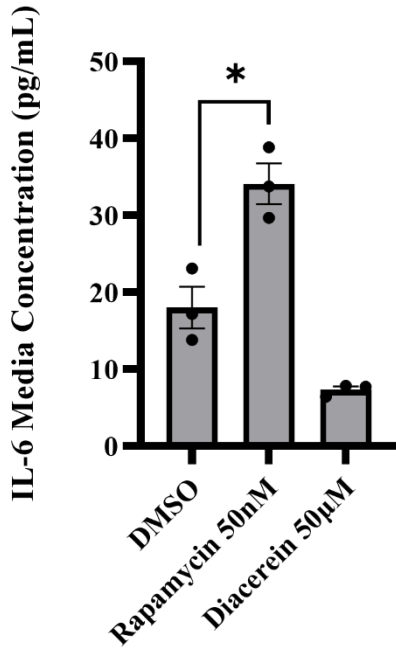


Figure 4.14. IL-6 secretion can be increased in *TSC2*-deficient neural cells by rapamycin, and reduced by DCN. IL-6 secretion was measured by ELISA in *TSC2*-deficient neural cells after 48 h treatment with either rapamycin, or DCN. Rapamycin treatment significantly increased IL-6 secretion. DCN reduced IL-6 secretion, however this did not reach statistical significance. $n = 3$, one-way ANOVA with Dunnett's multiple comparisons.

While the results here did not reach statistical significance, the data still shows a trend. DCN appears capable of reducing IL-6 secretion in *TSC2*-deficient neurons. This is in contrast to previous results, wherein DCN increased IL-6 production in AML cells significantly. It should be noted that treatment conditions were different between cell lines, with a 48 h treatment used rather than 24 h. While not directly compared, IL-6 levels appear far lower in *TSC2*-deficient neuronal cells than *TSC2*-deficient AML cells; media from untreated *TSC2*-deficient neurons had IL-6 at around 17.5 pg/mL, whereas this was closer to 500 pg/mL in the *TSC2*-deficient AML cells. This could highlight differential regulation of IL-6 in *TSC2*-deficient AML and neuronal cells, and thus highlight the need for *in vitro* neuronal models.

4.3 Conclusion

In this section, the influence of anti-inflammatory pathway inhibitors was analysed in *TSC2*-deficient cells. Specifically, the formation of anchorage-independent colonies of *TSC2*-deficient cells, as well as cell migration was reduced via direct IKK inhibition (with BMS345541), or drugs that could indirectly inhibit NF- κ B. The potential therapeutic applicability for using IL-1 β inhibitors was demonstrated. DCN was highlighted as a potent drug that markedly reduced the elevated inflammatory pathways in TSC cell line models. Most obvious was the very strong inhibition of phosphorylation of STAT3 on the Y705 residue. DCN was also effective at slowing colony formation and cell migration of *TSC2*-deficient cells, and reduced the gene expression of various inflammatory cytokines and immune checkpoint regulators. As an approved drug with relatively mild side effects, DCN may be appropriate for the treatment of TSC (476). However, due to a lack of inhibition on RelA phosphorylation and the knowledge that DCN may function to block STAT3 activity through inhibition of IL-6 receptor binding, it is not possible to confirm if the effects seen after DCN treatment are due to IL-1 β inhibition. To confirm this, investigation with specific IL-1 β inhibitors would be required. Further investigation into DCN within TSC will be carried out in the following chapter.

Chapter 5: *TSC2*-deficient iPSC Model for Neuronal Model Generation

5.1 Introduction

TSC patients typically present with SEN/SEGA and cortical tubers. Cortical tubers occur in around 80-90% of TSC patients and typically develop in the cerebral cortex, but can also occur deeper within the brain (323). Cortical tubers are believed to be a key determining site in TSC-associated epilepsy, with a distinction being made between non-epileptogenic tubers and “hot” cortical tubers. Surgery is often employed to remove these “hot” cortical tubers, providing an effective but invasive means of alleviating treatment-refractory epilepsy (324). Cortical tubers are associated with a prevalence of astrocytes and other glial cells, malformed/dysplastic neurons, and giant cells that are believed to arise as poorly differentiated astrocytes or neurons (490). Enhanced cytokine activity as well as receptors for excitatory neurotransmission has been observed in cortical tubers, likely hinting towards a derivation of epilepsy (491). SEN/SEGAs refer to two categories of related tumours. Importantly, SENs are typically thought to be asymptomatic, and like cortical tubers, contain a mixture of neurons, glial, and giant cells (492). The growth of SEGAs (typically near the foramen of Monro) can cause obstruction of cerebrospinal fluid leading to hydrocephalus and increasing the morbidity of TSC patients (493). SEN/SEGAs typically show no specific symptoms until hydrocephalus occurs (300), meaning that routine monitoring of TSC patients is advisable for positive patient outcomes. Tumours of the CNS are believed to be the leading cause of death in TSC patients (494), highlighting the importance of research into this subset of TSC-associated tumours.

Various *in vitro* models have been employed to investigate the development of brain tumours in TSC patients. Costa *et al.* (2016) investigated mTORC1 inhibition on the outcome of neurodevelopment in *TSC2*-deficient iPSCs (495), demonstrating that early inhibition of mTORC1 in development is capable of correcting much of the dysregulated neurodevelopment that may occur in TSC. Many other studies have utilised stem cell based approaches to investigate neurodevelopment within TSC, some of which utilise sophisticated three-dimensional approaches to better recapitulate the complex tumour microenvironment (496). A particularly interesting study by Blair *et al.* (2018) utilised a three-dimensional model of TSC to investigate cortical tuber development, within which STAT3 activity was a large component of investigation (362). However, many of these models have not focused

specifically on the neuroinflammatory signature of TSC-associated brain tumours, with the role of NF- κ B signalling seeming to be unexplored within *in vitro* TSC brain tumour models. This may be a key oversight, as previous data showed that NF- κ B signalling was dysregulated in TSC patient-derived brain tumours, and NF- κ B can play a key role in the development of epilepsy (214).

Within this chapter, *TSC2*-knockout iPSCs were generated. These cells were then differentiated into neuronal cell lineages to serve as a model for TSC-associated brain tumours. A summary of this process and the biomarkers used to identify cell types are shown here (Figure 5.1).

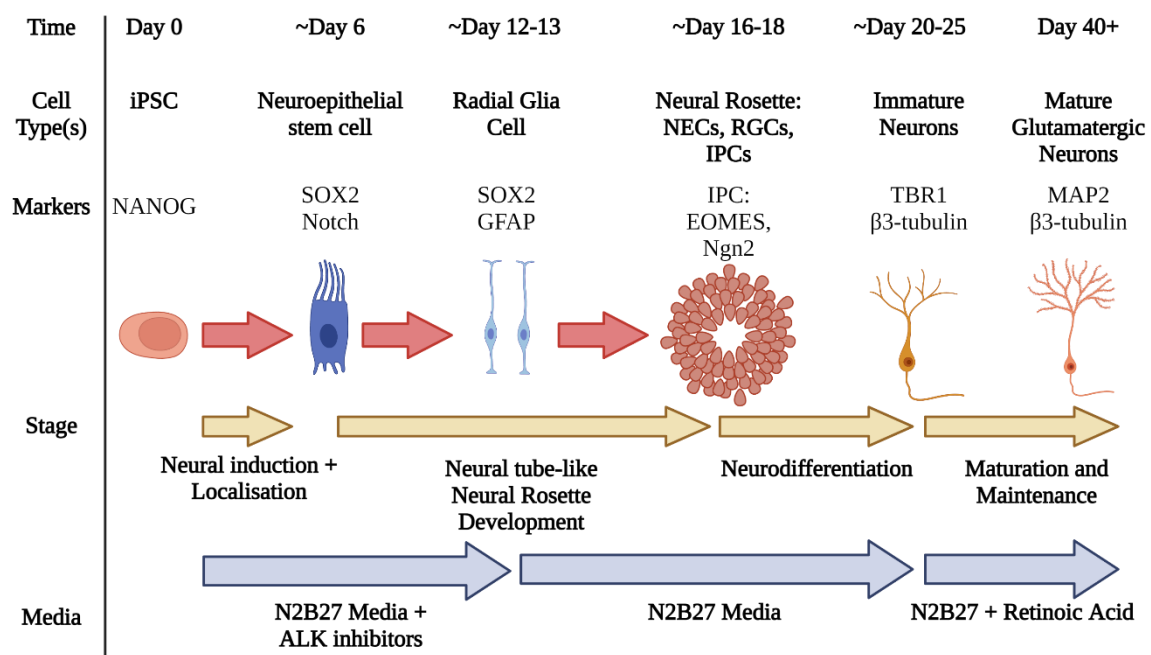


Figure 5.1. Steps of neurodifferentiation and markers of cell types. Neurodifferentiation begins with iPSCs. These are subject to neural induction and localisation to become glutamatergic neurons by incubation in N2B27 media with ALK inhibitors (LDN193189 and SB505124). iPSCs become neuroepithelial cells, which proliferate and differentiate into radial glia cells. From here, ALK inhibitors are removed. Radial glial cells arrange into neural rosettes: an *in vitro* representation of the neural tube. Radial glial cells divide asymmetrically to generate intermediate progenitor cells which migrate and then differentiation into immature neurons. Cells are then maintained within N2B27 media with supplemented retinoic acid to generate mature glutamatergic neurons. Illustration was developed in BioRender.

These cell models were used to analyse the inflammatory pathways that were identified in earlier chapters, with the aim to see how a *TSC2*-deficient *in vitro* brain cell line model might compare to other available *in vitro* TSC cell line models. Specifically, this chapter aimed to

see how inflammatory pathways could be influenced within TSC-derived brain tumours via NF- κ B pathway or mTORC1 inhibition, as well as to gain insight into the developmental stages of TSC-derived brain tumours. Data gained from this chapter revealed dysregulated inflammatory pathways in *TSC2*-deficient neurons which could be linked to epilepsy and autism in TSC.

5.2 Results

5.2.1 *TSC2* knockout verification and sequencing

Following revival, cell lines were expanded and the PGP1-*TSC2*⁽⁻⁾ cell pool was subject to single-cell cloning to isolate a pure *TSC2* knockout. Colonies were selected and expanded before being used to generate protein lysates. 6 clones which showed likely *TSC2* knockout were expanded and sequenced. The presence or absence of *TSC2* protein was confirmed with western blot, with clone A5 (PGP1-A5) used for further analysis (Figure 5.2a). The presence of pluripotency was confirmed with protein expression of OCT4A, NANOG, and SOX2 levels and compared to wild-type PGP1. AML *TSC2*⁽⁻⁾ cells were used as a negative control. Sequencing data is shown as in Chapter 2 with a discordance plot (Figure 5.2b) and Sanger sequencing (Figure 5.2c). With confirmation of *TSC2* knockout, PGP1-A5 was used to develop stocks as a human *TSC2* knockout iPSC model. Other clones were also developed, but PGP1-A5 appeared to be the most suitable based off of sequencing data.

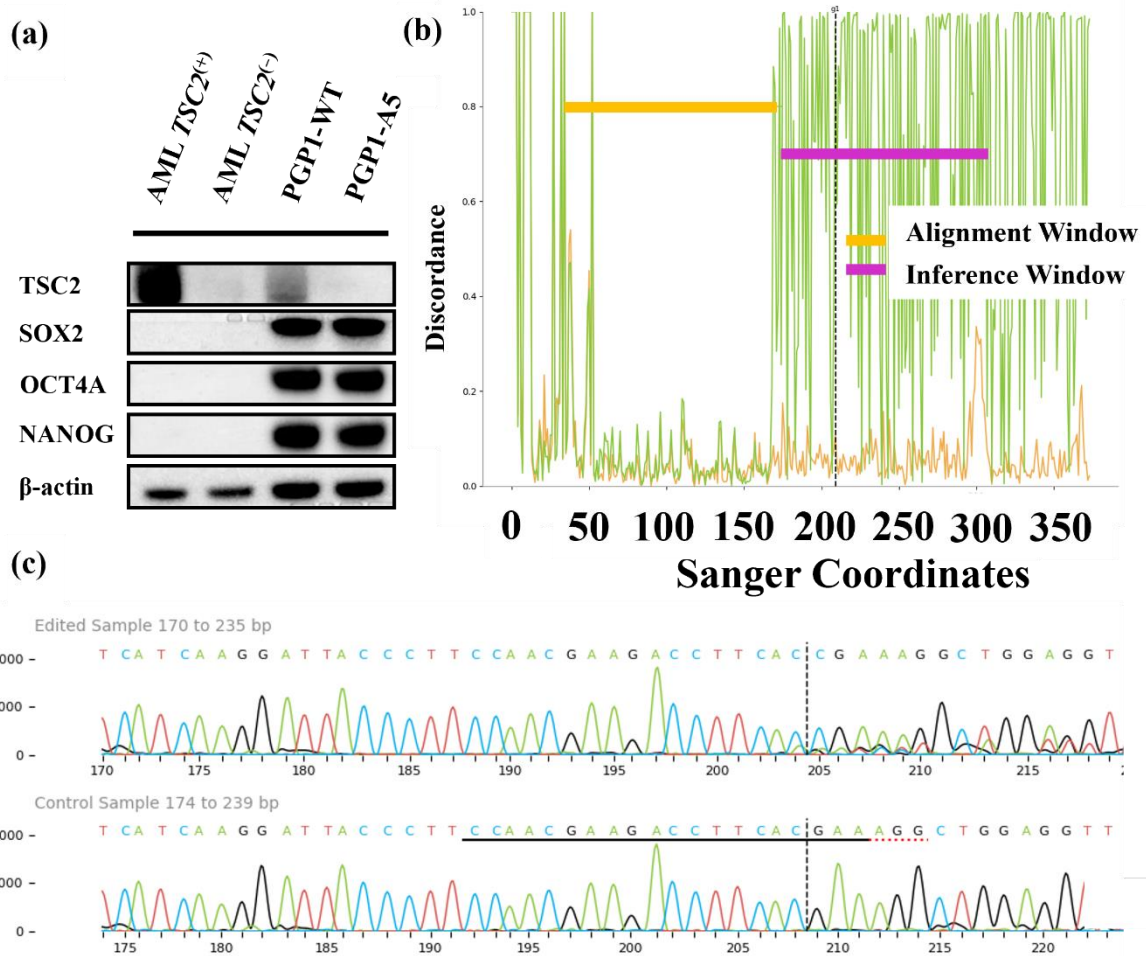


Figure 5.2. Confirmation of purified *TSC2*-KO PGP1 iPSCs following PGP1 subcloning and sequencing. **(a)** Western blot comparing *TSC2*⁽⁺⁾ and *TSC2*⁽⁻⁾ AMLs, as well as wild-type PGP1 (PGP1-WT) and PGP1 subclone A5 (PGP1-A5). Protein expression of *TSC2* was probed, as well as three pluripotency markers: *SOX2*, *OCT4A*, and *NANOG*. As expected, PGP1-A5 showed no *TSC2* expression, but retained pluripotency. $n = 1$. **(b)** Discordance plot showing a change in overall alignment between bases of the wild-type control and the CRISPR-Cas9-edited sample. An indel plot (not shown) demonstrates a 97% presence of indels resulting in frameshift mutations for *TSC2*. The remaining 3% is possibly due to discrepancy in sample preparation resulting in sanger sequencing error, as *TSC2* protein expression seemed to be null in western blots. **(c)** Sanger sequence read showing the edited region (top) of DNA around the selected guide sequence following CRISPR-Cas9 transfection. The black dotted line shows the cut location.

5.2.2 Neurodifferentiation Optimisation for *TSC2*-KO PGP1

Initial attempts to differentiate PGP1 cell lines into neuronal cell lineages were unsuccessful with regards to PGP1-A5. PGP1-WT and PGP1-A5 cells were differentiated with mirrored conditions to generate wild type versus *TSC2*-deficient neurons. Lysates generated from these

cells would have been assayed at varying timepoints to determine differentiation states. However, initial differentiation of PGP1-A5 proved unsuccessful, with excessive cell death occurring post-passage to fibronectin in *TSC2*⁽⁻⁾ cells (Figure 5.3.1). Unfortunately, the cell density was deemed too low to proceed with neurodifferentiation.

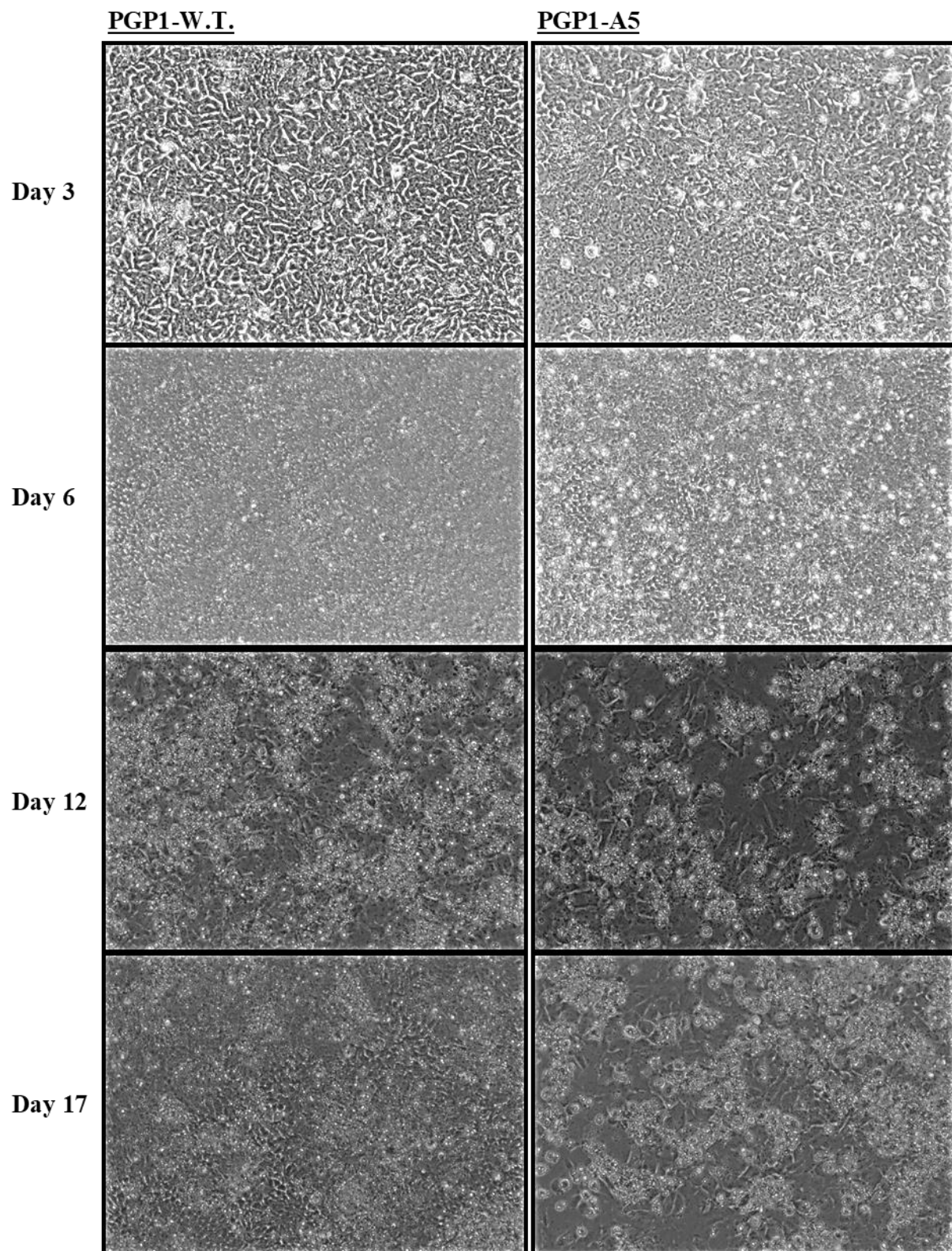


Figure 5.3.1. PGP1-A5 iPSCs demonstrate reduced viability in neurodifferentiation. PGP1-WT and PGP1-A5 iPSCs were subjected to neurodifferentiation (Section 2.14) over a time span of 17 days, and which point neurodifferentiation was terminated. PGP1-A5 showed differing morphology of a neuroepithelial layer at day 6 with larger, less densely packed cells, compared to PGP1-WT.

Following a passage to fibronectin coated plates at day 10, PGP1-A5 showed markedly reduced confluency at days 12 and 17, compared to PGP1-WT.

Figure 5.3.1 shows an initial hint of the altered differentiation processes within *TSC2*-KO iPSCs. Altered morphology was observed early in the differentiation process with a visually lower cell-density in PGP1-A5 cells, as compared to PGP1-WT cells at day 6 of neurodifferentiation. By day 10, cell density in PGP1-WT cells was becoming too high, requiring a passage to fibronectin coated plates to continue the neurodifferentiation process. The density of PGP1-A5 was deemed sufficiently high for a passage at this point also.

Following passaging, PGP1-A5 showed lower cell attachment compared to PGP1-WT, leading to markedly reduced confluency. This difference in confluency would significantly alter differentiation capacity, as high confluency is required for efficient differentiation within this protocol. Therefore, the neurodifferentiation protocol was adjusted to provide higher cell seeding densities for the early stages of PGP1-A5 differentiation.

It is unclear why *TSC2*-KO iPSCs differentiate in such a different way. However, samples generated at day ten of differentiation were generated to re-confirm *TSC2*-knockout (Figure 5.3.2).

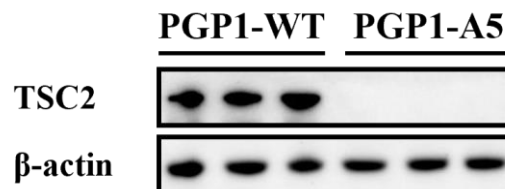


Figure 5.3.2. PGP1-A5 cells do not express TSC2 protein. These samples were generated at day 10 of neurodifferentiation. Each lane represents one sample harvested from separate wells.

5.3 *TSC2*⁽⁻⁾ iPSC model final usage

5.3.1 Neurodifferentiation of PGP1-A5 cells

Following initial attempts at neurodifferentiation, it was decided to re-attempt neurodifferentiation using higher passage ratios for PGP1-A5 at key stages in neurodifferentiation. Important to note is that at this stage, PGP1-WT stocks were unable to be revived after freezing. As a substitute, iBJ4 iPSCs were used as a wild-type control.

iBJ4-WT and PGP1-A5 iPSCs were subject to neurodifferentiation, and images were taken at day zero, eight (pre-passage), ten (post-passage), and fourteen (Figure 5.4.1). Within this neurodifferentiation, the passage to fibronectin coated plates was performed at a ratio of 1:3 for iBJ4-WT, and 1:2 for PGP1-A5. Notably, cell density was still relatively low post-passage for PGP1-A5 cells, as seen at day 10. Higher passage ratios were not used (*i.e.*, 1:1.5 or 1:1), because at later stages of neurodifferentiation it was found that PGP1-A5 cells would proliferate and metabolise very rapidly, leading to an ultimately higher cell density than iBJ4 cells. By day fourteen, rapid cell proliferation allowed PGP1-A5 cells to return to 100% confluency, like iBJ4. It is likely that low confluency would impact differentiation states.

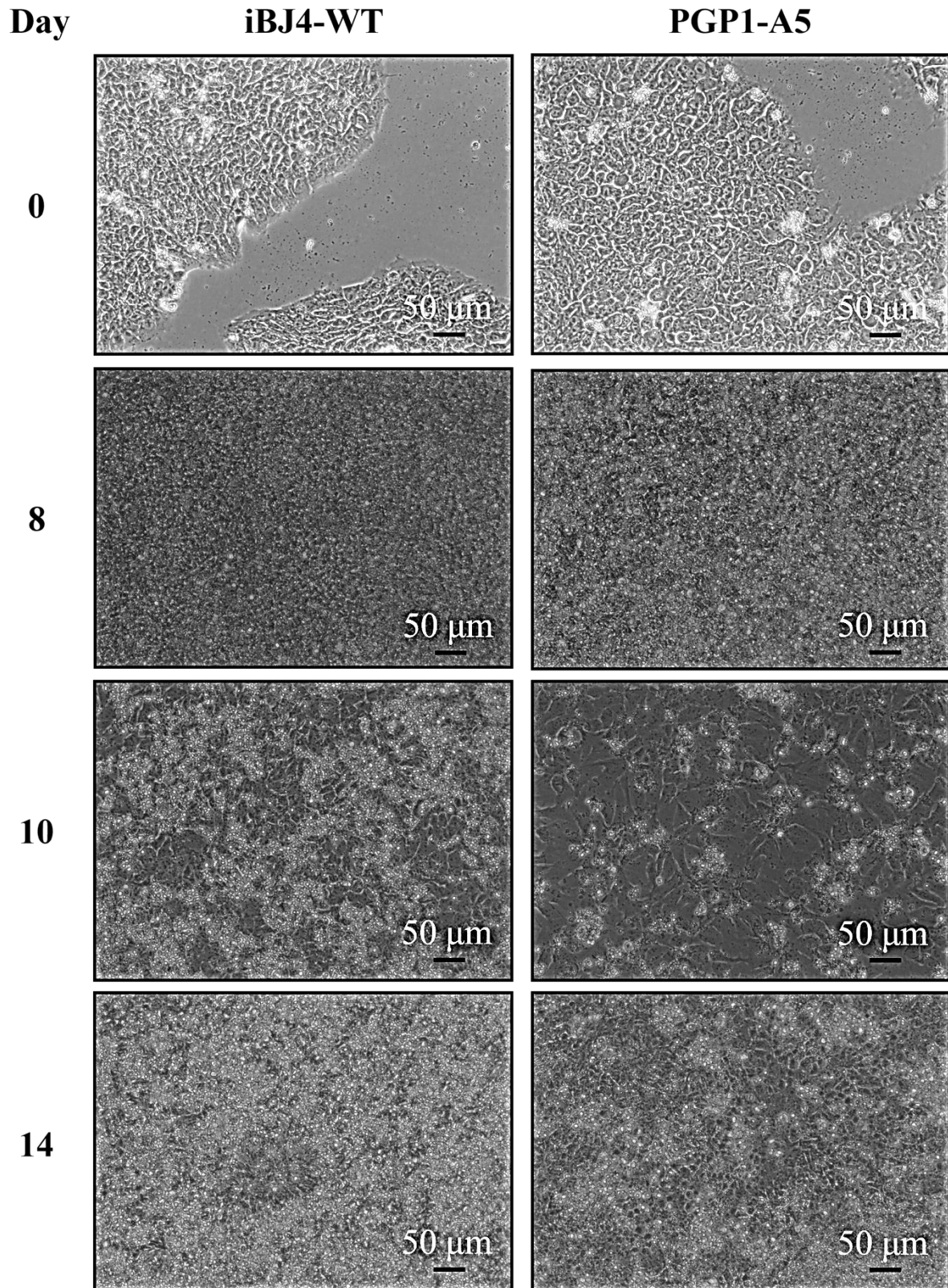


Figure 5.4.1. PGP1-A5 cells can progress with neurodifferentiation following passage to fibronectin if passaged at a higher ratio than iBJ4-WT. iBJ4-WT and PGP1-A5 were subject to neurodifferentiation and imaged over several time points. PGP1-A5 exhibited differing morphology and lower cell attachment post-passage at day 10, but would proliferate sufficiently to proceed with

neurodifferentiation. This comparison was performed over a singular neurodifferentiation of multiple wells.

Neurodifferentiation was continued and images were continuously taken (Figure 5.4.2).

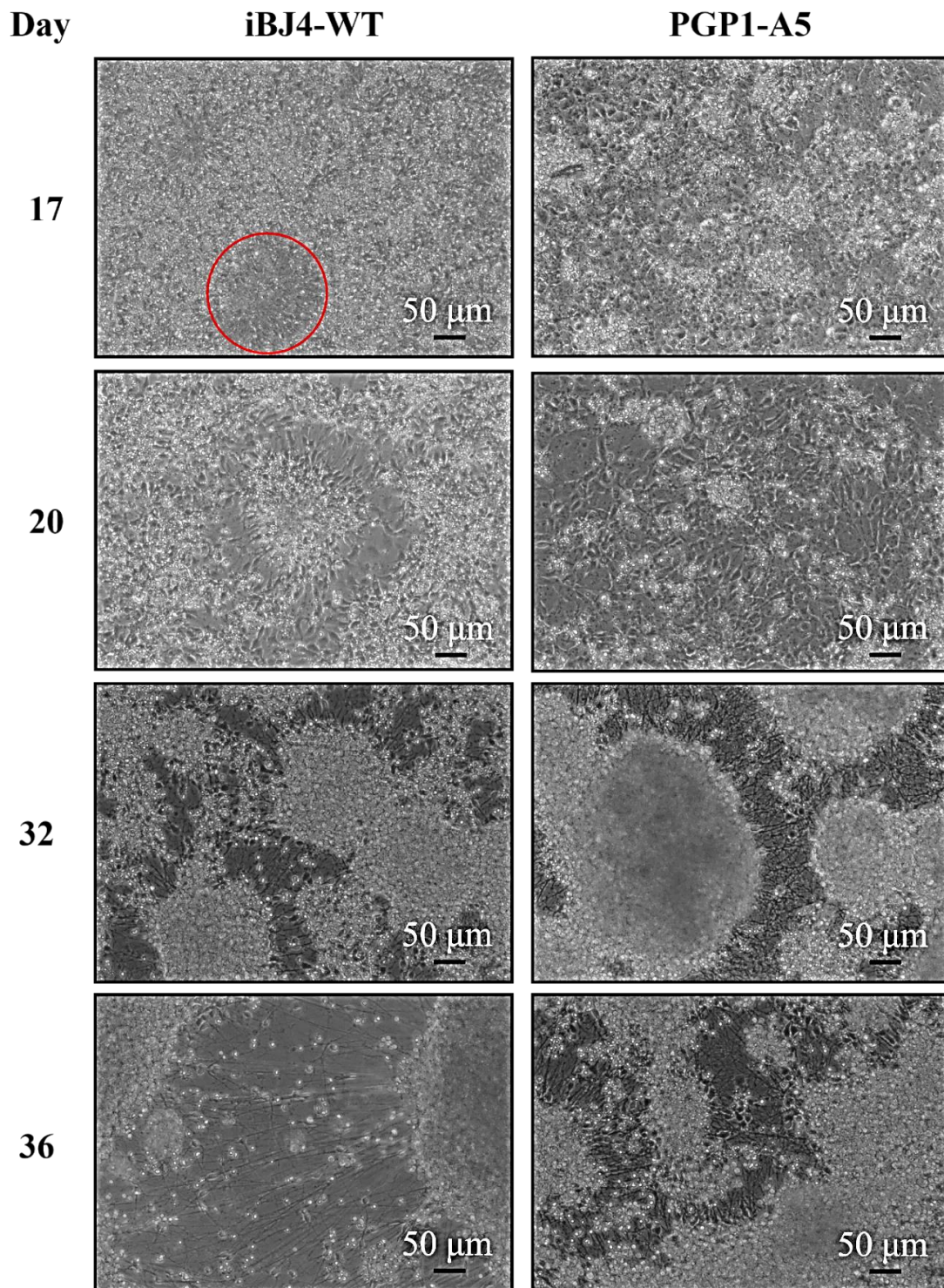


Figure 5.4.2 Differentiation of PGP1-A5 cells and iBJ4-WT cells. At day 17 of differentiation, rosette formation can be seen in iBJ4-WT (red circle), but this is not apparent in PGP1-A5.

Post passage to PDL-Laminin plates, by day 20 iBJ4-WT had clear rosette formation with neurite outgrowth starting to occur, whereas this was once again less apparent in PGP1-A5 cells (Figure 5.4.2). Following another passage at day 31, neural growth became more apparent in both cell lines at day 32, although this was much denser in PGP1-A5 cell. By day 36, neurons were beginning to mature in iBJ4-WT, with longer axons and dendrites beginning to form. Maturation was less clear in PGP1-A5, with a highly dense, disorganised morphology of neural outgrowths. However, neural growth was still apparent.

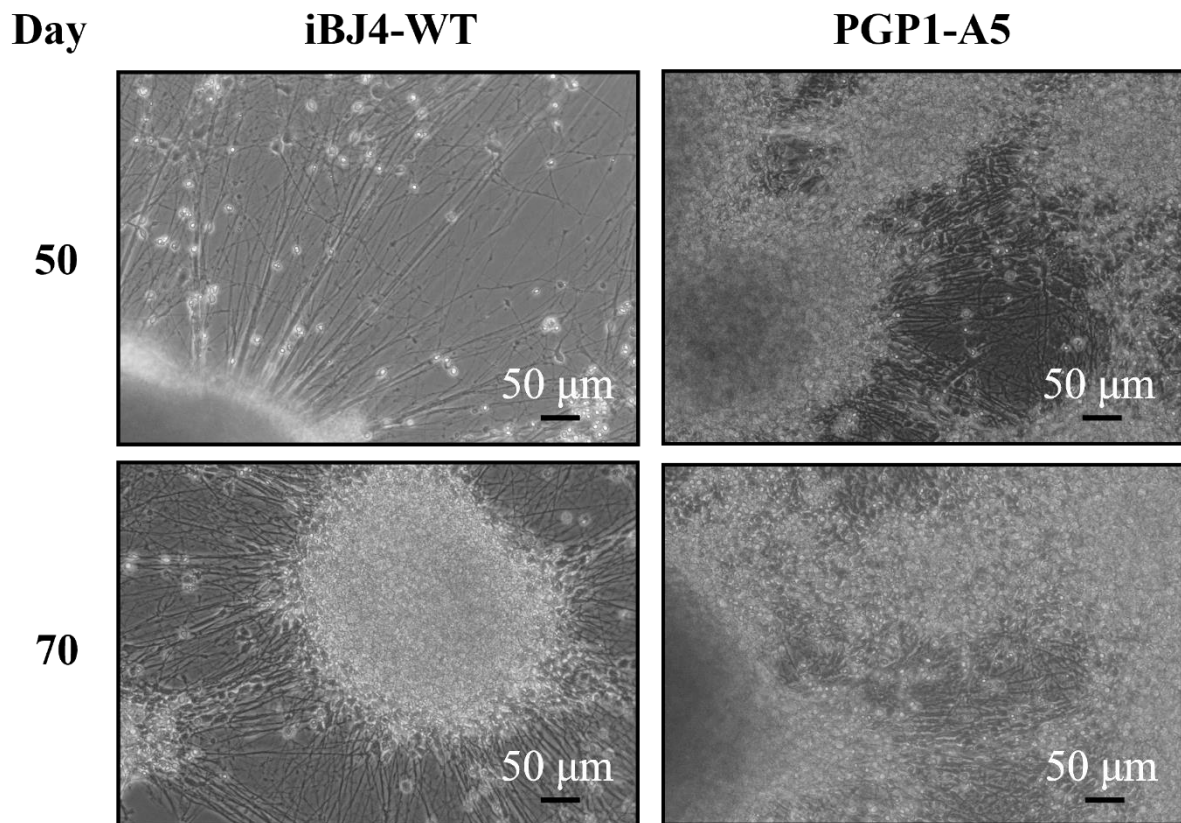


Figure 5.4.3. Maturation of iBJ4-WT and PGP1-A5 neurons. By day 50 of neurodifferentiation, iBJ4-WT cells demonstrated long, highly organised neural outgrowth. While neural generation was also visibly apparent within PGP1-A5, the cells remained highly disorganised and densely packed. This trend was maintained at day 70.

At the time points of day 50 and day 70, PGP1-A5 appeared to be growing progressively more densely packed when compared to iBJ4-WT cells, making it more difficult to identify axon formation (Figure 5.4.3). While neural development did visually appear to be occurring, dense packing of cells in PGP1-A5 cells were obscuring this development. In earlier stages, neurite outgrowth appeared disorganised and tangled, and were surrounded by apparent non-neuronal cells. Though this is only based on visual identification, the images give interesting hints to what

we may see at the protein level of *TSC2*⁽⁻⁾ neurons. Specifically, it suggests a presence of non-neuronal cells, as well as high mTORC1 activity (as expected) from still differentiating cells and neurons, since typically non proliferating neurons will not exhibit high degrees of mTORC1 activity (362).

To gain a visual idea of cell type, cells were seeded at low density (1:48) from day 64 and imaged at 20X (Figure 5.4.4a). A general macroscopic view was also taken at 4X of non-passaged cells (Figure 5.4.4b).

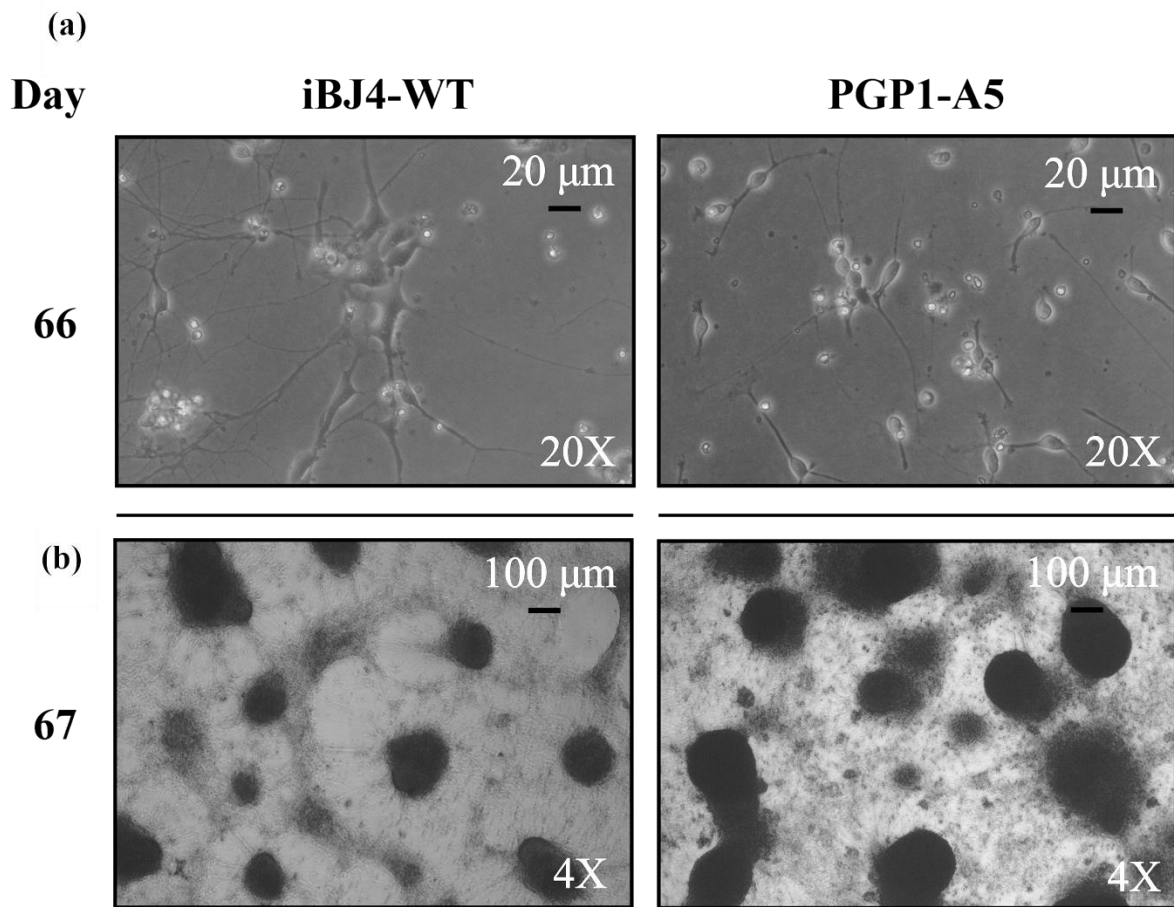


Figure 5.4.4. Neuronal differentiation of *TSC2*⁽⁻⁾ iPSCs results in mixed cell outcomes, and differential macroscopic structures. Cells were imaged at (a) day 66 with a low seeding density at 20X, and (b) at day 67 at 4X without passage.

At day 64, iBJ4-WT and PGP1-A5 cells were passaged at low density and then imaged at day 66 (Figure 5.4.4a). iBJ4-WT cells demonstrated neuronal-like cells and other unidentified cell types. PGP1-A5 presented with neurons, but also appeared to have a high degree of what appear to be RGCs, signifying a stall in differentiation. At a macroscopic view, PGP1-A5-derived neurons exhibited slightly larger, more dense neuronal clusters when compared to

wild-type (Figure 5.4.4b). It is possible that the apparent representative presence of neurons is lower than the actual presence when cells were passaged at a low seeding density. This is because mature neurons at this stage of growth are sensitive to passaging.

Two key features were noted in this section.

- 1) $TSC2^{(-)}$ PGP1-A5 iPSCs can be differentiated alongside wild-type iPSCs, however the differentiation process exhibits different structural features and milestones. Notably, despite severe cell loss upon passages, $TSC2^{(-)}$ cells are able to proliferate in order to “catch up”, and then overtake $TSC2^{(+)}$ cells in terms of cell density. It is difficult to determine the impact that this drop, and subsequent excess in cell density exerts on neurodifferentiation. Cell density is an important component of neural differentiation protocols, with high cell density playing a key role in efficient neuron outcomes (497). Massively reduced cell density is not a feature that would occur during brain tumour formation, so it is difficult to say that this is a reminiscent feature of *in vivo* neuronal growth. Additionally, cell density was relatively quick to recover, so the impact of low density was not detrimental to neural differentiation.
- 2) The presence of neurons is masked by a comparatively high cell density emerging at later stages of neurodifferentiation within $TSC2^{(-)}$ PGP1-A5 cells, compared to wild-type. While iBJ4-WT showed clear, organised neurite outgrowth and axon extension, PGP1-A5 demonstrated tangled and packed neurites, with other crowded cell types present. While neurons appear to form in $TSC2^{(-)}$ cells during neurodifferentiation, there also appears to be a high presence of other cell types. These cells appear to be radial glia, which should not normally be present at this stage of differentiation. Notably, this was identified visually, and will be explored more in later sections. From these images alone, it is difficult to confirm that the cells pictured in Figure 5.4.4a (iBJ4-WT) are neurons, and not other cell types such as oligodendrocytes. Similarly, from this image alone it is not possible to confirm that the cells imaged for PGP1-A5 are radial glia.

This data shows that overall, this model can be used to observe TSC neural cell production. It is important to note that due to differing neurodifferentiation conditions and genetic lineages, outcomes may not be perfectly representative.

5.3.2 Protein expression during neurodifferentiation of *TSC2*⁽⁻⁾ PGP1-A5

There was a visually striking difference in neurodifferentiation between wild type and *TSC2*⁽⁻⁾ iPSCs. It is reasonable to assume that the overcrowding of cells and especially around neuronal clusters in later stages of neurodifferentiation is due to mTORC1 hyperactivity. Naturally, we would assume that mTORC1 hyperactivity upon loss of *TSC2* would result in greater proliferation of precursor cells (neuronal epithelium cells, intermediate progenitors, and radial glia). However, the effect of mTORC1 hyperactivity on the actual signalling pathways present during neurodifferentiation is less obvious.

mTORC1 activity is undeniably essential in brain development, particularly within NECs. This has been demonstrated in multiple studies that typically use conditional or induced knockouts of mTOR activity (498–500). Knockout of mTOR activity in the developing brain of mice normally results in reduced cortical thickness, microcephaly, a reduction in postmitotic neurons, and a reduction in proliferation of *EOMES* and *Ki-67* positive IPCs.

mTORC1 hyperactivation shows the opposite effect. Specifically, mTORC1 hyperactivation through loss of *Tsc1* or *Tsc2* in early stages of development results in megalencephaly in mice studies, and increased cortical thickness (501). The study cited here focused on mTOR loss in RGCs and interestingly reported that the effects of *Tsc1* or *Tsc2* loss were identical. This contrasts with the general consensus that *TSC2* (or *Tsc2*) mutations are more severe than *TSC1* (or *Tsc1*) and suggests that the effect of *TSC1* versus *TSC2* loss is dependent on cell type. Specifically, astrocytes harbouring *TSC2* mutation may be more pathogenic than those harbouring *TSC1* mutations. This study also noted that STAT3 hyperactivation was likely important in the dysregulated differentiation in *Tsc1*-mutant RGCs.

mTORC1 hyperactivation also results in a failure of IPCs to migrate. Magri *et al.* (2011) (502) provided an in depth look into how *Tsc1* mutations lead to migration defects in neural progenitors. Normal brain development requires migration of neural progenitors from the dorsal SVZ to the ventral SVZ. mTORC1 hyperactivation has been shown to compromise this migration, leading to a build-up of poorly differentiated cells within the dorsal SVZ. As outlined by Magri *et al.* (2011) (and mentioned above), the cell type which harbours *TSC1/TSC2* deficiency is of high importance in determining the outcome of brain development in TSC.

Overall, neuronal differentiation is largely dependent on a selection of sequentially regulated transcription factors that guide progression to the next state of differentiation. Samples were collected over days 0-40 of neurodifferentiation, and probed for a range of proteins, including NANOG, β 3-tubulin, Notch2, Eomesodermin (EOMES), T-box brain protein 1 (TBR1), Microtubule associated protein 2 (MAP2), Neurogenin 2 (Ngn2), and SOX2. By observing relative levels of these factors, we can discern how neurodifferentiation is progressing within *TSC2*⁽⁻⁾ cells, and how this may differ from the differentiation of wild-type cells (Figure 5.5.1).

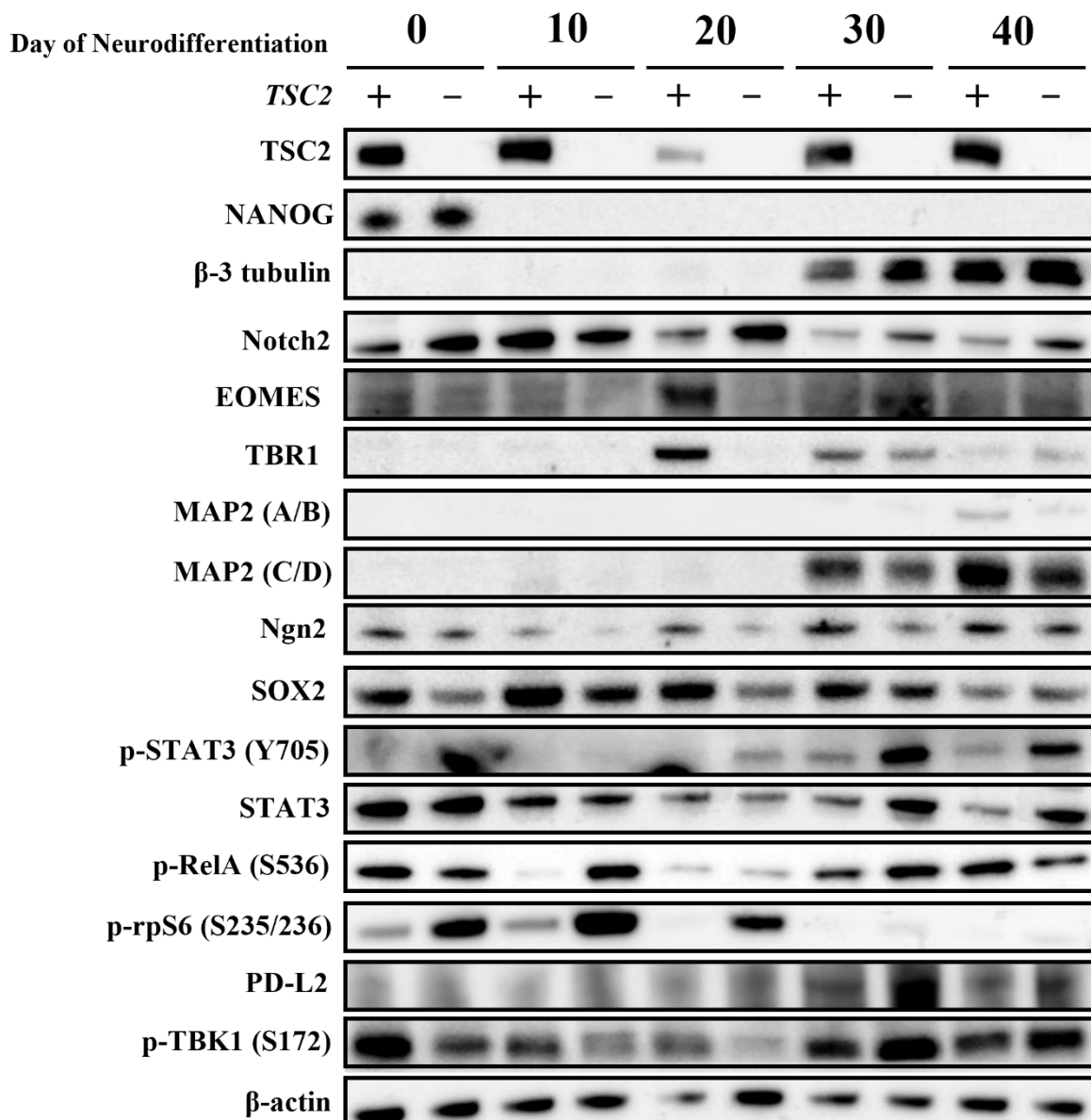


Figure 5.5.1. Differential protein expression in PGP1-A5 vs iBJ4-WT during neurodifferentiation. Samples were collected during neurodifferentiation at days 0, 10, 20, 30, and 40. Samples were then analysed via SDS-PAGE and western blot. Most blots were performed as $n = 3$, although EOMES and S536 p-RelA were $n = 2$.

Subsequent densitometry analysis of these western blots is shown below (Figure 5.5.2-5.5.4).

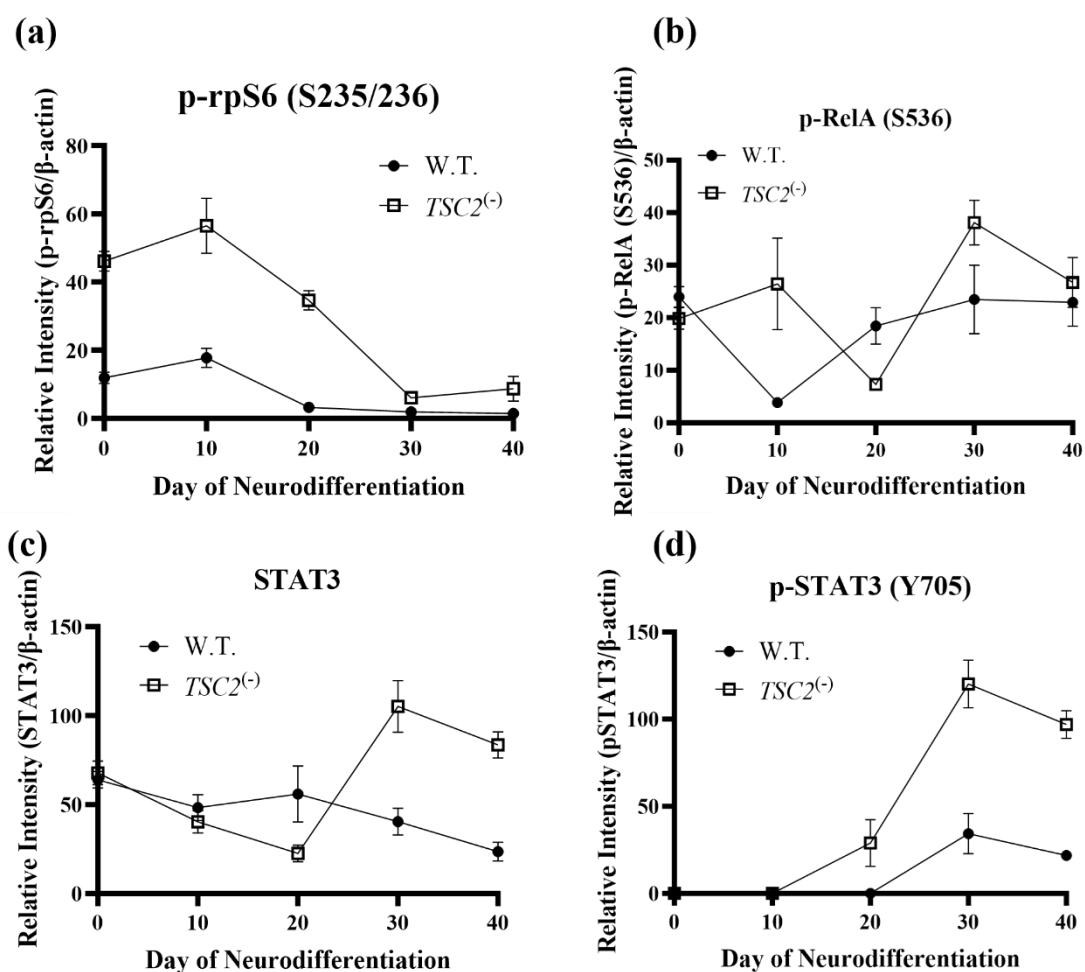


Figure 5.5.2. mTORC1, NF- κ B, and STAT3 signalling is dysregulated through neurodifferentiation in PGP1-A5 iPSCs. Densitometry analysis was performed on western blots of (a) p-rpS6 (S236/236), (b) p-RelA (S536), (c) STAT3, and (d) p-STAT3 (Y705) through neurodifferentiation, comparing iBJ4-WT and PGP1-A5. a, c, and d: $n = 3$, two-way ANOVA with Šídák's multiple comparisons test. b: $n = 2$. Data normalised to β -actin expression. Relative signal intensity is shown.

This data showed interesting trends in the development of inflammatory signals during neurodifferentiation. High mTORC1 activity, as denoted by rpS6 phosphorylation at early time points is likely playing a significant role in determining cell fate. As reviewed in the paper by Tee *et al.* (2016) (286), mTORC1 signalling plays a vital role in various stages of neurogenesis. One component of this is the generation of radial glia from neuroepithelial cells, which should be occurring at early times of neurodifferentiation. Disruption of this

delicate process by enhanced mTORC1 signalling is likely enhanced by high RelA phosphorylation.

Interestingly, STAT3 activity does not seem particularly accompanied by NF- κ B activity in these cells. Previous chapters demonstrated a link between NF- κ B signalling and STAT3 activation, but this is not recapitulated through neurodifferentiation. For example, we would expect to see heightened STAT3 phosphorylation on Y705 in PGP1-A5 cells at day 10, but this is not the case. Instead, p-STAT3 increases initially during a dampening of NF- κ B activity, with both inflammatory signalling pathways active at day 30. In the context of neurodifferentiation, the close signalling interplay between NF- κ B and STAT3 is not as clearly apparent compared to non-neuronal cell models of TSC.

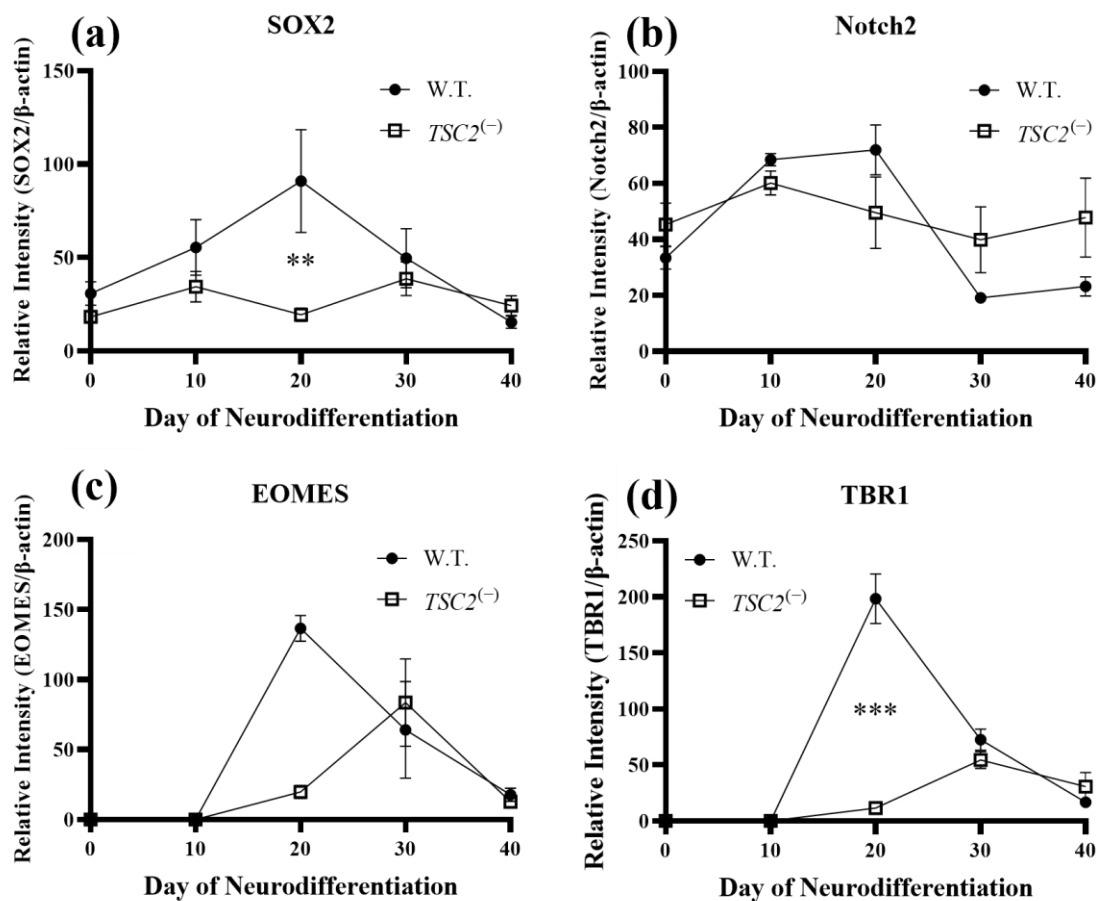


Figure 5.5.3. Neurodifferentiation markers are dysregulated in *TSC2*-deficient cells. Densitometry analysis was performed on western blots of (a) SOX2, (b) Notch2, (c) EOMES, and (d) TBR1 through neurodifferentiation, comparing iBJ4-WT and *TSC2*^(-/-) PGP1-A5. *TSC2*-deficient cells show differing expression patterns of key differentiation markers. a, b, and d: $n = 3$, two-way ANOVA with Šidák's multiple comparisons test. c: $n = 2$. Data normalised to β -actin expression. Relative signal intensity is shown.

Figure 5.5.3 demonstrates differences in the developmental processes undergone in *TSC2*-deficient cells within the earlier stages of neural development. NANOG (shown in Figure 5.5.1) is one of many proteins responsible for maintaining pluripotency in stem cells (503), and NANOG expression is totally removed upon neural induction by day 10. At this point, SOX2 and Notch2 levels in both iBJ4-WT and PGP1-A5 begin rising (less so for PGP1-A5). SOX2 also functions as a marker for stem cells (504), however is also indicative of the presence of radial glia (505), which likely explains the peak in SOX2 expression at day 20 in iBJ4-WT cells. At this point, as shown in Figure 5.4.2, neural rosettes are forming.

Heightening expression of Notch2 was also apparent. Notch2 increased in both cell lines from day 0, and by day 30, Notch2 levels drop significantly in iBJ4-wt. Meanwhile, the increase in Notch2 levels were less pronounced in the *TSC2*⁽⁻⁾ cells. While this was a trend in the data, it did not reach significance. Notch2 is a transmembrane receptor and can maintain radial glia. Thus, the high expression of Notch2 in this scenario may maintain a radial glial population in *TSC2*⁽⁻⁾ cells, which should otherwise be used up in the asymmetric generation of neurons.

The transcription factors, EOMES (also known as TBR2), and TBR1 are typically expressed sequentially and serve as markers of neural development. EOMES expression is typically a marker of IPCs, while also serving to epigenetically induce the activation of TBR1 that is expressed in immature neurons (278). The blots for EOMES in this set of experiments were relatively unclear due to technical issues with antibody, resulting in an $n = 2$. Measurements of bands at the timepoints of day 0 and day 10 were not measured due to a level of background noise in the antibody signal. As a comparison, blots from a similar *TSC1*-deficient neurodifferentiation experiment will be shown in Figures 5.8.1-5.8.3.

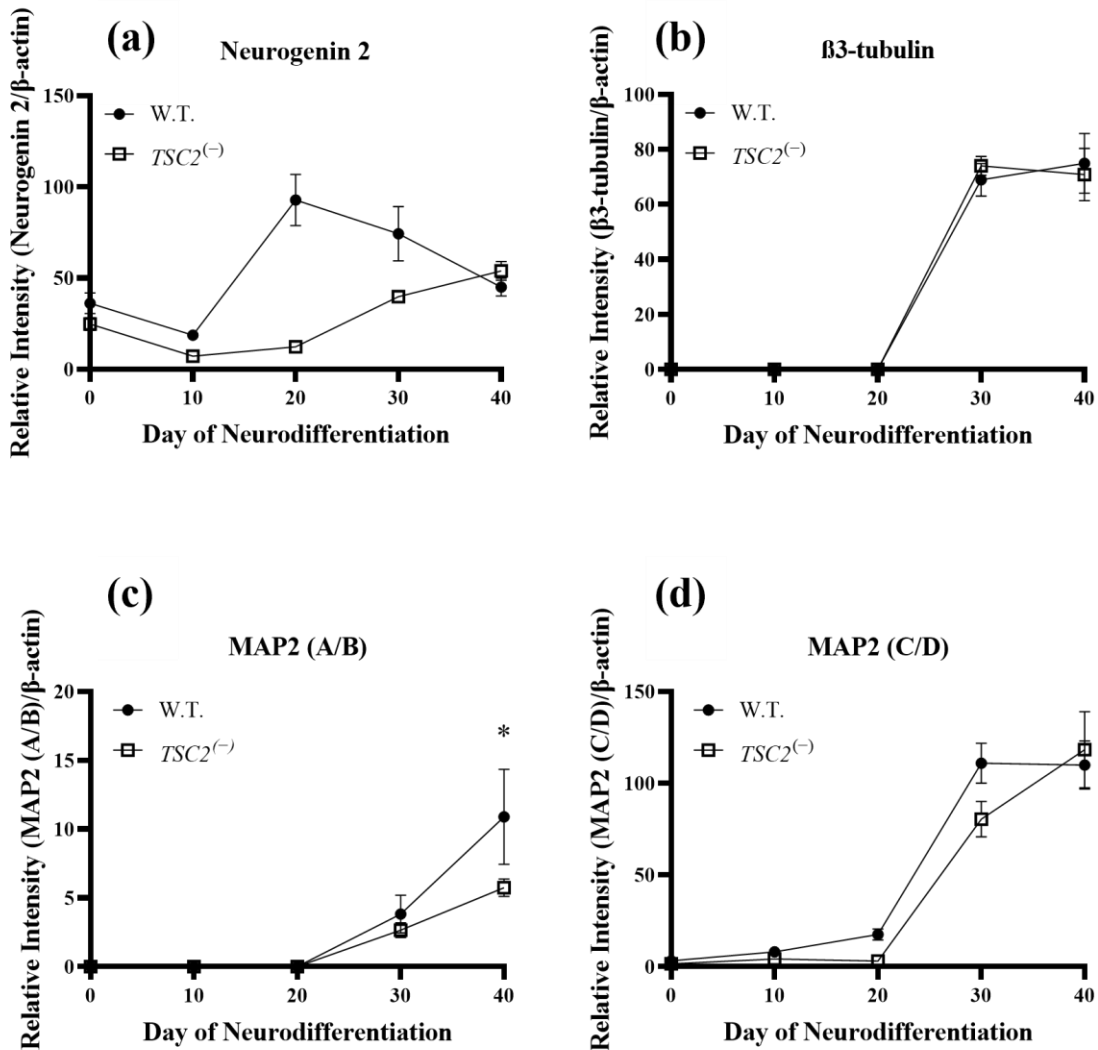


Figure 5.5.4. Later stage neural markers develop more slowly in *TSC2*^(-/-) PGP1-A5 cells.

Densitometry analysis was performed by western blots analysis of (a) neurogenin 2, (b) β3-tubulin, (c) MAP2 (A/B isoforms), and (d) MAP2 (C/D isoforms) through neurodifferentiation, comparing iBJ4-WT and *TSC2*^(-/-) PGP1-A5. *n* = 3, two-way ANOVA with Šídák's multiple comparisons test. Data normalised to β-actin expression. Relative signal intensity is shown.

Neurogenin 2 is typically expressed within IPCs. As such, it is unsurprising that wild type cells express high levels of neurogenin 2 at days 20 and 30 of neurodifferentiation, and the overall expression patterns are similar to that of EOMES (Figure 5.5.3). The presence of β3-tubulin typically signifies the formation of neurons (506). Surprisingly, β3-tubulin shows little difference between the cell types, although we may have expected reduction in *TSC2*^(-/-) cells due to a reduction in earlier developmental markers. Conversely, MAP2 (A/B) seemed to increase more within the iBJ4-WT cells.

Similarly, MAP2 (C/D) was detectable at earlier stages in iBJ4-WT cells, compared to PGP1-A5, before having similar expression at day 40.

Here, we see slight differences in neurodevelopmental processes occurring in *TSC2*⁽⁻⁾ cells, compared to wild type (Figure 5.5.4). The delay in markers for IPCs may explain the small, but apparent delay in MAP2 expression (Figure 5.5.4c and 5.5.4d). Notably, the development of the larger A/B isoforms of MAP2 appears to be greater in wild-type cells, signifying the development of more mature, and longer neural projections (507). In contrast to this slight but significant result, β 3-tubulin levels appear to develop at a similar level in both cell lines by day 30 and 40 (Figure 5.5.4b). As a cytoskeletal protein associated with neurons, this also signifies the development of neurons. Due to a later and lower transient expression of neurodevelopmental markers such as neurogenin 2, EOMES, and TBR1, we might expect overall neuronal cell development to be lower within *TSC2*⁽⁻⁾ cells. However, the development of neurons was apparent visually (Figure 5.4.2 – 5.4.3), although obscured with the overgrowth of other cell types. The abundance of other cell types that arise during development may be dampening the signal of normalised data for markers such as EOMES and TBR1, which otherwise may show a high expression and thus development of neurons alongside other glial cells. This may be mediated through the expression of proteins such as SOX2 and notch2. As observed, notch2 levels in *TSC2*⁽⁻⁾ cells do not exhibit the same spike in expression by day 20 as in wild-type cells. In this way, notch2 may be maintaining a population of radial glia. This may be demonstrated by overall SOX2 levels that spike in a similar way within wild-type populations, but are generally maintained at a low but persistent level in the *TSC2*⁽⁻⁾ cells. This would match with visual data of cells plated at low density, as shown in Figure 5.4.4, where *TSC2*⁽⁻⁾ cells at day 66 show a morphology which is similar to that of RGCs.

Data (not shown) obtained by another lab member, Dr Laura Kleckner, hinted at a similar expression pattern in *TSC1*⁽⁻⁾ iBJ4 cells. Specifically, mRNA expression of vimentin, and PAX6 were both significantly upregulated within neuronal populations at day 50 of neurodifferentiation, when compared to wild-type iBJ4 cells. This would suggest an abundance of radial glia in samples (508,509). To accompany this, fluorescent images and the outcome of image analysis for *TSC1*⁽⁻⁾ and wild-type iBJ4 cells were also kindly provided (Figure 5.6).

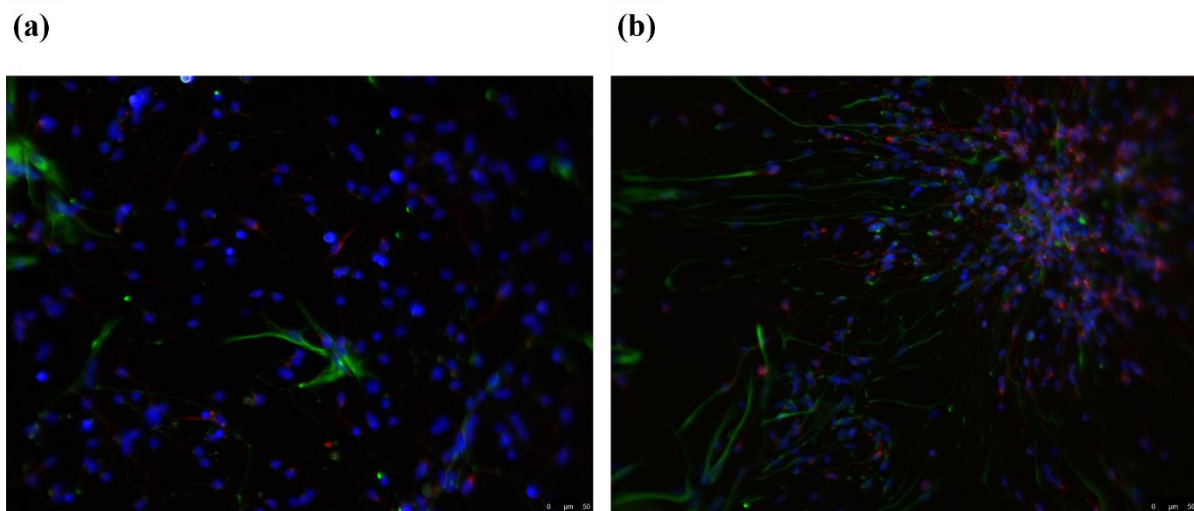


Figure 5.6. *TSC1*⁽⁻⁾ cells develop more astrocytes than wild-type during neurodifferentiation. *TSC1*⁽⁻⁾ iBJ4 cells were differentiated alongside iBJ4 wild-type cells by Dr Laura Kleckner. Following fixing at day 53 of neurodifferentiation, cells were probed fluorescently for S100 calcium binding protein B (S100b) (green), MAP2 (red), and nuclei (DAPI, blue). The images and image analysis were kindly donated. The analysis identified a higher proportion of S100b-positive cells within *TSC1*⁽⁻⁾ cells than wild-type.

Fluorescent image analysis of this data may indirectly support the theory of TSC1/2 protein-deficient cells being locked into radial glia populations for a prolonged period. Once radial glia are formed, they will either form IPCs (which later become neurons), differentiate into astrocytes once neuronal generation is complete, or alternatively differentiate directly into postmitotic neurons (286,510).

To accompany this data, we can also look towards transcriptomic data of TSC patient-derived brain tumours (Table 5.2, Figure 5.7).

Gene	Fold Change (SEN/SEGA)	Fold Change (Cortical Tuber)	Significant? (SEN/SEGA;Cortical Tuber)		
<i>NOTCH1</i>	2.3	1.7	(Y;N)	NEC	
<i>SOX10</i>	0.2	1.12	(Y;N)		
<i>CDH1</i>	4.2	1.4	(Y;N)		
<i>HES1</i>	4.6	2.3	(Y;Y*)		
<i>NES</i>	11.9	2.9	(Y;Y)		
<i>SOX2</i>	4.3	2.8	(Y;Y)		
<i>VIM</i>	29.3	9.3	(Y;Y)		
<i>FABP7</i>	2.5	3.2	(Y;Y)		RGC
<i>CDH2</i>	1.1	1.2	(N;N)		
<i>TNC</i>	21.1	25.5	(Y;Y)		IPC
<i>NOTCH2</i>	2.8	2.3	(Y;Y)		
<i>PAX6</i>	1.04	2	(N;Y)		
<i>EOMES</i>	35.0	1.3	(Y;N)	Neuron	
<i>NGN2</i>	0.1	0.5	(Y;N)		
<i>TBR1</i>	0.03	0.3	(Y;Y)		
<i>DCX</i>	0.04	0.9	(Y;N)		
<i>NEUROD1</i>	0.01	0.3	(Y;Y)		
<i>MAP2</i>	0.1	0.5	(Y;N)		
<i>NEUN</i>	< 0.01	0.4	(Y;Y)		
<i>MAPT</i>	0.2	0.8	(Y;N)		
<i>TUBB3</i>	0.85	0.83	(Y;N)		
<i>GFAP</i>	7.41	25.2	(Y;Y)		AC
<i>S100B</i>	0.9	2.1	(N;N)		
<i>ALDH1L1</i>	1.3	2.9	(N;N)		
<i>EAAT2</i>	0.1	0.8	(Y;N)		
<i>GJA1</i>	3.1	5.1	(Y;Y)		
<i>GJB6</i>	0.01	0.4	(Y;N)		
<i>NDRG2</i>	0.6	1.02	(Y;N)		

Table 5.2. Transcriptomic neurodevelopmental markers in TSC patient-derived brain tumours. Using transcriptomic data obtained from the brain tumours of TSC patients, as referred to in section 2.2.4, the relative expression of various genes relating to neural and glial cell types were analysed. Significance refers to $p < 0.05$. (*: $p = 0.052$) (NEC = Neuroepithelial cell, RGC = Radial Glial Cell, IPC = Intermediate Progenitor Cell, AC = Astrocyte.) *Note: GFAP is also a marker for RGCs.*

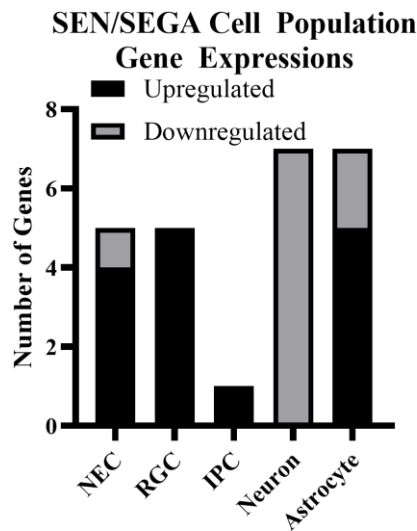


Figure 5.7. Pre-neural cell types are upregulated in SEN/SEGA. Significantly upregulated/downregulated genes of specific cell types were plotted, corresponding to Table 5.2.

The data from Table 5.2 and Figure 5.7 highlight that in general, SEN/SEGA tumours exhibit an upregulation of pre-neural cell types, whereas neuron formation is downregulated. Astrocytes also appear to be upregulated.

5.3.3 Protein expression during neurodifferentiation of *TSC1*⁽⁻⁾ iBJ4

To support the data obtained from the *TSC2*⁽⁻⁾ iPSC model, a second neurodifferentiation was performed with iBJ4 *TSC1*⁽⁻⁾ and iBJ4 wild-type cells (Figure 5.8.1). This *TSC1*-deficient model was engineered and kindly donated by Dr Laura Kleckner (Harwood Lab, NMHRI, Cardiff University) to be used in this project.

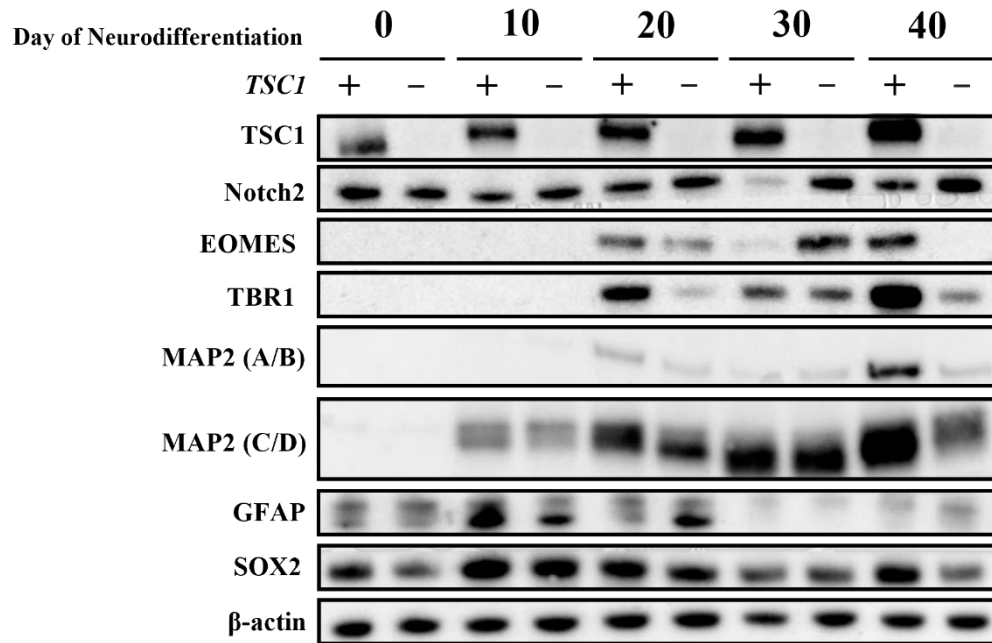


Figure 5.8.1. Differential protein expression in iBJ4-*TSC1*⁽⁻⁾ vs iBJ4-WT during neurodifferentiation. Samples were collected during neurodifferentiation at days 0, 10, 20, 30, and 40. Samples were then analysed via SDS-PAGE and western blot.

For this set of experiments, it should be noted that the comparatively high expression and late spike of SOX2 in wild-type iBJ4 cells possibly signifies the presence of radial glia. This would demonstrate issues through the neurodifferentiation process, and therefore, the data cannot provide a perfectly clear interpretation. If SOX2 expression relates to a high RGC population, the spike at day 40 in EOMES expression may relate to the generation of a new set of IPCs. The pattern of EOMES expression is strikingly similar to the data obtained from neurodifferentiation of *TSC2*-deficient cells.

Regardless, a general interpretation of these markers shows a similar set of results to those observed in the *TSC2*-deficient cells, with an overall trend of delayed differentiation, and a difficulty in progression to the immature neuron stage, as shown by a weakened expression of TBR1 (Figure 5.8.2).

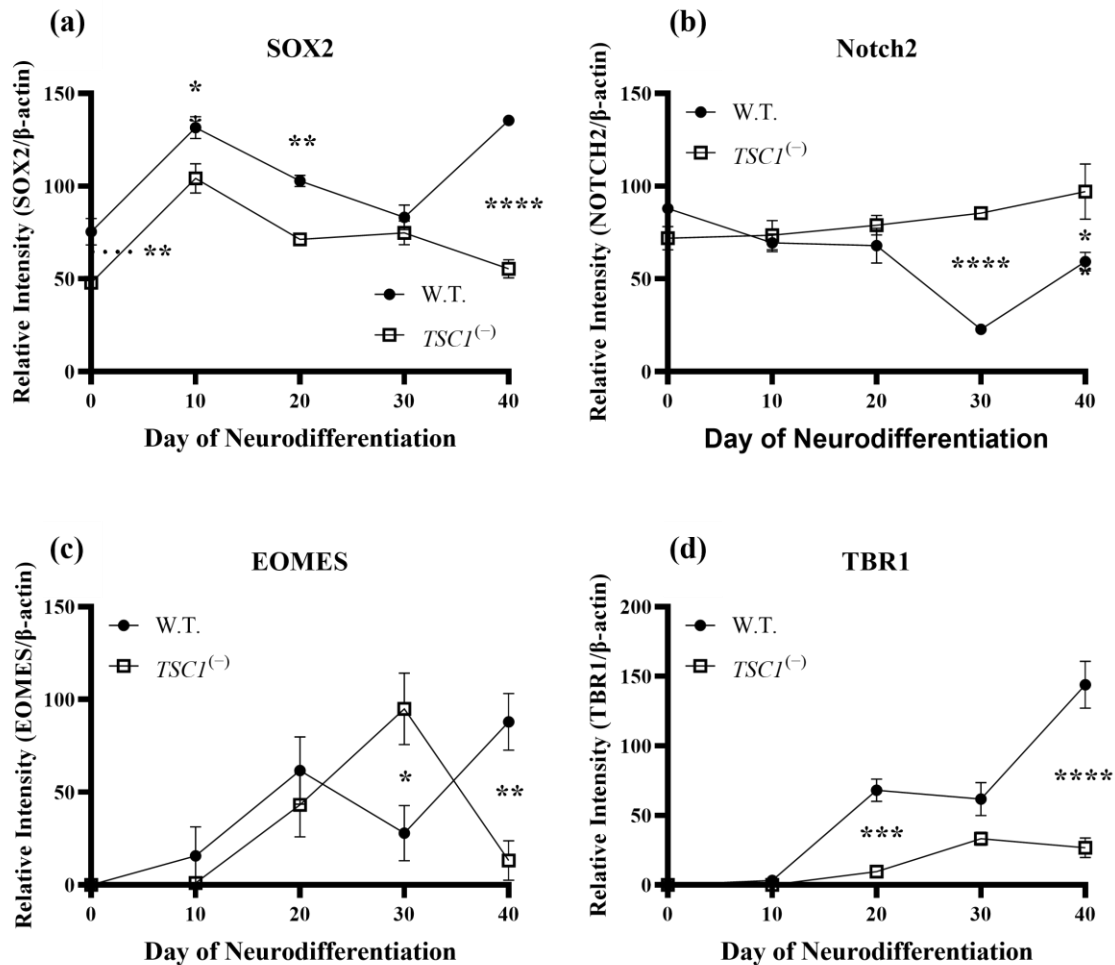


Figure 5.8.2. Early to intermediate neurodifferentiation markers are dysregulated in *TSCI*-deficient cells. Densitometry analysis was performed on Western blots of (a) SOX2, (b) notch2, (c) EOMES, and (d) TBR1 through neurodifferentiation, comparing iBJ4-WT and *TSCI*⁽⁻⁾ iBJ4. $n = 3$, two-way ANOVA with Šídák's multiple comparisons test. Data normalised to β -actin expression. Relative signal intensity is shown.

Overall, *TSCI*-deficient neurons seem to show overall lower levels of SOX2 throughout neurodifferentiation (Figure 5.8.2a). At earlier stages, this may show a failure to form RGCs. This is in contrast to Notch2 expression, where Notch2 gradually appeared to increase in expression within *TSCI*-deficient cells (Figure 5.8.2b). Of note, the expression pattern of EOMES are strikingly similar in to the previous data obtained from *TSC2*-deficient cells. *TSCI*-deficient cells show a delayed upregulation of EOMES expression, suggesting a delay in IPC generation (Figure 5.8.2c). This likely corresponds with delayed TBR1 expression (Figure 5.8.2d). It is unclear why EOMES spikes for a second time in iBJ4-WT cells. This may be representative of a second round of differentiation.

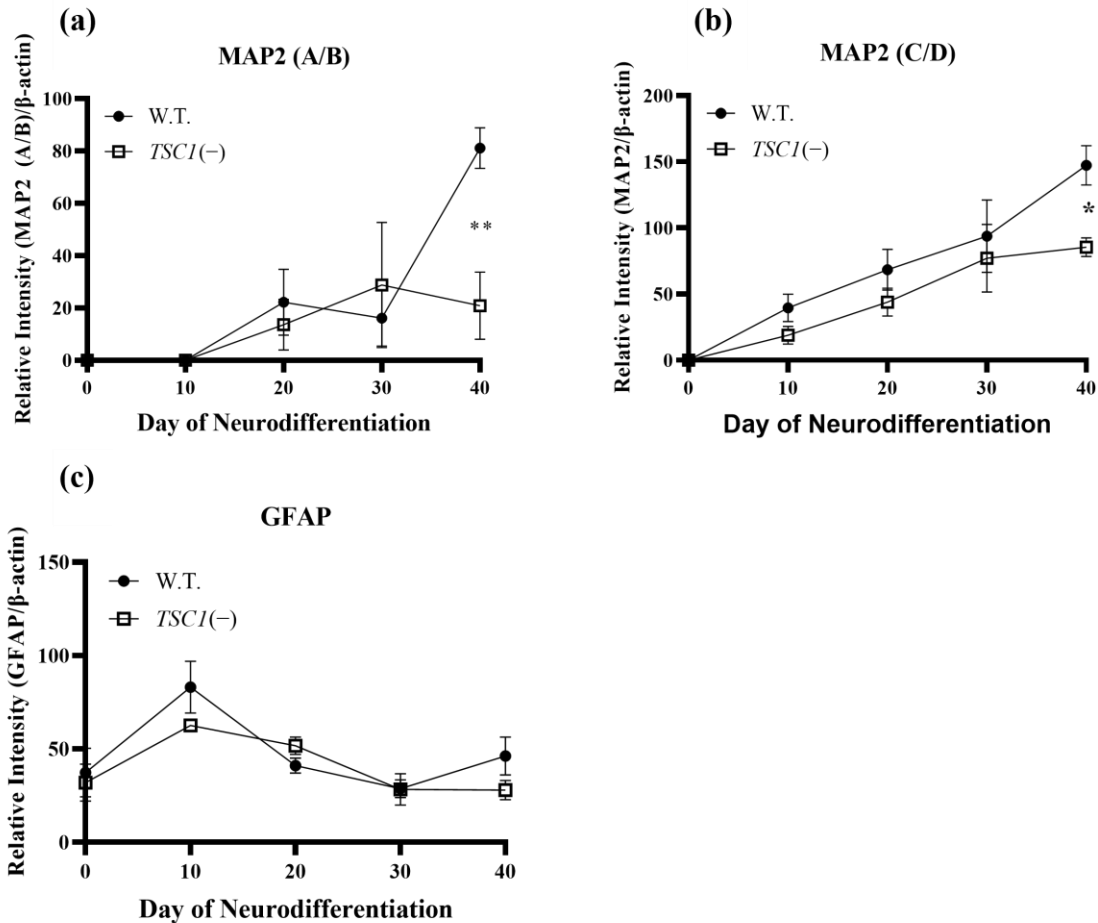


Figure 5.8.3. Neurodifferentiation markers are dysregulated in *TSC1*-deficient cells. Densitometry analysis was performed on Western blots of (a) MAP2 (A/B) and (b) MAP2 (C/D), and (c) GFAP through neurodifferentiation, comparing iBJ4-WT and *TSC1*⁽⁻⁾ iBJ4. $n = 3$, two-way ANOVA with Šídák's multiple comparisons test. Data normalised to β -actin expression. Relative signal intensity is shown.

Notably, MAP2 expression appears higher in wild-type cells than *TSC1*-deficient cells, as previously shown in the comparison including *TSC2*-deficient cells (Figure 5.8.3a-b). Blots for GFAP were also performed over the duration. Delayed upregulation of MAP2 isoforms in *TSC1*-deficient cells is likely resultant of delayed EOMES/TBR1 expression, as shown in Figure 5.8.2. The initial spike in GFAP expression around day 10 likely corresponds to an emergence of RGCs. Notably, this is dampened in *TSC1*-deficient cells compared to wild type, but persists slightly more into day 20. While multiple comparisons showed no significance, the overall expression patterns through two-way ANOVA reached $p = 0.0004$.

With the conflation of Table 2 and the other Figures shown here, an overall trend appears to emerge. Within TSC patients, tumours appear to have a large comprisal of pre-neural cells. Specifically, we see an upregulation of genes which would suggest the presence of NECs, RGCs, and IPCs. Conversely, the presence of neurons is significantly downregulated. This is not entirely matched by the *in vitro* data, wherein a somewhat delayed but clear upregulation of neural cell markers are observed (such as MAP2 and TBR1). However, development is clearly delayed.

As outlined in the paper by Englund *et al.* (2005) (511), neurodevelopmental markers occur in a sequential fashion. In short, PAX6 is expressed in radial glia, TBR2 (EOMES) is expressed in migrating intermediate precursor cells, and TBR1 is expressed in immature postmitotic neurons. With additional data that demonstrates dysregulated NF- κ B, STAT3, and mTORC1 activity in *TSC2*-deficient neural cells (Figure 5.5.2), we can begin to suggest why the delays in neuronal development are observed in *TSC1/TSC2*-deficient cells.

As outlined by Tee *et al.* (2016) (286), mTORC1 activity plays a significant role in neural development. Specifically, it guides the stages between differentiation and can lead to the generation of IPCs from RGCs. It is interesting to note that while TBR2-positive IPCs and RGCs are upregulated upon mTORC1 hyperactivity, the number of postmitotic neurons does not increase (512,513). In this case, mTORC1 activity is essential for the generation of IPCs from an NPC population (514). Therefore, we may hypothesise that if RGCs are not terminally committing to neurons in TSC-derived brain tumours, RGCs may instead be committing to glial lineages or remaining as dysregulated RGCs. mTORC1 activity also guides the migration of IPCs along the processes of RGCs, and a final conversion of dividing neuroblasts to mature postmitotic neurons (286). This is not necessarily represented within our *in vitro TSC2*-deficient model, where we see delayed but apparent neural development. This is in contrast to the findings in a study which observed mTORC1 hyperactivity leading to the formation of highly proliferating IPCs (500). If this were the case, an early and high expression of EOMES/Neurogenin 2 within *TSC2*-deficient cells may have been observed. Instead, EOMES expression was delayed in *TSC1/TSC2*-deficient cells. Similarly, Neurogenin 2 expression was delayed in *TSC2*-deficient cells. However, *TSC2*-deficient cells do appear to exhibit a propensity to delayed terminal differentiation to non-mitotic neurons, as marked by a downregulation in TBR1 within *TSC1/TSC2*-deficient cells, and also a slight delay in MAP2 expression. It should be also noted that while mTORC1 hyperactivity diminishes over time in both cell lines, it remains higher in *TSC2*⁽⁻⁾ cells overall at all time

points measured, as marked by rpS6 phosphorylation. A diminishment in the level of rpS6 phosphorylation over time could be due to differentiation into non-dividing neurons with lower available rpS6. This was suggested in the paper by Blair *et al.* (362). The studies referenced above (except Blair *et al.*) are generally performed on *in vivo* models of mice. Therefore, their results may not be perfectly recapitulated by the *in vitro* human cell model used here. The expression patterns of rpS6 phosphorylation were relatively predictable. Earlier data and the general knowledge surrounding TSC indicates that mTORC1 activity is higher within *TSC2*-deficient cells and would likely remain higher throughout neurodifferentiation.

The activity of NF- κ B in TSC neural development is much less well studied. A recent study found an elevation of NF- κ B related proteins (TNF α , ICAM1, MAPK) within cortical tubers of TSC patients (335), but barring this, specific NF- κ B targeted research in the neural development of TSC patients is incredibly limited. Our data shows dysregulation in the expression patterns of NF- κ B. Specifically, RelA phosphorylation on serine 536 fluctuates throughout days 0-40 of differentiation, but in general appears to be higher within *TSC2*⁽⁻⁾ cells. NF- κ B activity is known to play a variety of roles in the brain, regulating axonal function and morphology, while also exerting both neuroprotective and neural-apoptotic effects (515). The effects of NF- κ B signalling on neural process outgrowth seem to be mixed. NF- κ B activity inhibits the growth of neuronal axons in a canonical, TNF α stimulated manner (516). However, in the presence of BDNF, NF- κ B inhibition appears to have the opposite effect, wherein neuron arbor size was reduced (517). In broad studies to assess the overall effect of NF- κ B knockout in mice, NF- κ B has been demonstrated as important in neural activity, playing roles in memory and learning (518).

A review by Dresselhaus and Meffert (2019) (519) looked at NF- κ B activity across neural cell types. Overall, NF- κ B in neurons likely controls inhibitory or excitatory signal transmission, and influences control over dendrite/axon formation and plasticity. Interestingly, glutamatergic excitatory signals increase NF- κ B activity. Meanwhile, glutamate can cause excessive NF- κ B activity in astrocytes, leading to oxidative stress-induced cell toxicity. Under basal conditions, astrocytes do not normally exert NF- κ B activity, however, upon injury or disease, p-RelA is stimulated to drive NF- κ B activity in astrocytes. RelB also plays roles in NF- κ B activity under injury or disease, but the assays in our study focus predominantly on RelA. Perhaps most interestingly, cultured neural NECs expressing a NF- κ B super-inhibitor dominant negative I κ B α transgene to suppress NF- κ B activity would

enhance differentiation into glial lineages rather than neurons (520). This transgene was under the expression of the GFAP promoter. Thus, blocking NF- κ B activity within radial glia which express GFAP was likely preventing neuron formation in this context. Unsurprisingly, NF- κ B activity also plays a significant role in microglia, controlling activation and inflammatory/neurotoxic properties of the immune cells (521). Reduction in microglial-specific NF- κ B activity would lead to the reduced expression of NF- κ B target cytokines such as IL-6 or IL-1 β . Using mice with a conditional knockout of IKK β in microglia, it has been shown that inhibition of NF- κ B protects against neural cell death that would occur from excessive inflammatory stimulation from a microglial origin (522), but also induces behavioural defects in mice (523). This shows the multi-faceted role of NF- κ B in microglia; NF- κ B exerts damaging effects on neurons in the presence of excessive inflammatory stimulation, but NF- κ B activity in microglia is evidently important in the immune system and contributes to proper neuronal function. The *in vitro* model used in our study does not specifically investigate microglia, however the role of the immune system will be investigated in TSC patient-derived tumours via transcriptomic analysis later in this chapter.

A study by FitzPatrick *et al.* (2018) (524) investigated the longitudinal role that NF- κ B plays during the neural development process using an *in vitro* model. Gene ontology analysis highlighted an NF- κ B activation signature (with regards to TNF α , cytokine, and inflammatory signalling). This NF- κ B activation signature was high at the stage of differentiation between RGC to IPC, suggesting that high NF- κ B activity plays a significant role in the transition between these two cell types. IPCs were also found to typically express higher canonical NF- κ B activity. NF- κ B activity was also shown to influence maturation of IPCs, wherein high NF- κ B expression was correlated with low SOX2 and high nestin expression in IPCs. Moreover, IPCs with high NF- κ B expression committed to less β 3-tubulin expressing neurons, as well as a reduction in SOX10; a neural crest marker which would signify the presence of NECs. This corresponded with IPCs that had a relatively high level of metabolic activity with enhanced NF- κ B. Lastly, autophagy is increased within NF- κ B activated cells. This is interesting, as high mTORC1 activity would normally result in the repression of autophagy in *TSC2*-deficient cells. The overall role that autophagy plays in neural differentiation is poorly understood, so it is difficult to say what role the ‘push and pull’ of NF- κ B/mTORC1 activity has on autophagy and how this might be involved in the commitment of neurons during differentiation. It is interesting to note that RelA phosphorylation within our data shows comparatively high peaks within *TSC2*-deficient cells

at day 10 and day 30 of neurodifferentiation. The presence of NF- κ B activity at day 30 may correlate with the presence of IPCs. If related to the study of FitzPatrick *et al.* (524), this would lead to a reduction or delay in neuron formation. This is, in part, shown in our data through slightly reduced MAP2 expression at day 30. However, this was not significantly reported by 2-way ANOVA.

STAT3 signalling in neurogenesis has been investigated to a greater depth, however the results are still fairly non-conclusive. Most notably, (and probably similarly to mTORC1 and NF- κ B activity), STAT3 activity likely possesses a temporal component in determining cell fate during neurogenesis. One study (which did not discern between neural progenitor cell types), determined that STAT3 activity can promote proliferation and suppress the formation of neurons (525). Furthermore, while it was previously thought that STAT3 drives the formation of astrocytes, this study identified that astrocyte formation is not strictly dependent on STAT3 expression, but that STAT3 drives GFAP expression. An RNA-seq analysis was also performed, which identified that STAT3-knockout cells expressed markers which would correspond with radial glia, and less so with neurons and IPCs. In general, glial markers were upregulated upon STAT3 loss. Another key point is that upon STAT3 knockdown, mTOR phosphorylation also reduced, suggesting that STAT3 is able to promote mTOR signalling. Conversely, STAT3 knockdown lead to a decrease in markers for IPCs and neurons. Thus, STAT3 activity is likely implicated in the commitment of neural differentiation.

Another related study described that activation of STAT3 occurred in neural stem cells (526), which is partially shown in our data with STAT3 expression at day 10 of neurodifferentiation, and by slight downregulation over time as populations of cell types change over time in wild-type cells. Interestingly, STAT3 drug inhibition in rats resulted in increased neuron generation, demonstrating that the activity of STAT3 is likely inhibiting neuron formation. Conversely, following spinal cord injury, STAT3 activity was shown to be beneficial in the recruitment of active astrocytes for the repair of damaged neuronal tissue (527). This shows that the general knowledge on STAT3 activity in neural development is inconsistent and complicated. Importantly, this study demonstrated that total STAT3 knockout was detrimental to neural repair and resulted in a large increase in immune cell infiltration, while SOCS3 knockout (which would boost STAT3 activity) could improve neural repair. The data collectively demonstrated that the total level of STAT3 protein was involved in the general neural function and repair, whereas phosphorylated STAT3 was driving the reported pathogenic signals. The different roles that unphosphorylated and phosphorylated STAT3

have is an important point to discuss and is raised in newer studies (as referenced in Chapter 3, (383)). For instance, it has been demonstrated that unphosphorylated STAT3 still plays a role in transcriptional target activation. Thus, STAT3 expression is likely necessary for neuroprotective and regenerative effects via slight inflammatory activity, but excessive inflammation is detrimental to repair (where STAT3 would become chronically phosphorylated). If we compare this to the data shown previously, high STAT3 expression (and phosphorylation) in *TSC2*-deficient cells may be stalling neural development and instead retaining cells in precursor states. This is marked by a delay in EOMES and TBR1 expression, and a relatively consistent SOX2 and Notch2 expressive state. STAT3 nuclear activity in rat brains appears to be more apparent within glial cells, rather than in neurons (528). Further adding to this, RGCs were identified as expressing high levels of STAT3, and enhanced STAT3 causes a maintained presence of RGCs and reduced neural development (529). In this same study, STAT3 was also shown to induce proliferation via symmetrical division in RGCs, replicated both *in vivo* and *in vitro*. Typically, symmetrical division occurs early in development in order to expand the number of RGCs, followed later by asymmetrical division which gives rise to more neurons (530), however this appears dysregulated upon STAT3 upregulation. This would support the notion that *TSC2*-deficient cells are promoting a glial lineage of astrocytes or RGCs, rather than neurons, and that this is being mediated through STAT3 or phospho-STAT3. The levels of SOX2 in our data seem relatively low, and variation is not especially pronounced between the timepoints for *TSC2*-deficient cells, however if we look at general pattern alone, the levels of SOX2 seem to roughly mimic that of STAT3 total levels. *i.e.*, higher expression at day 10, diminishment at day 20, and then increased again at day 30.

Unlike NF- κ B, the role of STAT3 in the development of neurons in TSC has also been investigated. A study by Blair *et al.* (362) utilised *TSC1* and *TSC2* knockout, or Cre-knockout systems to investigate the impact of loss of function in TSC-proteins during neural development, within a cortical spheroid model. Importantly, they noted that *TSC1*- or *TSC2*-deficient cortical spheroids generated a greater glial population. They also noted that *TSC1/TSC2*-homozygous knockout cells exhibited a delay in neural protein expression, similar to what we observed in the results listed here. To compare, Blair *et al.* noted significant differences in these protein expressions at significantly later timepoints than in our data (day 50, 100, and 150), which we were unable to perform due to time constraints. Slightly later timepoints in our data will be reviewed shortly. Interestingly, Blair *et al.*

reported an increase in Y705 STAT3 phosphorylation over all timepoints for *TSC2*-deficient cells. *TSC1*-deficient cells also exhibited greater STAT3 phosphorylation than wild type, but less so than for *TSC2*-deficient cells. In this case, STAT3 phosphorylation gradually increased, similar to what was observed with western blot analysis at day 0 to day 40 in our results. The variation in observed results may be related to the different types of models used, *i.e.*, a three-dimensional spheroid model versus a two-dimensional model. Blair *et al.* arrived at a similar hypothesis: *TSC2* knockout could be promoting the formation of glial cells, likely through STAT3 activity. Since we previously identified that NF- κ B activity may be a driver of STAT3, this could suggest that dysregulated NF- κ B signalling in neural development is driving gliogenic signalling. However, this logic is hampered by a mismatch in expression patterns between p-RelA and p-STAT3 in our neurodifferentiation. Blair *et al.* also identified that mTORC1 inhibition with persistent rapamycin treatment was able to reduce the glial outcome of *TSC2*-deficient neural generation, highlighting the prevalent role of mTORC1 hyperactivation in cell composition of TSC patient-derived tumours. They also noted that the timing of mTORC1 hyperactivation (through Cre-knockout of *TSC2*) played a significant role in the outcome of the cells, which is to be expected. Conditional knockout of *TSC2* at day 12 of neurodifferentiation resulted in the highly glial phenotype as exhibited in regular *TSC2*-deficient cells. Based on their methodology, this was during the precursor expansion stage, likely containing NECs and RGCs. Similarly, mTORC1 inhibition at this stage of neural development was beneficial in reversing this phenotype, whereas mTORC1 inhibition at later stages did not significantly alter the end result of cell type composition. This is complimented by similar data produced by Dr Laura Kleckner, as mentioned before, who utilised a reversible Cas13 knockout system of *TSC1* (not shown). In this data, a 24 h knockout of *TSC1* (resulting in a short burst of mTORC1 hyperactivity) at day 8 was sufficient to drastically increase expression of vimentin, CD44, PAX6, and S100b1 at day 50 of neurodifferentiation. This signifies that mTORC1 hyperactivation is incredibly important at the stage of NECs and RGCs in determining cell fate. It also highlights, as mentioned by Blair *et al.*, that there is a window of development where mTORC1 inhibition is key in preventing the dysregulated glial phenotype that is typically observed in TSC patient-derived brain tumours.

With all of this considered, we can conclude that the inflammatory pathways, NF- κ B and STAT3, are dysregulated in *TSC2*-deficient cells of a neural lineage, and that it is likely that these are contributing to the dysregulated macro-morphology observed across development.

It is likely that mTORC1 hyperactivity is playing a significant role in guiding the inflammatory state, as well as playing direct roles in preventing neuron generation. Further work would need to be carried out to investigate this further. Mild inhibition of NF- κ B, STAT3, or mTORC1 throughout the differentiation process would be interesting to observe, with regards to how inhibition of these three pathways might interact with one another and influence the final morphology of cells. In our experimentation, we did attempt an exploratory treatment of long-term rapamycin or BMS345541 supplementation, but due to time constraints we were not able to optimise dosage, and neurodifferentiation failed because of this.

5.3.4 Inflammatory pathways in mature *TSC2*⁽⁻⁾ neurons

An insight into how mTORC1 effects the neurodifferentiation process has now been observed. A dysregulated inflammatory phenotype throughout neurodifferentiation has also been observed. The study next aimed to investigate how these inflammatory pathways persist later into differentiation by probing them at days 60 and 70. At this point, cells were able to be maintained for prolonged periods with little manipulation, although *TSC2*-deficient cells continued to proliferate and metabolise, as represented by increasing plate cell-packing and media acidification. Morphology at day 60 is shown in iBJ4-WT and PGP1-A5 cells (Figure 9.1a), highlighting the sparse, easily discernible nature of neural projections in wild type cells versus the disorganised and clustered organisation in *TSC2*⁽⁻⁾ PGP1-A5 cells. Protein samples were also generated at day 60 and used for western blots, comparing protein expression of neural markers and STAT3 expression between wild-type and *TSC2*-deficient neurons (Figure 9.1b).

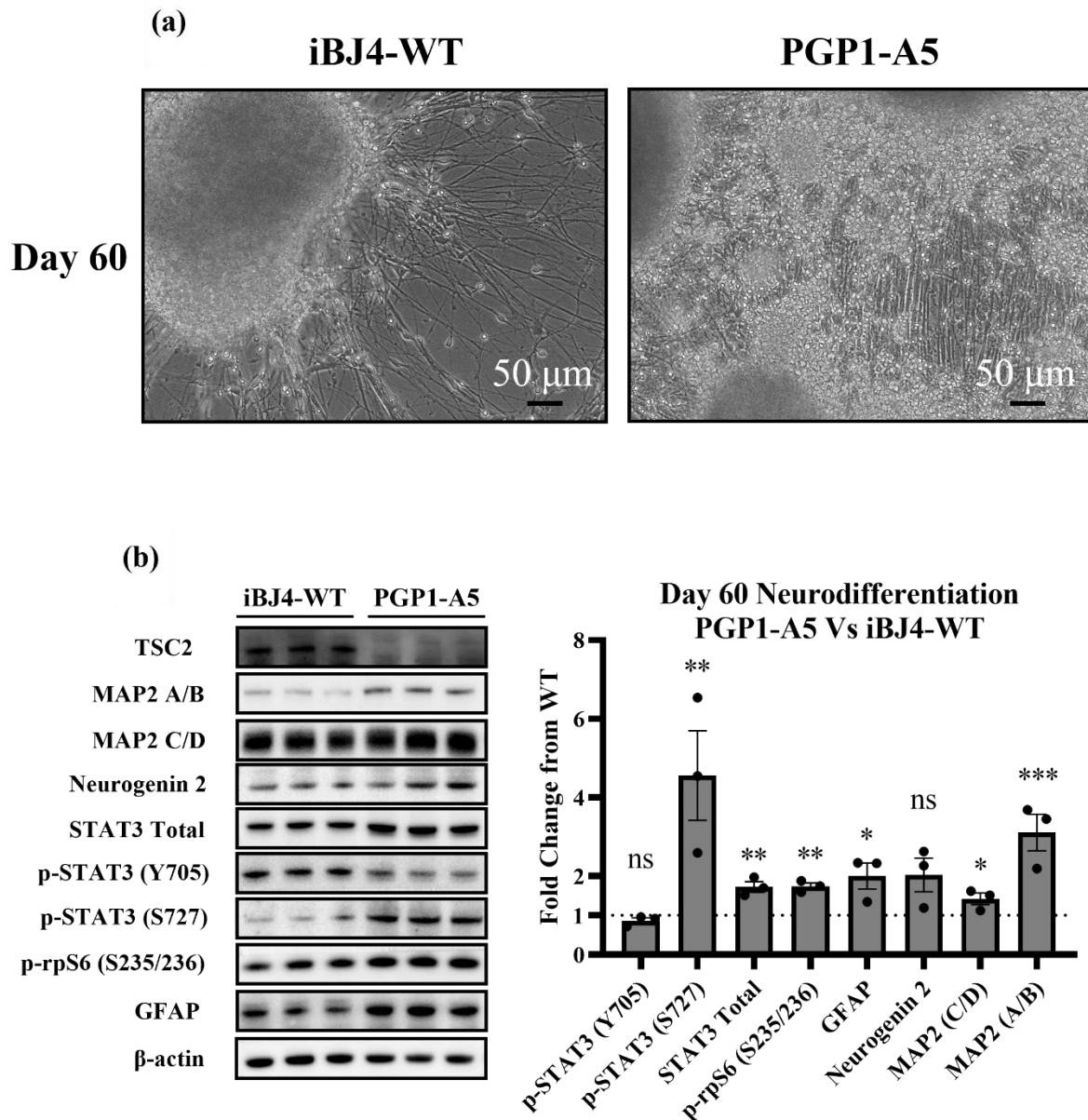


Figure 5.9.1. Neurodifferentiation of *TSC2*⁽⁻⁾ cells produces neurons and GFAP positive cells. (a) Images were taken at day 60 of neurodifferentiation, comparing wild-type cells and *TSC2*⁽⁻⁾ cells. Wild type cells demonstrate clear projection of axons or dendrites, with minimal other cell types grouping around neural clusters. Conversely, while neural projections can be seen in *TSC2*-deficient cells, other cell types appear to be present. (b) Western blots were performed on samples collected at day 60, comparing wild-type cells and *TSC2*⁽⁻⁾ cells. A corresponding densitometry analysis is included, with protein expression normalised to β-actin and fold changes from iBJ4-WT samples are shown. *n* = 3, multiple t-tests. Data normalised to β-actin expression.

Notably, morphology of *TSC2*⁽⁻⁾ cells varied across wells, with patches of high-density, poorly differentiated cells accompanied by less dense patches of well-formed neural projections (Figure 9.2)

PGP1-A5

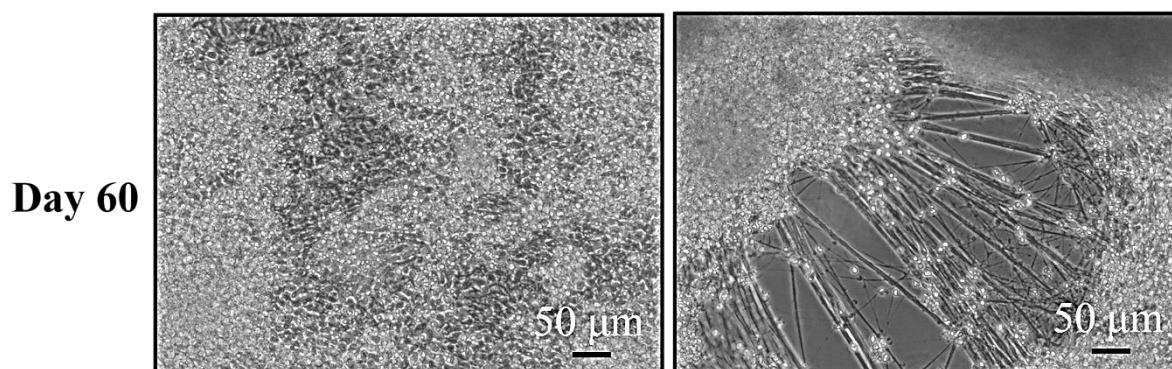


Figure 5.9.2. Morphology and cell types vary within populations of *TSC2*-deficient neural cells. Images were taken at 20X of *TSC2*-deficient neurons at day 60 of neurodifferentiation. Different regions of the same well are compared to show heterogeneity in cell populations and morphology.

Samples and images at day 60 provide an insight into how *TSC2*⁽⁻⁾ cells form neuronal cells. Beginning the analysis at MAP2 expression, we see that neural formation appears to be progressing within *TSC2*⁽⁻⁾ cells, demonstrating a surprisingly upregulated level of MAP2 across the C/D and A/B isoforms. Considering our previous data, this is somewhat unexpected. When compared to images taken in Figure 5.9.1 and 5.9.2, it is possible that the MAP2-expressing neurons are growing underneath the larger number of poorly differentiated (and presumably proliferating) cells. While hard to determine with phase contrast images, MAP2-expressing neurons remain abundant, buried underneath other cell types. While neural formation is clear in this case, it is likely that their function would be dysregulated.

Comparatively high rpS6 phosphorylation was also observed in PGP1-A5 cells versus iBJ4-WT cells, signifying mTORC1 activation. This would likely contribute to neuropathological processes, such as epilepsy (531). Neurogenin 2 was also slightly upregulated which may signify a higher presence of IPCs, although this did not reach statistical significance. It was previously suggested that mTORC1 hyperactivation may be stalling neurodifferentiation, leading to an upregulation of RGCs and other neural precursors. We may hypothesise that while RGCs are upregulated, at some point they may finally commit to conversion to terminal neural differentiation. Therefore, high RGC content of *TSC2*-deficient tumours may ultimately cause neural generation, at least within our *TSC2*⁽⁻⁾ *in vitro* model.

The results we see in STAT3 activity are unexpected, given the high STAT3 phosphorylation on Y705 during earlier stages of differentiation. At day 60, we instead see lower levels of Y705 p-STAT3, although once adjusted for by normalisation to β -actin, this difference is

minimal and did not reach significance. Based on previous data shown in chapter 3, this might suggest that cytokines such as IL-6 are reduced, although it is not clear why this would occur. Within TSC patient-derived brain tumours, transcriptomic data shows no significant change in IL-6 mRNA in either SEN/SEGAs or cortical tubers ($p = 0.424$ and 0.889 respectively), so it appears that IL-6 is not as significantly dysregulated in TSC patient-derived brain tumours as in their non-neuronal counterparts. STAT3, however, is significantly upregulated by 3-fold and 1.8-fold in SEN/SEGAs and Cortical Tubers, respectively. This is mirrored in our data wherein STAT3 total expression is nearly 2-fold higher in *TSC2*⁽⁻⁾ cells than wild-type. Phosphorylation on the serine 727 residue of STAT3 is upregulated by >4-fold in *TSC2*⁽⁻⁾ cells. This is unsurprising, as this serine phosphorylation site of STAT3 can be directly phosphorylated by mTORC1 (44). The relationship between the serine and tyrosine phosphorylation sites of STAT3 has been unclear, with both old and new studies determining that S727 phosphorylation exerted regulatory effects on Y705 phosphorylation (532,533). However, other studies have reported that S727 phosphorylation of STAT3 may work synergistically with Y705 phosphorylation for maximal STAT3 transcriptional activation (534,535). The role that S727 phosphorylation plays on overall STAT3 activity, particular with regards to Y705-phosphorylation, is likely cell type and context dependent. Overall, the function of S727 phosphorylation on STAT3 is relatively unclear compared to Y705 phosphorylation, but it is believed to play a role in mitochondrial function (536), and otherwise has oncogenic effects (82).

The high S727-phosphorylation of STAT3 in day 60 *TSC2*-deficient neurons may therefore be exerting regulatory effects on Y705 phosphorylation in a manner which is not recapitulated in the other *TSC2*-deficient models shown in earlier data. Alternatively, cytokine production may not be as severe in *TSC2*-deficient brain cells as in the other models and therefore less capable of overriding S727-induced regulation on the STAT3 tyrosine site. Cytokine production may also be more focused on the promotion of other pathways such as NF- κ B, rather than STAT3. However, total levels of STAT3 are elevated in *TSC2*-deficient cells, which as mentioned prior, may be able to drive pro-inflammatory action regardless of their phosphorylation status on Y705.

Lastly, we see that GFAP expression is upregulated by approximately 2-fold in *TSC2*-deficient cells. This fits with the earlier ideas presented, since GFAP may demonstrate the presence of either astrocytes or RGCs. To further explore these trends, *TSC1*-deficient neuronal samples at day 60 of differentiation were also analysed (Figure 5.9.3).

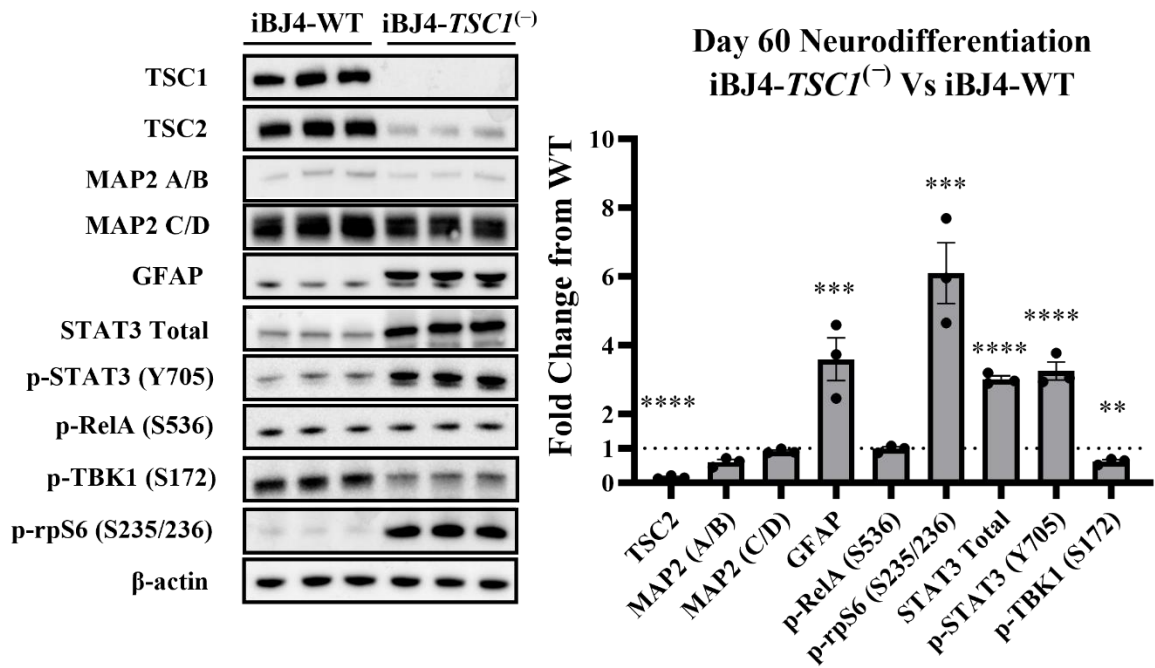


Figure 5.9.3. *TSC1*-deficient neurons exhibit enhanced STAT3 signalling at day 60. Western blots were performed on samples collected at day 60 of differentiation, comparing wild-type cells and *TSC1*⁽⁻⁾ cells. A corresponding densitometry analysis is included. *n* = 3, multiple t-tests. Data normalised to β-actin expression and fold changes from iBJ4-WT samples are shown.

Aiming to validate previous data, *TSC1*-deficient neurons at day 60 were also analysed. The results observed here are not fully congruent with those shown in Figure 5.9.2. Specifically, STAT3 signalling appears increased in *TSC1*-deficient neurons, whereas it is decreased in *TSC2*-deficient neurons. In both samples, however, GFAP is expressed at a higher level in *TSC1/TSC2*-deficient cells, signifying the previously discussed hypothesis of either a blockade within neurodifferentiation, or enhanced glial differentiation.

To further explore the data presented here, samples were also collected at day 70 of neurodifferentiation in *TSC2*-deficient neurons and probed for various targets (Figure 10).

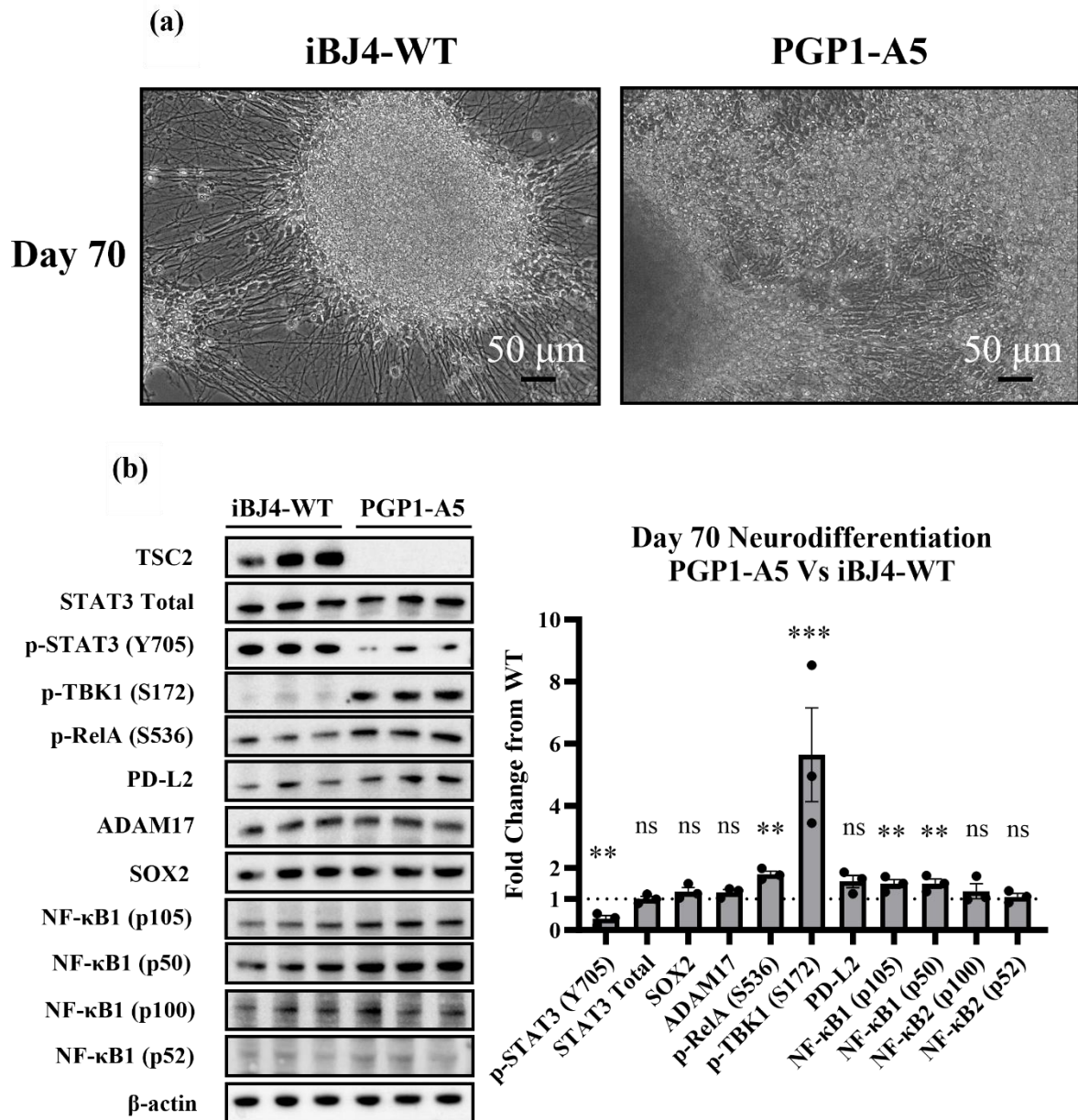


Figure 5.10. *TSC2*-deficient neurons exhibit enhanced NF-κB signalling and decreased STAT3 activity. (a) Images were taken at day 70 of neurodifferentiation, comparing wild-type cells and *TSC2*⁽⁻⁾ cells. As before, wild type cells demonstrate a clearer neuronal morphology, while *TSC2*⁽⁻⁾ cells were packed with cells. (b) Western blots were performed on samples collected at day 70, comparing wild-type cells and *TSC2*⁽⁻⁾ cells. A corresponding densitometry analysis is included, with protein expression normalised to β-actin. *n* = 3, multiple t-tests. Data normalised to β-actin expression and fold changes from iBJ4-WT samples are shown.

Previously it was observed that STAT3 phosphorylation on Y705 was slightly decreased in *TSC2*-deficient neural cells at day 60, compared to wild type, however we observed an

upregulation in total STAT3 protein. The difference is now far more pronounced, with STAT3 phosphorylation on Y705 being approximately 2.8-fold higher in wild-type cells than *TSC2*-deficient cells. Additionally, the slight upregulation in STAT3 protein which was previously observed in *TSC2*-deficient cells was not apparent, with equal STAT3 protein expressed across both cell lines. The meaning of this is unclear but suggests stark differences between the dysregulation of STAT3 between neural cells and the previously analysed *in vitro* AMLs and MEFs (and ELT3s). We previously proposed that STAT3 dysregulation could be driven through NF- κ B. It seems that this prior theory is inaccurate in the neural model since NF- κ B is upregulated, whereas STAT3 is downregulated. In the discussion of Figure 5.9 we discussed why STAT3 may be downregulated in this scenario, however the data here contradicts the data obtained by Blair *et al.*, (2018) (362), where they saw that STAT3 phosphorylation on Y705 was consistently higher in *TSC2*-deficient lines over the 5 timepoints sampled. Overall, the resolution in our study at earlier stages was much higher (with sampling every 10 days, rather than with 30-50 day interludes) and we could potentially attribute a difference in STAT3 phosphorylation between the two studies to this. For example, longer gaps between sampling time may have missed fluctuating STAT3 signals, and it may be possible that if allowed to continue growing our model would have once again shown high STAT3 phosphorylation on Y705, as in the earlier timepoints of day 0 to day 40. The neurodifferentiation models and protocols are not the same and could also be a cause of the differences in the data obtained. The issue of genetic lineage may also offer an explanation here, since the *TSC2*-deficient model is a different lineage of iPSCs than the wild-type cells. Therefore, results in this chapter cannot be taken with full confidence, however by usage of a *TSC1*-deficient model wherein the genetic lineage is matched between wild-type and *TSC1*-deficient cells, similar trends can be observed and taken with better credulity. Further confirmation of dysregulated NF- κ B activity can be seen by a roughly 1.5-fold increase in both the NF- κ B1 p105 precursor and the cleaved (active) p50 subunit. Conversely, the NF- κ B2 proteins, p100 and p52, are not dysregulated within *TSC2*-deficient neurons. This provides evidence that *TSC2*-deficient NF- κ B signalling typically occurs through the canonical NF- κ B pathway rather than the non-canonical pathway. Due to a lack of a transcriptional activation domain, p50 homodimers could repress NF- κ B activity by competing with other NF- κ B dimers for κ B promoter sites, meaning that p50 can act as a tumour suppressor (537). However, the high abundance of p-RelA probably means that pro-inflammatory effects through canonical NF- κ B signalling are more prevalent.

SOX2 was upregulated by approximately 1.2-fold in *TSC2*-deficient cells, but this did not reach significance. A lack of enhanced SOX2 expression but enhanced GFAP (at day 60) suggests an increased presence of astrocytes. This would also be supported by fluorescence imaging as demonstrated in Figure 5.6. However, astrocyte markers are not necessarily upregulated within TSC patient-derived SEN/SEGAs (Table 5.2), while cortical tubers do seem to express higher astrocyte markers (with low significance). This suggests discrepancy between the *in vitro* model and the *in vivo* brain tumours. While it is still likely true that *TSC2* inactivation is resulting in a blockade during the differentiation process, it may also seem apparent that astrocytes are then a final point of termination of the differentiation process. More analysis would be needed to confirm this, but due to an inferred overall lower astrocyte abundance in SEN/SEGAs, our *in vitro* model may be a closer approximation of cortical tubers in terms of cell types and therefore neuropathology.

Of note here are the differences in inflammatory signalling mechanisms between *TSC1* and *TSC2*-deficient neurons. As previously stated, the lack of a true control within *TSC2*-deficient neurodifferentiation experiments means that results may be difficult to validate. However, the results seem to indicate that inflammation within *TSC1*-deficient neurons is linked more closely to STAT3 signalling, whereas *TSC2*-deficient neurons is more dependent on NF- κ B signalling. Despite this, both models presented some similar trends. Both *TSC1* and *TSC2*-deficient cells appear to show delays in the neurodevelopmental process, and both appear to lead to a dysregulated generation of GFAP-expressing cells.

Despite the confusing nature of STAT3 activity in *TSC2*-deficient neural cells, the dysregulation of NF- κ B provides a more consistent story with regards to the data in Chapter 3. Firstly, significant upregulation of RelA phosphorylation on serine 536. Secondly, a stark upregulation in TBK1 phosphorylation on serine 172 was observed. As described in prior chapters, this signifies activation of the cGAS/STING pathway, which may be responsible for the activation of NF- κ B through RelA. However, this is contrasted in Figure 5.9.3 where TBK1 phosphorylation was greater in wild-type cells than *TSC1*-deficient cells. Lastly, while PD-L2 upregulation did not reach significance through a t-test, PD-L2 was upregulated by roughly 1.5-fold in *TSC2*-deficient cells. It is possible that PD-L2 is increased through NF- κ B since PD-L2 could be reduced through NF- κ B inhibition in previous experiments. PD-L2 is also highly upregulated in TSC patient-derived SEN/SEGAs and cortical tubers (3.9-fold and 2.4-fold respectively). With this as a basis, we can look to pathway inhibitors as performed in

previous chapters with the goal of reducing dysregulated signalling in *TSC2*-deficient brain cells.

5.3.4 IKK and mTORC1 inhibition in *TSC2*⁽⁻⁾ neural cells

PGP1-A5 cells were treated at day 68 of neurodifferentiation with either BMS345541 10 μ M or rapamycin 50nM and lysed on day 70 in sample buffer (48 h treatment). These samples were then probed for inflammatory pathway activation (Figure 5.11).

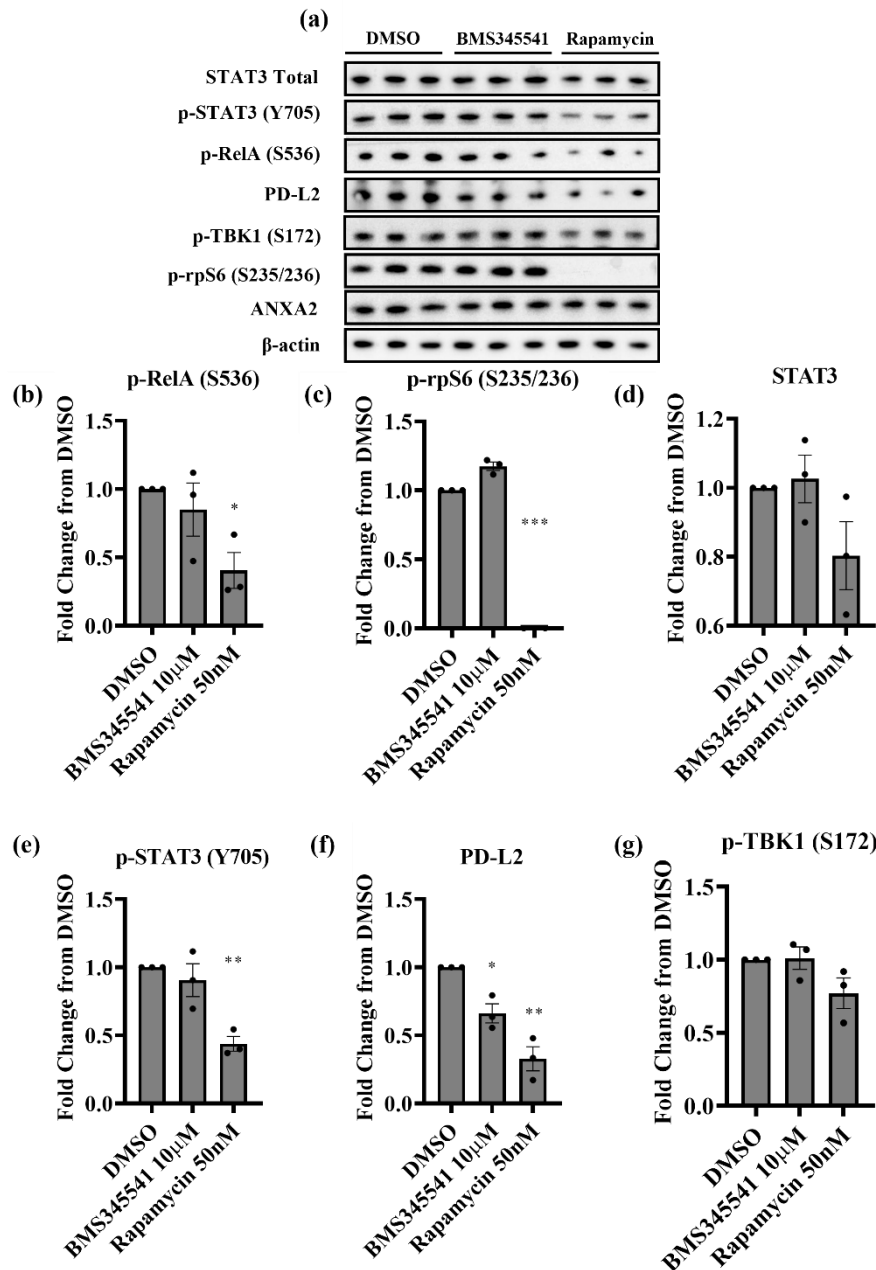


Figure 5.11. IKK or mTORC1 inhibition can reduce some inflammatory signalling in *TSC2*-deficient PGP1-A5 cells. (a) PGP1-A5 neuronal cells were treated at day 68 with either 48 h BMS345541 10 μ M or rapamycin 50 nM, prior to lysis and Western Blot. Corresponding densitometry analysis was

performed on (b) p-RelA (S536), (c) p-rpS6 (S235/236), (d) STAT3, (e) p-STAT3 (Y705), (f) PD-L2, and (g) p-TBK1 (S172) $n = 3$, one-way ANOVA with Dunnett's multiple comparisons. Data normalised to β -actin expression and fold changes of signal intensity from DMSO are shown.

Inhibition of IKK or mTORC1 in day 70 neurons of *TSC2*-deficient cells show perplexing results. IKK inhibition had minimal inhibitory capacity on the targets assayed; while some targets did appear to be reduced, these typically did not reach significance. This likely correlates with an apparent failure to inhibit NF- κ B pathway activation (marked by RelA phosphorylation). Due to time constraints, optimisation of inhibitor dosage was not possible in the neural model, so the highest prior used concentration of BMS345541 was used for this experiment (10 μ M). It is possible that this dosage was not suitable due to either cell type or cell density. It should be noted that neurons tend to form in large three-dimensional neuronal clusters, shown best in figure 5.4.4b. These may provide an insulating effect for *in vitro* drug inhibition. Typically, the concentration of rapamycin used (50 nM) is able to mostly inhibit mTORC1 signalling *in vitro* (as shown by a lack of detected rpS6 phosphorylation), so this comparatively high dose was able to produce more substantial effects.

It is possible that the lack of inhibitory effect by BMS345541 on STAT3 is due to the low basal expression of STAT3 in *TSC2*-deficient neurons anyway. Furthermore, there is likely a lack of direct control over STAT3 activity by NF- κ B in the neural model. As demonstrated in prior data using this model, STAT3 phosphorylation on tyrosine 705 is downregulated when compared to wild type. Conversely, NF- κ B signalling is upregulated and does not appear to be driving STAT3 activity in these cells. Therefore, it is not entirely surprising that IKK inhibition with BMS345541 does not alter STAT3 activity. Strangely, mTORC1 inhibition was able to reduce both RelA phosphorylation and STAT3 phosphorylation on both the S536 and Y705 sites, respectively. In Chapter 3, we demonstrated that mTORC1 inhibition was not capable of reducing RelA or STAT3 phosphorylation in *TSC2*⁽⁻⁾ cells. This further demonstrates differences between an *in vitro* neural model when compared to an *in vitro* kidney model of TSC, and further suggests the issues of using a singular model for research of the pathology of TSC.

This may link to the state of TBK1 phosphorylation. As previously demonstrated, TBK1 phosphorylation on serine 176 is highly upregulated in both *TSC2*-deficient AMLs and neural cells, as shown in Chapter 3 and this chapter (Figure 10) respectively. However, pTBK1 is significantly more upregulated in neural cells than the previously assayed AMLs. This is possibly due to metabolic differences between the cells. *TSC2*-deficient cells are most likely

suppressing mitophagy via mTORC1 hyperactivation, leading to a build-up of dysfunctional, “leaky” mitochondria. These release ROS as well as mtDNA which is likely stimulating the cGAS/STING pathway and driving pTBK1 phosphorylation, which in turn stimulates the NF- κ B pathway. Neurons are non-mitotic cells, meaning that there is a comparatively small turnover of cells in neural cultures (excluding non-neuronal, poorly differentiated cells). They are also highly energy-dependent cells, and typically contain a far larger number of mitochondria than other cell types (538). In the current hypothesis, this means that we are likely to have a more pronounced build-up of *TSC2*-deficient cells with even more faulty mitochondria. This hypothesis may be partially confirmed by the increase in TBK1 phosphorylation at day 30 of neurodifferentiation (Figure 5.1, $n = 1$)), when neurons are beginning to arise in the cell population. Therefore, we hypothesise that this may explain the comparative difference in TBK1 activation. In turn, this may explain why mTORC1 inhibition shows a more pronounced effect on NF- κ B activation in neural cells than in AMLs. mTORC1 inhibition may be capable of removing the blockade on mitophagy and lead to mitochondrial recycling, therefore removing this inflammatory process. This may also have been altered by longer treatment duration in neural samples (48 h) versus the treatments in AMLs in Chapter 3 (24 h), wherein more time was permitted for mitochondrial turnover. Phosphorylation of TBK1 was reduced slightly (Figure 5.11g) by mTORC1 inhibition. This did not quite reach significance via one-way ANOVA ($p = 0.08$), but with more repeats or a longer treatment duration, this effect may become statistically significant.

Notably, both IKK and mTORC1 inhibition were able to reduce levels of PD-L2, which we previously identified as being dysregulated in our datasets.

Overall, this data shows potential benefit of both treatments in reducing the pathology of TSC. The difference in the effect of mTORC1 inhibition at reducing these molecular phenotypes in neural cells compared to *in vitro* AMLs is interesting and highlights a key difference between the models. This must be investigated further, specifically with regards to NF- κ B hyperactivation and pTBK1 activation. It would also benefit to assay combinatorial approaches of these drugs.

5.3.6 Diacerein in *TSC2*⁽⁻⁾ neural cells

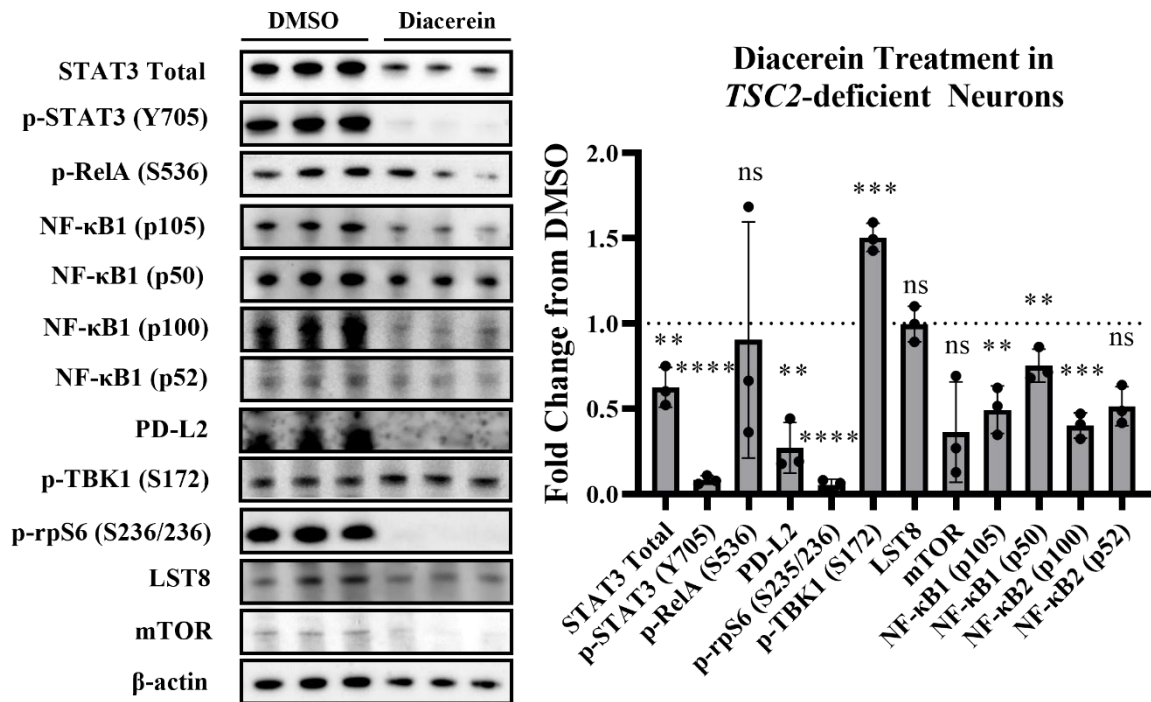


Figure 5.12. Diacerein is highly effective at inhibiting mTORC1 and STAT3 activity in *TSC2*-deficient cells. *TSC2*⁽⁻⁾ PGP1-A5 cells were treated at day 68 with DCN 50 μ M for a total of 48 h, with lysis on day 70. Lysates were then probed for various biomarkers. Western blots are shown alongside representative pixel densitometry. The contrast for mTOR was adjusted for visualisation in the blot panel to better demonstrate difference in expression, but densitometry was performed on the original, unedited image. Data normalised to β -actin expression and fold changes of signal intensity from DMSO are shown.

Treatment with DCN yielded positive results in *TSC2*-deficient cells. As previously shown in other cell lines, DCN is highly effective at suppressing STAT3 activity. Notably, we did not identify high STAT3 activity in neural samples, but this is not entirely consistent with other studies such as Blair *et al* (2018). Therefore, we may suggest that STAT3 inhibitory potential is still a relevant factor to consider in drug targeting of TSC. As identified in previous results, the inhibitory effect of DCN on RelA phosphorylation appears inconsistent, suggesting that IL-1 β signalling may not be primarily driving RelA phosphorylation. However, DCN was able to reduce NF- κ B1 p50, likely through reduction of the NF- κ B1 p105 precursor. This could reduce the formation of p-RelA/p50 heterodimers and thus possibly reduce NF- κ B transcriptional activity. While non-canonical NF- κ B activity has not been observed as upregulated (marked by relative protein levels of p100/p52) in *TSC2*-deficient neurons, DCN also reduced NF- κ B2 p100 significantly. DCN also reduced p52, but this did not reach

statistical significance. Alternatively, DCN may be exerting anti-inflammatory effects through other unidentified pathways.

The effect of DCN on PD-L2 expression was more pronounced, with a significant reduction in PD-L2 expression in neurons. Since this reduction does not appear to be reduced alongside NF- κ B activity, it suggests that PD-L2 is regulated through non-NF- κ B-dependent mechanisms. Potentially this is through STAT3 activity, although if this were the case, we would expect to see STAT3 hyperactivity in the assayed neural samples at day 70. The overall mechanism is unclear, but DCN appears potent for reducing this immune-evading protein.

Lastly, and perhaps most surprisingly, DCN potently reduced phosphorylation of rpS6, suggesting a reduction in mTORC1 activity is achieved via suppression of inflammatory pathways. This is unexpected, since mTORC1 activity should be constitutive through the loss of *TSC2*. This result possibly comes from a downregulation of the expression of mTOR, the catalytic core factor of mTORC1. This may suggest that DCN is downregulating mTORC1 activity by reducing expression of the core components of mTORC1. As shown above, DCN has a highly potent capacity for reducing STAT3 phosphorylation on Y705. Unpublished data from within the lab has shown that inhibition of STAT3 can downregulate subunits of mTORC1 at the level of gene expression, and increase levels of DEPTOR, and this may further elaborate on how DCN might reduce mTORC1 activity. However, DCN increased phosphorylation of TBK1 on the serine-172 site. This further complicates the relationship between mTORC1, NF- κ B, and cGAS/STING signalling in TSC. The previous hypothesis was that sustained mTORC1 signalling leads to a build-up of dysfunctional mitochondria due to a reduction in mitophagy, and this results ultimately in TBK1 phosphorylation. However, as DCN potently reduces mTORC1 activity, we would assume that through the described process that TBK1 phosphorylation would reduce. Via direct inhibition of IL-1 β signalling, we would also expect DCN to lower NF- κ B activity. However, this was only partially observed. This suggests further complexity to the pathways which needs further exploration. Exploration of more specific IL-1 β inhibitors would be required to further investigate the role of IL-1 β signalling in TSC.

Notably the metabolite of DCN, Rhein, also has neuroprotective effects (539). Despite being apparently able to reduce neuroinflammation, Rhein is not believed to cross the BBB, although has been detected following traumatic brain injury (540). Arguably, if the blood brain barrier is compromised in TSC, this may result in uptake of the drug to the brain. There

is credible belief that due to the connection between mTOR activity and angiogenic dysregulation, the BBB in TSC patients may be compromised (541). This could be an exploitable feature for usage of drugs such as DCN which are not typically thought to permeate the BBB.

5.4 Conclusion

This chapter demonstrated the development of a novel *TSC2*-deficient iPSC model that was used to explore neurodevelopment in the context of TSC. Notably, we show delayed neural development and dysregulated (and fluctuating) inflammatory signalling. While it was not possible to precisely confirm what cell populations were formed after loss of *TSC2* in neural development, our data seemed to complement other studies showing that neurodifferentiation was also delayed at early stages. *TSC2*-deficient cells appear to remain as proliferating RGCs for a longer duration before committing to terminal differentiation into either astrocytes or neurons. It was possible that oligodendrocytes were also formed, but these were not tested for within this study. A dramatic upregulation of TBK1 and RelA phosphorylation on serine 172 and serine 536, respectively, was observed in later stages of neurodifferentiation. In patients, this would likely result in the recruitment of immune cells to the lesions. Possibly, these events would contribute to TANDs such as epilepsy. Lastly, the potential applicability of IL-1 β inhibition with the rheumatoid arthritis drug, DCN, was identified. DCN was able to ablate PD-L2 expression, as well as drastically reduce rpS6 phosphorylation. DCN also strikingly blocked STAT3 phosphorylation. The applicability of DCN to reduce STAT3 activation could be considered as highly relevant for TSC-derived brain tumours and TANDs. However, it should be noted that it is not possible to confirm if the effects seen by DCN treatment are due to inhibition of IL-1 β signalling or IL-6 signalling, and further investigation with specific IL-1 β inhibitors should be considered. We did not observe an increase in the phosphorylation of STAT3 in *TSC2*-deficient neurons compared to control. This may be due to the limitation in the time-points used for analysis, or other confounding factors. Other related studies did observe STAT3 activation during neurodifferentiation for *TSC2*-deficient cells compared to control cells, notably Blair *et al.* (2018). However, even with these differences, the *TSC2*-deficient iPSC model used in this study had a higher basal level of some inflammatory signals, which is consistent with the pathology of TSC.

The data in this chapter is somewhat limited due to a lack of true wild-type control for comparison to *TSC2*-deficient iPSCs. However, comparisons to *TSC1*-deficient neurodifferentiation studies which possess suitable wild-type controls show similar trends. This provides some level of verification of the suitability of the used *TSC2*⁽⁻⁾ PGP1-A5 clone. The data here is also limited in the sense that samples at day 60-70 were intended to represent a final developmental stage of TSC-derived brain tumours. It should be noted that many aspects of the tumour microenvironment cannot be truly reproduced in an *in vitro* culture setting. These cell models lack the appropriate interactions with the immune system and dysregulated vascularisation which occurs in TSC. New studies may be able to recapitulate this further with three-dimensional organoid or assembloid cultures. Additionally, longer culture times, and perhaps a higher resolution in sample collection times, would have been preferential. However, these features were not possible due to time constraints.

Chapter 6 – Discussion

This project aimed to investigate inflammatory processes in *TSC2*-deficient cells.

Inflammatory signalling was examined within various pre-existing *in vitro* cell line models of TSC (MEF, AML, and ELT3 cells). By exploring inflammation, the project hoped to identify the origination of the inflammatory signature that is apparent in *TSC2*-deficient cells and delineate how this may arise from hyperactive mTORC1 signalling. The project also aimed to develop a *TSC2*-deficient iPSC model for the investigation of neural development in TSC, and the prevalence of inflammatory pathways within TSC-derived brain tumours. By using transcriptomic data obtained from TSC patient-derived brain tumours, the study also aimed to investigate the applicability of *in vitro* cell line model systems to better interpret *in vivo* TSC-derived tumours. By identifying inflammatory pathways in TSC, the project aimed to identify novel treatment options that would target dysregulated inflammatory pathways. Lastly, the presence of inflammatory signalling within TSC was to be analysed within the context of neural development. This data would be used to suggest how TSC-driven inflammation contributes to the development of TANDs.

Neuroinflammation is linked to a variety of neuropsychiatric disorders, both within and outside of the context of TANDs. For example, neuroinflammation has been characterised within psychiatric disorders such as schizophrenia and depression (542,543). A review by Matta *et al.* also highlights the prevalence of neuroinflammation within autism spectrum disorder (544), while a review by Aronica & Crino categorises the dominant role of neuroinflammation within epilepsy (545). Autism is rarely identified as the direct result of a known genetic cause, with TSC being one of these rare cases. Therefore, the known genetic causation of TSC as a disease and being able to identify its neuroinflammatory phenotype may offer drastic insights into the development of such neurological disorders. Furthermore, autism and epilepsy within TSC are intrinsically linked wherein the severity of epilepsy increases in the presence of autism (546), meaning that the research of one neurological condition within TSC may provide additional insights on the other. Since this heightened inflammatory phenotype is observed *in vitro* (through elevation of several biomarkers including STAT3 and NF- κ B activation) and *in vivo*, we could assume that inflammation may be contributing to the neurological disease state of TSC. Consequently, neuroinflammation is likely a key factor in TSC that is linked to autism and epilepsy. This sentiment has previously been suggested by others (333).

A dysregulated inflammatory phenotype was observed across all cell line models of TSC. Within these models, variation in the inflammatory signatures was apparent at both the transcriptomic and protein expression level. Non neuronal *in vitro* cell models demonstrated an upregulation in NF- κ B and STAT3 signalling. The *TSC2*-deficient neuronal cells exhibited high NF- κ B and low STAT3 activity, while *TSC1*-deficient neuronal cells demonstrated high STAT3 and low NF- κ B activity. Part of this study aimed to use a multitude of models to explore whether non-neuronal *in vitro* models were an appropriate model to study inflammation in the context of TSC, and whether this reflected the state of inflammation found within TSC patient-derived brain tumours. The transcriptomic analysis of TSC patient-derived brain tumours donated by Jeffrey Mackeigan proved invaluable for this study. The RNA sequencing data from *TSC2*-deficient AMLs allowed for a comparison between TSC patient-derived brain tumours and AML cell lines. It was found that many of the dysregulated genes associated with inflammatory/immune signalling were consistent between these transcriptomic data sets. For example, both *in vitro* AML cells and *in vivo* TSC-derived brain tumours showed a high upregulation in immune checkpoint regulators such as *PDCD1LG2*. Additionally, NF- κ B signalling appears dysregulated within both *TSC2*-deficient AML cells and TSC patient-derived brain tumours. This is matched within the *TSC2*-deficient neuronal model, but not the *TSC1*-deficient neuronal model. It is possible that this demonstrates a reason for the difference in severity between *TSC1* and *TSC2* mutations found in TSC patients; mutations in *TSC1* typically present with milder features associated with TSC disease. It is possible that *TSC2* mutations may present a more severe disease state due to dysregulated NF- κ B activity which is otherwise not present within *TSC1*-mutated cells. Within Chapters 3 and 4, a presumed feature of TSC was that upregulated STAT3 activity within TSC is dependent on upregulated NF- κ B activity. This was because both pathways seemed hyperactive in *TSC2*-deficient AML cells and *Tsc2*-deficient MEFs, and inhibition of IKK could reduce the heightened level of STAT3 activity. Data produced within the *TSC2*-deficient neuronal model seemed to contradict this. *TSC2*-deficient neurons exhibited high levels of NF- κ B activity and low levels of STAT3 (at the day 70 timepoint). Inhibition of IKK with BMS345541 seemed ineffective (possibly due to an insufficient concentration of the drug, so NF- κ B pathway inhibition was incomplete), but mTORC1 inhibition with rapamycin was effective at reducing phosphorylation of both RelA and STAT3. Even if the results of IKK inhibition within this setting are to be discounted, these results contradict those seen in *TSC2*-deficient AMLs. Results in AMLs seemed to suggest that inflammatory pathway activation was relatively independent of mTORC1 activity; mTORC1 inhibition was

generally insufficient for suppressing STAT3 or NF- κ B activity in AML cells. Overall, these patterns may suggest that STAT3 activity in TSC can be, but is not explicitly, driven by NF- κ B activity.

As described earlier, neuronal cells (due to their non-dividing nature) may demonstrate more mitochondrial build-up and therefore have a greater level of cGAS/STING pathway activation. This could be represented via the difference in fold change of TBK1 phosphorylation between *TSC2*-deficient and *TSC2*-restored AMLs, versus PGP1-A5 vs iBJ4-WT cells (2-fold vs 6-fold, respectively). NF- κ B may have an increased reliance on the cGAS/STING pathway within neural cells, and this may demonstrate why rapamycin appears marginally more effective at reducing inflammatory signalling in neuronal lines. This is only the case if we suppose that rapamycin may exert some degree of anti-inflammatory action by reactivation of mitophagy. However, the reduction in NF- κ B activity of day 70 in the *TSC2*-deficient neurons after treatment with rapamycin was marginal and did not reach statistical significance. It may be possible that longer treatment durations with rapamycin would have made this effect more pronounced.

The cGAS/STING/TBK1 pathway may offer explanation for the origination of inflammation in *TSC2*-deficient cells. However, it is clear that other inflammatory signalling mechanisms must play a role. This is demonstrated by the influence of *TSC2*-deficient cell-conditioned media on *TSC2*-expressing cells, wherein conditioned media of *TSC2*-deficient cells potently stimulates STAT3 activity. Notably, these experiments did not demonstrate an increase in RelA phosphorylation at the short timeframes used. Overall, the experiments with conditioned media from *TSC2*-deficient cells reveal that cytokines are likely propagating autocrine pro-inflammatory signalling in TSC. These autocrine mechanisms preferentially stimulate STAT3 (and probably other pathways), but not NF- κ B, signifying that NF- κ B hyperactivation may be coming from internal processes within the cell. By exploring this further, IL-6 secretion was found to be highly upregulated within *TSC2*-deficient AMLs, and this could be reduced by inhibition of IKK. Conversely, rapamycin treatment enhanced the levels of secreted IL-6. This data shows that IL-6 secretion is dependent on the NF- κ B pathway that then leads to STAT3 phosphorylation (likely via IL6 receptors and the JAK2/STAT3 pathway). Interestingly, rapamycin could markedly enhance the induction of IL-6 secretion after TNF α stimulation. Therefore, this study hypothesised that the inflammatory mechanisms observed in TSC may arise from inflammatory cytokines/chemokines resultant of NF- κ B hyperactivation, and these can then positively

influence additional inflammatory pathways. If IL-6 is taken as a broad indicator of the production of other NF- κ B-induced cytokines, it is possible that NF- κ B pathway inhibition could be sufficient to reduce inflammation, by attenuating cytokine production. Within brain tumours, cytokines and chemokines would serve as attractants and activators of immune cells, whilst also stimulating resident neurons. Immune infiltration to brain tumours is likely to contribute to the development of epilepsy due to even further cytokine release by active immune cells, such as IL-1 β , CXCL8, and TNF α (211). It should be noted that the TSC patient-derived brain tumour transcriptome data demonstrated a significant upregulation of *IL1B* and *TNF* (and also *CXCL8*, though not to statistical significance). Upregulation was also observed within cortical tubers, although were not statistically significant. Combined with gene ontology analysis, this data indicates that TSC-derived tumours have an increase of immune invasion. IL-1 β released from tumour-invading microglia may contribute to the enhanced excitability of neurons and would worsen seizures (547). In this context, immune infiltration may contribute to epilepsy in TSC. IL-6 is implicated within inflammation in TSC and is likely a contributing factor (434). An observation made within this study demonstrated that *IL6* was not significantly dysregulated within TSC-derived brain tumours. While this study did attempt to investigate IL-6 within *TSC2*-deficient neuronal cells, a direct comparison between *TSC2*-deficient and *TSC2*-expressing neurons was limited; the conditioned media samples collected did not demonstrate a high enough level of IL-6 for detection (data not shown), and time limits made repeats of this experiment not possible. When conditioned media was loaded at a much higher volume within ELISA experiments to investigate drug treatments in *TSC2*-deficient cells, IL-6 could be detected. While a direct comparison was not made between *in vitro* AML and *in vitro* neurons, the study seemed to suggest overall that IL-6 signalling may be less relevant within TSC-derived brain tumours than other TSC-associated tumours. It is possible that immune invasion to TSC-derived brain tumours may be the primary originators of IL-6, rather than the *TSC2*-deficient neurons and glia specifically. Alternative cytokines such as IL-1 β and TNF α may play a more significant role in the disease state, and further investigation into these may provide insight into new therapies.

Previous studies have investigated inflammation in TSC, and enhanced inflammatory signalling is often linked to epilepsy in TSC. Highly sophisticated organoid models of brain and kidney tumours have been used to investigate TSC, however these do not tend to investigate inflammatory pathways (548). A detailed statistical analysis of the SEN/SEGA and

cortical tuber datasets used within this study also identified a high inflammatory/immune signature in TSC, but did not go into the specific details of inflammatory pathways (51). Astrocyte-localised IL-1 β has been shown to play a role in the downstream generation of various cytokines, and inhibition of IL-1 β and CXCL10 has reduced seizure frequency in mouse TSC models (333). Notably, mTOR inhibition has been shown to enhance NF- κ B activity and reduce STAT3 activity (in immune cells when subject to inflammatory stimuli), suggesting that the current mTOR inhibitors may have a partially pro-inflammatory effect (49). With this information, alongside data presented in this study, it could be hypothesised that conventional mTORC1 inhibition is worsening the inflammatory state of TSC through NF- κ B. This could be attributed to TSC-associated conditions such as treatment-resistant epilepsy. FPR2, which is believed to dampen inflammatory and immune responses within neuroinflammation, is downregulated in TSC (549), and the expression of FPR2 is inversely correlated with NF- κ B activity. NF- κ B activity in TSC also seems highly context dependent, wherein the impact of *TSC2* loss (or presence) is dependent on Akt/PTEN or mTORC1 activity (48). These studies appear to present the limit of NF- κ B associated neuroinflammation in TSC. There is a high body of research detailing the role of NF- κ B in the development of epilepsy. The inhibition of NF- κ B associated cytokines such as TNF α and IL-1 β has proved effective at reducing epilepsy (550,551), although this is not in the context of TSC. The role of *TSC2* mutation in the development of TANDs is still not fully understood. Identifying TSC and TANDs through a neuroinflammatory lens may allow us to research treatments more effectively for the disease state, and hopefully reduce the neuropsychiatric burden on TSC patients as well as the development/re-emergence of tumours.

This study aimed to elaborate on the prevalence of neuroinflammation in TSC, and link neuroinflammation-associated TANDs to the dysregulation of NF- κ B signalling. A key component of this was to observe the state of STAT3 and NF- κ B throughout differentiation. Like Blair *et al.* (2018) (362), STAT3 activation seemed to increase drastically within the middle stages of neurodifferentiation within the data presented in this study. Strangely, STAT3 activity dropped in later sample collection times, but this may have been due to a flaw in the study design; *TSC2*-deficient iPSCs lacked a true wild-type control. Following a cell culture contamination, PGP1 wild-type cells were unable to be thawed, meaning that the PGP1-A5 *TSC2*-deficient clone was differentiated alongside iBJ4 wild-type iPSC cells. The difference in genetic background between these cells could present with different

neurodifferentiation and cell-signalling outcomes. To our knowledge, the state of NF- κ B signalling has not been observed within *TSC2*-deficient iPS cells throughout differentiation, so the study is unique in this regard. While NF- κ B appeared to fluctuate throughout the earlier stages of differentiation, by later stages the NF- κ B pathway was significantly upregulated. The heightened level of NF- κ B signalling could be linked to the development of epilepsy in TSC. As well as increased RelA phosphorylation, *TSC2*-deficient neurons also demonstrated an upregulation in NF- κ B1, in both the precursor (p105) and active (p50) forms, but not NF- κ B2. While RelB phosphorylation could not be probed for in this study, NF- κ B2 expression was upregulated in *TSC2*-deficient AMLs, but not NF- κ B1. IKK inhibition was unsuccessful with a standardly used concentration BMS345541 in the *TSC2*-deficient neuronal cells. This limits the conclusions that can be drawn this study regarding the involvement of NF- κ B. However, usage of non-neuronal *in vitro* models showed that IKK inhibition was effective at reducing the expression of STAT3 and PD-L2. mTORC1 inhibition was also able to inhibit these targets in neuronal cells, but less so within non-neuronal models. mTORC1 inhibition was also able to reduce RelA phosphorylation in neuronal cells. This may allow us to tentatively suggest that 1) NF- κ B activity in TSC is driven by different pathways depending on the cellular context, and 2) NF- κ B inhibition through mTORC1 inhibition may be partially responsible for the reduction in dysregulated markers such as PD-L2 in neuronal cells. Further testing of this could involve a transcriptomic analysis to determine differences in gene regulation upon NF- κ B inhibition between different cell types.

NF- κ B is notoriously difficult to inhibit pharmacologically within cancer cells. A review by Wang *et al.*, outlines some of these reasons (552). In brief, NF- κ B signalling is highly complex, and can be stimulated through a variety of inputs. While the canonical and non-canonical pathways are key drivers of NF- κ B activity, crosstalk with other pathways such as mTORC1 can also induce NF- κ B. NF- κ B signalling is the result of multiple steps, including nuclear shuttling, appropriate post-translational modifications (i.e., phosphorylation), and dimer formation. The complex nature of NF- κ B activation and a lack of appropriate biomarkers to determine the activity status of NF- κ B makes it difficult to gauge whether drug inhibitors are working effectively or not. Furthermore, as NF- κ B activity is so ubiquitously expressed, inhibition of NF- κ B can be accompanied with various side effects. As also mentioned prior, the role that RelA S536 phosphorylation may be contentious (485). Despite this, many therapies have been shown to reduce NF- κ B activity. Many of these function by preventing the degradation of the inhibitor, I κ B α . Aspirin is a good example (467), where

aspirin possibly prevents I κ B α degradation via inhibition of the relevant kinase, IKK (553). This potentially links to the previously referenced clinical trial in the applicability of aspirin for managing TSC-associated seizures (NCT03356769). Many of the drugs selected earlier in this study sought to inhibit NF- κ B activity indirectly via inhibition of upstream signalling events (for example TNFR inhibition by R-7050, and TLR inhibition via Resatorvid), or by poorly characterised anti-inflammatory activity (such as SAHA). One interesting modality of NF- κ B inhibition has been previously explored in TSC. Bortezomib is typically believed to exert NF- κ B inhibition indirectly by inhibiting the proteasome, leading to the prevention of degradation, and subsequent accumulation of I κ B α (442). Bortezomib, when combined with nelfinavir, which is thought to enhance ER stress via proteasome inhibition (554), was shown to have potent cytotoxic effects on *Tsc2*-deficient rodent cells (357). The authors of this study attributed this effect to excessive ER stress; *Tsc2*-deficient cells have higher basal levels of ER stress due to high protein synthesis leading to an abundance of unfolded protein.

This study highlighted the potential benefit of adjunctive therapy. Anchorage-independent growth assays, used as a simple *in vitro* system to represent tumour growth, demonstrated that while IKK inhibition was effective at reducing spheroid formation, this anti-tumour effect was further amplified upon dual treatment with rapamycin. Colony regrowth was slowed and a reduction in overall colonies was reduced after dual treatment, when compared to monotherapy. This work demonstrates the therapeutic potential of NF- κ B inhibitors when combined with the classical treatment with mTORC1 inhibitors. Combined drug inhibition of mTORC1 and NF- κ B might be more cytotoxic, resulting in the tumours not regrowing after treatment ends. IKK inhibition broadly reduced other phenotypic aspects of *TSC2*-deficient cells, which included proliferation and migration. This is also represented in STAT3 activity, wherein combinatorial treatment was more effective at reducing Y705 STAT3-phosphorylation over longer time periods. Additionally, while IKK inhibition could reduce mRNA expression of some inflammatory targets such as *FNI* and *PDCDILG2*, it would increase the expression of others, such as *CD276*. Combinatorial treatment with rapamycin seemed to nullify this effect, preserving the inhibitory capacity of some targets whilst dampening the pro-inflammatory signalling which was elicited by IKK inhibition in others.

This study also highlighted the complex signalling interplay between NF- κ B, STAT3, and mTORC1. Perhaps most striking is the biphasic response of IKK inhibition on STAT3 activity. For instance, STAT3 phosphorylation rapidly increased upon IKK inhibition before

dampening down at later timepoints. This highlights the complex, multi-faceted connections between inflammatory dysregulation in TSC, and is also likely due to the poorly characterised action of unphosphorylated STAT3. An increase in unphosphorylated STAT3 may be leading to a surge in IL-6 expression (383), which then drives STAT3 phosphorylation on the tyrosine site (Figure 6.1). However, not all of the details are clear with regards to how this signalling interplay occurs precisely within the context of TSC. While this study has made headway on delineating these processes, the overall sentiment is that further research must be conducted in the complex inflammatory signalling interplay in TSC.

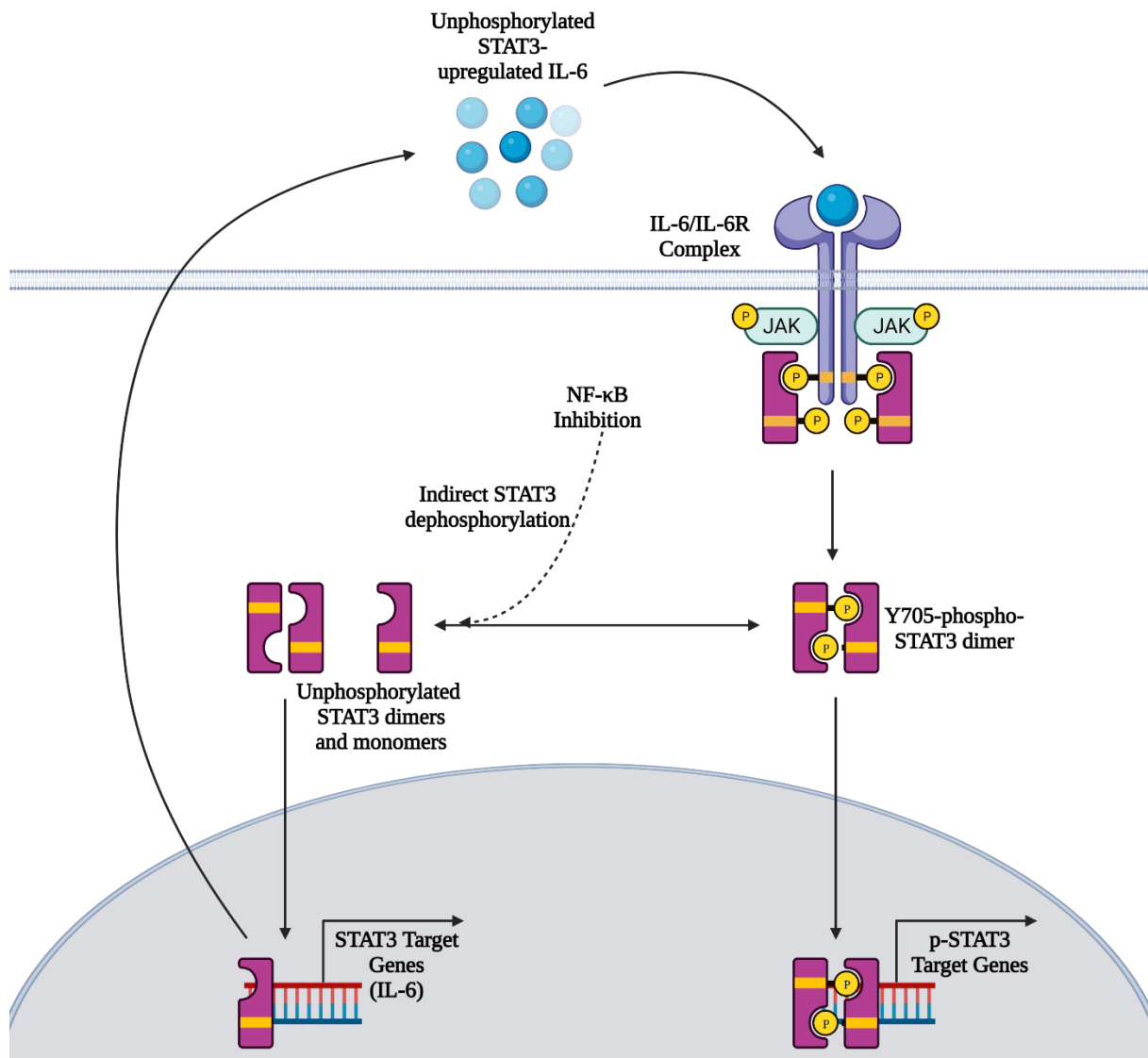


Figure 6.1. Indirect inhibition of phospho-STAT3 activity by NF-κB pathway inhibition leads to an increase in available unphosphorylated STAT3. Unphosphorylated STAT3 then upregulates IL-6, which in turn promotes STAT3 re-phosphorylation on Y705. Illustration produced in BioRender.

The cGAS/STING pathway has had little research in the context of TSC. Most related research has had varied conclusions, suggesting that cGAS/STING/TBK1 activation can both negatively or positively regulate mTORC1 (555,556), however no research appears to investigate the inverse. It is possible that in TSC, the cGAS/STING/TBK1 signalling pathway lies upstream of NF-κB activity. Here, the study reported heightened TBK1 activation in *TSC2*-deficient cells, and it is believed that this is at least partially responsible for the heightened activation of NF-κB. From this study, it is hypothesised that NF-κB contributes to the overall production of cytokines such as IL-6 that drives a positive inflammatory feedback loop. This is worsened *in vivo* with the recruitment of immune cells, particularly within brain tumours, which produce cytokines to prime neurons in a hyper-excitatory state, leading to

TANDs like epilepsy. Since epilepsy results in even further cytokine production, TANDs may result in a hyper inflammatory state that exacerbates the condition, suggesting why epilepsy in TSC is correlated with a worsening of the neuropsychiatric burden (557). Since TSC-associated epilepsy is among one of the leading causes of death and reduced quality of life in TSC patients, it is important to identify the causes and potential treatments to reduce epilepsy (111). This study does not present substantial proof that mTORC1 is a central driver of TBK1 activity but offers some insight. TBK1 activity could not be reduced significantly by mTORC1 inhibition over a 48 h treatment period, however this may be due to an insufficient duration of treatment. However, connecting the results presented herein with existing literature may make this claim more feasible. For instance, mTORC1 activity is known to regulate mitochondrial function (558) and mitophagy (559). This process is highly important for mitochondria in neurons, wherein mitochondria are continuously remodelled and recycled to prevent a build-up of ineffective, poorly functioning damaged mitochondria (560,561). In neurons, mitochondria are shuttled to remote axonal regions to provide ATP and assist in buffering calcium flux during synaptic transmission (562). Faulty mitochondria are known to leak cytosolic mtDNA which can stimulate the cGAS/STING pathway (418). The current literature generally links a TSC-implicated build-up of faulty mitochondria to TANDs like epilepsy due to increased cellular stress in excitatory neurons and astrocytes (563,564). Increased cellular stress from mitochondrial dysfunction also has links to a variety of neurodegenerative conditions such as Alzheimer's disease and Parkinson's disease (565). It is known that cGAS/STING activation can be derived from faulty mitochondria, but the neuroinflammatory implications of this signalling remain unexplored (555). Here, it could be suggested that an accumulation of faulty mitochondria is leading to an excess of cytosolic mitochondrial DNA. This is recognised within the cGAS/STING pathway, leading to TBK1 phosphorylation. p-TBK1 then activates NF- κ B, leading to inflammatory signals that worsen the development of TANDs. Seahorse XF was performed to try to analyse mitochondrial dysfunction, but ultimately proved unsuccessful, and would be a useful datapoint for future work. While not explored in this work, treatments to inhibit TBK1 activation may be beneficial in TSC. Amlexanox is a TBK1 inhibitor used for the relief of ulcers and other inflammatory conditions (566), and future research could explore the effect of amlexanox in TSC. Data on mitochondrial function in TSC is limited and with varied outcomes. One study identified higher extracellular acidification rates (ECAR) and lower oxygen consumption rates (OCR) in *TSC2*^(+/-) cells (567), and another demonstrated low OCR and high ECAR in LAM cells (568). Others have showed that *TSC2*-deficient cells present higher OCR and

ECAR (569,570). These differences may be due to the design of the study and cell type. If we speculate that high ECAR and low OCR levels are resultant of the presence of a build-up of faulty mitochondria, then this may be implicated in the stimulation of NF- κ B in TSC. Ultimately, a build-up of faulty mitochondria may be the event that kick starts the inflammatory positive feedback mechanisms which are hypothesised here. Once these mechanisms exist for a certain period (and are worsened by pro-inflammatory events such as seizures and immune infiltration), they may become independently functional of mTORC1 activity and thus not respond to traditional mTORC1 inhibition. It has been shown that long-term treatment of Everolimus has greater effects in the reduction of TSC-associated epilepsy, meaning that longer treatment durations could be more efficacious in the reduction of neuroinflammation (571). A speculative representative diagram of this proposed mechanism of inflammation is shown here (Figure 6.2)

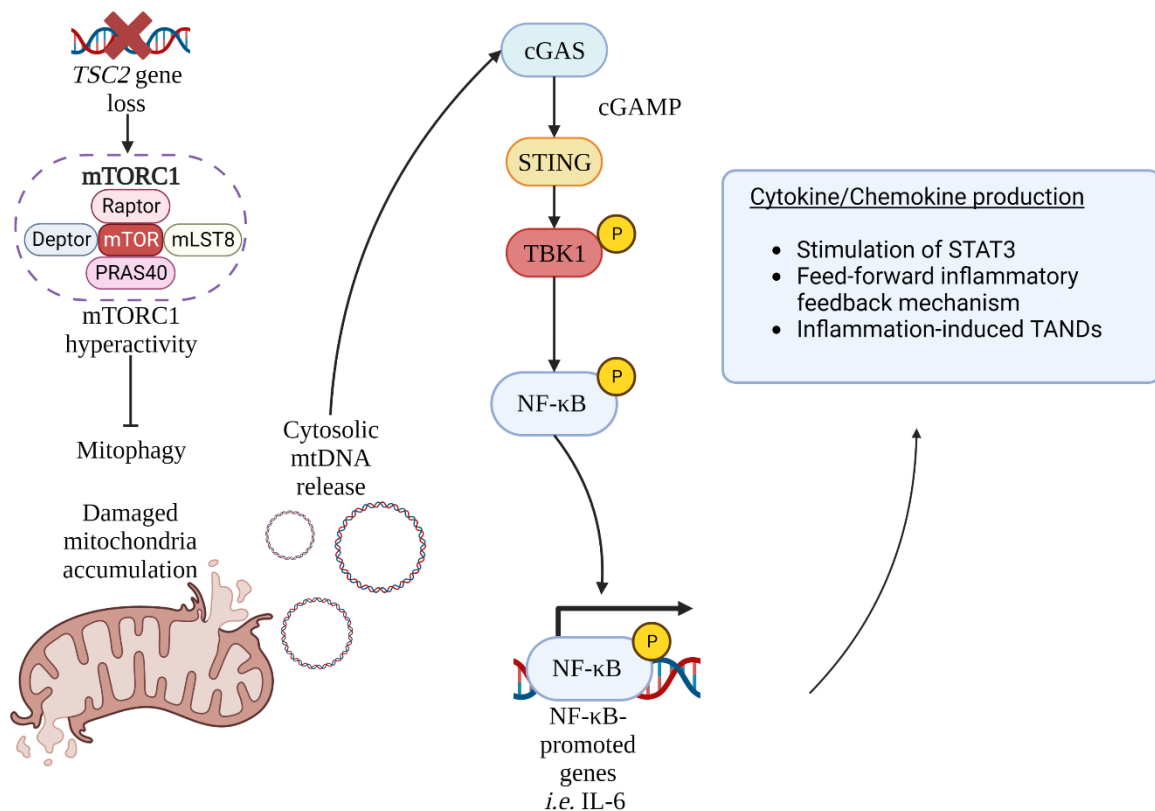


Figure 6.2. Proposed mechanism of the development of inflammation in *TSC2*-deficient cells. Loss of functional *TSC2* results in mTORC1 hyperactivation, which in turn leads to an inhibition of autophagy and mitophagy. This results in a build-up of faulty, damaged mitochondria. Damaged mitochondria release ROS and mtDNA to the cytoplasm, leading to cGAS/STING activation. TBK1 is phosphorylated through STING activation, resulting in NF- κ B activity which drives neuroinflammatory processes and TAND development. Illustration produced in BioRender.

A rheumatoid arthritis gene signature was identified in TSC patient derived tumours and cell line models, which lead to identifying IL-1 β as a potential drug target. To explore this further, *TSC2*-deficient cells were treated with DCN, an IL-1 β inhibitor that is used in the treatment of rheumatoid arthritis, and the effect of treatment was tested on the inflammatory pathways. DCN proved effective to reduce inflammatory signalling, although DCN did not show a significant reduction in RelA phosphorylation. However, other components of the NF- κ B pathway showed a trend in reduction, including NF- κ B1 and NF- κ B2. Importantly, DCN potently reduced STAT3 activation as well as mTORC1 activity. The reduction in mTORC1 activity was believed to be attributed to a reduction in the mTORC1 core components, LST8 and mTOR. Unpublished in-lab data demonstrated that these core mTOR components can be reduced at the transcriptomic level by STAT3 inhibition, as well as upregulating DEPTOR, suggesting a potential mechanism for DCN's ability to reduce mTORC1 activity.

DCN's drug action is to inhibit IL-1 β signalling, which would theoretically result in inhibition of NF- κ B, since IL-1 β typically stimulates NF- κ B through the canonical pathway. It is generally understood that DCN can reduce NF- κ B activity in this way (476). While this effect was limited *in vitro*, more prominent inhibition of NF- κ B may arise *in vivo* from DCN, since DCN is metabolised to rhein in humans (572). While both DCN and rhein function to suppress the IL-1 β receptor, rhein is also able to regulate IL-1 β signalling by reducing the production of IL-1 converting enzyme (ICE), which prevents the cleavage of pro-IL- β to mature IL-1 β (477). Rhein also blocks MEK/ERK signalling (477). Still, DCN should present with some inhibition of the NF- κ B pathway *in vitro*, since it is able to prevent the functional assembly of IL-1 β receptors. It is possible that some of the effects of DCN shown in this study are due to the capability of DCN to block the IL-6 receptor (487), however it is unknown whether rhein would also exert this activity. Regardless, the correlation of a rheumatoid arthritis gene signature in TSC has not been investigated prior to this study, and nor has the translational usage of rheumatoid arthritis drugs in TSC been previously considered. The data presented within this study suggests that DCN may have significant disease altering effects in TSC. IL-1 β is significant within the context of epilepsy, since microglia-derived IL-1 β can promote hyperexcitability of neurons, and excessive cytokine production is also linked to neuronal cell death (217). Due to the mTORC1-inhibiting potential of DCN, this study may even propose the substitution of traditional mTORC1 inhibition by rapamycin with DCN treatment. Issues with the usage of DCN in treating TSC should be acknowledged. Firstly, DCN (or rhein) is not typically believed to cross the blood

brain barrier (540). As mentioned previously though, the blood brain barrier may be compromised within TSC, and this may allow rhein to exert anti-inflammatory effects within the brains of TSC patients. Inflammation would also increase the permeability of the BBB (573). Within this study, it is not possible to directly assess the condition of the BBB, and this may warrant further investigation. Additionally, due to the renal mode of rhein clearance from the body, it could be suggested that TSC patients with impaired renal function (due to angiomyolipoma) could be at risk of complications from DCN treatment, as DCN treatment is typically administered at a low dose in patients with renal complications (574). However, DCN has also demonstrated positive effects on renal function by suppressing inflammation (575). Aside from these points, DCN generally presents with relatively mild side effects, with gastrointestinal issues and mild skin reactions being the most prevalent adverse events (476). Further research may determine the potential applicability for this drug in the treatment of TSC.

In conclusion, this study has provided insights on the significant role that inflammation plays in the disease state of TSC. Specifically, dysregulated NF- κ B signalling was identified, and it has been shown that inhibition of the NF- κ B pathway is able to reduce a range of inflammatory biomarkers in TSC. While non-neuronal *in vitro* models shared some similar inflammatory characteristics to neuronal *in vitro* models of TSC, the variation in inflammatory activation demonstrate that non-neuronal models are insufficient for modelling neuroinflammation in TSC. Thus, usage of the neuronal models highlighted important mechanisms of NF- κ B-driven neuroinflammation, and suggested the cGAS/STING pathway as an overall source of this inflammation. Lastly, the study showed potential repurposing of the rheumatoid arthritis drug, diacerein, for the treatment of inflammation in TSC. Future work may seek to further investigate the state of NF- κ B signalling in TSC patient-derived brain tumours. *In vitro* RNA-sequencing would be beneficial to employ in this regard and would provide a useful comparison to *in vivo* TSC patient-derived brain tumour datasets. Future studies could also seek to further investigate the applicability of DCN for the treatment of TSC, with further research into IL-1 β signalling to support this. Furthermore, additional readouts of NF- κ B activity could be employed by investigating the nuclear localisation of NF- κ B transcription factors to a higher level.

Bibliography

1. Gómez MR. History of the tuberous sclerosis complex. *Brain Dev* (1995) 17:55–57. doi: 10.1016/0387-7604(94)00130-8
2. Northrup H, Krueger DA, Roberds S, Smith K, Sampson J, Korf B, Kwiatkowski DJ, Mowat D, Nellist M, Povey S, et al. Tuberous sclerosis complex diagnostic criteria update: Recommendations of the 2012 international tuberous sclerosis complex consensus conference. *Pediatr Neurol* (2013) 49:243–254. doi: 10.1016/j.pediatrneurol.2013.08.001
3. Pounders AJ, Rushing G V., Mahida S, Nonyane BAS, Thomas EA, Tameez RS, Gipson TT. Racial differences in the dermatological manifestations of tuberous sclerosis complex and the potential effects on diagnosis and care. *Therapeutic Advances in Rare Disease* (2022) 3: doi: 10.1177/26330040221140125/ASSET/IMAGES/LARGE/10.1177_26330040221140125-FIG13.JPEG
4. Rebaine Y, Nasser M, Cottin V, Girerd B, Leroux C. Tuberous sclerosis complex for the pulmonologist. *European Respiratory Review* (2021) 30: doi: 10.1183/16000617.0348-2020
5. Graham EG. Section of Dermatology Case of Adenoma Sebaceum: Pringle Type.
6. Jansen FE, Van Nieuwenhuizen O, Van Huffelen AC. Tuberous sclerosis complex and its founders. *J Neurol Neurosurg Psychiatry* (2004) 75:770. doi: 10.1136/jnnp.2003.027524
7. Moolten SE. Hamartial nature of the tuberous sclerosis complex and its bearing on the tumor problem: Report of a case with tumor anomaly of the kidney and adenoma sebaceum. *Arch Intern Med* (1942) 69:589–623. doi: 10.1001/archinte.1942.00200160040005
8. The European Chromosome 16 Tuberous Sclerosis Consortium. Identification and characterization of the tuberous sclerosis gene on chromosome 16. *Cell* (1993) 75:1305–1315. doi: 10.1016/0092-8674(93)90618-Z
9. Van Slegtenhorst M, De Hoogt R, Hermans C, Nellist M, Janssen B, Verhoef S, Lindhout D, Van Den Ouweland A, Halley D, Young J, et al. Identification of the tuberous sclerosis gene TSC1 on chromosome 9q34. *Science* (1979) (1997) 277:805–808. doi: 10.1126/science.277.5327.805
10. Chong-Kopera H, Inoki K, Li Y, Zhu T, Garcia-Gonzalo FR, Rosa JL, Guan KL. TSC1 stabilizes TSC2 by inhibiting the interaction between TSC2 and the HERC1 ubiquitin ligase. *Journal of Biological Chemistry* (2006) 281:8313–8316. doi: 10.1074/jbc.C500451200
11. Yang H, Jiang X, Li B, Yang HJ, Miller M, Yang A, Dhar A, Pavletich NP. Mechanisms of mTORC1 activation by RHEB and inhibition by PRAS40. *Nature* 2017 552:7685 (2017) 552:368–373. doi: 10.1038/nature25023
12. Knudson AG. Mutation and cancer: statistical study of retinoblastoma. *Proc Natl Acad Sci U S A* (1971) 68:820–823. doi: 10.1073/pnas.68.4.820
13. Krueger DA, Northrup H, Krueger DA, Roberds S, Smith K, Sampson J, Korf B, Kwiatkowski DJ, Mowat D, Nellist M, et al. Tuberous sclerosis complex surveillance and management: Recommendations of the 2012 international tuberous sclerosis complex consensus conference. *Pediatr Neurol* (2013) 49:255–265. doi: 10.1016/j.pediatrneurol.2013.08.002

14. Sampson JR, Yates JRW, Pirrit LA, Fleury P, Winship I, Beighton P, Connor JM. Evidence for genetic heterogeneity in tuberous sclerosis. *J Med Genet* (1989) 26:511–516. doi: 10.1136/jmg.26.8.511
15. Reyna-Fabián ME, Hernández-Martínez NL, Alcántara-Ortigoza MA, Ayala-Summano JT, Enríquez-Flores S, Velázquez-Aragón JA, Varela-Echavarría A, Todd-Quiñones CG, González-del Angel A. First comprehensive TSC1/TSC2 mutational analysis in Mexican patients with Tuberous Sclerosis Complex reveals numerous novel pathogenic variants. *Sci Rep* (2020) 10:1–14. doi: 10.1038/s41598-020-62759-5
16. Napolioni V, Curatolo P. Genetics and Molecular Biology of Tuberous Sclerosis Complex. *Curr Genomics* (2008) 9:475–487. doi: 10.2174/138920208786241243
17. Dibble CC, Elis W, Menon S, Qin W, Klekota J, Asara JM, Finan PM, Kwiatkowski DJ, Murphy LO, Manning BD. TBC1D7 Is a Third Subunit of the TSC1-TSC2 Complex Upstream of mTORC1. *Mol Cell* (2012) 47:535–546. doi: 10.1016/j.molcel.2012.06.009
18. Rosset C, Netto CBO, Ashton-Prolla P. TSC1 and TSC2 gene mutations and their implications for treatment in Tuberous Sclerosis Complex: a review. *Genet Mol Biol* (2017) 40:69. doi: 10.1590/1678-4685-GMB-2015-0321
19. Liu GY, Sabatini DM. mTOR at the nexus of nutrition, growth, ageing and disease. *Nat Rev Mol Cell Biol* (2020) 1–21. doi: 10.1038/s41580-019-0199-y
20. Inoki K, Ouyang H, Zhu T, Lindvall C, Wang Y, Zhang X, Yang Q, Bennett C, Harada Y, Stankunas K, et al. TSC2 Integrates Wnt and Energy Signals via a Coordinated Phosphorylation by AMPK and GSK3 to Regulate Cell Growth. *Cell* (2006) 126:955–968. doi: 10.1016/j.cell.2006.06.055
21. Lee DF, Kuo HP, Chen C Te, Hsu JM, Chou CK, Wei Y, Sun HL, Li LY, Ping B, Huang WC, et al. IKK β Suppression of TSC1 Links Inflammation and Tumor Angiogenesis via the mTOR Pathway. *Cell* (2007) 130:440–455. doi: 10.1016/j.cell.2007.05.058
22. Pennington K, Chan T, Torres M, Andersen J. The dynamic and stress-adaptive signaling hub of 14-3-3: emerging mechanisms of regulation and context-dependent protein–protein interactions. *Oncogene* (2018) 37:5587–5604. doi: 10.1038/s41388-018-0348-3
23. Margaria JP, Campa CC, De Santis MC, Hirsch E, Franco I. The PI3K/Akt/mTOR pathway in polycystic kidney disease: A complex interaction with polycystins and primary cilium. *Cell Signal* (2020) 66:109468. doi: 10.1016/j.cellsig.2019.109468
24. McEneaney LJ, Tee AR. “Finding a cure for tuberous sclerosis complex: From genetics through to targeted drug therapies.” *Advances in Genetics*. Academic Press Inc. (2019). p. 91–118 doi: 10.1016/bs.adgen.2018.11.003
25. Zamora EA, Aeddula NR. *Tuberous Sclerosis*. StatPearls Publishing (2021).
26. Grajkowska W, Kotulska K, Jurkiewicz E, Matyja E. Brain lesions in tuberous sclerosis complex. Review. *Folia Neuropathol* (2010) 48:139–149.
27. Nabbout R, Belousova E, Benedik MP, Carter T, Cottin V, Curatolo P, Dahlin M, D’Amato L, d’Augères GB, de Vries PJ, et al. Epilepsy in tuberous sclerosis complex: Findings from the TOSCA Study. *Epilepsia Open* (2019) 4:73–84. doi: 10.1002/epi4.12286

28. Taveira-Da Silva AM, Jones AM, Julien-Williams P, Yao J, Stylianou M, Moss J. Severity and outcome of cystic lung disease in women with tuberous sclerosis complex. *European Respiratory Journal* (2015) 45:171–180. doi: 10.1183/09031936.00088314
29. Cudzilo CJ, Szczesniak RD, Brody AS, Rattan MS, Krueger DA, Bissler JJ, Franz DN, McCormack FX, Young LR. Lymphangioliomyomatosis screening in women with tuberous sclerosis. *Chest* (2013) 144:578–585. doi: 10.1378/CHEST.12-2813
30. Zak S, Mokhallati N, Su W, McCormack FX, Franz DN, Mays M, Krueger DA, Szczesniak RD, Gupta N. Lymphangioliomyomatosis mortality in patients with tuberous sclerosis complex. *Ann Am Thorac Soc* (2019) 16:509–512. doi: 10.1513/ANNALSATS.201807-471RL/SUPPL_FILE/DISCLOSURES.PDF
31. Berger U, Khaghani A, Pomerance A, Yacoub MH, Coombes RC. Pulmonary lymphangioliomyomatosis and steroid receptors. An immunocytochemical study. *Am J Clin Pathol* (1990) 93:609–614. doi: 10.1093/AJCP/93.5.609
32. Kinoshita M, Yokoyama T, Hisashiwatanabe EH, Rikimaru T, Ichikawa Y, Oizumi K. Hormone receptors in pulmonary lymphangiomyomatosis. *Kurume Med J* (1995) 42:141–144. doi: 10.2739/KURUMEMEDJ.42.141
33. Hancock E, Osborne J. Lymphangioliomyomatosis: A review of the literature. *Respir Med* (2002) 96:1–6. doi: 10.1053/RMED.2001.1207
34. Uysal SP, Şahin M. Tuberous sclerosis: A review of the past, present, and future. *Turk J Med Sci* (2020) 50:1665–1676. doi: 10.3906/sag-2002-133
35. Li J, Kim SG, Blenis J. Rapamycin: One drug, many effects. *Cell Metab* (2014) 19:373–379. doi: 10.1016/j.cmet.2014.01.001
36. Canpolat M, Gumus H, Kumandas S, Coskun A, Per H. The use of rapamycin in patients with tuberous sclerosis complex: Long-term results. *Epilepsy and Behavior* (2018) 88:357–364. doi: 10.1016/j.yebeh.2018.09.020
37. Li M, Zhou Y, Chen C, Yang T, Zhou S, Chen S, Wu Y, Cui Y. Efficacy and safety of mTOR inhibitors (rapamycin and its analogues) for tuberous sclerosis complex: A meta-analysis. *Orphanet J Rare Dis* (2019) 14:1–9. doi: 10.1186/s13023-019-1012-x
38. van der Poest Clement EA, Sahin M, Peters JM. Vigabatrin for Epileptic Spasms and Tonic Seizures in Tuberous Sclerosis Complex. *J Child Neurol* (2018) 33:519–524. doi: 10.1177/0883073818768309
39. De Vries PJ, Whittemore VH, Leclezio L, Byars AW, Dunn D, Ess KC, Hook D, King BH, Sahin M, Jansen A. Tuberous sclerosis associated neuropsychiatric disorders (TAND) and the TAND Checklist. *Pediatr Neurol* (2015) 52:25–35. doi: 10.1016/J.PEDIATRNEUROL.2014.10.004
40. Leclezio L, de Vries P. Towards an improved understanding of TSC-Associated Neuropsychiatric Disorders (TAND). *Advances in Autism* (2016) 2:76–83. doi: 10.1108/AIA-12-2015-0025/FULL/XML
41. Hsieh DT, Whiteway SL, Rohena LO, Thiele EA. Tuberous sclerosis complex. *Neurol Clin Pract* (2016) 6:339–347. doi: 10.1212/CPJ.0000000000000260

42. Di Nardo A, Lenoël I, Winden KD, Rühmkorf A, Modi ME, Barrett L, Ercan-Herbst E, Venugopal P, Behne R, Lopes CAM, et al. Phenotypic Screen with TSC-Deficient Neurons Reveals Heat-Shock Machinery as a Druggable Pathway for mTORC1 and Reduced Cilia. *Cell Rep* (2020) 31:107780. doi: 10.1016/J.CELREP.2020.107780/ATTACHMENT/E16BDBE0-4A58-405B-96DC-95CBA1D10FF2/MMC4.XLSX
43. Zhang C, Wan X, Tang S, Li K, Wang Y, Liu Y, Sha Q, Zha X, Liu Y. miR-125b-5p/STAT3 Pathway Regulated by mTORC1 Plays a Critical Role in Promoting Cell Proliferation and Tumor Growth. *J Cancer* (2020) 11:919. doi: 10.7150/JCA.33696
44. Yokogami K, Wakisaka S, Avruch J, Reeves SA. Serine phosphorylation and maximal activation of STAT3 during CNTF signaling is mediated by the rapamycin target mTOR. *Curr Biol* (2000) 10:47–50. doi: 10.1016/S0960-9822(99)00268-7
45. Laplante M, Sabatini DM. Regulation of mTORC1 and its impact on gene expression at a glance. *J Cell Sci* (2013) 126:1713–1719. doi: 10.1242/jcs.125773
46. Wang Y tian, Tang F, Hu X, Zheng C xi, Gong T jun, Zhou Y, Luo Y, Min L. Role of crosstalk between STAT3 and mTOR signaling in driving sensitivity to chemotherapy in osteosarcoma cell lines. *IUBMB Life* (2020) 72:2146–2153. doi: 10.1002/IUB.2349
47. Dan HC, Cooper MJ, Cogswell PC, Duncan JA, Ting JPY, Baldwin AS. Akt-dependent regulation of NF- κ B is controlled by mTOR and Raptor in association with IKK. *Genes Dev* (2008) 22:1490–1500. doi: 10.1101/GAD.1662308
48. Gao Y, Gartenhaus RB, Lapidus RG, Hussain A, Zhang Y, Wang X, Dan HC. Differential IKK/NF- κ B Activity Is Mediated by TSC2 through mTORC1 in PTEN-Null prostate cancer and tuberous sclerosis complex tumor cells. *Molecular Cancer Research* (2015) 13:1602–1614. doi: 10.1158/1541-7786.MCR-15-0213
49. Weichhart T, Costantino G, Poglitsch M, Rosner M, Zeyda M, Stuhlmeier KM, Kolbe T, Stulnig TM, Hörl WH, Hengstschläger M, et al. The TSC-mTOR Signaling Pathway Regulates the Innate Inflammatory Response. *Immunity* (2008) 29:565–577. doi: 10.1016/j.immuni.2008.08.012
50. Avgeris S, Fostira F, Vagena A, Ninios Y, Delimitsou A, Vodicka R, Vrtel R, Youroukos S, Stravopodis DJ, Vlassi M, et al. Mutational analysis of TSC1 and TSC2 genes in Tuberous Sclerosis Complex patients from Greece. *Sci Rep* (2017) 7: doi: 10.1038/S41598-017-16988-W
51. Martin KR, Zhou W, Bowman MJ, Shih J, Au KS, Dittenhafer-Reed KE, Sisson KA, Koeman J, Weisenberger DJ, Cottingham SL, et al. The genomic landscape of tuberous sclerosis complex. *Nat Commun* (2017) 8: doi: 10.1038/ncomms15816
52. Winden KD, Sundberg M, Yang C, Wafa SMA, Dwyer S, Chen PF, Buttermore ED, Sahin M. Biallelic Mutations in TSC2 Lead to Abnormalities Associated with Cortical Tubers in Human iPSC-Derived Neurons. *Journal of Neuroscience* (2019) 39:9294–9305. doi: 10.1523/JNEUROSCI.0642-19.2019
53. Ehninger D, Han S, Shilyansky C, Zhou Y, Li W, Kwiatkowski DJ, Ramesh V, Silva AJ. Reversal of learning deficits in a Tsc2^{+/-} mouse model of tuberous sclerosis. *Nature Medicine* 2008 14:8 (2008) 14:843–848. doi: 10.1038/nm1788
54. Hsieh CC jung, Lo YC, Li SJ, Lin TC, Chang CW, Chen TC, Yang SH, Lee YC, Chen YY. Detection of endophenotypes associated with neuropsychiatric deficiencies in a mouse model of tuberous

- sclerosis complex using diffusion tensor imaging. *Brain Pathology* (2021) 31:4–19. doi: 10.1111/BPA.12870
55. Sundberg M, Tochitsky I, Buchholz DE, Winden K, Kujala V, Kapur K, Cataltepe D, Turner D, Han MJ, Woolf CJ, et al. Purkinje cells derived from TSC patients display hypoexcitability and synaptic deficits associated with reduced FMRP levels and reversed by rapamycin. *Molecular Psychiatry* 2018 23:11 (2018) 23:2167–2183. doi: 10.1038/s41380-018-0018-4
 56. Chan JA, Zhang H, Roberts PS, Jozwiak S, Wieslawa G, Lewin-Kowalik J, Kotulska K, Kwiatkowski DJ. Pathogenesis of tuberous sclerosis subependymal giant cell astrocytomas: biallelic inactivation of TSC1 or TSC2 leads to mTOR activation. *J Neuropathol Exp Neurol* (2004) 63:1236–1242. doi: 10.1093/JNEN/63.12.1236
 57. Niida Y, Stemmer-Rachamimov AO, Logrip M, Tapon D, Perez R, Kwiatkowski DJ, Sims K, MacCollin M, Louis DN, Ramesh V. Survey of somatic mutations in tuberous sclerosis complex (TSC) hamartomas suggests different genetic mechanisms for pathogenesis of TSC lesions. *Am J Hum Genet* (2001) 69:493–503. doi: 10.1086/321972
 58. Sepp T, Yates JRW, Green AJ, Sepp T, Yates W, Green AJ. Loss of heterozygosity in tuberous sclerosis hamartomas. *J Med Genet* (1996) 33:962. doi: 10.1136/JMG.33.11.962
 59. Henske EP, Scheithauer BW, Short MP, Wollmann R, Nahmias J, Hornigold N, Van Slegtenhorst M, Welsh CT, Kwiatkowski DJ. Allelic loss is frequent in tuberous sclerosis kidney lesions but rare in brain lesions. *Am J Hum Genet* (1996) 59:400.
 60. Nie D, Di Nardo A, Han JM, Baharanyi H, Kramvis I, Huynh T, Dabora S, Codeluppi S, Pandolfi PP, Pasquale EB, et al. Tsc2-Rheb signaling regulates EphA-mediated axon guidance. *Nature Neuroscience* 2010 13:2 (2010) 13:163–172. doi: 10.1038/nn.2477
 61. Pradhan SA, Rather MI, Tiwari A, Bhat VK, Kumar A. Evidence that TSC2 acts as a transcription factor and binds to and represses the promoter of Epregrulin. *Nucleic Acids Res* (2014) 42:6243–6255. doi: 10.1093/NAR/GKU278
 62. Sarbassov DD, Ali SM, Sengupta S, Sheen JH, Hsu PP, Bagley AF, Markhard AL, Sabatini DM. Prolonged Rapamycin Treatment Inhibits mTORC2 Assembly and Akt/PKB. *Mol Cell* (2006) 22:159–168. doi: 10.1016/J.MOLCEL.2006.03.029
 63. Saxton RA, Sabatini DM. mTOR Signaling in Growth, Metabolism, and Disease. *Cell* (2017) 168:960. doi: 10.1016/J.CELL.2017.02.004
 64. Schalm SS, Fingar DC, Sabatini DM, Blenis J. TOS motif-mediated raptor binding regulates 4E-BP1 multisite phosphorylation and function. *Curr Biol* (2003) 13:797–806. doi: 10.1016/S0960-9822(03)00329-4
 65. Yang H, Rudge DG, Koos JD, Vaidialingam B, Yang HJ, Pavletich NP. mTOR kinase structure, mechanism and regulation. *Nature* 2013 497:7448 (2013) 497:217–223. doi: 10.1038/nature12122
 66. Wang L, Harris TE, Roth RA, Lawrence JC. PRAS40 regulates mTORC1 kinase activity by functioning as a direct inhibitor of substrate binding. *Journal of Biological Chemistry* (2007) 282:20036–20044. doi: 10.1074/jbc.M702376200

67. Peterson TR, Laplante M, Thoreen CC, Sancak Y, Kang SA, Kuehl WM, Gray NS, Sabatini DM. DEPTOR is an mTOR inhibitor frequently overexpressed in multiple myeloma cells and required for their survival. *Cell* (2009) 137:873–886. doi: 10.1016/J.CELL.2009.03.046
68. Valvezan AJ, Manning BD. Molecular logic of mTORC1 signalling as a metabolic rheostat. *Nature Metabolism* 2019 1:3 (2019) 1:321–333. doi: 10.1038/s42255-019-0038-7
69. Laplante M, Sabatini DM. mTOR signaling in growth control and disease. *Cell* (2012) 149:274. doi: 10.1016/J.CELL.2012.03.017
70. Martineau Y, Azar R, Bousquet C, Pyronnet S. Anti-oncogenic potential of the eIF4E-binding proteins. *Oncogene* 2013 32:6 (2012) 32:671–677. doi: 10.1038/onc.2012.116
71. Gingras AC, Gygi SP, Raught B, Polakiewicz RD, Abraham RT, Hoekstra MF, Aebersold R, Sonenberg N. Regulation of 4E-BP1 phosphorylation: a novel two-step mechanism. *Genes Dev* (1999) 13:1422–1437. doi: 10.1101/GAD.13.11.1422
72. Zoncu R, Efeyan A, Sabatini DM. MTOR: From growth signal integration to cancer, diabetes and ageing. *Nat Rev Mol Cell Biol* (2011) 12:21–35. doi: 10.1038/nrm3025
73. Ang Z, Koean RAG, Er JZ, Lee LT, Tam JKC, Guo H, Ding JL. Novel AU-rich proximal UTR sequences (APS) enhance CXCL8 synthesis upon the induction of rpS6 phosphorylation. *PLoS Genet* (2019) 15: doi: 10.1371/JOURNAL.PGEN.1008077
74. Raught B, Peiretti F, Gingras AC, Livingstone M, Shahbazian D, Mayeur GL, Polakiewicz RD, Sonenberg N, Hershey JWB. Phosphorylation of eucaryotic translation initiation factor 4B Ser422 is modulated by S6 kinases. *EMBO J* (2004) 23:1761–1769. doi: 10.1038/SJ.EMBOJ.7600193
75. Hong S, Freeberg MA, Han T, Kamath A, Yao Y, Fukuda T, Suzuki T, Kim JK, Inoki K. LARP1 functions as a molecular switch for mTORC1-mediated translation of an essential class of mRNAs. *Elife* (2017) 6: doi: 10.7554/ELIFE.25237
76. Jia JJ, Lahr RM, Solgaard MT, Moraes BJ, Pointet R, Yang AD, Celucci G, Graber TE, Hoang HD, Niklaus MR, et al. mTORC1 promotes TOP mRNA translation through site-specific phosphorylation of LARP1. *Nucleic Acids Res* (2021) 49:3461. doi: 10.1093/NAR/GKAA1239
77. Gomes C, Smith SC, Youssef MN, Zheng JJ, Hagg T, Hetman M. RNA Polymerase 1-driven Transcription as a Mediator of BDNF-induced Neurite Outgrowth. *J Biol Chem* (2011) 286:4357. doi: 10.1074/JBC.M110.170134
78. Betz C, Hall MN. Where is mTOR and what is it doing there? *Journal of Cell Biology* (2013) 203:563–574. doi: 10.1083/JCB.201306041
79. Rosner M, Hengstschläger M. Cytoplasmic and nuclear distribution of the protein complexes mTORC1 and mTORC2: rapamycin triggers dephosphorylation and delocalization of the mTORC2 components rictor and sin1. *Hum Mol Genet* (2008) 17:2934–2948. doi: 10.1093/HMG/DDN192
80. Ortells MC, Morancho B, Drews-Elger K, Viollet B, Laderoute KR, López-Rodríguez C, Aramburu J. Transcriptional regulation of gene expression during osmotic stress responses by the mammalian target of rapamycin. *Nucleic Acids Res* (2012) 40:4368. doi: 10.1093/NAR/GKS038

81. Tsang CK, Liu H, Zheng XFS. mTOR binds to the promoters of RNA polymerase I- and III-transcribed genes. *Cell Cycle* (2010) 9:953. doi: 10.4161/CC.9.5.10876
82. Lin WH, Chang YW, Hong MX, Hsu TC, Lee KC, Lin C, Lee JL. STAT3 phosphorylation at Ser727 and Tyr705 differentially regulates the EMT–MET switch and cancer metastasis. *Oncogene* 2020 40:4 (2020) 40:791–805. doi: 10.1038/s41388-020-01566-8
83. Giguère V. Canonical signaling and nuclear activity of mTOR—a teamwork effort to regulate metabolism and cell growth. *FEBS J* (2018) 285:1572–1588. doi: 10.1111/FEBS.14384
84. Li K, Wei X, Zhang L, Chi H, Yang J. Raptor/mTORC1 Acts as a Modulatory Center to Regulate Anti-bacterial Immune Response in Rockfish. *Front Immunol* (2019) 10:2953. doi: 10.3389/FIMMU.2019.02953/BIBTEX
85. Dumont FJ, Su Q. Mechanism of action of the immunosuppressant rapamycin. *Life Sci* (1995) 58:373–395. doi: 10.1016/0024-3205(95)02233-3
86. Nandagopal N, Ali AK, Komal AK, Lee SH. The critical role of IL-15-PI3K-mTOR pathway in natural killer cell effector functions. *Front Immunol* (2014) 5:187. doi: 10.3389/FIMMU.2014.00187/BIBTEX
87. Guertin DA, Stevens DM, Thoreen CC, Burds AA, Kalaany NY, Moffat J, Brown M, Fitzgerald KJ, Sabatini DM. Ablation in mice of the mTORC components raptor, rictor, or mLST8 reveals that mTORC2 is required for signaling to Akt-FOXO and PKCalpha, but not S6K1. *Dev Cell* (2006) 11:859–871. doi: 10.1016/J.DEVCEL.2006.10.007
88. Laplante M, Sabatini DM. mTOR signaling at a glance. *J Cell Sci* (2009) 122:3589. doi: 10.1242/JCS.051011
89. Oshiro N, Yoshino KI, Hidayat S, Tokunaga C, Hara K, Eguchi S, Avruch J, Yonezawa K. Dissociation of raptor from mTOR is a mechanism of rapamycin-induced inhibition of mTOR function. *Genes to Cells* (2004) 9:359–366. doi: 10.1111/J.1356-9597.2004.00727.X
90. Yao CA, Ortiz-Vega S, Sun YY, Chien CT, Chuang JH, Lin Y. Association of mSin1 with mTORC2 Ras and Akt reveals a crucial domain on mSin1 involved in Akt phosphorylation. *Oncotarget* (2017) 8:63392. doi: 10.18632/ONCOTARGET.18818
91. Jacinto E, Facchinetti V, Liu D, Soto N, Wei S, Jung SY, Huang Q, Qin J, Su B. SIN1/MIP1 maintains rictor-mTOR complex integrity and regulates Akt phosphorylation and substrate specificity. *Cell* (2006) 127:125–137. doi: 10.1016/J.CELL.2006.08.033
92. Qian J, Su S, Liu P. Experimental Approaches in Delineating mTOR Signaling. *Genes* 2020, Vol 11, Page 738 (2020) 11:738. doi: 10.3390/GENES11070738
93. Fu W, Hall MN. Regulation of mTORC2 Signaling. *Genes (Basel)* (2020) 11:1–19. doi: 10.3390/GENES11091045
94. Sarbassov DD, Guertin DA, Ali SM, Sabatini DM. Phosphorylation and regulation of Akt/PKB by the rictor-mTOR complex. *Science (1979)* (2005) 307:1098–1101. doi: 10.1126/SCIENCE.1106148/SUPPL_FILE/SARBASSOV.SOM.PDF
95. Oh WJ, Wu CC, Kim SJ, Facchinetti V, Julien LA, Finlan M, Roux PP, Su B, Jacinto E. mTORC2 can associate with ribosomes to promote cotranslational phosphorylation and stability of nascent Akt polypeptide. *EMBO J* (2010) 29:3939–3951. doi: 10.1038/EMBOJ.2010.271

96. Oh WJ, Jacinto E. mTOR complex 2 signaling and functions. *Cell Cycle* (2011) 10:2305. doi: 10.4161/CC.10.14.16586
97. Masui K, Cavenee WK, Mischel PS. mTORC2 in the center of cancer metabolic reprogramming. *Trends Endocrinol Metab* (2014) 25:364. doi: 10.1016/J.TEM.2014.04.002
98. Schreiber KH, Ortiz D, Academia EC, Anies AC, Liao CY, Kennedy BK. Rapamycin-mediated mTORC2 inhibition is determined by the relative expression of FK506-binding proteins. *Aging Cell* (2015) 14:265. doi: 10.1111/ACEL.12313
99. Cusmai R, Moavero R, Bombardieri R, Vigeveno F, Curatolo P. Long-term neurological outcome in children with early-onset epilepsy associated with tuberous sclerosis. *Epilepsy Behav* (2011) 22:735–739. doi: 10.1016/J.YEBEH.2011.08.037
100. Kossoff EH, Zupec-Kania BA, Auvin S, Ballaban-Gil KR, Christina Bergqvist AG, Blackford R, Buchhalter JR, Caraballo RH, Cross JH, Dahlin MG, et al. Optimal clinical management of children receiving dietary therapies for epilepsy: Updated recommendations of the International Ketogenic Diet Study Group. *Epilepsia Open* (2018) 3:175–192. doi: 10.1002/EPI4.12225
101. Elliott RE, Carlson C, Kalhorn SP, Moshel YA, Weiner HL, Devinsky O, Doyle WK. Refractory epilepsy in tuberous sclerosis: vagus nerve stimulation with or without subsequent resective surgery. *Epilepsy Behav* (2009) 16:454–460. doi: 10.1016/J.YEBEH.2009.08.018
102. Hobby G, Clark R, Woywodt A. A treasure from a barren island: the discovery of rapamycin. *Clin Kidney J* (2022) 15:1971. doi: 10.1093/CKJ/SFAC116
103. Luo C, Ye WR, Shi W, Yin P, Chen C, He YB, Chen MF, Zu X Bin, Cai Y. Perfect match: mTOR inhibitors and tuberous sclerosis complex. *Orphanet Journal of Rare Diseases* 2022 17:1 (2022) 17:1–16. doi: 10.1186/S13023-022-02266-0
104. He W, Chen J, Wang YY, Zhang MN, Qian-Lu, Wang QH, Luo XM, Chen XQ, Zou LP. Sirolimus improves seizure control in pediatric patients with tuberous sclerosis: A prospective cohort study. *Seizure* (2020) 79:20–26. doi: 10.1016/J.SEIZURE.2020.03.018
105. McCormack FX, Inoue Y, Moss J, Singer LG, Strange C, Nakata K, Barker AF, Chapman JT, Brantly ML, Stocks JM, et al. Efficacy and Safety of Sirolimus in Lymphangiomyomatosis. *New England Journal of Medicine* (2011) 364:1595–1606. doi: 10.1056/NEJMOA1100391
106. Cabrera-López C, Martí T, Catalá V, Torres F, Mateu S, Ballarín J, Torra R. Assessing the effectiveness of rapamycin on angiomyolipoma in tuberous sclerosis: a two years trial. *Orphanet J Rare Dis* (2012) 7:87. doi: 10.1186/1750-1172-7-87
107. Sadowski K, Sijko K, Domańska-Pakieła D, Borkowska J, Chmielewski D, Ulatowska A, Józwiak S, Kotulska K. Antiepileptic Effect and Safety Profile of Rapamycin in Pediatric Patients With Tuberous Sclerosis Complex. *Front Neurol* (2022) 13:346. doi: 10.3389/FNEUR.2022.704978/BIBTEX
108. Overwater IE, Rietman AB, Mous SE, Bindels-De Heus K, Rizopoulos D, Ten Hoopen LW, Van Der Vaart T, Jansen FE, Elgersma Y, Moll HA, et al. A randomized controlled trial with everolimus for IQ and autism in tuberous sclerosis complex. *Neurology* (2019) 93:E200–E209. doi: 10.1212/WNL.0000000000007749

109. Krueger DA, Sadhwani A, Byars AW, de Vries PJ, Franz DN, Whittemore VH, Filip-Dhima R, Murray D, Kapur K, Sahin M. Everolimus for treatment of tuberous sclerosis complex-associated neuropsychiatric disorders. *Ann Clin Transl Neurol* (2017) 4:877–887. doi: 10.1002/ACN3.494
110. Overwater IE, Rietman AB, van Eeghen AM, de Wit MCY. Everolimus for the treatment of refractory seizures associated with tuberous sclerosis complex (TSC): current perspectives. *Ther Clin Risk Manag* (2019) 15:951. doi: 10.2147/TCRM.S145630
111. Amin S, Lux A, Calder N, Laugharne M, Osborne J, O’callaghan F. Causes of mortality in individuals with tuberous sclerosis complex. *Dev Med Child Neurol* (2017) 59:612–617. doi: 10.1111/DMCN.13352
112. Specchio N, Pavia GC, de Palma L, De Benedictis A, Pepi C, Conti M, Marras CE, Vigevano F, Curatolo P. Current role of surgery for tuberous sclerosis complex-associated epilepsy. *Pediatr Investig* (2022) 6:16. doi: 10.1002/PED4.12312
113. Bissler JJ, Nonomura N, Budde K, Zonnenberg BA, Fischereder M, Voi M, Louveau AL, Herbst F, Bebin EM, Curatolo P, et al. Angiomyolipoma rebound tumor growth after discontinuation of everolimus in patients with tuberous sclerosis complex or sporadic lymphangioleiomyomatosis. *PLoS One* (2018) 13: doi: 10.1371/JOURNAL.PONE.0201005
114. Palavra F, Robalo C, Reis F. Recent Advances and Challenges of mTOR Inhibitors Use in the Treatment of Patients with Tuberous Sclerosis Complex. *Oxid Med Cell Longev* (2017) 2017: doi: 10.1155/2017/9820181
115. MacKeigan JP, Krueger DA. Differentiating the mTOR inhibitors everolimus and sirolimus in the treatment of tuberous sclerosis complex. *Neuro Oncol* (2015) 17:1550. doi: 10.1093/NEUONC/NOV152
116. Huang J, Dibble CC, Matsuzaki M, Manning BD. The TSC1-TSC2 Complex Is Required for Proper Activation of mTOR Complex 2. *Mol Cell Biol* (2008) 28:4104. doi: 10.1128/MCB.00289-08
117. Wataya-Kaneda M, Ohno Y, Fujita Y, Yokozeki H, Niizeki H, Ogai M, Fukai K, Nagai H, Yoshida Y, Hamada I, et al. Sirolimus Gel Treatment vs Placebo for Facial Angiofibromas in Patients With Tuberous Sclerosis Complex: A Randomized Clinical Trial. *JAMA Dermatol* (2018) 154:781–788. doi: 10.1001/JAMADERMATOL.2018.1408
118. Luo C, Zhang YS, Zhang MX, Chen MF, Li Y, Qi L, Li HZ, Zu X Bin, Cai Y. Everolimus versus sirolimus for angiomyolipoma associated with tuberous sclerosis complex: a multi-institutional retrospective study in China. *Orphanet J Rare Dis* (2021) 16:1–8. doi: 10.1186/S13023-021-01932-Z/TABLES/3
119. Klawitter J, Nashan B, Christians U. Everolimus and Sirolimus in Transplantation-Related but Different. *Expert Opin Drug Saf* (2015) 14:1055. doi: 10.1517/14740338.2015.1040388
120. Ben-Menachem E. Mechanism of action of vigabatrin: correcting misperceptions. *Acta Neurol Scand Suppl* (2011) 124:5–15. doi: 10.1111/J.1600-0404.2011.01596.X
121. Friedman D, Bogner M, Parker-Menzer K, Devinsky O. Vigabatrin for partial-onset seizure treatment in patients with tuberous sclerosis complex. *Epilepsy Behav* (2013) 27:118–120. doi: 10.1016/J.YEBEH.2012.12.033

122. Wild JM, Chiron C, Ahn H, Baulac M, Bursztyjn J, Gandolfo E, Goldberg I, Goñi FJ, Mercier F, Nordmann JP, et al. Visual field loss in patients with refractory partial epilepsy treated with vigabatrin: Final results from an open-label, observational, multicentre study. *CNS Drugs* (2009) 23:965–982. doi: 10.2165/11317650-000000000-00000
123. James Willmore L, Abelson MB, Ben-Menachem E, Pellock JM, Donald Shields W. Vigabatrin: 2008 Update. *Epilepsia* (2009) 50:163–173. doi: 10.1111/j.1528-1167.2008.01988.x
124. Neal MJ, Shah MA. Development of tolerance to the effects of vigabatrin (gamma-vinyl-GABA) on GABA release from rat cerebral cortex, spinal cord and retina. *Br J Pharmacol* (1990) 100:324–328. doi: 10.1111/J.1476-5381.1990.TB15803.X
125. Overwater IE, Bindels-De Heus K, Rietman AB, Ten Hoopen LW, Vergouwe Y, Moll HA, De Wit MCY. Epilepsy in children with tuberous sclerosis complex: Chance of remission and response to antiepileptic drugs. *Epilepsia* (2015) 56:1239–1245. doi: 10.1111/EPI.13050
126. Wang S, Fallah A, Fallah A. Optimal management of seizures associated with tuberous sclerosis complex: Current and emerging options. *Neuropsychiatr Dis Treat* (2014) 10:2021–2030. doi: 10.2147/NDT.S51789
127. Specchio N, Pepi C, de Palma L, Moavero R, De Benedictis A, Marras CE, Vigevano F, Curatolo P. Surgery for drug-resistant tuberous sclerosis complex-associated epilepsy: who, when, and what. *Epileptic Disord* (2021) 23:53–73. doi: 10.1684/EPD.2021.1253
128. Vannicola C, Tassi L, Barba C, Boniver C, Cossu M, de Curtis M, De Palma L, D’Errico I, Didato G, Guerrini R, et al. Seizure outcome after epilepsy surgery in tuberous sclerosis complex: Results and analysis of predictors from a multicenter study. *J Neurol Sci* (2021) 427: doi: 10.1016/J.JNS.2021.117506
129. Treiber JM, Curry DJ, Weiner HL, Roth J. Epilepsy surgery in tuberous sclerosis complex (TSC): emerging techniques and redefinition of treatment goals. *Childs Nerv Syst* (2020) 36:2519–2525. doi: 10.1007/S00381-020-04715-2
130. Stellon MA, Cobourn K, Whitehead MT, Elling N, McClintock W, Oluigbo CO. “Laser and the Tuber”: thermal dynamic and volumetric factors influencing seizure outcomes in pediatric subjects with tuberous sclerosis undergoing stereoencephalography-directed laser ablation of tubers. *Childs Nerv Syst* (2019) 35:1333–1340. doi: 10.1007/S00381-019-04255-4
131. Sylantyev S, Jensen TP, Ross RA, Rusakov DA. Cannabinoid- and lysophosphatidylinositol-sensitive receptor GPR55 boosts neurotransmitter release at central synapses. *Proc Natl Acad Sci U S A* (2013) 110:5193–5198. doi: 10.1073/PNAS.1211204110/-/DCSUPPLEMENTAL/PNAS.201211204SI.PDF
132. Nichol K, Stott C, Jones N, Gray RA, Bazelot M, Whalley BJ. The proposed multimodal mechanism of action of cannabidiol (CBD) in epilepsy: modulation of intracellular calcium and adenosine-mediated signaling (P5.5-007). *Neurology* (2019) 92:
133. Gray RA, Whalley BJ. The proposed mechanisms of action of CBD in epilepsy. *Epileptic Disorders* (2020) 22:S10–S15. doi: 10.1684/EPD.2020.1135
134. Atalay S, Jarocka-karpowicz I, Skrzydlewska E. Antioxidative and Anti-Inflammatory Properties of Cannabidiol. *Antioxidants* (2020) 9: doi: 10.3390/ANTIOX9010021

135. Seltzer ES, Watters AK, Mackenzie D, Granat LM, Zhang D. Cannabidiol (CBD) as a Promising Anti-Cancer Drug. *Cancers (Basel)* (2020) 12:1–26. doi: 10.3390/CANCERS12113203
136. Massi P, Vaccani A, Bianchessi S, Costa B, Macchi P, Parolaro D. The non-psychoactive cannabidiol triggers caspase activation and oxidative stress in human glioma cells. *Cell Mol Life Sci* (2006) 63:2057–2066. doi: 10.1007/S00018-006-6156-X
137. Shrivastava A, Kuzontkoski PM, Groopman JE, Prasad A. Cannabidiol induces programmed cell death in breast cancer cells by coordinating the cross-talk between apoptosis and autophagy. *Mol Cancer Ther* (2011) 10:1161–1172. doi: 10.1158/1535-7163.MCT-10-1100
138. Sultan AS, Marie MA, Sheweita SA. Novel mechanism of cannabidiol-induced apoptosis in breast cancer cell lines. *Breast* (2018) 41:34–41. doi: 10.1016/J.BREAST.2018.06.009
139. O'Brien K. Cannabidiol (CBD) in Cancer Management. *Cancers (Basel)* (2022) 14: doi: 10.3390/CANCERS14040885
140. Wiemer-Kruel A, Stiller B, Bast T. Cannabidiol Interacts Significantly with Everolimus-Report of a Patient with Tuberous Sclerosis Complex. *Neuropediatrics* (2019) 50:400–403. doi: 10.1055/S-0039-1695786
141. Ebrahimi-Fakhari D, Agricola KD, Tudor C, Krueger D, Franz DN. Cannabidiol Elevates Mechanistic Target of Rapamycin Inhibitor Levels in Patients With Tuberous Sclerosis Complex. *Pediatr Neurol* (2020) 105:59–61. doi: 10.1016/J.PEDIATRNEUROL.2019.11.017
142. Geffrey AL, Pollack SF, Bruno PL, Thiele EA. Drug–drug interaction between clobazam and cannabidiol in children with refractory epilepsy. *Epilepsia* (2015) 56:1246–1251. doi: 10.1111/EPI.13060
143. Gaston TE, Bebin EM, Cutter GR, Liu Y, Szaflarski JP. Interactions between cannabidiol and commonly used antiepileptic drugs. *Epilepsia* (2017) 58:1586–1592. doi: 10.1111/EPI.13852
144. Devinsky O, Patel AD, Cross JH, Villanueva V, Wirrell EC, Privitera M, Greenwood SM, Roberts C, Checketts D, VanLandingham KE, et al. Effect of Cannabidiol on Drop Seizures in the Lennox–Gastaut Syndrome. *New England Journal of Medicine* (2018) 378:1888–1897. doi: 10.1056/NEJMOA1714631/SUPPL_FILE/NEJMOA1714631_DISCLOSURES.PDF
145. Devinsky O, Cross JH, Laux L, Marsh E, Miller I, Nabbout R, Scheffer IE, Thiele EA, Wright S. Trial of Cannabidiol for Drug-Resistant Seizures in the Dravet Syndrome. *N Engl J Med* (2017) 376:2011–2020. doi: 10.1056/NEJMOA1611618
146. Golub V, Reddy DS. “Cannabidiol Therapy for Refractory Epilepsy and Seizure Disorders.” *Advances in Experimental Medicine and Biology*. Springer (2021). p. 93–110 doi: 10.1007/978-3-030-57369-0_7
147. Thiele EA, Bebin EM, Filloux F, Kwan P, Loftus R, Sahebkar F, Sparagana S, Wheless J. Long-term cannabidiol treatment for seizures in patients with tuberous sclerosis complex: An open-label extension trial. *Epilepsia* (2022) 63:426–439. doi: 10.1111/EPI.17150
148. Schubert-Bast S, Strzelczyk A. Review of the treatment options for epilepsy in tuberous sclerosis complex: towards precision medicine. *Ther Adv Neurol Disord* (2021) 14: doi: 10.1177/17562864211031100

149. Hall MN. mTOR-what does it do? *Transplant Proc* (2008) 40:55-8. doi: 10.1016/j.transproceed.2008.10.009
150. Mecca C, Giambanco I, Donato R, Arcuri C. Targeting mTOR in glioblastoma: Rationale and preclinical/clinical evidence. *Dis Markers* (2018) 2018: doi: 10.1155/2018/9230479
151. Conciatori F, Bazzichetto C, Falcone I, Pilotto S, Bria E, Cognetti F, Milella M, Ciuffreda L. Role of mTOR signaling in tumor microenvironment: An overview. *Int J Mol Sci* (2018) 19: doi: 10.3390/ijms19082453
152. Dibble CC, Manning BD. Signal integration by mTORC1 coordinates nutrient input with biosynthetic output. *Nat Cell Biol* (2013) 15:555–564. doi: 10.1038/ncb2763
153. Ilagan E, Manning BD. Emerging Role of mTOR in the Response to Cancer Therapeutics. *Trends Cancer* (2016) 2:241–251. doi: 10.1016/j.trecan.2016.03.008
154. Parry L, Maynard J, Patel A, Hodges A, Von Deimling A, Sampson J, Cheadle J. Molecular analysis of the TSC1 and TSC2 tumour suppressor genes in sporadic glial and glioneuronal tumours. *Hum Genet* (2000) 107:350–356. doi: 10.1007/S004390000390
155. Zhu QY, He ZM, Cao WM, Li B. The role of TSC2 in breast cancer: a literature review. *Front Oncol* (2023) 13: doi: 10.3389/FONC.2023.1188371
156. Kwiatkowski DJ, Choueiri TK, Fay AP, Rini BI, Thorner AR, De Velasco G, Tyburczy ME, Hamieh L, Albiges L, Agarwal N, et al. Mutations in TSC1, TSC2, and MTOR are associated with response to rapalogs in patients with metastatic Renal Cell Carcinoma. *Clin Cancer Res* (2016) 22:2445. doi: 10.1158/1078-0432.CCR-15-2631
157. Ryskalin L, Lazzeri G, Flaibani M, Biagioni F, Gambardella S, Frati A, Fornai F. mTOR-Dependent Cell Proliferation in the Brain. *Biomed Res Int* (2017) 2017: doi: 10.1155/2017/7082696
158. Furnari FB, Fenton T, Bachoo RM, Mukasa A, Stommel JM, Stegh A, Hahn WC, Ligon KL, Louis DN, Brennan C, et al. Malignant astrocytic glioma: genetics, biology, and paths to treatment. *Genes Dev* (2007) 21:2683–2710. doi: 10.1101/GAD.1596707
159. Tamimi AF, Juweid M. Epidemiology and Outcome of Glioblastoma. *Glioblastoma* (2017) 143–153. doi: 10.15586/CODON.GLIOMASTOMA.2017.CH8
160. Kim HJ, Park JW, Lee JH. Genetic Architectures and Cell-of-Origin in Glioblastoma. *Front Oncol* (2020) 10: doi: 10.3389/FONC.2020.615400
161. Duzgun Z, Eroglu Z, Biray Avci C. Role of mTOR in glioblastoma. *Gene* (2016) 575:187–190. doi: 10.1016/J.GENE.2015.08.060
162. Divé I, Klann K, Michaelis JB, Heinzen D, Steinbach JP, Münch C, Ronellenfitsch MW. Inhibition of mTOR signaling protects human glioma cells from hypoxia-induced cell death in an autophagy-independent manner. *Cell Death Discovery* 2022 8:1 (2022) 8:1–8. doi: 10.1038/s41420-022-01195-y
163. Heinzen D, Divé I, Lorenz NI, Luger A-L, Steinbach JP, Ronellenfitsch MW. Second Generation mTOR Inhibitors as a Double-Edged Sword in Malignant Glioma Treatment. *Int J Mol Sci* (2019) 20:4474. doi: 10.3390/ijms20184474

164. Hütt-Cabezas M, Karajannis MA, Zagzag D, Shah S, Horkayne-Szakaly I, Rushing EJ, Cameron JD, Jain D, Eberhart CG, Raabe EH, et al. Activation of mTORC1/mTORC2 signaling in pediatric low-grade glioma and pilocytic astrocytoma reveals mTOR as a therapeutic target. *Neuro Oncol* (2013) 15:1604. doi: 10.1093/NEUONC/NOT132
165. Chakravarti A, Zhai G, Suzuki Y, Sarkesh S, Black PM, Muzikansky A, Loeffler JS. The prognostic significance of phosphatidylinositol 3-kinase pathway activation in human gliomas. *J Clin Oncol* (2004) 22:1926–1933. doi: 10.1200/JCO.2004.07.193
166. Wang H, Wang H, Zhang W, Huang HJ, Liao WSL, Fuller GN. Analysis of the activation status of Akt, NFκB, and Stat3 in human diffuse gliomas. *Laboratory Investigation* (2004) 84:941–951. doi: 10.1038/labinvest.3700123
167. Korkolopoulou P, Levidou G, El-Habr EA, Piperi C, Adamopoulos C, Samaras V, Boviatsis E, Thymara I, Trigka EA, Sakellariou S, et al. Phosphorylated 4E-binding protein 1 (p-4E-BP1): a novel prognostic marker in human astrocytomas. *Histopathology* (2012) 61:293–305. doi: 10.1111/J.1365-2559.2012.04236.X
168. Li XY, Zhang LQ, Zhang XG, Li X, Ren YB, Ma XY, Li XG, Wang LX. Association between AKT/mTOR signalling pathway and malignancy grade of human gliomas. *J Neurooncol* (2011) 103:453–458. doi: 10.1007/S11060-010-0424-1
169. Dumas AA, Pomella N, Rosser G, Guglielmi L, Vinel C, Millner TO, Rees J, Aley N, Sheer D, Wei J, et al. Microglia promote glioblastoma via mTOR-mediated immunosuppression of the tumour microenvironment. *EMBO J* (2020) 39:e103790. doi: 10.15252/EMBJ.2019103790
170. Behrooz AB, Talaie Z, Jusheghani F, Łos MJ, Klonisch T, Ghavami S. Wnt and PI3K/Akt/mTOR Survival Pathways as Therapeutic Targets in Glioblastoma. *International Journal of Molecular Sciences* 2022, Vol 23, Page 1353 (2022) 23:1353. doi: 10.3390/IJMS23031353
171. Masri J, Bernath A, Martin J, Jo OD, Vartanian R, Funk A, Gera J. mTORC2 activity is elevated in gliomas and promotes growth and cell motility via overexpression of rictor. *Cancer Res* (2007) 67:11712–20. doi: 10.1158/0008-5472.CAN-07-2223
172. Tanaka K, Babic I, Nathanson D, Akhavan D, Guo D, Gini B, Dang J, Zhu S, Yang H, de Jesus J, et al. Oncogenic EGFR signaling activates an mTORC2-NF-κB pathway that promotes chemotherapy resistance. *Cancer Discov* (2011) 1:524–538. doi: 10.1158/2159-8290.CD-11-0124
173. Fan QW, Weiss WA. Inhibition of PI3K-Akt-mTOR Signaling in Glioblastoma by mTORC1/2 Inhibitors. *Methods Mol Biol* (2012) 821:349. doi: 10.1007/978-1-61779-430-8_22
174. Janes MR, Limon JJ, So L, Chen J, Lim RJ, Chavez MA, Vu C, Lilly MB, Mallya S, Ong ST, et al. Effective and selective targeting of leukemia cells using a TORC1/2 kinase inhibitor. *Nat Med* (2010) 16:205–213. doi: 10.1038/NM.2091
175. Peddi PF, Hurvitz SA. PI3K pathway inhibitors for the treatment of brain metastases with a focus on HER2+ breast cancer. *J Neurooncol* (2014) 117:7. doi: 10.1007/S11060-014-1369-6
176. Cloughesy TF, Yoshimoto K, Nghiemphu P, Brown K, Dang J, Zhu S, Hsueh T, Chen Y, Wang W, Youngkin D, et al. Antitumor Activity of Rapamycin in a Phase I Trial for Patients with Recurrent PTEN-Deficient Glioblastoma. *PLoS Med* (2008) 5:0139–0151. doi: 10.1371/JOURNAL.PMED.0050008

177. Singer E, Walter C, Fabbro D, Rageot D, Beaufile F, Wymann MP, Rischert N, Riess O, Hillmann P, Nguyen HP. Brain-penetrant PQR620 mTOR and PQR530 PI3K/mTOR inhibitor reduce huntingtin levels in cell models of HD. *Neuropharmacology* (2020) 162:107812. doi: 10.1016/J.NEUROPHARM.2019.107812
178. Wesseling P, van den Bent M, Perry A. Oligodendroglioma: pathology, molecular mechanisms and markers. *Acta Neuropathol* (2015) 129:809–827. doi: 10.1007/S00401-015-1424-1
179. Komori T. Pathology of oligodendroglia: An overview. *Neuropathology* (2017) 37:465–474. doi: 10.1111/NEUP.12389
180. Hoch MJ, Franceschi AM, Shepherd TM. Oligodendroglioma. *PET/MR Imaging: A Case-Based Approach* (2022)281–283. doi: 10.1007/978-3-319-65106-4_115
181. Liu S, Liu X, Xiao Y, Chen S, Zhuang W. Prognostic factors associated with survival in patients with anaplastic oligodendroglioma. *PLoS One* (2019) 14:e0211513. doi: 10.1371/JOURNAL.PONE.0211513
182. Tateishi K, Nakamura T, Juratli TA, Williams EA, Matsushita Y, Miyake S, Nishi M, Miller JJ, Tummala SS, Fink AL, et al. PI3K/AKT/mTOR Pathway Alterations Promote Malignant Progression and Xenograft Formation in Oligodendroglial Tumors. *Clin Cancer Res* (2019) 25:4375–4387. doi: 10.1158/1078-0432.CCR-18-4144
183. Iddrissu M, Dakurah T, Wepeba G. Anaplastic Ependymoma of the Fourth Ventricle Causing Obstructive Hydrocephalus. *Ghana Med J* (2005) 39:33. doi: 10.4314/GMJ.V39I1.35979
184. Wu J, Armstrong TS, Gilbert MR. Biology and management of ependymomas. *Neuro Oncol* (2016) 18:902–913. doi: 10.1093/NEUONC/NOW016
185. Chai Y-H, Jung S, Lee J-K, Kim I-Y, Jang W-Y, Moon K-S, Kim J-H, Lee K-H, Kim S-K, Jung T-Y. Ependymomas: Prognostic Factors and Outcome Analysis in a Retrospective Series of 33 Patients. *Brain Tumor Res Treat* (2017) 5:70. doi: 10.14791/BTRT.2017.5.2.70
186. Bowers DC, Kucejova B, Margraf L, Gargan L, Brugarolas J. mMTORC1 activation in childhood ependymoma and response to sirolimus. *J Neurooncol* (2011) 103:797–801. doi: 10.1007/S11060-010-0455-7/TABLES/1
187. Dewi FRP, Jiapaer S, Kobayashi A, Hazawa M, Ikliptikawati DK, Hartono, Sabit H, Nakada M, Wong RW. Nucleoporin TPR (translocated promoter region, nuclear basket protein) upregulation alters MTOR-HSF1 trails and suppresses autophagy induction in ependymoma. *Autophagy* (2021) 17:1001–1012. doi: 10.1080/15548627.2020.1741318
188. Bowers DC, Rajaram V, Karajannis MA, Gardner SL, Su JM-F, Baxter P, Partap S, Klesse LJ. Phase II study of everolimus for recurrent or progressive pediatric ependymoma. *Neurooncol Adv* (2023) 5:1–7. doi: 10.1093/NOAJNL/VDAD011
189. Boer K, Troost D, Timmermans W, Van Rijen PC, Spliet WGM, Aronica E. Pi3K-mTOR signaling and AMOG expression in epilepsy-associated glioneuronal tumors. *Brain Pathol* (2010) 20:234–244. doi: 10.1111/J.1750-3639.2009.00268.X
190. Pekmezci M, Villanueva-Meyer JE, Goode B, Van Ziffle J, Onodera C, Grenert JP, Bastian BC, Chamyan G, Maher OM, Khatib Z, et al. The genetic landscape of ganglioglioma. *Acta Neuropathol Commun* (2018) 6:47. doi: 10.1186/S40478-018-0551-Z/FIGURES/3

191. Mei H, Wang Y, Lin Z, Tong Q. The mTOR Signaling Pathway in Pediatric Neuroblastoma. <http://dx.doi.org/10.3109/088800182013798058> (2013) 30:605–615. doi: 10.3109/08880018.2013.798058
192. Al-Saleem T, Wessner LL, Scheithauer BW, Patterson K, Roach ES, Dreyer SJ, Fujikawa K, Bjornsson J, Bernstein J, Henske EP. Malignant Tumors of the Kidney, Brain, and Soft Tissues in Children and Young Adults with the Tuberous Sclerosis Complex. (1998)
193. Kidney cancer risk | Cancer Research UK. <https://www.cancerresearchuk.org/health-professional/cancer-statistics/statistics-by-cancer-type/kidney-cancer/risk-factors#ref1> [Accessed May 16, 2023]
194. Azriel A, Gogos A, Rogers TW, Moscovici S, Lo P, Drummond K. Glioblastoma in a patient with tuberous sclerosis. *Journal of Clinical Neuroscience* (2019) 60:153–155. doi: 10.1016/J.JOCN.2018.10.083
195. Chen L, Deng H, Cui H, Fang J, Zuo Z, Deng J, Li Y, Wang X, Zhao L. Inflammatory responses and inflammation-associated diseases in organs. *Oncotarget* (2018) 9:7204–7218. doi: 10.18632/oncotarget.23208
196. Coussens LM, Werb Z. Inflammation and cancer. *Nature* (2002) 420:860–867. doi: 10.1038/nature01322
197. Muldoon LL, Alvarez JI, Begley DJ, Boado RJ, Del Zoppo GJ, Doolittle ND, Engelhardt B, Hallenbeck JM, Lonser RR, Ohlfest JR, et al. Immunologic privilege in the central nervous system and the blood–brain barrier. *Journal of Cerebral Blood Flow & Metabolism* (2013) 33:13. doi: 10.1038/JCBFM.2012.153
198. Dotiwala AK, McCausland C, Samra NS. Anatomy, Head and Neck, Blood Brain Barrier. *StatPearls* (2022)
199. Stanimirovic D, Kemmerich K, Haqqani AS, Farrington GK. Engineering and Pharmacology of Blood–Brain Barrier-Permeable Bispecific Antibodies. *Adv Pharmacol* (2014) 71:301–335. doi: 10.1016/BS.APHA.2014.06.005
200. Yarlagadda A, Alfson E, Clayton AH. The Blood Brain Barrier and the Role of Cytokines in Neuropsychiatry. *Psychiatry (Edgmont)* (2009) 6:18.
201. Frost JL, Schafer DP. Microglia: Architects of the Developing Nervous System. *Trends Cell Biol* (2016) 26:587–597. doi: 10.1016/J.TCB.2016.02.006
202. Li Q, Barres BA. Microglia and macrophages in brain homeostasis and disease. *Nature Reviews Immunology* 2017 18:4 (2017) 18:225–242. doi: 10.1038/nri.2017.125
203. Li Y, Du XF, Liu CS, Wen ZL, Du JL. Reciprocal regulation between resting microglial dynamics and neuronal activity in vivo. *Dev Cell* (2012) 23:1189–1202. doi: 10.1016/J.DEVCEL.2012.10.027
204. Sato K. Effects of Microglia on Neurogenesis. *Glia* (2015) 63:1394. doi: 10.1002/GLIA.22858
205. Ferrini F, De Koninck Y. Microglia control neuronal network excitability via BDNF signalling. *Neural Plast* (2013) 2013: doi: 10.1155/2013/429815

206. Woodburn SC, Bollinger JL, Wohleb ES. The semantics of microglia activation: neuroinflammation, homeostasis, and stress. *Journal of Neuroinflammation* 2021 18:1 (2021) 18:1–16. doi: 10.1186/S12974-021-02309-6
207. Jurga AM, Paleczna M, Kuter KZ. Overview of General and Discriminating Markers of Differential Microglia Phenotypes. *Front Cell Neurosci* (2020) 14:198. doi: 10.3389/FNCEL.2020.00198/BIBTEX
208. Rogers J, Mastroeni D, Leonard B, Joyce J, Grover A. Neuroinflammation in Alzheimer's disease and Parkinson's disease: are microglia pathogenic in either disorder? *Int Rev Neurobiol* (2007) 82:235–246. doi: 10.1016/S0074-7742(07)82012-5
209. Rana A, Musto AE. The role of inflammation in the development of epilepsy. *Journal of Neuroinflammation* 2018 15:1 (2018) 15:1–12. doi: 10.1186/S12974-018-1192-7
210. Vezzani A, French J, Bartfai T, Baram TZ. The role of inflammation in epilepsy. *Nat Rev Neurol* (2011) 7:31–40. doi: 10.1038/nrneurol.2010.178
211. Kinoshita S, Koyama R. Pro- and anti-epileptic roles of microglia. *Neural Regen Res* (2021) 16:1369. doi: 10.4103/1673-5374.300976
212. Kagitani-Shimono K, Kato H, Soeda F, Iwatani Y, Mukai M, Ogawa K, Tominaga K, Nabatame S, Taniike M. Extension of microglial activation is associated with epilepsy and cognitive dysfunction in Tuberous sclerosis complex: A TSPO-PET study. *Neuroimage Clin* (2023) 37:103288. doi: 10.1016/J.NICL.2022.103288
213. Zhang B, Zou J, Han L, Rensing N, Wong M. Microglial activation during epileptogenesis in a mouse model of tuberous sclerosis complex. *Epilepsia* (2016) 57:1317. doi: 10.1111/EPI.13429
214. Cai M, Lin W. The Function of NF-Kappa B During Epilepsy, a Potential Therapeutic Target. *Front Neurosci* (2022) 16:851394. doi: 10.3389/FNINS.2022.851394
215. Martín-Suárez S, Cortes JM, Bonifazi P. Blockage of STAT3 during epileptogenesis prevents GABAergic loss and imprinting of the epileptic state. *Brain* (2023) doi: 10.1093/BRAIN/AWAD055
216. Michev A, Orsini A, Santi V, Bassanese F, Veraldi D, Brambilla I, Marseglia GL, Savasta S, Foadelli T. An Overview of The Role of Tumor Necrosis Factor-Alpha in Epileptogenesis and Its Therapeutic Implications. *Acta Bio Medica : Atenei Parmensis* (2021) 92:2021418. doi: 10.23750/ABM.V92IS4.12667
217. Vezzani A, Baram TZ. New Roles for Interleukin-1 Beta in the Mechanisms of Epilepsy. *Epilepsy Curr* (2007) 7:45–50. doi: 10.1111/J.1535-7511.2007.00165.X
218. Aggarwal BB. Signalling pathways of the TNF superfamily: A double-edged sword. *Nat Rev Immunol* (2003) 3:745–756. doi: 10.1038/nri1184
219. Brenner D, Blaser H, Mak TW. Regulation of tumour necrosis factor signalling: Live or let die. *Nat Rev Immunol* (2015) 15:362–374. doi: 10.1038/nri3834
220. Emmerich CH, Bakshi S, Kelsall IR, Ortiz-Guerrero J, Shpiro N, Cohen P. Lys63/Met1-hybrid ubiquitin chains are commonly formed during the activation of innate immune signalling. *Biochem Biophys Res Commun* (2016) 474:452–461. doi: 10.1016/j.bbrc.2016.04.141

221. Haas TL, Emmerich CH, Gerlach B, Schmukle AC, Cordier SM, Rieser E, Feltham R, Vince J, Warnken U, Wenger T, et al. Recruitment of the Linear Ubiquitin Chain Assembly Complex Stabilizes the TNF-R1 Signaling Complex and Is Required for TNF-Mediated Gene Induction. *Mol Cell* (2009) 36:831–844. doi: 10.1016/j.molcel.2009.10.013
222. Sabio G, Davis RJ. TNF and MAP kinase signalling pathways. *Semin Immunol* (2014) 26:237–245. doi: 10.1016/j.smim.2014.02.009
223. Holbrook J, Lara-Reyna S, Jarosz-Griffiths H, McDermott M. Tumour necrosis factor signalling in health and disease [version 1; referees: 2 approved]. *F1000Res* (2019) 8: doi: 10.12688/f1000research.17023.1
224. Wajant H, Scheurich P. TNFR1-induced activation of the classical NF- κ B pathway. *FEBS J* (2011) 278:862–876. doi: 10.1111/J.1742-4658.2011.08015.X
225. Yu H, Lin L, Zhang Z, Zhang H, Hu H. Targeting NF- κ B pathway for the therapy of diseases: mechanism and clinical study. *Signal Transduction and Targeted Therapy* 2020 5:1 (2020) 5:1–23. doi: 10.1038/s41392-020-00312-6
226. Oeckinghaus A, Ghosh S. The NF-kappaB family of transcription factors and its regulation. *Cold Spring Harb Perspect Biol* (2009) 1: doi: 10.1101/cshperspect.a000034
227. Lang V, Janzen J, Fischer GZ, Soneji Y, Beinke S, Salmeron A, Allen H, Hay RT, Ben-Neriah Y, Ley SC. betaTrCP-mediated proteolysis of NF-kappaB1 p105 requires phosphorylation of p105 serines 927 and 932. *Mol Cell Biol* (2003) 23:402–413. doi: 10.1128/MCB.23.1.402-413.2003
228. Guan H, Hou S, Ricciardi RP. DNA binding of repressor nuclear factor-kappaB p50/p50 depends on phosphorylation of Ser337 by the protein kinase A catalytic subunit. *J Biol Chem* (2005) 280:9957–9962. doi: 10.1074/JBC.M412180200
229. Kuntzen C, Zazzeroni F, Pham CG, Papa S, Bubici C, Knabb JR, Franzoso G. A method for isolating prosurvival targets of NF-kappaB/Rel transcription factors. *Methods Mol Biol* (2007) 399:99–124. doi: 10.1007/978-1-59745-504-6_8
230. Chen FE, Huang D Bin, Chen YQ, Ghosh G. Crystal structure of p50/p65 heterodimer of transcription factor NF- κ B bound to DNA. *Nature* 1998 391:6665 (1998) 391:410–413. doi: 10.1038/34956
231. Chen YQ, Sengchanthalangsy LL, Hackett A, Ghosh G. NF-kappaB p65 (RelA) homodimer uses distinct mechanisms to recognize DNA targets. *Structure* (2000) 8:419–428. doi: 10.1016/S0969-2126(00)00123-4
232. Kaneko N, Kurata M, Yamamoto T, Morikawa S, Masumoto J. The role of interleukin-1 in general pathology. *Inflammation and Regeneration* 2019 39:1 (2019) 39:1–16. doi: 10.1186/S41232-019-0101-5
233. Weber A, Wasiliew P, Kracht M. Interleukin-1 (IL-1) pathway. *Sci Signal* (2010) 3:1. doi: 10.1126/SCISIGNAL.3105CM1/ASSET/016ED8E6-3CC3-495E-97EE-99B43F69CD9F/ASSETS/GRAPHIC/3105CM1-F1.JPEG
234. Motwani M, Pesiridis S, Fitzgerald KA. DNA sensing by the cGAS–STING pathway in health and disease. *Nat Rev Genet* (2019) 20:657–674. doi: 10.1038/s41576-019-0151-1

235. Cheng Z, Dai T, He X, Zhang Z, Xie F, Wang S, Zhang L, Zhou F. The interactions between cGAS-STING pathway and pathogens. *Signal Transduct Target Ther* (2020) 5:1–15. doi: 10.1038/s41392-020-0198-7
236. Gao P, Ascano M, Wu Y, Barchet W, Gaffney BL, Zillinger T, Serganov AA, Liu Y, Jones RA, Hartmann G, et al. Cyclic [G(2',5')pA(3',5')p] is the metazoan second messenger produced by DNA-activated cyclic GMP-AMP synthase. *Cell* (2013) 153:1094–1107. doi: 10.1016/j.cell.2013.04.046
237. Won JK, Bakhom SF. The cytosolic DNA-sensing cGAS–sting pathway in cancer. *Cancer Discov* (2020) 10:26–39. doi: 10.1158/2159-8290.CD-19-0761
238. Xiao TS, Fitzgerald KA. The cGAS-STING Pathway for DNA Sensing. *Mol Cell* (2013) 51:135–139. doi: 10.1016/j.molcel.2013.07.004
239. Civril F, Deimling T, De Oliveira Mann CC, Ablasser A, Moldt M, Witte G, Hornung V, Hopfner KP. Structural mechanism of cytosolic DNA sensing by cGAS. *Nature* (2013) 498:332–337. doi: 10.1038/nature12305
240. Zhao B, Du F, Xu P, Shu C, Sankaran B, Bell SL, Liu M, Lei Y, Gao X, Fu X, et al. A conserved PLPLRT/SD motif of STING mediates the recruitment and activation of TBK1. *Nature* (2019) 569:718–722. doi: 10.1038/s41586-019-1228-x
241. Tanaka Y, Chen ZJ. STING specifies IRF3 phosphorylation by TBK1 in the cytosolic DNA signaling pathway. *Sci Signal* (2012) 5:ra20–ra20. doi: 10.1126/scisignal.2002521
242. Dunphy G, Flannery SM, Almine JF, Connolly DJ, Paulus C, Jønsson KL, Jakobsen MR, Nevels MM, Bowie AG, Unterholzner L. Non-canonical Activation of the DNA Sensing Adaptor STING by ATM and IFI16 Mediates NF-κB Signaling after Nuclear DNA Damage. *Mol Cell* (2018) 71:745–760.e5. doi: 10.1016/j.molcel.2018.07.034
243. Möser C V., Stephan H, Altenrath K, Kynast KL, Russe OQ, Olbrich K, Geisslinger G, Niederberger E. TANK-binding kinase 1 (TBK1) modulates inflammatory hyperalgesia by regulating MAP kinases and NF-κB dependent genes. *J Neuroinflammation* (2015) 12:1–13. doi: 10.1186/S12974-015-0319-3/FIGURES/7
244. Tanaka T, Narazaki M, Kishimoto T. Il-6 in inflammation, Immunity, And disease. *Cold Spring Harb Perspect Biol* (2014) 6: doi: 10.1101/cshperspect.a016295
245. Luo Y, Zheng SG. Hall of fame among pro-inflammatory cytokines: Interleukin-6 gene and its transcriptional regulation mechanisms. *Front Immunol* (2016) 7:604. doi: 10.3389/fimmu.2016.00604
246. Su H, Lei CT, Zhang C. Interleukin-6 signaling pathway and its role in kidney disease: An update. *Front Immunol* (2017) 8:405. doi: 10.3389/fimmu.2017.00405
247. Kumar H, Kawai T, Akira S. Pathogen recognition by the innate immune system. *Int Rev Immunol* (2011) 30:16–34. doi: 10.3109/08830185.2010.529976
248. Barnes TC, Anderson ME, Moots RJ. The Many Faces of Interleukin-6: The Role of IL-6 in Inflammation, Vasculopathy, and Fibrosis in Systemic Sclerosis. *Int J Rheumatol* (2011) 2011: doi: 10.1155/2011/721608

249. Rose-John S. Il-6 trans-signaling via the soluble IL-6 receptor: Importance for the proinflammatory activities of IL-6. *Int J Biol Sci* (2012) 8:1237–1247. doi: 10.7150/ijbs.4989
250. Reeh H, Rudolph N, Billing U, Christen H, Streif S, Bullinger E, Schliemann-Bullinger M, Findeisen R, Schaper F, Huber HJ, et al. Response to IL-6 trans- and IL-6 classic signalling is determined by the ratio of the IL-6 receptor α to gp130 expression: Fusing experimental insights and dynamic modelling. *Cell Communication and Signaling* (2019) 17: doi: 10.1186/s12964-019-0356-0
251. Rose-John S. Interleukin-6 biology is coordinated by membrane-bound and soluble receptors: role in inflammation and cancer. *J Leukoc Biol* (2006) 80:227–236. doi: 10.1189/jlb.1105674
252. Scheller J, Schuster B, Hölscher C, Yoshimoto T, Rose-John S. No inhibition of IL-27 signaling by soluble gp130. *Biochem Biophys Res Commun* (2005) 326:724–728. doi: 10.1016/j.bbrc.2004.11.098
253. Kagan P, Sultan M, Tachlytski I, Safran M, Ben-Ari Z. Both MAPK and STAT3 signal transduction pathways are necessary for IL-6-dependent hepatic stellate cells activation. *PLoS One* (2017) 12: doi: 10.1371/journal.pone.0176173
254. Kamran MZ, Patil P, Gude RP. Role of STAT3 in cancer metastasis and translational advances. *Biomed Res Int* (2013) 2013:421821. doi: 10.1155/2013/421821
255. Hillmer EJ, Zhang H, Li HS, Watowich SS. STAT3 signaling in immunity. *Cytokine Growth Factor Rev* (2016) 31:1–15. doi: 10.1016/j.cytogfr.2016.05.001
256. Wormald S, Zhang JG, Krebs DL, Mielke LA, Silver J, Alexander WS, Speed TP, Nicola NA, Hilton DJ. The comparative roles of suppressor of cytokine signaling-1 and -3 in the inhibition and desensitization of cytokine signaling. *Journal of Biological Chemistry* (2006) 281:11135–11143. doi: 10.1074/jbc.M509595200
257. Samavati L, Rastogi R, Du W, Hüttemann M, Fite A, Franchi L. STAT3 tyrosine phosphorylation is critical for interleukin 1 beta and interleukin-6 production in response to lipopolysaccharide and live bacteria. *Mol Immunol* (2009) 46:1867–1877. doi: 10.1016/J.MOLIMM.2009.02.018
258. Valin A, Ruano Y, Del Rey MJ, García-Herrero CM, Martín-Guerrero E, Bravo B, Cañete JD, Rodríguez-Peralto JL PJL. Crosstalk Between IL-6 and TNF-Alpha Signaling Pathway in Rheumatoid Arthritis Synovial Fibroblasts [abstract]. *Arthritis Rheumatol* (2016) 68:
259. Rotter V, Nagaev I, Smith U. Interleukin-6 (IL-6) Induces Insulin Resistance in 3T3-L1 Adipocytes and Is, Like IL-8 and Tumor Necrosis Factor- α , Overexpressed in Human Fat Cells from Insulin-resistant Subjects. *Journal of Biological Chemistry* (2003) 278:45777–45784. doi: 10.1074/jbc.M301977200
260. Matsusaka T, Fujikawa K, Nishio Y, Mukaida N, Matsushima K, Kishimoto T, Akira S. Transcription factors NF-IL6 and NF- κ B synergistically activate transcription of the inflammatory cytokines, interleukin 6 and interleukin 8. *Proc Natl Acad Sci U S A* (1993) 90:10193–10197. doi: 10.1073/pnas.90.21.10193
261. Libermann TA, Baltimore D. Activation of interleukin-6 gene expression through the NF-kappa B transcription factor. *Mol Cell Biol* (1990) 10:2327–2334. doi: 10.1128/mcb.10.5.2327

262. Squarize CH, Castilho RM, Sriuranpong V, Pinto DS, Gutkind JS. Molecular cross-talk between the NF κ B and STAT3 signaling pathways in head and neck squamous cell carcinoma. *Neoplasia* (2006) 8:733–746. doi: 10.1593/neo.06274
263. West NR. Coordination of immune-stroma crosstalk by IL-6 family cytokines. *Front Immunol* (2019) 10:1093. doi: 10.3389/fimmu.2019.01093
264. Hungness ES, Luo G, Pritts TA, Sun X, Robb BW, Hershko D, Hasselgren P-O. Transcription factors C/EBP- β and - δ regulate IL-6 production in IL-1 β -stimulated human enterocytes. *J Cell Physiol* (2002) 192:64–70. doi: 10.1002/jcp.10116
265. Tian Q, Miyazaki R, Ichiki T, Imayama I, Inanaga K, Ohtsubo H, Yano K, Takeda K, Sunagawa K. Inhibition of tumor necrosis factor- α -induced interleukin-6 expression by Telmisartan through cross-talk of peroxisome proliferator-activated receptor- γ with nuclear factor κ B and CCAAT/Enhancer-Binding protein- β . *Hypertension* (2009) 53:798–804. doi: 10.1161/HYPERTENSIONAHA.108.126656
266. Crosstalk between TNF and IL-6/STAT3 signaling revealed in HEK-Blue IL-6 cells | RISE:2020. <https://www.northeastern.edu/rise/presentations/crosstalk-between-tnf-and-il-6stat3-signaling-revealed-in-hek-blue-il-6-cells/> [Accessed April 3, 2020]
267. Al-Shanti N, Saini A, Faulkner SH, Stewart CE. Beneficial synergistic interactions of TNF- α and IL-6 in C2 skeletal myoblasts—Potential cross-talk with IGF system. *Growth Factors* (2008) 26:61–73. doi: 10.1080/08977190802025024
268. Xu Z, Xiao SB, Xu P, Xie Q, Cao L, Wang D, Luo R, Zhong Y, Chen HC, Fang LR. miR-365, a novel negative regulator of interleukin-6 gene expression, is cooperatively regulated by Sp1 and NF- κ B. *Journal of Biological Chemistry* (2011) 286:21401–21412. doi: 10.1074/jbc.M110.198630
269. Kiu H, Hilton DJ, Nicola NA, Ernst M, Marquez R, Alexander WS, Roberts AW, Mcmanus EJ. Mechanism of crosstalk inhibition of IL-6 signaling in response to LPS and TNF α . *Growth Factors* (2007) 25:319–328. doi: 10.1080/08977190701830151
270. Bode JG, Nimmesgern A, Schmitz J, Schaper F, Schmitt M, Frisch W, Häussinger D, Heinrich PC, Graeve L. LPS and TNF α induce SOCS3 mRNA and inhibit IL-6-induced activation of STAT3 in macrophages. *FEBS Lett* (1999) 463:365–370. doi: 10.1016/S0014-5793(99)01662-2
271. Bode JG, Schweigart J, Kehrmann J, Ehrling C, Schaper F, Heinrich PC, Häussinger D. TNF- α Induces Tyrosine Phosphorylation and Recruitment of the Src Homology Protein-Tyrosine Phosphatase 2 to the gp130 Signal-Transducing Subunit of the IL-6 Receptor Complex. *The Journal of Immunology* (2003) 171:257–266. doi: 10.4049/jimmunol.171.1.257
272. braintumourresearch.org. Exposing the Financial Impact of a Brain Tumour Diagnosis. <https://www.braintumourresearch.org/campaigning/stark-facts> [Accessed May 18, 2023]
273. Singh R, Munakomi S. Embryology, Neural Tube. *StatPearls* (2022)
274. Fedorova V, Vanova T, Elrefae L, Pospisil J, Petrasova M, Kolajova V, Hudacova Z, Baniariova J, Barak M, Peskova L, et al. Differentiation of neural rosettes from human pluripotent stem cells in vitro is sequentially regulated on a molecular level and accomplished by the mechanism reminiscent of secondary neurulation. *Stem Cell Res* (2019) 40:101563. doi: 10.1016/J.SCR.2019.101563
275. Gilbert SF. The Neural Crest. (2000)

276. Ackerman S. The Development and Shaping of the Brain. (1992)
277. Bystron I, Blakemore C, Rakic P. Development of the human cerebral cortex: Boulder Committee revisited. *Nature Reviews Neuroscience* 2008 9:2 (2008) 9:110–122. doi: 10.1038/nrn2252
278. Hevner RF. Intermediate progenitors and Tbr2 in cortical development. *J Anat* (2019) 235:616–625. doi: 10.1111/JOA.12939
279. Gil-Sanz C, Franco SJ, Martinez-Garay I, Espinosa A, Harkins-Perry S, Müller U. Cajal-Retzius cells instruct neuronal migration by coincidence signaling between secreted and contact-dependent guidance cues. *Neuron* (2013) 79:461. doi: 10.1016/J.NEURON.2013.06.040
280. Kaplan ES, Ramos-Laguna KA, Mihalas AB, Daza RAM, Hevner RF. Neocortical Sox9+ radial glia generate glutamatergic neurons for all layers, but lack discernible evidence of early laminar fate restriction. *Neural Dev* (2017) 12:1–10. doi: 10.1186/S13064-017-0091-4/FIGURES/3
281. Lavdas AA, Grigoriou M, Pachnis V, Parnavelas JG. The medial ganglionic eminence gives rise to a population of early neurons in the developing cerebral cortex. *J Neurosci* (1999) 19:7881–7888. doi: 10.1523/JNEUROSCI.19-18-07881.1999
282. Tramontin AD, García-Verdugo JM, Lim DA, Alvarez-Buylla A. Postnatal development of radial glia and the ventricular zone (VZ): a continuum of the neural stem cell compartment. *Cereb Cortex* (2003) 13:580–587. doi: 10.1093/CERCOR/13.6.580
283. Cuadros MA, Sepulveda MR, Martin-Oliva D, Marín-Teva JL, Neubrand VE. Microglia and Microglia-Like Cells: Similar but Different. *Front Cell Neurosci* (2022) 16:33. doi: 10.3389/FNCEL.2022.816439/BIBTEX
284. Mander PK, Jekabsone A, Brown GC. Microglia proliferation is regulated by hydrogen peroxide from NADPH oxidase. *J Immunol* (2006) 176:1046–1052. doi: 10.4049/JIMMUNOL.176.2.1046
285. Gómez-Nicola D, Fransen NL, Suzzi S, Hugh Perry V. Regulation of Microglial Proliferation during Chronic Neurodegeneration. *The Journal of Neuroscience* (2013) 33:2481. doi: 10.1523/JNEUROSCI.4440-12.2013
286. Tee AR, Sampson JR, Pal DK, Bateman JM. The role of mTOR signalling in neurogenesis, insights from tuberous sclerosis complex. *Semin Cell Dev Biol* (2016) 52:12. doi: 10.1016/J.SEMCDB.2016.01.040
287. Zimmer TS, Broekaart DWM, Gruber VE, van Vliet EA, Mühlebner A, Aronica E. Tuberous Sclerosis Complex as Disease Model for Investigating mTOR-Related Gliopathy During Epileptogenesis. *Front Neurol* (2020) 11:1028. doi: 10.3389/FNEUR.2020.01028/BIBTEX
288. Mühlebner A, Van Scheppingen J, De Neef A, Bongaarts A, Zimmer TS, Mills JD, Jansen FE, Spliet WGM, Krsek P, Zamecnik J, et al. Myelin Pathology Beyond White Matter in Tuberous Sclerosis Complex (TSC) Cortical Tubers. *J Neuropathol Exp Neurol* (2020) 79:1054. doi: 10.1093/JNEN/NLAA090
289. Xanthos DN, Sandkühler J. Neurogenic neuroinflammation: inflammatory CNS reactions in response to neuronal activity. *Nat Rev Neurosci* (2014) 15:43–53. doi: 10.1038/NRN3617
290. Boer K, Jansen F, Nellist M, Redeker S, van den Ouweland AMW, Spliet WGM, van Nieuwenhuizen O, Troost D, Crino PB, Aronica E. Inflammatory processes in cortical tubers

- and subependymal giant cell tumors of tuberous sclerosis complex. *Epilepsy Res* (2008) 78:7–21. doi: 10.1016/j.eplepsyres.2007.10.002
291. Wildonger J, Jan LY, Jan YN. The Tsc1–Tsc2 complex influences neuronal polarity by modulating TORC1 activity and SAD levels. *Genes Dev* (2008) 22:2447. doi: 10.1101/GAD.1724108
 292. Kalantari BN, Salamon N. Neuroimaging of Tuberous Sclerosis: Spectrum of Pathologic Findings and Frontiers in Imaging. *http://dx.doi.org/102214/AJR072928* (2012) 190: doi: 10.2214/AJR.07.2928
 293. Alshoabi SA, Hamid AM, Alhazmi FH, Qurashi AA, Abdulaal OM, Aloufi KM, Daqqaq TS. Diagnostic features of tuberous sclerosis complex: case report and literature review. *Quant Imaging Med Surg* (2022) 12:84661–84861. doi: 10.21037/QIMS-21-412
 294. Wataya-Kaneda M, Tanaka M, Hamasaki T, Katayama I. Trends in the Prevalence of Tuberous Sclerosis Complex Manifestations: An Epidemiological Study of 166 Japanese Patients. *PLoS One* (2013) 8:63910. doi: 10.1371/JOURNAL.PONE.0063910
 295. O’Callaghan FJK, Martyn CN, Renowden S, Noakes M, Presdee D, Osborne JP. Subependymal nodules, giant cell astrocytomas and the tuberous sclerosis complex: a population-based study. *Arch Dis Child* (2008) 93:751–754. doi: 10.1136/ADC.2007.125880
 296. Stein JR, Reidman DA. Imaging Manifestations of a Subependymal Giant Cell Astrocytoma in Tuberous Sclerosis. *Case Rep Radiol* (2016) 2016:1–5. doi: 10.1155/2016/3750450
 297. How TSC Affects Brain Anatomy. <https://www.massgeneral.org/neurology/tsc/patient-education/how-tsc-affects-brain-anatomy> [Accessed May 18, 2023]
 298. Jansen AC, Belousova E, Benedik MP, Carter T, Cottin V, Curatolo P, Dahlin M, D’Amato L, D’Augères GB, De Vries PJ, et al. Clinical Characteristics of Subependymal Giant Cell Astrocytoma in Tuberous Sclerosis Complex. *Front Neurol* (2019) 10:705. doi: 10.3389/FNEUR.2019.00705
 299. Elousrouti LT, Lamchahab M, Bougtoub N, Elfatemi H, Chbani L, Harmouch T, Maaroufi M, Amarti Riffi A. Subependymal giant cell astrocytoma (SEGA): a case report and review of the literature. *J Med Case Rep* (2016) 10: doi: 10.1186/S13256-016-0818-6
 300. Bongaarts A, Giannikou K, Reinten RJ, Anink JJ, Mills JD, Jansen FE, Spliet WGM, den Dunnen WFA, Coras R, Blümcke I, et al. Subependymal giant cell astrocytomas in Tuberous Sclerosis Complex have consistent TSC1/TSC2 biallelic inactivation, and no BRAF mutations. *Oncotarget* (2017) 8:95516–95529. doi: 10.18632/oncotarget.20764
 301. SHEPHERD CW, GOMEZ MR, LIE JT, CROWSON CS. Causes of death in patients with tuberous sclerosis. *Mayo Clin Proc* (1991) 66:792–796. doi: 10.1016/S0025-6196(12)61196-3
 302. Curatolo P, Moavero R, de Vries PJ. Neurological and neuropsychiatric aspects of tuberous sclerosis complex. *Lancet Neurol* (2015) 14:733–745. doi: 10.1016/S1474-4422(15)00069-1
 303. Nishio S, Morioka T, Suzuki S, Kira R, Mihara F, Fukui M. Subependymal giant cell astrocytoma: clinical and neuroimaging features of four cases. *J Clin Neurosci* (2001) 8:31–34. doi: 10.1054/JOCN.2000.0767
 304. Campen CJ, Porter BE. Subependymal Giant Cell Astrocytoma (SEGA) Treatment Update. *Curr Treat Options Neurol* (2011) 13:380. doi: 10.1007/S11940-011-0123-Z

305. Tang X, Angst G, Haas M, Yang F, Wang C. The Characterization of a Subependymal Giant Astrocytoma-Like Cell Line from Murine Astrocyte with mTORC1 Hyperactivation. *Int J Mol Sci* (2021) 22: doi: 10.3390/IJMS22084116
306. Ebrahimi-Fakhari D, Franz DN. Pharmacological treatment strategies for subependymal giant cell astrocytoma (SEGA). <https://doi.org/10.1080/1465656620201751124> (2020) 21:1329–1336. doi: 10.1080/14656566.2020.1751124
307. Danassegarane G, Tinois J, Sahler Y, Aouaissa S, Riffaud L. Subependymal giant-cell astrocytoma: A surgical review in the modern era of mTOR inhibitors. *Neurochirurgie* (2022) 68:627–636. doi: 10.1016/J.NEUCHI.2022.07.003
308. Tomoto K, Fujimoto A, Inenaga C, Okanishi T, Imai S, Ogai M, Fukunaga A, Nakamura H, Sato K, Obana A, et al. Experience using mTOR inhibitors for subependymal giant cell astrocytoma in tuberous sclerosis complex at a single facility. *BMC Neurol* (2021) 21:1–7. doi: 10.1186/S12883-021-02160-5/FIGURES/1
309. Weidman DR, Palasamudram S, Zak M, Whitney R, McCoy B, Bouffet E, Taylor M, Shroff M, Bartels U. The effect of mTOR inhibition on obstructive hydrocephalus in patients with tuberous sclerosis complex (TSC) related subependymal giant cell astrocytoma (SEGA). *J Neurooncol* (2020) 147:731–736. doi: 10.1007/S11060-020-03487-8/FIGURES/2
310. Franz DN, Agricola K, Mays M, Tudor C, Care MM, Holland-Bouley K, Berkowitz N, Miao S, Peyrard S, Krueger DA. Everolimus for subependymal giant cell astrocytoma: 5-year final analysis. *Ann Neurol* (2015) 78:929–938. doi: 10.1002/ANA.24523
311. Franz DN, Belousova E, Sparagana S, Bebin EM, Frost MD, Kuperman R, Witt O, Kohrman MH, Flamini JR, Wu JY, et al. Long-Term Use of Everolimus in Patients with Tuberous Sclerosis Complex: Final Results from the EXIST-1 Study. *PLoS One* (2016) 11: doi: 10.1371/JOURNAL.PONE.0158476
312. Van Tassel P, Curé JK, Holden KR. Cystlike white matter lesions in tuberous sclerosis. *AJNR Am J Neuroradiol* (1997) 18:1367.
313. Shahid A. Resecting the epileptogenic tuber: what happens in the long term? *Epilepsia* (2013) 54 Suppl 9:135–138. doi: 10.1111/EPI.12458
314. Baskin HJ. The pathogenesis and imaging of the tuberous sclerosis complex. *Pediatr Radiol* (2008) 38:936–952. doi: 10.1007/S00247-008-0832-Y/TABLES/3
315. Wang MX, Segaran N, Bhalla S, Pickhardt PJ, Lubner MG, Katabathina VS, Ganeshan D. Tuberous sclerosis: Current update. *Radiographics* (2021) 41:1992–2010. doi: 10.1148/RG.2021210103/ASSET/IMAGES/LARGE/RG.2021210103TBL4.JPEG
316. Chu-Shore CJ, Major P, Montenegro M, Thiele E. Cyst-like tubers are associated with TSC2 and epilepsy in tuberous sclerosis complex. *Neurology* (2009) 72:1165–1169. doi: 10.1212/01.WNL.0000345365.92821.86
317. Mühlebner A, Van Scheppingen J, Hulshof HM, Scholl T, Iyer AM, Anink JJ, Nellist MD, Jansen FE, Spliet WGM, Krsek P, et al. Novel Histopathological Patterns in Cortical Tubers of Epilepsy Surgery Patients with Tuberous Sclerosis Complex. *PLoS One* (2016) 11: doi: 10.1371/JOURNAL.PONE.0157396

318. Pascual-Castroviejo I, Hernández-Moneo JL, Pascual-Pascual SI, Viaño J, Gutiérrez-Molina M, Velazquez-Fragua R, Quiñones Tapia D, Morales Bastos C. Significance of tuber size for complications of tuberous sclerosis complex. *Neurología (English Edition)* (2013) 28:550–557. doi: 10.1016/J.NRLENG.2013.10.013
319. Ruppe V, Dilsiz P, Reiss CS, Carlson C, Devinsky O, Zagzag D, Weiner HL, Talos DM. Developmental brain abnormalities in tuberous sclerosis complex: A comparative tissue analysis of cortical tubers and perituberal cortex. *Epilepsia* (2014) 55:539–550. doi: 10.1111/EPI.12545/SUPPINFO
320. Mühlebner A, Iyer AM, Van Scheppingen J, Anink JJ, Jansen FE, Veersema TJ, Braun KP, Spliet WGM, Van Hecke W, Söylemezoğlu F, et al. Specific pattern of maturation and differentiation in the formation of cortical tubers in tuberous sclerosis complex (TSC): Evidence from layer-specific marker expression. *J Neurodev Disord* (2016) 8:1–14. doi: 10.1186/S11689-016-9142-0/FIGURES/6
321. Talos DM, Kwiatkowski DJ, Cordero K, Black PM, Jensen FE. Cell-specific alterations of glutamate receptor expression in tuberous sclerosis complex cortical tubers. *Ann Neurol* (2008) 63:454–465. doi: 10.1002/ANA.21342
322. Cepeda C, Levinson S, Yazon VW, Barry J, Mathern GW, Fallah A, Vinters H V., Levine MS, Wu JY. Cellular antiseizure mechanisms of everolimus in pediatric tuberous sclerosis complex, cortical dysplasia, and non-mTOR-mediated etiologies. *Epilepsia Open* (2018) 3:180. doi: 10.1002/EPI4.12253
323. Feliciano DM. The Neurodevelopmental Pathogenesis of Tuberous Sclerosis Complex (TSC). *Front Neuroanat* (2020) 14: doi: 10.3389/FNANA.2020.00039
324. Lachhwani DK, Pestana E, Gupta A, Kotagal P, Bingaman W, Wyllie E. Identification of candidates for epilepsy surgery in patients with tuberous sclerosis. *Neurology* (2005) 64:1651–1654. doi: 10.1212/01.WNL.0000160389.93984.53
325. Zhang K, Hu W han, Zhang C, Meng F gang, Chen N, Zhang J guo. Predictors of seizure freedom after surgical management of tuberous sclerosis complex: A systematic review and meta-analysis. *Epilepsy Res* (2013) 105:377–383. doi: 10.1016/J.EPILEPSYRES.2013.02.016
326. Watrin F, Manent JB, Cardoso C, Represa A. Causes and Consequences of Gray Matter Heterotopia. *CNS Neurosci Ther* (2015) 21:112. doi: 10.1111/CNS.12322
327. Chu-Shore CJ, Major P, Camposano S, Muzykewicz D, Thiele EA. The natural history of epilepsy in tuberous sclerosis complex. *Epilepsia* (2010) 51:1236–1241. doi: 10.1111/J.1528-1167.2009.02474.X
328. O’Callaghan FJK, Harris T, Joinson C, Bolton P, Noakes M, Presdee D, Renowden S, Shiell A, Martyn CN, Osborne JP. The relation of infantile spasms, tubers, and intelligence in tuberous sclerosis complex. *Arch Dis Child* (2004) 89:530–533. doi: 10.1136/ADC.2003.026815
329. Jansen FE, Vincken KL, Algra A, Anbeek P, Braams O, Nellist M, Zonnenberg BA, Jennekens-Schinkel A, Van Den Ouweland A, Halley D, et al. Cognitive impairment in tuberous sclerosis complex is a multifactorial condition. *Neurology* (2008) 70:916–923. doi: 10.1212/01.WNL.0000280579.04974.C0
330. McIntosh WC, Das JM. Temporal Seizure. *StatPearls* (2022)

331. Mukonoweshuro W, Wilkinson ID, Griffiths PD. Proton MR Spectroscopy of Cortical Tubers in Adults with Tuberous Sclerosis Complex. *AJNR Am J Neuroradiol* (2001) 22:1920.
332. Prabowo AS, Anink JJ, Lammens M, Nellist M, Van Den Ouweland AMW, Adle-Biassette H, Sarnat HB, Flores-Sarnat L, Crino PB, Aronica E. Fetal Brain Lesions in Tuberous Sclerosis Complex: TORC1 Activation and Inflammation. *Brain Pathology* (2013) 23:45. doi: 10.1111/J.1750-3639.2012.00616.X
333. Zhang B, Zou J, Rensing NR, Yang M, Wong M. Inflammatory mechanisms contribute to the neurological manifestations of tuberous sclerosis complex. *Neurobiol Dis* (2015) 80:70–79. doi: 10.1016/j.nbd.2015.04.016
334. Balosso S, Maroso M, Sanchez-Alavez M, Ravizza T, Frasca A, Bartfai T, Vezzani A. A novel non-transcriptional pathway mediates the proconvulsive effects of interleukin-1beta. *Brain* (2008) 131:3256–3265. doi: 10.1093/BRAIN/AWN271
335. Maldonado M, Baybis M, Newman D, Kolson DL, Chen W, McKhann G, Gutmann DH, Crino PB. Expression of ICAM-1, TNF- α , NF κ B, and MAP kinase in tubers of the tuberous sclerosis complex. *Neurobiol Dis* (2003) 14:279–290. doi: 10.1016/S0969-9961(03)00127-X
336. Gruber VE, Luinenburg MJ, Colleselli K, Endmayr V, Anink JJ, Zimmer TS, Jansen F, Gosselaar P, Coras R, Scholl T, et al. Increased expression of complement components in tuberous sclerosis complex and focal cortical dysplasia type 2B brain lesions. *Epilepsia* (2022) 63:364. doi: 10.1111/EPI.17139
337. Kopczyńska M, Zelek WM, Vespa S, Touchard S, Wardle M, Loveless S, Thomas RH, Hamandi K, Morgan BP. Complement system biomarkers in epilepsy. *Seizure* (2018) 60:1–7. doi: 10.1016/J.SEIZURE.2018.05.016
338. Maroso M, Balosso S, Ravizza T, Iori V, Wright CI, French J, Vezzani A. Interleukin-1 β biosynthesis inhibition reduces acute seizures and drug resistant chronic epileptic activity in mice. *Neurotherapeutics* (2011) 8:304–315. doi: 10.1007/S13311-011-0039-Z
339. Digital J, Commons Phase JD, Sansalone K, Dilsiz P, Weiner H, Devinsky O, Talos DM. Neoangiogenesis and Blood-brain Barrier Dysfunction in Human Neoangiogenesis and Blood-brain Barrier Dysfunction in Human TSC Brain Lesions TSC Brain Lesions.
340. Ballabh P, Braun A, Nedergaard M. The blood–brain barrier: an overview: Structure, regulation, and clinical implications. *Neurobiol Dis* (2004) 16:1–13. doi: 10.1016/J.NBD.2003.12.016
341. Zhang ZG, Zhang L, Jiang Q, Zhang R, Davies K, Powers C, Van Bruggen N, Chopp M. VEGF enhances angiogenesis and promotes blood-brain barrier leakage in the ischemic brain. *J Clin Invest* (2000) 106:829–838. doi: 10.1172/JCI9369
342. Kiani L. Blood–brain barrier disruption following seizures. *Nature Reviews Neurology* 2023 19:4 (2023) 19:196–196. doi: 10.1038/s41582-023-00794-2
343. Marchi N, Granata T, Ghosh C, Janigro D. Blood–brain barrier dysfunction and epilepsy: Pathophysiologic role and therapeutic approaches. *Epilepsia* (2012) 53:1877. doi: 10.1111/J.1528-1167.2012.03637.X

344. Galvan V, Hart MJ. Vascular mTOR-dependent mechanisms linking the control of aging to Alzheimer's disease. *Biochim Biophys Acta* (2016) 1862:992. doi: 10.1016/J.BBADIS.2015.11.010
345. Eissa N, Sadeq A, Sasse A, Sadek B. Role of Neuroinflammation in Autism Spectrum Disorder and the Emergence of Brain Histaminergic System. Lessons Also for BPSD? *Front Pharmacol* (2020) 11:886. doi: 10.3389/FPHAR.2020.00886/BIBTEX
346. Hu C, Li H, Li J, Luo X, Hao Y. Microglia: Synaptic modulator in autism spectrum disorder. *Front Psychiatry* (2022) 13:2601. doi: 10.3389/FPSYT.2022.958661/BIBTEX
347. Rodriguez JI, Kern JK. Evidence of microglial activation in autism and its possible role in brain underconnectivity. *Neuron Glia Biol* (2011) 7:205. doi: 10.1017/S1740925X12000142
348. Young AMH, Campbell E, Lynch S, Suckling J, Powis SJ. Aberrant NF-KappaB Expression in Autism Spectrum Condition: A Mechanism for Neuroinflammation. *Front Psychiatry* (2011) 2: doi: 10.3389/FPSYT.2011.00027
349. Malik M, Tauqeer Z, Sheikh AM, Wen G, Nagori A, Yang K, Brown WT, Li X. NF-κB Signaling in the Brain of Autistic Subjects. *Mediators Inflamm* (2011) 2011: doi: 10.1155/2011/785265
350. Yu J, Astrinidis A, Howard S, Henske EP. Estradiol and tamoxifen stimulate LAM-associated angiomyolipoma cell growth and activate both genomic and nongenomic signaling pathways. *Am J Physiol Lung Cell Mol Physiol* (2004) 286:694–700. doi: 10.1152/AJPLUNG.00204.2003/ASSET/IMAGES/LARGE/ZH50040416920005.JPEG
351. Dabora SL, Kwiatkowski DJ, Franz DN, Roberts PS, Nieto A, Chung J, Choy YS, Reeve MP, Thiele E, Egelhoff JC, et al. Mutational analysis in a cohort of 224 tuberous sclerosis patients indicates increased severity of TSC2, compared with TSC1, disease in multiple organs. *Am J Hum Genet* (2001) 68:64–80. doi: 10.1086/316951
352. Hong F, Larrea MD, Doughty C, Kwiatkowski DJ, Squillace R, Slingerland JM. mTOR-raptor binds and activates SGK1 to regulate p27 phosphorylation. *Mol Cell* (2008) 30:701–711. doi: 10.1016/J.MOLCEL.2008.04.027
353. Zhang H, Cicchetti G, Onda H, Koon HB, Asrican K, Bajraszewski N, Vazquez F, Carpenter CL, Kwiatkowski DJ. Loss of Tsc1/Tsc2 activates mTOR and disrupts PI3K-Akt signaling through downregulation of PDGFR. *J Clin Invest* (2003) 112:1223–1233. doi: 10.1172/JCI17222
354. Astrinidis A, Cash TP, Hunter DS, Walker CL, Chernoff J, Henske EP. Tuberlin, the tuberous sclerosis complex 2 tumor suppressor gene product, regulates Rho activation, cell adhesion and migration. *Oncogene* (2002) 21:8470–8476. doi: 10.1038/SJ.ONC.1205962
355. Alsaqati M, Davis BA, Wood J, Jones MM, Jones L, Westwood A, Petter O, Isles AR, Linden D, Van den Bree M, et al. NRSF/REST lies at the intersection between epigenetic regulation, miRNA-mediated gene control and neurodevelopmental pathways associated with Intellectual disability (ID) and Schizophrenia. *Transl Psychiatry* (2022) 12: doi: 10.1038/S41398-022-02199-Z
356. Cellosaurus cell line GM23338 (CVCL_F182). https://www.cellosaurus.org/CVCL_F182 [Accessed August 18, 2023]
357. Johnson CE, Dunlop EA, Seifan S, McCann HD, Hay T, Parfitt GJ, Jones AT, Giles PJ, Shen MH, Sampson JR, et al. Loss of tuberous sclerosis complex 2 sensitizes tumors to

- nelfinavir–bortezomib therapy to intensify endoplasmic reticulum stress-induced cell death. *Oncogene* (2018) 37:5913–5925. doi: 10.1038/s41388-018-0381-2
358. Love MI, Huber W, Anders S. Moderated estimation of fold change and dispersion for RNA-seq data with DESeq2. *Genome Biol* (2014) 15:1–21. doi: 10.1186/S13059-014-0550-8/FIGURES/9
359. Siniscalco D, Schultz S, Brigida AL, Antonucci N. Inflammation and neuro-immune dysregulations in autism spectrum disorders. *Pharmaceuticals* (2018) 11: doi: 10.3390/ph11020056
360. Zimmer TS, Korotkov A, Zwakenberg S, Jansen FE, Zwartkuis FJT, Rensing NR, Wong M, Mühlebner A, van Vliet EA, Aronica E, et al. Upregulation of the pathogenic transcription factor SPI1/PU.1 in tuberous sclerosis complex and focal cortical dysplasia by oxidative stress. *Brain Pathology* (2021) doi: 10.1111/bpa.12949
361. Nechama M, Makayes Y, Resnick E, Meir K, Volovelsky O. Rapamycin and dexamethasone during pregnancy prevent tuberous sclerosis complex–associated cystic kidney disease. *JCI Insight* (2020) 5: doi: 10.1172/jci.insight.136857
362. Blair JD, Hockemeyer D, Bateup HS. Genetically engineered human cortical spheroid models of tuberous sclerosis. *Nat Med* (2018) 24:1568–1578. doi: 10.1038/s41591-018-0139-y
363. Jeong A, Nakagawa JA, Wong M. Predictors of Drug-Resistant Epilepsy in Tuberous Sclerosis Complex. *J Child Neurol* (2017) 32:1092–1098. doi: 10.1177/0883073817737446
364. Moavero R, Pinci M, Bombardieri R, Curatolo P. The management of subependymal giant cell tumors in tuberous sclerosis: A clinician’s perspective. *Child’s Nervous System* (2011) 27:1203–1210. doi: 10.1007/s00381-011-1406-0
365. Goncharova EA, Goncharov DA, Damera G, Tliba O, Amrani Y, Panettieri RA, Krymskaya VP. Signal transducer and activator of transcription 3 is required for abnormal proliferation and survival of TSC2-deficient cells: Relevance to pulmonary lymphangiomyomatosis. *Mol Pharmacol* (2009) 76:766–777. doi: 10.1124/mol.109.057042
366. Dodd KM, Tee AR. STAT3 and mTOR: Co-operating to drive HIF and angiogenesis. *Oncoscience* (2015) 2:913–914. doi: 10.18632/oncoscience.272
367. Nagarkatti P, Pandey R, Rieder SA, Hegde VL, Nagarkatti M. Cannabinoids as novel anti-inflammatory drugs. *Future Med Chem* (2009) 1:1333–1349. doi: 10.4155/fmc.09.93
368. Nickels K. Cannabidiol in patients with intractable epilepsy due to TSC: A possible medication but not a miracle. *Epilepsy Curr* (2017) 17:91–92. doi: 10.5698/1535-7511.17.2.91
369. Xu Z, Xue T, Zhang Z, Wang X, Xu P, Zhang J, Lei X, Li Y, Xie Y, Wang L, et al. Role of signal transducer and activator of transcription-3 in up-regulation of GFAP after epilepsy. *Neurochem Res* (2011) 36:2208–2215. doi: 10.1007/s11064-011-0576-1
370. Reichenbach N, Delekate A, Plescher M, Schmitt F, Krauss S, Blank N, Halle A, Petzold GC. Inhibition of Stat3-mediated astrogliosis ameliorates pathology in an Alzheimer’s disease model. *EMBO Mol Med* (2019) 11: doi: 10.15252/emmm.201809665
371. Piperi C, Papavassiliou KA, Papavassiliou AG. Pivotal Role of STAT3 in Shaping Glioblastoma Immune Microenvironment. *Cells* (2019) 8: doi: 10.3390/cells8111398

372. Flynn CM, Garbers Y, Düsterhöft S, Wichert R, Lokau J, Lehmann CHK, Dudziak D, Schröder B, Becker-Pauly C, Rose-John S, et al. Cathepsin S provokes interleukin-6 (IL-6) trans-signaling through cleavage of the IL-6 receptor in vitro. *Scientific Reports* 2020 10:1 (2020) 10:1–13. doi: 10.1038/s41598-020-77884-4
373. van Horssen R, ten Hagen TLM, Eggermont AMM. TNF- α in Cancer Treatment: Molecular Insights, Antitumor Effects, and Clinical Utility. *Oncologist* (2006) 11:397–408. doi: 10.1634/THEONCOLOGIST.11-4-397
374. Park J, Shim JK, Yoon SJ, Kim SH, Chang JH, Kang SG. Transcriptome profiling-based identification of prognostic subtypes and multi-omics signatures of glioblastoma. *Sci Rep* (2019) 9:1–11. doi: 10.1038/s41598-019-47066-y
375. Pan Y, Wang S, Yang B, Jiang Z, Lenahan C, Wang J, Zhang J, Shao A. Transcriptome analyses reveal molecular mechanisms underlying phenotypic differences among transcriptional subtypes of glioblastoma. *J Cell Mol Med* (2020) 24:3901–3916. doi: 10.1111/jcmm.14976
376. Tang J, He D, Yang P, He J, Zhang Y. Genome-wide expression profiling of glioblastoma using a large combined cohort. *Sci Rep* (2018) 8:1–12. doi: 10.1038/s41598-018-33323-z
377. Yang J, Amiri KI, Burke JR, Schmid JA, Richmond A. BMS-345541 Targets Inhibitor of κ B Kinase and Induces Apoptosis in Melanoma: Involvement of Nuclear Factor κ B and Mitochondria Pathways. *Clin Cancer Res* (2006) 12:950. doi: 10.1158/1078-0432.CCR-05-1220
378. Silva KAS, Dong J, Dong Y, Dong Y, Schor N, Tweardy DJ, Zhang L, Mitch WE. Inhibition of Stat3 activation suppresses caspase-3 and the ubiquitin-proteasome system, leading to preservation of muscle mass in cancer cachexia. *J Biol Chem* (2015) 290:11177–11187. doi: 10.1074/JBC.M115.641514
379. Atkinson GP, Nozell SE, Benveniste EN. NF- κ B and STAT3 signaling in glioma: Targets for future therapies. *Expert Rev Neurother* (2010) 10:575–586. doi: 10.1586/ern.10.21
380. Grivennikov SI, Karin M. Dangerous liaisons: STAT3 and NF- κ B collaboration and crosstalk in cancer. *Cytokine Growth Factor Rev* (2010) 21:11–19. doi: 10.1016/j.cytogfr.2009.11.005
381. Grivennikov S, Karin E, Terzic J, Mucida D, Yu GY, Vallabhapurapu S, Scheller J, Rose-John S, Cheroutre H, Eckmann L, et al. IL-6 and Stat3 Are Required for Survival of Intestinal Epithelial Cells and Development of Colitis-Associated Cancer. *Cancer Cell* (2009) 15:103–113. doi: 10.1016/j.ccr.2009.01.001
382. Yang J, Liao X, Agarwal MK, Barnes L, Auron PE, Stark GR. Unphosphorylated STAT3 accumulates in response to IL-6 and activates transcription by binding to NF κ B. *Genes Dev* (2007) 21:1396. doi: 10.1101/GAD.1553707
383. Yang J, Chatterjee-Kishore M, Staugaitis SM, Nguyen H, Schlessinger K, Levy DE, Stark GR. Novel Roles of Unphosphorylated STAT3 in Oncogenesis and Transcriptional Regulation. *Cancer Res* (2005) 65:939–947. doi: 10.1158/0008-5472.939.65.3
384. Groblewska M, Litman-Zawadzka A, Mroczko B. The role of selected chemokines and their receptors in the development of gliomas. *Int J Mol Sci* (2020) 21: doi: 10.3390/ijms21103704
385. Roebuck KA, Finnegan A. Regulation of intercellular adhesion molecule-1 (CD54) gene expression. *J Leukoc Biol* (1999) 66:876–888. doi: 10.1002/jlb.66.6.876

386. Haskill S, Peace A, Morris J, Sporn SA, Anisowicz A, Lee SW, Smith T, Martin G, Ralph P, Sager R. Identification of three related human GRO genes encoding cytokine functions. *Proc Natl Acad Sci U S A* (1990) 87:7732–7736. doi: 10.1073/pnas.87.19.7732
387. Anisowicz A, Messineo M, Lee SW, Sager R. An NF-kappa B-like transcription factor mediates IL-1/TNF-alpha induction of gro in human fibroblasts. *J Immunol* (1991) 147:520–7.
388. Skinner DD, Lane TE. CXCR2 Signaling and Remyelination in Preclinical Models of Demyelination. *DNA Cell Biol* (2020) 39:3–7. doi: 10.1089/dna.2019.5182
389. Johnson EA, Dao TL, Guignet MA, Geddes CE, Koemeter-Cox AI, Kan RK. Increased expression of the chemokines CXCL1 and MIP-1 α by resident brain cells precedes neutrophil infiltration in the brain following prolonged soman-induced status epilepticus in rats. *J Neuroinflammation* (2011) 8:41. doi: 10.1186/1742-2094-8-41
390. Pacheco-Rodriguez G, Kumaki F, Steagall WK, Zhang Y, Ikeda Y, Lin J-P, Billings EM, Moss J. Chemokine-Enhanced Chemotaxis of Lymphangiomyomatosis Cells with Mutations in the Tumor Suppressor TSC2 Gene. *The Journal of Immunology* (2009) 182:1270–1277. doi: 10.4049/jimmunol.182.3.1270
391. Burke JR, Pattoli MA, Gregor KR, Brassil PJ, MacMaster JF, McIntyre KW, Yang X, Iotzova VS, Clarke W, Strnad J, et al. BMS-345541 is a highly selective inhibitor of I κ B kinase that binds at an allosteric site of the enzyme and blocks NF- κ B-dependent transcription in mice. *Journal of Biological Chemistry* (2003) 278:1450–1456. doi: 10.1074/jbc.M209677200
392. Kaya-Aksoy E, Cingoz A, Senbabaoglu F, Seker F, Sur-Erdem I, Kayabolen A, Lokumcu T, Sahin GN, Karahuseyinoglu S, Bagci-Onder T. The pro-apoptotic Bcl-2 family member Harakiri (HRK) induces cell death in glioblastoma multiforme. *Cell Death Discovery 2019 5:1* (2019) 5:1–12. doi: 10.1038/s41420-019-0144-z
393. De Benedetti A, Graff JR. eIF-4E expression and its role in malignancies and metastases. *Oncogene* (2004) 23:3189–3199. doi: 10.1038/sj.onc.1207545
394. Campbell KJ, Tait SWG. Targeting BCL-2 regulated apoptosis in cancer. *Open Biol* (2018) 8: doi: 10.1098/rsob.180002
395. Freilinger A, Rosner M, Hengstschlager M. Tuberin negatively affects BCL-2's cell survival function. *Amino Acids* (2006) 30:391–396. doi: 10.1007/s00726-006-0359-1
396. Lopez-Guerra M, Roue G, Perez-Galan P, Alonso R, Villamor N, Montserrat E, Campo E, Colomer D. P65 activity and ZAP-70 status predict the sensitivity of chronic lymphocytic leukemia cells to the selective I κ B kinase inhibitor BMS-345541. *Clinical Cancer Research* (2009) 15:2767–2776. doi: 10.1158/1078-0432.CCR-08-2382
397. Lee H, Herrmann A, Deng JH, Kujawski M, Niu G, Li Z, Forman S, Jove R, Pardoll DM, Yu H. Persistently Activated Stat3 Maintains Constitutive NF- κ B Activity in Tumors. *Cancer Cell* (2009) 15:283–293. doi: 10.1016/j.ccr.2009.02.015
398. Yu Z, Zhang W, Kone BC. Signal transducers and activators of transcription 3 (STAT3) inhibits transcription of the inducible nitric oxide synthase gene by interacting with nuclear factor κ B. *Biochemical Journal* (2002) 367:97–105. doi: 10.1042/BJ20020588

399. Wu Z, Zhang X, Yang J, Wu G, Zhang Y, Yuan Y, Jin C, Chang Z, Wang J, Yang X, et al. Nuclear protein I κ B- ζ inhibits the activity of STAT3. *Biochem Biophys Res Commun* (2009) 387:348–352. doi: 10.1016/j.bbrc.2009.07.023
400. Champion JD, Dodd KM, Lam HC, Alzahrani MAM, Seifan S, Rad E, Scourfield DO, Fishel ML, Calver BL, Ager A, et al. Drug Inhibition of Redox Factor-1 Restores Hypoxia-Driven Changes in Tuberous Sclerosis Complex 2 Deficient Cells. *Cancers (Basel)* (2022) 14: doi: 10.3390/CANCERS14246195
401. Niehof M, Streetz K, Rakemann T, Bischoff SC, Manns MP, Horn F, Trautwein C. Interleukin-6-induced Tethering of STAT3 to the LAP/C/EBP β Promoter Suggests a New Mechanism of Transcriptional Regulation by STAT3. *Journal of Biological Chemistry* (2001) 276:9016–9027. doi: 10.1074/jbc.M009284200
402. Kuilman T, Michaloglou C, Vredeveld LCW, Douma S, van Doorn R, Desmet CJ, Aarden LA, Mooi WJ, Peeper DS. Oncogene-Induced Senescence Relayed by an Interleukin-Dependent Inflammatory Network. *Cell* (2008) 133:1019–1031. doi: 10.1016/j.cell.2008.03.039
403. Calkhoven CF, Mü C, Leutz A. Translational control of C/EBP and C/EBP isoform expression. (2000)
404. Smink JJ, Leutz A. Rapamycin and the transcription factor C/EBP β as a switch in osteoclast differentiation: Implications for lytic bone diseases. *J Mol Med* (2010) 88:227–233. doi: 10.1007/S00109-009-0567-8/FIGURES/3
405. Yang T, Zhu L, Zhai Y, Zhao Q, Peng J, Zhang H, Yang Z, Zhang L, Ding W, Zhao Y. TSC1 controls IL-1 β expression in macrophages via mTORC1-dependent C/EBP β pathway. *Cellular & Molecular Immunology* 2016 13:5 (2015) 13:640–650. doi: 10.1038/cmi.2015.43
406. Cappello C, Zwergal A, Kanclerski S, Haas SC, Kandemir JD, Huber R, Page S, Brand K. C/EBP β enhances NF- κ B-associated signalling by reducing the level of I κ B- α . *Cell Signal* (2009) 21:1918–1924. doi: 10.1016/J.CELLSIG.2009.08.009
407. Solinas C, Aiello M, Rozali E, Lambertini M, Willard-Gallo K, Migliori E. Programmed Cell Death-Ligand 2: A Neglected But Important Target in the Immune Response to Cancer? *Transl Oncol* (2020) 13:100811. doi: 10.1016/J.TRANON.2020.100811
408. Astarci E, Sade A, Çimen I, Savaş B, Banerjee S. The NF- κ B target genes ICAM-1 and VCAM-1 are differentially regulated during spontaneous differentiation of Caco-2 cells. *FEBS J* (2012) 279:2966–2986. doi: 10.1111/J.1742-4658.2012.08677.X
409. Fabene PF, Mora GN, Martinello M, Rossi B, Merigo F, Ottoboni L, Bach S, Angiari S, Benati D, Chakir A, et al. A role for leukocyte-endothelial adhesion mechanisms in epilepsy. *Nat Med* (2008) 14:1377. doi: 10.1038/NM.1878
410. Uknowledge U, Cai L, Wang Z, Ji A, Meyer JM, Van Der Westhuyzen DR. Scavenger Receptor CD36 Expression Contributes to Adipose Scavenger Receptor CD36 Expression Contributes to Adipose Tissue Inflammation and Cell Death in Diet-Induced Obesity Tissue Inflammation and Cell Death in Diet-Induced Obesity. (2012) doi: 10.1371/journal.pone.0036785
411. Cao D, Luo J, Chen D, Xu H, Shi H, Jing X, Zang W. CD36 regulates lipopolysaccharide-induced signaling pathways and mediates the internalization of Escherichia coli in cooperation with TLR4 in goat mammary gland epithelial cells. *Sci Rep* (2016) 6: doi: 10.1038/SREP23132

412. Chen Y, Zhang J, Cui W, Silverstein RL. CD36, a signaling receptor and fatty acid transporter that regulates immune cell metabolism and fate. *J Exp Med* (2022) 219: doi: 10.1084/JEM.20211314
413. Gil-Yarom N, Radomir L, Sever L, Kramer MP, Lewinsky H, Bornstein C, Blecher-Gonen R, Barnett-Itzhaki Z, Mirkin V, Friedlander G, et al. CD74 is a novel transcription regulator. *Proc Natl Acad Sci U S A* (2017) 114:562–567. doi: 10.1073/PNAS.1612195114/SUPPL_FILE/PNAS.201612195SI.PDF
414. Wang HX, Zhang Q, Zhang J, Luan R, Liang Z, Tan L, Xu Y, Zhang P, Zheng L, Zhao Y, et al. CD74 regulates cellularity and maturation of medullary thymic epithelial cells partially by activating the canonical NF- κ B signaling pathway. *FASEB Journal* (2021) 35: doi: 10.1096/FJ.202100139R
415. Berkova Z, Tao RH, Samaniego F. Milatuzumab - a promising new immunotherapeutic agent. *Expert Opin Investig Drugs* (2010) 19:141–149. doi: 10.1517/13543780903463854
416. Beswick EJ, Reyes VE. CD74 in antigen presentation, inflammation, and cancers of the gastrointestinal tract. *World J Gastroenterol* (2009) 15:2855–2861. doi: 10.3748/wjg.15.2855
417. Valiño-Rivas L, Cuarental L, Grana O, Bucala R, Leng L, Sanz A, Gomez G, Ortiz A, Sanchez-Niño MD. TWEAK increases CD74 expression and sensitizes to DDT proinflammatory actions in tubular cells. *PLoS One* (2018) 13:e0199391. doi: 10.1371/JOURNAL.PONE.0199391
418. Zhang W, Li G, Luo R, Lei J, Song Y, Wang B, Ma L, Liao Z, Ke W, Liu H, et al. Cytosolic escape of mitochondrial DNA triggers cGAS-STING-NLRP3 axis-dependent nucleus pulposus cell pyroptosis. *Experimental & Molecular Medicine* 2022 54:2 (2022) 54:129–142. doi: 10.1038/s12276-022-00729-9
419. Basit A, Cho MG, Kim EY, Kwon D, Kang SJ, Lee JH. The cGAS/STING/TBK1/IRF3 innate immunity pathway maintains chromosomal stability through regulation of p21 levels. *Experimental & Molecular Medicine* 2020 52:4 (2020) 52:643–657. doi: 10.1038/s12276-020-0416-y
420. Li S, Zou H, Shao YY, Mei Y, Cheng Y, Hu DL, Tan ZR, Zhou HH. Pseudogenes of annexin A2, novel prognosis biomarkers for diffuse gliomas. *Oncotarget* (2017) 8:106962–106975. doi: 10.18632/oncotarget.22197
421. Zhai H, Acharya S, Gravanis I, Mehmood S, Seidman RJ, Shroyer KR, Hajjar KA, Tsirka SE. Annexin A2 promotes glioma cell invasion and tumor progression. *Journal of Neuroscience* (2011) 31:14346–14360. doi: 10.1523/JNEUROSCI.3299-11.2011
422. Jung H, Kim JS, Kim WK, Oh KJ, Kim JM, Lee HJ, Han BS, Kim DS, Seo YS, Lee SC, et al. Intracellular annexin A2 regulates NF- κ B signaling by binding to the p50 subunit: implications for gemcitabine resistance in pancreatic cancer. *Cell Death Dis* (2015) 6:e1606. doi: 10.1038/CDDIS.2014.558
423. Schumacher N, Rose-John S. ADAM17 orchestrates Interleukin-6, TNF α and EGF-R signaling in inflammation and cancer. *Biochimica et Biophysica Acta (BBA) - Molecular Cell Research* (2022) 1869:119141. doi: 10.1016/J.BBAMCR.2021.119141
424. Jha NK, Jha SK, Sharma R, Kumar D, Ambasta RK, Kumar P. Hypoxia-Induced Signaling Activation in Neurodegenerative Diseases: Targets for New Therapeutic Strategies. *Journal of Alzheimer's Disease* (2018) 62:15–38. doi: 10.3233/JAD-170589

425. Lall R, Mohammed R, Ojha U. What are the links between hypoxia and alzheimer's disease? *Neuropsychiatr Dis Treat* (2019) 15:1343–1354. doi: 10.2147/NDT.S203103
426. Schöenberger MJ, Kovacs WJ. Hypoxia signaling pathways: Modulators of oxygen-related organelles. *Front Cell Dev Biol* (2015) 3:42. doi: 10.3389/fcell.2015.00042
427. Muz B, de la Puente P, Azab F, Azab AK. The role of hypoxia in cancer progression, angiogenesis, metastasis, and resistance to therapy. *Hypoxia* (2015) 3:83. doi: 10.2147/hp.s93413
428. Monteiro A, Hill R, Pilkington G, Madureira P. The Role of Hypoxia in Glioblastoma Invasion. *Cells* (2017) 6:45. doi: 10.3390/cells6040045
429. Eltzschig HK, Carmeliet P. Hypoxia and Inflammation. *New England Journal of Medicine* (2011) 364:656–665. doi: 10.1056/nejmra0910283
430. Xu C, Li X, Guo P, Wang J. Hypoxia-induced activation of JAK/STAT3 signaling pathway promotes trophoblast cell viability and angiogenesis in preeclampsia. *Medical Science Monitor* (2017) 23:4909–4917. doi: 10.12659/MSM.905418
431. D'ignazio L, Rocha S. Hypoxia Induced NF-κB. *Cells* (2016) 5:1–8. doi: 10.3390/CELLS5010010
432. Harvey DM, Levine AJ. p53 alteration is a common event in the spontaneous immortalization of primary BALB/c murine embryo fibroblasts. *Genes Dev* (1991) 5:2375–2385. doi: 10.1101/GAD.5.12B.2375
433. El-Hashemite N, Kwiatkowski DJ. Interferon-γ-Jak-Stat signaling in pulmonary lymphangiomyomatosis and renal angiomyolipoma: A potential therapeutic target. *Am J Respir Cell Mol Biol* (2005) 33:227–230. doi: 10.1165/rcmb.2005-0152RC
434. Shu HF, Zhang CQ, Yin Q, An N, Liu SY, Yang H. Expression of the Interleukin 6 System in Cortical Lesions From Patients With Tuberous Sclerosis Complex and Focal Cortical Dysplasia Type IIb. *J Neuropathol Exp Neurol* (2010) 69:838–849. doi: 10.1097/NEN.0B013E3181EAEAE5
435. la Iglesia N, Puram S, Bonni A. STAT3 Regulation of Glioblastoma Pathogenesis. *Curr Mol Med* (2009) 9:580–590. doi: 10.2174/156652409788488739
436. Haftchenary S, Luchman HA, Jouk AO, Veloso AJ, Page BDG, Cheng XR, Dawson SS, Grinshtein N, Shahani VM, Kerman K, et al. Potent targeting of the STAT3 protein in brain cancer stem cells: A promising route for treating glioblastoma. *ACS Med Chem Lett* (2013) 4:1102–1107. doi: 10.1021/ml4003138
437. Soubannier V, Stifani S. NF-κB signalling in glioblastoma. *Biomedicines* (2017) 5: doi: 10.3390/biomedicines5020029
438. Puliyappadamba VT, Hatanpaa KJ, Chakraborty S, Habib AA. The role of NF-κB in the pathogenesis of glioma. *Mol Cell Oncol* (2014) 1: doi: 10.4161/23723548.2014.963478
439. Tang J, He D, Yang P, He J, Zhang Y. Genome-wide expression profiling of glioblastoma using a large combined cohort. *Sci Rep* (2018) 8:1–12. doi: 10.1038/s41598-018-33323-z
440. Yuan J, Mendes Levitin H, Frattini V, Bush EC, Samanamud J, Ceccarelli M, Dovas A, Zanazzi G, Canoll P, Bruce JN, et al. Single-Cell Transcriptome Analysis of Lineage Diversity and Microenvironment in High-Grade Glioma. doi: 10.1101/250704

441. Hideshima T, Ikeda H, Chauhan D, Okawa Y, Raje N, Podar K, Mitsiades C, Munshi NC, Richardson PG, Carrasco RD, et al. Bortezomib induces canonical nuclear factor-kappaB activation in multiple myeloma cells. *Blood* (2009) 114:1046–1052. doi: 10.1182/BLOOD-2009-01-199604
442. Sung MH, Bagain L, Chen Z, Karpova T, Yang X, Silvin C, Voss TC, McNally JG, Van Waes C, Hager GL. Dynamic Effect of Bortezomib on NF-κB Activity and Gene Expression in Tumor Cells. *Mol Pharmacol* (2008) 74:1215. doi: 10.1124/MOL.108.049114
443. Johnson CE, Dunlop EA, Seifan S, McCann HD, Hay T, Parfitt GJ, Jones AT, Giles PJ, Shen MH, Sampson JR, et al. Loss of tuberous sclerosis complex 2 sensitizes tumors to nelfinavir–bortezomib therapy to intensify endoplasmic reticulum stress-induced cell death. *Oncogene* (2018) 37:5913–5925. doi: 10.1038/S41388-018-0381-2
444. Auricchio N, Malinowska I, Shaw R, Manning BD, Kwiatkowski DJ. Therapeutic Trial of Metformin and Bortezomib in a Mouse Model of Tuberous Sclerosis Complex (TSC). *PLoS One* (2012) 7:31900. doi: 10.1371/JOURNAL.PONE.0031900
445. Marcum ZA, Hanlon JT. Recognizing the Risks of Chronic Nonsteroidal Anti-Inflammatory Drug Use in Older Adults. *Ann Longterm Care* (2010) 18:24. /pmc/articles/PMC3158445/ [Accessed August 20, 2023]
446. Kapałczyńska M, Kolenda T, Przybyła W, Zajączkowska M, Teresiak A, Filas V, Ibbs M, Bliźniak R, Łuczewski Ł, Lamperska K. 2D and 3D cell cultures – a comparison of different types of cancer cell cultures. *Archives of Medical Science* (2018) 14:910–919. doi: 10.5114/aoms.2016.63743
447. Mokhtari RB, Homayouni TS, Baluch N, Morgatskaya E, Kumar S, Das B, Yeger H. Combination therapy in combating cancer. *Oncotarget* (2017) 8:38022. doi: 10.18632/ONCOTARGET.16723
448. Prizant H, Hammes SR. Minireview: Lymphangioleiomyomatosis (LAM): The “Other” Steroid-Sensitive Cancer. *Endocrinology* (2016) 157:3374. doi: 10.1210/EN.2016-1395
449. Heerboth S, Housman G, Leary M, Longacre M, Byler S, Lapinska K, Willbanks A, Sarkar S. EMT and tumor metastasis. *Clin Transl Med* (2015) 4: doi: 10.1186/S40169-015-0048-3
450. Huber MA, Azoitei N, Baumann B, Grünert S, Sommer A, Pehamberger H, Kraut N, Beug H, Wirth T. NF-kappaB is essential for epithelial-mesenchymal transition and metastasis in a model of breast cancer progression. *J Clin Invest* (2004) 114:569–581. doi: 10.1172/JCI21358
451. Wu Y, Zhou BP. TNF-α/NF-κB/Snail pathway in cancer cell migration and invasion. *British Journal of Cancer* 2010 102:4 (2010) 102:639–644. doi: 10.1038/sj.bjc.6605530
452. Pires BRB, Mencialha AL, Ferreira GM, De Souza WF, Morgado-Díaz JA, Maia AM, Corrêa S, Abdelhay ESW. NF-kappaB Is Involved in the Regulation of EMT Genes in Breast Cancer Cells. *PLoS One* (2017) 12:e0169622. doi: 10.1371/JOURNAL.PONE.0169622
453. Huo JL, Wang YT, Fu WJ, Lu N, Liu ZS. The promising immune checkpoint LAG-3 in cancer immunotherapy: from basic research to clinical application. *Front Immunol* (2022) 13:4133. doi: 10.3389/FIMMU.2022.956090/BIBTEX
454. Liu J, Chen Z, Li Y, Zhao W, Wu JB, Zhang Z. PD-1/PD-L1 Checkpoint Inhibitors in Tumor Immunotherapy. *Front Pharmacol* (2021) 12: doi: 10.3389/FPHAR.2021.731798

455. Liu HJ, Du H, Khabibullin D, Zarei M, Wei K, Freeman GJ, Kwiatkowski DJ, Henske EP. mTORC1 upregulates B7-H3/CD276 to inhibit antitumor T cells and drive tumor immune evasion. *Nat Commun* (2023) 14: doi: 10.1038/S41467-023-36881-7
456. Liu HJ, Lizotte PH, Du H, Speranza MC, Lam HC, Vaughan S, Alesi N, Wong KK, Freeman GJ, Sharpe AH, et al. TSC2-deficient tumors have evidence of T cell exhaustion and respond to anti-PD-1/anti-CTLA-4 immunotherapy. *JCI Insight* (2018) 3: doi: 10.1172/JCI.INSIGHT.98674
457. Gentilella A, Kozma SC, Thomas G. A liaison between mTOR signaling, ribosome biogenesis and cancer. *Biochim Biophys Acta* (2015) 1849:812. doi: 10.1016/J.BBAGRM.2015.02.005
458. Xiao J, Yang W, Xu B, Zhu H, Zou J, Su C, Rong J, Wang T, Chen Z. Expression of fibronectin in esophageal squamous cell carcinoma and its role in migration. *BMC Cancer* (2018) 18:1–9. doi: 10.1186/S12885-018-4850-3/FIGURES/3
459. Taftaf R, Liu X, Singh S, Jia Y, Dashzeveg NK, Hoffmann AD, El-Shennawy L, Ramos EK, Adorno-Cruz V, Schuster EJ, et al. ICAM1 initiates CTC cluster formation and trans-endothelial migration in lung metastasis of breast cancer. *Nature Communications* 2021 12:1 (2021) 12:1–15. doi: 10.1038/s41467-021-25189-z
460. Blaber R, Stylianou E, Clayton A, Steadman R. Selective regulation of ICAM-1 and RANTES gene expression after ICAM-1 ligation on human renal fibroblasts. *J Am Soc Nephrol* (2003) 14:116–127. doi: 10.1097/01.ASN.0000040595.35207.62
461. Vorinostat by Merck for Follicular Lymphoma: Likelihood of Approval. <https://www.pharmaceutical-technology.com/data-insights/vorinostat-merck-follicular-lymphoma-likelihood-of-approval/> [Accessed April 20, 2023]
462. Chong W, Li Y, Liu B, Zhao T, Fukudome EY, Liu Z, Smith WM, Velmahos GC, Demoya MA, Alam HB. Histone Deacetylase Inhibitor SAHA Attenuates TLR4 Signaling in LPS-Stimulated Mouse Macrophages. *J Surg Res* (2012) 178:851. doi: 10.1016/J.JSS.2012.07.023
463. Dai Y, Rahmani M, Dent P, Grant S. Blockade of histone deacetylase inhibitor-induced RelA/p65 acetylation and NF-kappaB activation potentiates apoptosis in leukemia cells through a process mediated by oxidative damage, XIAP downregulation, and c-Jun N-terminal kinase 1 activation. *Mol Cell Biol* (2005) 25:5429–5444. doi: 10.1128/MCB.25.13.5429-5444.2005
464. Wong AHH, Shin EM, Tergaonkar V, Chng WJ. Targeting NF-κB Signaling for Multiple Myeloma. *Cancers (Basel)* (2020) 12:1–20. doi: 10.3390/CANCERS12082203
465. Hideshima T, Raje N, Richardson PG, Anderson KC. A review of lenalidomide in combination with dexamethasone for the treatment of multiple myeloma. *Ther Clin Risk Manag* (2008) 4:129–136. doi: 10.2147/TCRM.S1445
466. Mitsiades N, Mitsiades CS, Poulaki V, Chauhan D, Richardson PG, Hideshima T, Munshi NC, Treon SP, Anderson KC. Apoptotic signaling induced by immunomodulatory thalidomide analogs in human multiple myeloma cells: therapeutic implications. *Blood* (2002) 99:4525–4530. doi: 10.1182/BLOOD.V99.12.4525
467. Kopp E, Ghosh S. Inhibition of NF-kappa B by sodium salicylate and aspirin. *Science* (1994) 265:956–959. doi: 10.1126/SCIENCE.8052854

468. Kim SR, Bae MK, Kim JY, Wee HJ, Yoo MA, Bae SK. Aspirin induces apoptosis through the blockade of IL-6-STAT3 signaling pathway in human glioblastoma A172 cells. *Biochem Biophys Res Commun* (2009) 387:342–347. doi: 10.1016/J.BBRC.2009.07.022
469. Matsunaga N, Tsuchimori N, Matsumoto T, Ii M. TAK-242 (resatorvid), a small-molecule inhibitor of Toll-like receptor (TLR) 4 signaling, binds selectively to TLR4 and interferes with interactions between TLR4 and its adaptor molecules. *Mol Pharmacol* (2011) 79:34–41. doi: 10.1124/MOL.110.068064
470. Feng Y, Gao J, Cui Y, Li M, Li R, Cui C, Cui J. Neuroprotective Effects of Resatorvid Against Traumatic Brain Injury in Rat: Involvement of Neuronal Autophagy and TLR4 Signaling Pathway. *Cell Mol Neurobiol* (2017) 37:155–168. doi: 10.1007/S10571-016-0356-1
471. Luo W, Han Y, Meng P, Yang Q, Zhao H, Ling J, Wang Y. Resatorvid Relieves Breast Cancer Complicated with Depression by Inactivating Hippocampal Microglia Through TLR4/NF- κ B/NLRP3 Signaling Pathway. *Cancer Manag Res* (2020) 12:13003. doi: 10.2147/CMAR.S279800
472. Zandi Z, Kashani B, Bashash D, Poursani EM, Mousavi SA, Chahardoli B, Ghaffari SH. The anticancer effect of the TLR4 inhibition using TAK-242 (resatorvid) either as a single agent or in combination with chemotherapy: A novel therapeutic potential for breast cancer. *J Cell Biochem* (2020) 121:1623–1634. doi: 10.1002/JCB.29397
473. Lucas-Ruiz F, Galindo-Romero C, Salinas-Navarro M, González-Riquelme MJ, Vidal-Sanz M, Agudo Barriuso M. Systemic and Intravitreal Antagonism of the TNFR1 Signaling Pathway Delays Axotomy-Induced Retinal Ganglion Cell Loss. *Front Neurosci* (2019) 13:1096. doi: 10.3389/FNINS.2019.01096
474. Qiu L, Zhang D, Sang Y, Zheng N, Chen J, Qiu X, Liu X. Relationship between Tumor Necrosis Factor-Alpha and Neuropeptide Y Expression and Neurological Function Score in Epileptic Children. *Iran J Public Health* (2021) 50:1056. doi: 10.18502/IJPH.V50I5.6123
475. Cheng S, Wang H-N, Xu L-J, Li F, Miao Y, Lei B, Sun X, Wang Z. Soluble tumor necrosis factor-alpha-induced hyperexcitability contributes to retinal ganglion cell apoptosis by enhancing Nav1.6 in experimental glaucoma. *J Neuroinflammation* (2021) 18:182. doi: 10.1186/S12974-021-02236-6
476. Pavelka K, Bruyère O, Cooper C, Kanis JA, Leeb BF, Maheu E, Martel-Pelletier J, Monfort J, Pelletier JP, Rizzoli R, et al. Diacerein: Benefits, Risks and Place in the Management of Osteoarthritis. An Opinion-Based Report from the ESCEO. *Drugs Aging* (2016) 33:75. doi: 10.1007/S40266-016-0347-4
477. Martel Pelletier J, Pelletier JP. Effects of diacerein at the molecular level in the osteoarthritis disease process. *Ther Adv Musculoskelet Dis* (2010) 2:95–104. doi: 10.1177/1759720X09359104
478. Rossi M, Sharkey AM, Viganò P, Fiore G, Furlong R, Florio P, Ambrosini G, Smith SK, Petraglia F. Identification of genes regulated by interleukin-1 β in human endometrial stromal cells. *Reproduction* (2005) 130:721–729. doi: 10.1530/REP.1.00688
479. Swindell WR, Beamer MA, Sarkar MK, Loftus S, Fullmer J, Xing X, Ward NL, Tsoi LC, Kahlenberg MJ, Liang Y, et al. RNA-seq analysis of IL-1B and IL-36 responses in epidermal keratinocytes

- identifies a shared MyD88-dependent gene signature. *Front Immunol* (2018) 9:80. doi: 10.3389/FIMMU.2018.00080/BIBTEX
480. Rheumatoid Arthritis disease: Malacards - Research Articles, Drugs, Genes, Clinical Trials. https://www.malacards.org/card/rheumatoid_arthritis#related_genes [Accessed May 9, 2023]
481. Nicolas P, Tod M, Padoin C, Petitjean O. Clinical pharmacokinetics of diacerein. *Clin Pharmacokinet* (1998) 35:347–359. doi: 10.2165/00003088-199835050-00002
482. Rex J, Lutz A, Faletti LE, Albrecht U, Thomas M, Bode JG, Borner C, Sawodny O, Merfort I. IL-1 β and TNF α differentially influence NF- κ B activity and FasL-induced apoptosis in primary murine hepatocytes during LPS-induced inflammation. *Front Physiol* (2019) 10:117. doi: 10.3389/FPHYS.2019.00117/BIBTEX
483. Schroder K, Tschopp J. The Inflammasomes. *Cell* (2010) 140:821–832. doi: 10.1016/J.CELL.2010.01.040
484. Wang N, Liang H, Zen K. Molecular mechanisms that influence the macrophage M1-M2 polarization balance. *Front Immunol* (2014) 5:614. doi: 10.3389/FIMMU.2014.00614/BIBTEX
485. Pradère JP, Hernandez C, Koppe C, Friedman RA, Luedde T, Schwabe RF. Negative regulation of NF- κ B p65 activity by serine 536 phosphorylation. *Sci Signal* (2016) 9:ra85. doi: 10.1126/SCISIGNAL.AAB2820
486. Eisa NH, Said E, Khodir AE, Sabry D, Ebrahim HA, Elsherbini DMA, Altemani R, Alnasser DM, Elsherbiny NM, El-Sherbiny M. Effect of Diacerein on HOTAIR/IL-6/STAT3, Wnt/ β -Catenin and TLR-4/NF- κ B/TNF- α axes in colon carcinogenesis. *Environ Toxicol Pharmacol* (2022) 95:103943. doi: 10.1016/J.ETAP.2022.103943
487. Bharti R, Dey G, Ojha PK, Rajput S, Jaganathan SK, Sen R, Mandal M. Diacerein-mediated inhibition of IL-6/IL-6R signaling induces apoptotic effects on breast cancer. *Oncogene* 2016 35:30 (2015) 35:3965–3975. doi: 10.1038/onc.2015.466
488. Rébé C, Ghiringhelli F. Interleukin-1 β and Cancer. *Cancers (Basel)* (2020) 12:1–31. doi: 10.3390/CANCERS12071791
489. Chen LC, Wang LJ, Tsang NM, Ojcius DM, Chen CC, Ouyang CN, Hsueh C, Liang Y, Chang KP, Chen CC, et al. Tumour inflammasome-derived IL-1 β recruits neutrophils and improves local recurrence-free survival in EBV-induced nasopharyngeal carcinoma. *EMBO Mol Med* (2012) 4:1276–1293. doi: 10.1002/EMMM.201201569
490. Mizuguchi M, Takashima S. Neuropathology of tuberous sclerosis. *Brain Dev* (2001) 23:508–515. doi: 10.1016/S0387-7604(01)00304-7
491. Boer K, Crino PB, Gorter JA, Nellist M, Jansen FE, Spliet WGM, Van Rijen PC, Wittink FRA, Breit TM, Troost D, et al. Gene Expression Analysis of Tuberous Sclerosis Complex Cortical Tubers Reveals Increased Expression of Adhesion and Inflammatory Factors. *Brain Pathology* (2010) 20:704. doi: 10.1111/J.1750-3639.2009.00341.X
492. Bender BL, Yunis EJ. Central nervous system pathology of tuberous sclerosis in children. *Ultrastruct Pathol* (1980) 1:287–299. doi: 10.3109/01913128009141432

493. Kasper E, Laviv Y, Sebai M-AE, Lin N, Butler W. Subependymal Giant Cell Astrocytoma: Associated Hyperproteinorrachia Causing Shunt Failures and Nonobstructive Hydrocephalus - Report of Successful Treatment with Long-term Follow-up. *Asian J Neurosurg* (2017) 12:746. doi: 10.4103/AJNS.AJNS_231_16
494. Northrup H, Koenig MK, Pearson DA, Au KS. Tuberous Sclerosis Complex. *GeneReviews*® (2021)
495. Costa V, Aigner S, Vukcevic M, Sauter E, Behr K, Ebeling M, Dunkley T, Friedlein A, Zoffmann S, Meyer CA, et al. mTORC1 Inhibition Corrects Neurodevelopmental and Synaptic Alterations in a Human Stem Cell Model of Tuberous Sclerosis. *Cell Rep* (2016) 15:86–95. doi: 10.1016/J.CELREP.2016.02.090
496. Afshar Saber W, Sahin M. Recent advances in human stem cell-based modeling of Tuberous Sclerosis Complex. *Mol Autism* (2020) 11: doi: 10.1186/S13229-020-0320-2
497. Srimasorn S, Kirsch M, Hallmeyer-Ellgner S, Lindemann D, Storch A, Hermann A. Increased Neuronal Differentiation Efficiency in High Cell Density-Derived Induced Pluripotent Stem Cells. *Stem Cells Int* (2019) 2019: doi: 10.1155/2019/2018784
498. Ka M, Condorelli G, Woodgett JR, Kim WY. mTOR regulates brain morphogenesis by mediating GSK3 signaling. *Development* (2014) 141:4076–4086. doi: 10.1242/DEV.108282
499. Cloëtta D, Thomanetz V, Baranek C, Lustenberger RM, Lin S, Oliveri F, Atanasoski S, Rüegg MA. Inactivation of mTORC1 in the Developing Brain Causes Microcephaly and Affects Gliogenesis. *The Journal of Neuroscience* (2013) 33:7799. doi: 10.1523/JNEUROSCI.3294-12.2013
500. Hartman NW, Lin T V., Zhang L, Paquelet GE, Feliciano DM, Bordey A. mTORC1 Targets the Translational Repressor 4E-BP2, but Not S6 Kinase 1/2, to Regulate Neural Stem Cell Self-Renewal In Vivo. *Cell Rep* (2013) 5:433–444. doi: 10.1016/J.CELREP.2013.09.017
501. Magri L, Cominelli M, Cambiaghi M, Corsi M, Leocani L, Minicucci F, Poliani PL, Galli R. Timing of mTOR activation affects tuberous sclerosis complex neuropathology in mouse models. *DMM Disease Models and Mechanisms* (2013) 6:1185–1197. doi: 10.1242/DMM.012096/-/DC1
502. Magri L, Cambiaghi M, Cominelli M, Alfaro-Cervello C, Corsi M, Pala M, Bulfone A, Garca-Verdugo JM, Leocani L, Minicucci F, et al. Sustained Activation of mTOR Pathway in Embryonic Neural Stem Cells Leads to Development of Tuberous Sclerosis Complex-Associated Lesions. *Cell Stem Cell* (2011) 9:447–462. doi: 10.1016/J.STEM.2011.09.008
503. Heurtier V, Owens N, Gonzalez I, Mueller F, Proux C, Mornico D, Clerc P, Dubois A, Navarro P. The molecular logic of Nanog-induced self-renewal in mouse embryonic stem cells. *Nature Communications* 2019 10:1 (2019) 10:1–15. doi: 10.1038/s41467-019-09041-z
504. Niwa H, Ogawa K, Shimosato D, Adachi K. A parallel circuit of LIF signalling pathways maintains pluripotency of mouse ES cells. *Nature* (2009) 460:118–122. doi: 10.1038/NATURE08113
505. Hutton SR, Pevny LH. SOX2 expression levels distinguish between neural progenitor populations of the developing dorsal telencephalon. *Dev Biol* (2011) 352:40–47. doi: 10.1016/J.YDBIO.2011.01.015

506. Katsetos CD, Legido A, Perentes E, Mörk SJ. Class III beta-tubulin isotype: a key cytoskeletal protein at the crossroads of developmental neurobiology and tumor neuropathology. *J Child Neurol* (2003) 18:851–866. doi: 10.1177/088307380301801205
507. Sánchez C, Díaz-Nido J, Avila J. Phosphorylation of microtubule-associated protein 2 (MAP2) and its relevance for the regulation of the neuronal cytoskeleton function. *Prog Neurobiol* (2000) 61:133–168. doi: 10.1016/S0301-0082(99)00046-5
508. Kamei Y, Inagaki N, Nishizawa M, Tsutsumi O, Taketani Y, Inagaki M. Visualization of Mitotic Radial Glial Lineage Cells in the Developing Rat Brain by Cdc2 Kinase-Phosphorylated Vimentin. *Glia* (1998) 23:191–199. doi: 10.1002/(SICI)1098-1136(199807)23:3
509. Götz M, Stoykova A, Gruss P. Pax6 controls radial glia differentiation in the cerebral cortex. *Neuron* (1998) 21:1031–1044. doi: 10.1016/S0896-6273(00)80621-2
510. Kriegstein AR, Götz M. Radial glia diversity: A matter of cell fate. *Glia* (2003) 43:37–43. doi: 10.1002/GLIA.10250
511. Englund C, Fink A, Lau C, Pham D, Daza RAM, Bulfone A, Kowalczyk T, Hevner RF. Pax6, Tbr2, and Tbr1 Are Expressed Sequentially by Radial Glia, Intermediate Progenitor Cells, and Postmitotic Neurons in Developing Neocortex. *The Journal of Neuroscience* (2005) 25:247. doi: 10.1523/JNEUROSCI.2899-04.2005
512. Way SW, Mckenna J, Mietzsch U, Reith RM, Wu HCJ, Gambello MJ. Loss of Tsc2 in radial glia models the brain pathology of tuberous sclerosis complex in the mouse. *Hum Mol Genet* (2009) 18:1252–1265. doi: 10.1093/HMG/DDP025
513. Magri L, Cambiaghi M, Cominelli M, Alfaro-Cervello C, Corsi M, Pala M, Bulfone A, Garca-Verdugo JM, Leocani L, Minicucci F, et al. Sustained Activation of mTOR Pathway in Embryonic Neural Stem Cells Leads to Development of Tuberous Sclerosis Complex-Associated Lesions. *Cell Stem Cell* (2011) 9:447–462. doi: 10.1016/J.STEM.2011.09.008
514. Paliouras GN, Hamilton LK, Aumont A, Joppé SE, Barnabé-Heider F, Fernandes KJL. Mammalian target of rapamycin signaling is a key regulator of the transit-amplifying progenitor pool in the adult and aging forebrain. *J Neurosci* (2012) 32:15012–15026. doi: 10.1523/JNEUROSCI.2248-12.2012
515. Gutierrez H, Davies AM. Regulation of neural process growth, elaboration and structural plasticity by NF- κ B. *Trends Neurosci* (2011) 34:316. doi: 10.1016/J.TINS.2011.03.001
516. Gutierrez H, O’Keeffe GW, Gavalda N, Gallagher D, Davies AM. Nuclear factor kappa B signaling either stimulates or inhibits neurite growth depending on the phosphorylation status of p65/RelA. *J Neurosci* (2008) 28:8246–8256. doi: 10.1523/JNEUROSCI.1941-08.2008
517. Gutierrez H, Hale VA, Dolcet X, Davies A. NF-kappaB signalling regulates the growth of neural processes in the developing PNS and CNS. *Development* (2005) 132:1713–1726. doi: 10.1242/DEV.01702
518. Kaltschmidt B, Kaltschmidt C. NF-KappaB in Long-Term Memory and Structural Plasticity in the Adult Mammalian Brain. *Front Mol Neurosci* (2015) 8:1–11. doi: 10.3389/FNMOL.2015.00069
519. Dresselhaus EC, Meffert MK. Cellular specificity of NF- κ B function in the nervous system. *Front Immunol* (2019) 10:1043. doi: 10.3389/FIMMU.2019.01043/BIBTEX

520. Xiao X, Putatunda R, Zhang Y, Soni P V., Li F, Zhang T, Xin M, Luo JJ, Bethea JR, Cheng Y, et al. Lymphotoxin β receptor-mediated NF κ B signaling promotes glial lineage differentiation and inhibits neuronal lineage differentiation in mouse brain neural stem/progenitor cells. *J Neuroinflammation* (2018) 15:1–14. doi: 10.1186/S12974-018-1074-Z/FIGURES/7
521. Frakes AE, Ferraiuolo L, Haidet-Phillips AM, Schmelzer L, Braun L, Miranda CJ, Ladner KJ, Bevan AK, Foust KD, Godbout JP, et al. Microglia induce motor neuron death via the classical NF- κ B pathway in amyotrophic lateral sclerosis. *Neuron* (2014) 81:1009. doi: 10.1016/J.NEURON.2014.01.013
522. Cho IH, Hong J, Suh EC, Kim JH, Lee H, Lee JE, Lee S, Kim CH, Kim DW, Jo EK, et al. Role of microglial IKK β in kainic acid-induced hippocampal neuronal cell death. *Brain* (2008) 131:3019–3033. doi: 10.1093/BRAIN/AWN230
523. Kyrargyri V, Vega-Flores G, Gruart A, Delgado-García JM, Probert L. Differential contributions of microglial and neuronal IKK β to synaptic plasticity and associative learning in alert behaving mice. *Glia* (2015) 63:549–566. doi: 10.1002/GLIA.22756
524. FitzPatrick LM, Hawkins KE, Delhove JM, Fernandez E, Soldati C, Bullen LF, Nohturfft A, Waddington SN, Medina DL, Bolaños JP, et al. NF- κ B Activity Initiates Human ESC-Derived Neural Progenitor Cell Differentiation by Inducing a Metabolic Maturation Program. *Stem Cell Reports* (2018) 10:1766. doi: 10.1016/J.STEMCR.2018.03.015
525. Su Y, Zhang W, Patro CPK, Zhao J, Mu T, Ma Z, Xu J, Ban K, Yi C, Zhou Y. STAT3 Regulates Mouse Neural Progenitor Proliferation and Differentiation by Promoting Mitochondrial Metabolism. *Front Cell Dev Biol* (2020) 8:362. doi: 10.3389/fcell.2020.00362
526. Li T, Zhao X, Duan J, Cui S, Zhu K, Wan Y, Liu S, Peng Z, Wang L. Targeted inhibition of STAT3 in neural stem cells promotes neuronal differentiation and functional recovery in rats with spinal cord injury. *Exp Ther Med* (2021) 22:1–11. doi: 10.3892/ETM.2021.10143
527. Okada S, Nakamura M, Katoh H, Miyao T, Shimazaki T, Ishii K, Yamane J, Yoshimura A, Iwamoto Y, Toyama Y, et al. Conditional ablation of Stat3 or Socs3 discloses a dual role for reactive astrocytes after spinal cord injury. *Nat Med* (2006) 12:829–834. doi: 10.1038/NM1425
528. Gautron L, De Smedt-Peyrusse V, Layé S. Characterization of STAT3-expressing cells in the postnatal rat brain. *Brain Res* (2006) 1098:26–32. doi: 10.1016/J.BRAINRES.2006.04.115
529. Hong S, Song MR. Signal transducer and activator of transcription-3 maintains the stemness of radial glia at mid-neurogenesis. *Journal of Neuroscience* (2015) 35:1011–1023. doi: 10.1523/JNEUROSCI.2119-14.2015
530. Noctor SC, Flint AC, Weissman TA, Dammerman RS, Kriegstein AR. Neurons derived from radial glial cells establish radial units in neocortex. *Nature* (2001) 409:714–720. doi: 10.1038/35055553
531. Crino PB. mTOR Signaling in Epilepsy: Insights from Malformations of Cortical Development. *Cold Spring Harb Perspect Med* (2015) 5: doi: 10.1101/CSHPERSPECT.A022442
532. Jain N, Zhang T, Fong SL, Lim CP, Cao X. Repression of Stat3 activity by activation of mitogen-activated protein kinase (MAPK). *Oncogene* (1998) 17:3157–3167. doi: 10.1038/SJ.ONC.1202238

533. Yang J, Kunimoto H, Katayama B, Zhao H, Shiromizu T, Wang L, Ozawa T, Tomonaga T, Tsuruta D, Nakajima K. Phospho-Ser727 triggers a multistep inactivation of STAT3 by rapid dissociation of pY705–SH2 through C-terminal tail modulation. *Int Immunol* (2020) 32:73–88. doi: 10.1093/INTIMM/DXZ061
534. Lin GS, Chen YP, Lin Dr ZX, Wang XF, Zheng ZQ, Chen L. STAT3 serine 727 phosphorylation influences clinical outcome in glioblastoma. *Int J Clin Exp Pathol* (2014) 7:3141. /pmc/articles/PMC4097241/ [Accessed April 13, 2023]
535. Wen Z, Zhong Z, Darnell JE. Maximal activation of transcription by stat1 and stat3 requires both tyrosine and serine phosphorylation. *Cell* (1995) 82:241–250. doi: 10.1016/0092-8674(95)90311-9
536. Gough DJ, Koetz L, Levy DE. The MEK-ERK pathway is necessary for serine phosphorylation of mitochondrial STAT3 and Ras-mediated transformation. *PLoS One* (2013) 8: doi: 10.1371/JOURNAL.PONE.0083395
537. Elsharkawy AM, Oakley F, Lin F, Packham G, Mann DA, Mann J. The NF-kappaB p50:p50:HDAC-1 repressor complex orchestrates transcriptional inhibition of multiple pro-inflammatory genes. *J Hepatol* (2010) 53:519–527. doi: 10.1016/J.JHEP.2010.03.025
538. Misgeld T, Schwarz TL. Mitostasis in neurons: Maintaining mitochondria in an extended cellular architecture. *Neuron* (2017) 96:651. doi: 10.1016/J.NEURON.2017.09.055
539. Bi F, Ma H, Ji C, Chang C, Liu W, Xie K. Rhein Protects Against Neurological Deficits After Traumatic Brain Injury in Mice via Inhibiting Neuronal Pyroptosis. *Front Pharmacol* (2020) 11:1564. doi: 10.3389/FPHAR.2020.564367/BIBTEX
540. Wang Y, Fan R, Luo J, Tang T, Xing Z, Xia Z, Peng W, Wang W, Lv H, Huang W, et al. An ultra high performance liquid chromatography with tandem mass spectrometry method for plasma and cerebrospinal fluid pharmacokinetics of rhein in patients with traumatic brain injury after administration of rhubarb decoction. *J Sep Sci* (2015) 38:1100–1108. doi: 10.1002/JSSC.201401197
541. Gorter JA, Aronica E, van Vliet EA. The Roof is Leaking and a Storm is Raging: Repairing the Blood–Brain Barrier in the Fight Against Epilepsy. *Epilepsy Curr* (2019) 19:177. doi: 10.1177/1535759719844750
542. Trépanier MO, Hopperton KE, Mizrahi R, Mechawar N, Bazinet RP. Postmortem evidence of cerebral inflammation in schizophrenia: A systematic review. *Mol Psychiatry* (2016) 21:1009–1026. doi: 10.1038/mp.2016.90
543. Felger JC, Li Z, Haroon E, Woolwine BJ, Jung MY, Hu X, Miller AH. Inflammation is associated with decreased functional connectivity within corticostriatal reward circuitry in depression. *Mol Psychiatry* (2016) 21:1358–1365. doi: 10.1038/mp.2015.168
544. Matta SM, Hill-Yardin EL, Crack PJ. The influence of neuroinflammation in Autism Spectrum Disorder. *Brain Behav Immun* (2019) 79:75–90. doi: 10.1016/j.bbi.2019.04.037
545. Aronica E, Crino PB. Inflammation in epilepsy: Clinical observations. *Epilepsia* (2011) 52:26–32. doi: 10.1111/j.1528-1167.2011.03033.x

546. Specchio N, Pietrafusa N, Trivisano M, Moavero R, De Palma L, Ferretti A, Vigevano F, Curatolo P. Autism and Epilepsy in Patients With Tuberous Sclerosis Complex. *Front Neurol* (2020) 11:639. doi: 10.3389/fneur.2020.00639
547. Vezzani A, Conti M, De Luigi A, Ravizza T, Moneta D, Marchesi F, De Simoni MG. Interleukin-1beta immunoreactivity and microglia are enhanced in the rat hippocampus by focal kainate application: functional evidence for enhancement of electrographic seizures. *J Neurosci* (1999) 19:5054–5065. doi: 10.1523/JNEUROSCI.19-12-05054.1999
548. Blair JD, Bateup HS. New frontiers in modeling Tuberous Sclerosis with human stem cell-derived neurons and brain organoids. *Dev Dyn* (2020) 249:46. doi: 10.1002/DVDY.60
549. Huang K, Wang Z, He Z, Li Y, Li S, Shen K, Zhu G, Liu Z, Lv S, Zhang C, et al. Downregulated formyl peptide receptor 2 expression in the epileptogenic foci of patients with focal cortical dysplasia type IIb and tuberous sclerosis complex. *Immun Inflamm Dis* (2022) 10:e706. doi: 10.1002/IID3.706
550. Aguilar-Castillo MJ, Cabezudo-García P, Ciano-Petersen NL, García-Martin G, Marín-Gracia M, Estivill-Torrús G, Serrano-Castro PJ. Immune Mechanism of Epileptogenesis and Related Therapeutic Strategies. *Biomedicines* (2022) 10: doi: 10.3390/BIOMEDICINES10030716
551. Lünemann JD, Malhotra S, Shinohara ML, Montalban X, Comabella M. Targeting Inflammasomes to Treat Neurological Diseases. *Ann Neurol* (2021) 90:177–188. doi: 10.1002/ANA.26158
552. Wang W, Nag SA, Zhang R. Targeting the NFκB Signaling Pathways for Breast Cancer Prevention and Therapy. *Curr Med Chem* (2015) 22:264. doi: 10.2174/0929867321666141106124315
553. Yoo CG, Lee S, Lee CT, Kim YW, Han SK, Shim YS. Effect of acetylsalicylic acid on endogenous IκB kinase activity in lung epithelial cells. *Am J Physiol Lung Cell Mol Physiol* (2001) 280:3–9. doi: 10.1152/AJPLUNG.2001.280.1.L3/ASSET/IMAGES/LARGE/H50110206005.JPEG
554. Gills JJ, LoPiccolo J, Tsurutani J, Shoemaker RH, Best CJM, Abu-Asab MS, Borojerdi J, Warfel NA, Gardner ER, Danish M, et al. Nelfinavir, A lead HIV protease inhibitor, is a broad-spectrum, anticancer agent that induces endoplasmic reticulum stress, autophagy, and apoptosis in vitro and in vivo. *Clin Cancer Res* (2007) 13:5183–5194. doi: 10.1158/1078-0432.CCR-07-0161
555. Zheng W, Xia N, Zhang J, Chen N, Meurens F, Liu Z, Zhu J. How the Innate Immune DNA Sensing cGAS–STING Pathway Is Involved in Autophagy. *Int J Mol Sci* (2021) 22: doi: 10.3390/IJMS222413232
556. Bodur C, Kazyken D, Huang K, Ekim Ustunel B, Siroky KA, Tooley AS, Gonzalez IE, Foley DH, Acosta-Jaquez HA, Barnes TM, et al. The IKK-related kinase TBK1 activates mTORC1 directly in response to growth factors and innate immune agonists. *EMBO J* (2018) 37:19–38. doi: 10.15252/EMBJ.201696164
557. Fohlen M, Taussig D, Ferrand-Sorbets S, Chipaux M, Dorison N, Delalande O, Dorfmueller G. Refractory epilepsy in preschool children with tuberous sclerosis complex: Early surgical treatment and outcome. *Seizure* (2018) 60:71–79. doi: 10.1016/J.SEIZURE.2018.06.005

558. de la Cruz López KG, Toledo Guzmán ME, Sánchez EO, García Carrancá A. mTORC1 as a Regulator of Mitochondrial Functions and a Therapeutic Target in Cancer. *Front Oncol* (2019) 9:1373. doi: 10.3389/FONC.2019.01373
559. Bartolomé A, García-Aguilar A, Asahara S-I, Kido Y, Guillén C, Pajvani UB, Benito M. MTORC1 Regulates both General Autophagy and Mitophagy Induction after Oxidative Phosphorylation Uncoupling. *Mol Cell Biol* (2017) 37: doi: 10.1128/MCB.00441-17
560. Ebrahimi-Fakhari D, Saffari A, Wahlster L, Di Nardo A, Turner D, Lewis TL, Conrad C, Rothberg JM, Lipton JO, Kölker S, et al. Impaired Mitochondrial Dynamics and Mitophagy in Neuronal Models of Tuberous Sclerosis Complex. *Cell Rep* (2016) 17:1053–1070. doi: 10.1016/j.celrep.2016.09.054
561. Tang G, Gudsnuk K, Kuo SH, Cotrina ML, Rosoklija G, Sosunov A, Sonders MS, Kanter E, Castagna C, Yamamoto A, et al. Loss of mTOR-dependent macroautophagy causes autistic-like synaptic pruning deficits. *Neuron* (2014) 83:1131–1143. doi: 10.1016/J.NEURON.2014.07.040
562. Maday S, Twelvetrees AE, Moughamian AJ, Holzbaur ELF. Axonal transport: cargo-specific mechanisms of motility and regulation. *Neuron* (2014) 84:292–309. doi: 10.1016/J.NEURON.2014.10.019
563. McMahon J, Huang X, Yang J, Komatsu M, Yue Z, Qian J, Zhu X, Huang Y. Impaired Autophagy in Neurons after Disinhibition of Mammalian Target of Rapamycin and Its Contribution to Epileptogenesis. *The Journal of Neuroscience* (2012) 32:15704. doi: 10.1523/JNEUROSCI.2392-12.2012
564. Mishra E, Thakur MK. Mitophagy: A promising therapeutic target for neuroprotection during ageing and age-related diseases. *Br J Pharmacol* (2023) doi: 10.1111/BPH.16062
565. Cai Q, Jeong YY. Mitophagy in Alzheimer's Disease and Other Age-Related Neurodegenerative Diseases. *Cells 2020, Vol 9, Page 150* (2020) 9:150. doi: 10.3390/CELLS9010150
566. Bell J. Amlexanox for the treatment of recurrent aphthous ulcers. *Clin Drug Investig* (2005) 25:555–566. doi: 10.2165/00044011-200525090-00001/FIGURES/TAB4
567. Julian LM, Delaney SP, Wang Y, Goldberg AA, Doré C, Yockell-Lelièvre J, Tam RY, Giannikou K, McMurray F, Shoichet MS, et al. Human Pluripotent Stem Cell-Derived TSC2-Haploinsufficient Smooth Muscle Cells Recapitulate Features of Lymphangioliomyomatosis. *Cancer Res* (2017) 77:5491–5502. doi: 10.1158/0008-5472.CAN-17-0925
568. Abdelwahab EMM, Pal S, Kvell K, Sarosi V, Bai P, Rue R, Krymskaya V, McPhail D, Porter A, Pongracz JE. Mitochondrial dysfunction is a key determinant of the rare disease lymphangioliomyomatosis and provides a novel therapeutic target. *Oncogene* (2019) 38:3093. doi: 10.1038/S41388-018-0625-1
569. Liu X, Liu Y, Yang R xue, Ding X jiu, Liang E shun. Loss of myeloid Tsc2 predisposes to angiotensin II-induced aortic aneurysm formation in mice. *Cell Death Dis* (2022) 13: doi: 10.1038/S41419-022-05423-2
570. Oeing CU, Jun S, Mishra S, Dunkerly-Eyring BL, Chen A, Grajeda MI, Tahir UA, Gerszten RE, Paolocci N, Ranek MJ, et al. MTORC1-Regulated Metabolism Controlled by TSC2 Limits Cardiac Reperfusion Injury. *Circ Res* (2021) 128:639. doi: 10.1161/CIRCRESAHA.120.317710

571. Wiegand G, May TW, Lehmann I, Stephani U, Kadish NE. Long-term treatment with everolimus in TSC-associated therapy-resistant epilepsies. *Seizure* (2021) 93:111–119. doi: 10.1016/J.SEIZURE.2021.10.011
572. Nicolas P, Tod M, Padoin C, Petitjean O. Clinical pharmacokinetics of diacerein. *Clin Pharmacokinet* (1998) 35:347–359. doi: 10.2165/00003088-199835050-00002
573. Galea I. The blood–brain barrier in systemic infection and inflammation. *Cellular & Molecular Immunology* 2021 18:11 (2021) 18:2489–2501. doi: 10.1038/s41423-021-00757-x
574. Kaur D, Kaur J, Kamal SS. Diacerein, its beneficial impact on chondrocytes and notable new clinical applications. *Brazilian Journal of Pharmaceutical Sciences* (2019) 54:e17534. doi: 10.1590/S2175-97902018000417534
575. Yu G, Liu Q, Dong X, Tang K, Li B, Liu C, Zhang W, Wang Y, Jin Y. Inhibition of inflammation using diacerein markedly improved renal function in endotoxemic acute kidney injured mice. *Cell Mol Biol Lett* (2018) 23:1–12. doi: 10.1186/S11658-018-0107-Z/FIGURES/6